Amino-Quat-Primer Polymer stabilized Silica-Nanoparticle-Dispersions

Dissertation

zur Erlangung des Grades eines

Doktors der Naturwissenschaften

im Fachbereich Biologie/Chemie

der Universität Osnabrück

vorgelegt von

Miriam Brandt

Osnabrück 2015

This work was carried out in the group Organic Materials Chemistry, at the Institute of Chemistry of New Materials, University of Osnabrück, under the supervision of Prof. Dr. Beginn. The studies were performed in the period from May 2012 to August 2015.

1. Referee : Prof. Dr. Uwe Beginn,

Organic Materials Chemistry,

University of Osnabrück

2. Referee : Prof. Dr. Lorenz Walder,

Molecular Electrochemistry,

University of Osnabrück

Enhancing the colloidal stability of nanoparticles dispersions, in order to extend the utilization time without any loss of performance, is desired. Prior works have confirmed the electrosteric stabilization of colloidal particles by so-called “amino-quat-primer” polymers, hyperbranched poly(ethylenimine) polymers containing amino groups and quaternized groups. In this work, a systematic investigation on the factors influencing the polymer-particle-interactions was carried out. Hence, aqueous silica-nanoparticle-dispersions were polymer-functionalized; their dispersions stability was studied using turbidity analysis; and the particle surface charge was examined employing electrophoretic measurements. Five key factors influencing the polymer-particle-interaction were defined, including: the polymer-particle-ratio, the degree of polymerization and the degree of functionalization of the polymer, the dispersion pH and the salt concentration. Alternatingly occurring areas of stable, unstable and again stable dispersions with an increasing polymer-particle-ratio occurred due to a charge reversal of bare, negatively charged to polymer-covered, positively charged particles. An additional area of unstable dispersions at very high polymer concentrations was assumed to arise from depletion forces of non-adsorbed free polymer. Stable, positively charged, polymer-covered silica nanoparticles were obtained for optimized conditions regarding the five key factors. After the dispersion stability enhancement, the new amino-functionalized surface could be used for further modifications, e.g. to result in a compatibility with a polymer matrix to fabricate highly functional polymer / inorganic hybrid materials.

Table of content

Chapter 1:

Introduction

1. Introduction

Dispersions of solid nanoparticles in liquid phases are widely employed in application areas such as cosmetics, coatings, and catalysis [1]. For these applications, a high stability of colloidal dispersions is required; however, dispersions are often thermodynamically unstable and tend to agglomerate over time. Therefore, in order to extend the utilization time without any loss of performance, an enhancement of the colloidal stability is desired.

The approach followed by this work to enhance the stability of colloidal dispersions is the particle surface functionalization by using so-called “amino-quat-primer” polymers. An amino-quat-primer polymer is a hyperbranched poly(ethylenimine) polymer which contains amino groups and quaternized groups (cf. Figure 1-1,1) [2]. Such polymers strongly adsorb on even slightly negatively charged surfaces by cooperative ionic interactions (cf. Figure 1-1,2). This approach provides two main advantages over a physical modification by low molecular weight compounds with only one ionic group per molecule: The numerous ionic bonds between one macromolecule and the surface cause a highly stable connection and besides, the new generated surface exhibits a high density of functional groups.

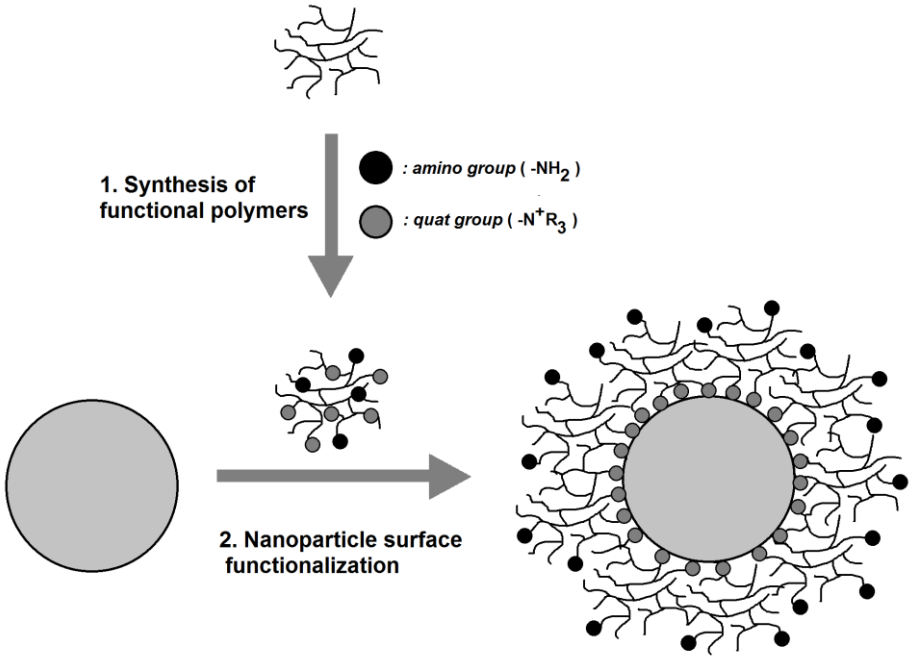

Figure 1-1: Scheme of 1) Synthesis of functional polymers and 2) Nanoparticle surface functionalization

Even though prior studies have revealed the positive effects of amino-quat-primer polymers on the stability of colloidal particles [3,4,5], deeper investigations of the occurring polymer-particle-interactions had not been carried out. To address this gap, in this work a systematic

study on the factors influencing the interaction of colloidal particles with amino-quat-primer polymers was performed. To investigate this interaction, five key factors were defined, including: the polymer-particle-ratio, the degree of polymerization and the degree of functionalization of the polymers, the dispersion pH and the salt concentration.

For the present study, colloidal silica was chosen as a model system to investigate dispersion stability, because it exhibits several desired properties, e.g. an easy and precise size control, low manufacturing costs, broad application spectrum, and an inherent stability in aqueous solution without further additives [6].

To achieve the objective of this thesis, firstly, amino-quat-primer polymers were synthesized and characterized; secondly, these polymers were employed to functionalize the surface of silica nanoparticles; and finally, the dispersion stability and the particle surface charge of these produced silica-polymer-dispersions were analyzed.

In Chapter 2 the following relevant literature for this work is reviewed: polyelectrolytes in general and hyperbranched poly(ethylenimine) in particular; silica nanoparticles; the electric double layer - and the DLVO theory; dynamic light scattering and laser-Doppler-velocimetry; the adsorption of charged polyelectrolytes on oppositely charged particles in general, as well as the adsorption of poly(ethylenimine) on silica surfaces in particular.

The experimental data of the synthesis of amino-quat-primer polymers and the preparation of silica-polymer-dispersions is given in Chapter 3.

Chapter 4 deals with the synthesis and characterization of amino-quat-primer polymers. The structure and degree of quaternization of the products are confirmed. Moreover, the protonation behavior upon variation of polymer concentration, pH and salt concentration is investigated.

The preparation of silica-nanoparticle-dispersions containing amino-quat-primer polymers is described in Chapter 5. In addition, the optical investigation of the dispersions concerning their stability by means of turbidity measurements is discussed.

In Chapter 6, the results of the investigation of the stability of silica-polymer-dispersions regarding the defined key factors are given.

Chapter 7 summarizes the results of this thesis and gives an outlook of further possible uses of these findings.

[1] Iler, R.K.; The Chemistry of Silica, Chapter 1, pp. 1-115, John Wiley & Sons, 1979

[2] Möller, M.; Beginn, U.; Keul, H.; Thomas, H.; European Patent Application, 060-07066 (to: DWI, RWTH Aachen e.V.), 03.04.2006 (EP 1710283A1)

[3] Komban, R.; Beckmann, R.; Rode, S.; Ichilmann, S.; Kühnle, A.; Beginn, U.; Haase, M.; Langmuir 2011, 27, 10174-10183

[4] Goel, V.; Beginn, U.; Mourran, A.; Möller, M., Macromolecules 2008, 41, 8187-8197

[5] Beckmann, R.; Beginn, U.; Journal of Polymer Science, Part A 2013, 51, 3700-3715

[6] Rahman, I.A.; Padavettan, V.; Journal of Nanomaterials 2012, 1-15

Chapter 2:

Literature Review

2. Literature Review

This chapter summarizes the “state of the art” as documented in the public literature concerning the stability of silica-nanoparticle-dispersions in the presence of amino-quat-primer polymers. The properties and the applications of polyelectrolytes in general, as well as the synthesis, their modification with epoxides, the properties, and the applications of hyperbranched poly(ethylenimine) are summarized in particular. The synthesis, the properties, and applications of silica nanoparticles are described and the theoretical background of the electric double layer and the DLVO theory are explained. Two measurement methods, namely dynamic light scattering and laser-Doppler-velocimetry, are introduced. The adsorption of charged polyelectrolytes on oppositely charged particles in general, as well as the adsorption of poly(ethylenimine) on silica surfaces in particular are described, and the properties, as well as the applications of polymer-silica-nanocomposites are summarized.

2.1. Polyelectrolytes

Polymer molecules, which carry covalently bonded ionic groups are called polyelectrolytes (PELs) [1].

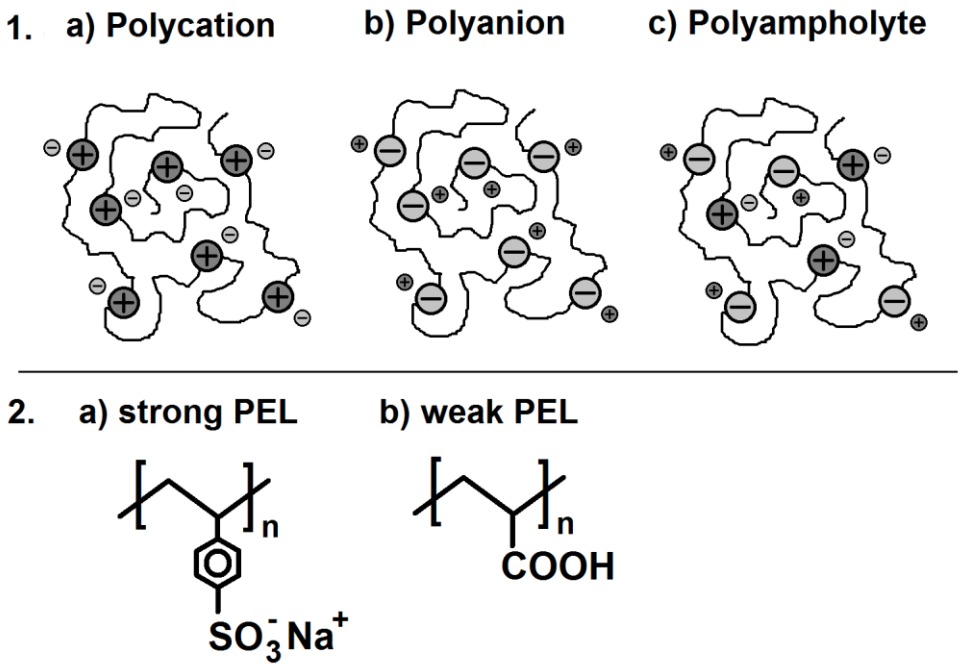

Figure 2-1: 1. Sketch of a) a polycation, b) a polyanion, and c) a polyampholyte; 2. Examples of a) a strong polyelectrolyte poly(sodium styrene sulfonate) and b) a weak polyelectrolyte poly(acrylic acid)

PELs can be classified according to their ionic charges as polycations, polyanions or polyampholytes (see Figure 2-1,1). Polycations or polybases (cf. Figure 2-1,1.a) bear cationic charges; polyanions or polyacids (cf. Figure 2-1,1.b) exhibit anionic charges; and polyampholytes (cf. Figure 2-1,1.c), carry cationic, as well as anionic charges. Polyelectrolytes can also be divided into strong and weak PELs regarding their degree of dissociation. Strong PELs are fully ionized and their charge is independent of the solution pH (see Figure 2-1,2.a). In contrast to this, a weak PEL carries ionizable groups and its charge density varies with pH and ionic strength of the solution (see Figure 2-1,2.b).

2.1.1. Properties of polyelectrolytes

Polyelectrolytes combine properties of macromolecules and electrolytes. However, their properties are far beyond the simple superposition of the properties of both species. The properties of polyelectrolyte solutions are less well described theoretically than the ones of uncharged polymer solutions [1]. Reasons are experimental problems such as aggregation phenomena, and theoretical difficulties like the handling of long-ranged Coulomb interactions.

The conformation of polyelectrolytes in solution depends strongly, among other things, on the polymer architecture, the solvent quality, the solution pH, as well as the ionic strength. Charges of the same type repel each other and lead to an elongation of the polymer molecule. The polyelectrolyte charge can be screened by addition of counterions [2], which leads to a random coil formation. The ionic charges of individual polyelectrolyte chains interact with each other and tend to form ordered ionic clusters. This leads to a failure of basic coil theories. Charges of the same type are less strongly screened at a higher dilution, which leads to an increase of the repulsive forces and the stiffness of the polyelectrolyte molecules. This effect is called “polyelectrolyte effect” [3]. The viscosity of polymer solutions decreases with an increasing dilution, however the reduced viscosity of polyelectrolyte solutions simultaneously increases.

2.1.2. Applications of polyelectrolytes

Polyelectrolytes are applied in a variety of different fields. Commercially PELs are used, among other things, as flocculants in wastewater treatment [4], as retention agents in the

paper industry [5], as stabilizators for colloidal systems [6], and as thickeners in foods [7] and cosmetics [8]. Current research interests including polyelectrolytes are for example polyelectrolyte multilayers produced by layer-by-layer deposition technique [9] and in the field of biochemical and medical applications, where biocompatible polyelectrolytes are used e.g. for implant coatings [10] and for controlled drug release [11].

2.2. Hyperbranched poly(ethylenimine)

The weak, cationic polyelectrolyte poly(ethylenimine) (PEI) can be obtained with a linear (LPEI), branched (BPEI), or dendritic (DPEI) architecture. LPEI consists of a chain of secondary amino groups terminated by two primary amino groups (see Figure 2-2a). DPEI consists of a core of tertiary amino groups and a shell of primary amino groups (see Figure 2-2c). In contrast to dendrimers which exhibit a perfect branched structure, there is also a certain amount of secondary amino groups present in hyperbranched polymers (see Figure 2-2b). Because of this imperfectness, the synthesis of hyperbranched polymers is much easier and cheaper than the one of dendrimers [12]. Nevertheless the properties of hyperbranched polymers like global structure, low viscosity and high solubility are close to the ones of dendrimers [13].

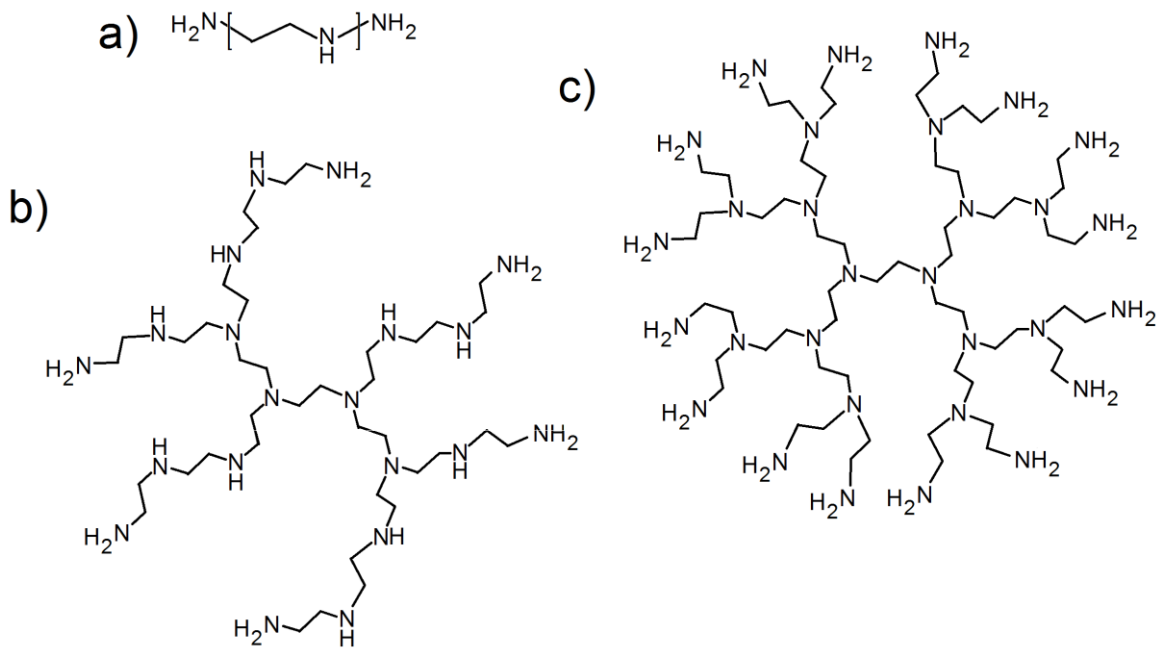

Figure 2-2a): Linear poly(ethylenimine) (LPEI), b) hyperbranched poly(ethylenimine) (BPEI), c) dendritic poly(ethylenimine) (DPEI)

2.2.1. Synthesis of hyperbranched poly(ethylenimine)

Hyperbranched poly(ethylenimine) is synthesized via the cationic ring-opening polymerization of aziridine [14], involving the "active chain end" (= ACE) mechanism. The reaction is initiated by a proton transfer to aziridine (see Figure 2-3a).

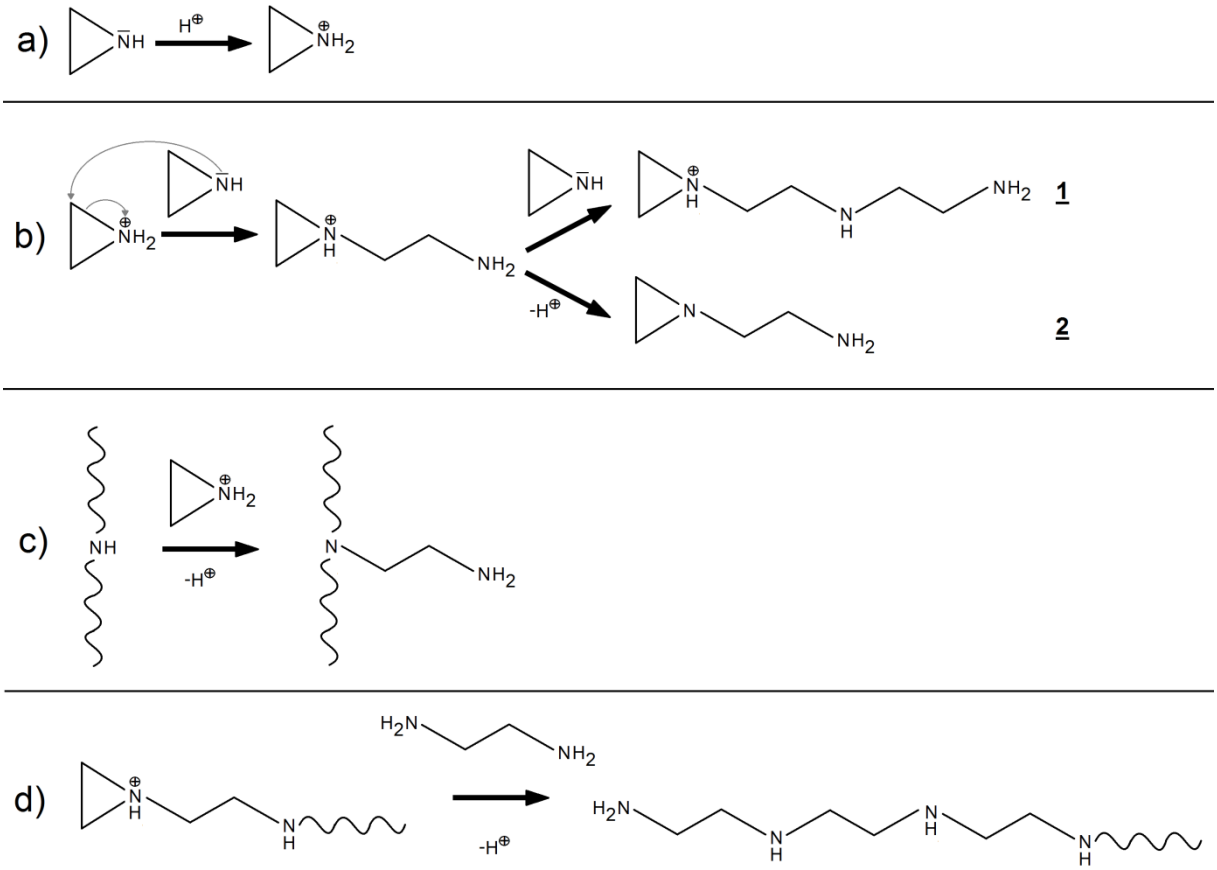

Figure 2-3: Synthesis of hyperbranched poly(ethylenimine): a) Initiation, b) propagation, c) branching, d) termination

The propagation takes places by a nucleophilic attack of the nitrogen atom of a neutral aziridine molecule on a carbon atom of the aziridinium species with simultaneous ring-opening of the latter unit (see Figure 2-3b,1). Since this addition transforms the added aziridine molecule into a new aziridinium unit, the growth-active species remains at the chain end. On dissociation of the proton from the terminal aziridinium, a "dormant species" is created (cf. Figure 2-3b,2). Branching frequently occurs due to nucleophilic attack of arbitrary chain-bonded nitrogen atoms to either aziridinium molecules or terminal aziridinium units. If a secondary amino group of an existing chain reacts with an aziridinium cation, a tertiary amino group is formed (see Figure 2-3c). The molecular weight can be controlled by addition of

ethylenediamine, because the reaction of this substance with the aziridinium cation leads to a chain termination (see Figure 2-3d).

According to pure statistical considerations the values of the ratio of primary, secondary and tertiary amino groups in hyperbranched poly(ethylenimine) should be 25:50:25 [15]. More recently the degree of branching was determined by inverse gated-^{13}C-NMR-spectroscopy. The ^{13}C-NMR- spectra of BPEI (shown in Figure 2-4b) exhibits eight signals caused by the eight different occurring chemical surroundings of the backbone carbon atoms in neighborhood of terminal, linear and dendritic amino groups (listed in Figure 2-4a) [16]. The measured molar fractions of primary, secondary and tertiary amino groups were 31:40:29, and 31:38:31, respectively, for investigated polymers with a molecular weight M_W of 25,000 and 750,000g/mol [17].

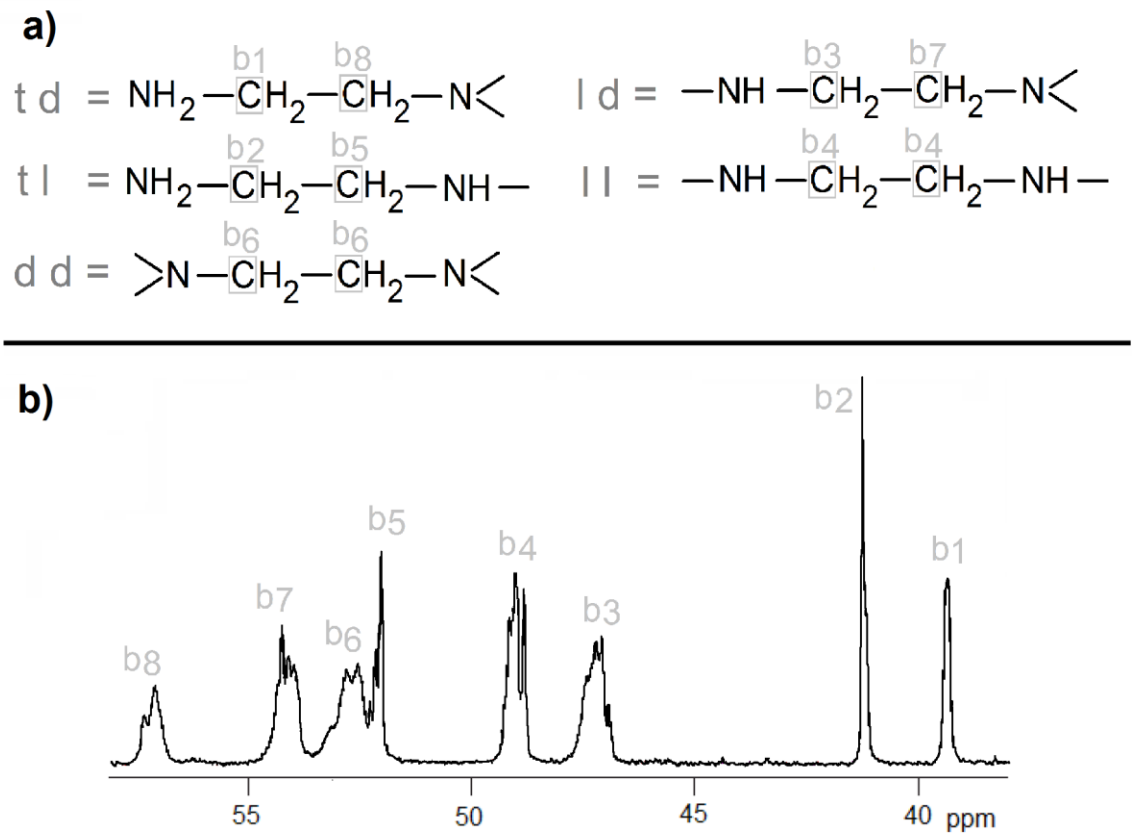

Figure 2-4: Possible combinations of neighboring terminal, linear and dendritic amino groups of hyperbranched poly(ethylenimine), b) ^{13}C-NMR-spectra of BPEI, denotation of backbone carbon atoms b_1 – b_8 according to a)

2.2.2. Modification of hyperbranched poly(ethylenimine) with epoxides

An epoxide is a cyclic ether consisting of three ring atoms, two carbon atoms and an oxygen atom. The ring is highly strained and this strain makes the epoxide highly reactive towards nuleophiles. The so-called “Prilezhaev reaction” describes the conversion of an alkene to an epoxide by employing a peroxycarboxylic acid (cf. Figure 2-5).

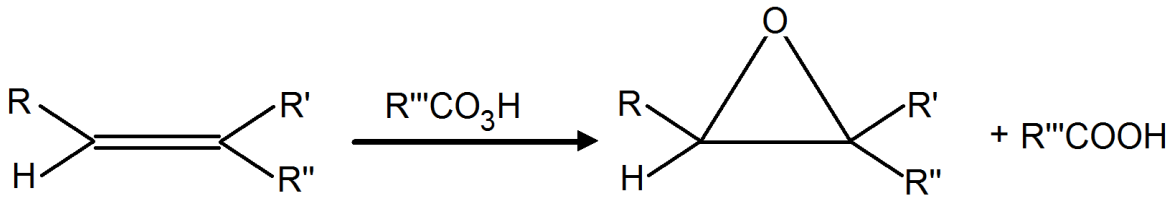

Figure 2-5: Prilezhaev reaction – reaction of alkenes with peroxycarboxylic acids to epoxides

During a nucleophilic addition to epoxides, the nucleophile could attack both carbon ring atoms and two isomers could be formed. It was found that during the reaction of epoxides with amines in aqueous solution under acid catalysis, unsymmetrical substituted epoxides are always attacked at the carbon atom with the higher number of free protons and only one isomer is found [18].

Figure 2-6 shows the reaction products of the reactions of an epoxide with a) a primary amine, b) a secondary amine, c) a tertiary amine, and d) an alcohol. Table 2-1 lists the reactivity constants of the reactions of propylene oxide with different amines [19]. The reactivity constant for the shortest rest, the methyl groups, is the highest for the tertiary amines. For the ethyl groups all reactivity constants are smaller than for the methyl groups, and for the propyl groups the reactivity constants for secondary and tertiary amines are almost zero. The bigger the rest bounded to the amino group, the higher is the steric hindrance and the smaller is the reactivity.

Table 2-1: Reactivity constants of the reactions of propylene oxide with different amines (values were normalized for RNH_3 = 0.0046 L^2 / mol^2; data taken from [19])

	NH_3	RNH_2	R_2NH	R_3N
R = -CH_3	1	8.04	36.96	57.83
R = -C_2H_5	1	2.61	4.56	0.84
R = -C_3H_7	1	5.87	-	-

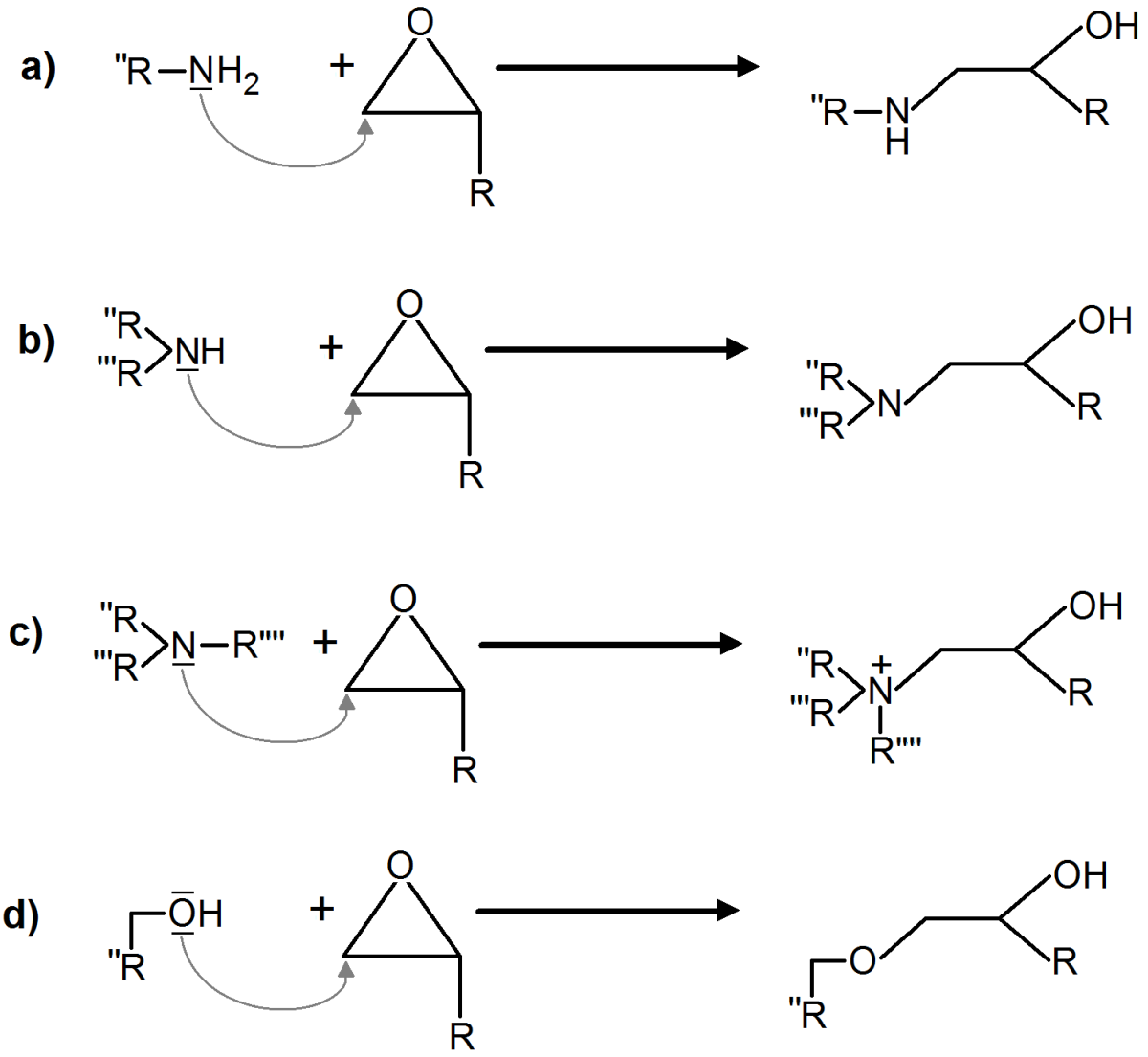

Figure 2-6: Reactions of an epoxide with a primary amine (a), a secondary amine (b), a tertiary amine (c), and an alcohol (d)

2.2.3. Properties of hyperbranched poly(ethylenimine)

Hyperbranched poly(ethylenimine) is a yellowish, viscous liquid with a glass temperature of -55°C [20]. It is soluble in polar solvents like dimethylformamide, water, methanol, and ethanol, but also in moderate nonpolar solvents like ethyl acetate, chloroform, and tetrahydrofuran.

The weak polyelectrolyte poly(ethylenimine) exists in a protonated state in aqueous solution. Figure 2-7a) illustrates the titration curves of hyperbranched poly(ethylenimine) [22]. The

experimental data is compared with calculated results. Figure 2-7b) depicts site specific degree of protonation for primary, secondary, and tertiary amines as a function of the solution pH obtained by Monte Carlo simulations. The point of zero charge of poly(ethylenimine) is at pH 10.8 [21]. Due to the hydration of amines in water and the resultant influence of the steric hindrance on the basicity of the amines, the following protonation behavior in dependence on the pH is found. At pH 8 all primary amines and half of the secondary amino groups are protonated. At pH 4 almost all secondary amino groups are protonated, but only around 10% of the tertiary amino groups. Tertiary amino groups only start to protonate under very acidic conditions. Hyperbranched poly(ethylenimine) is never completely protonated in an accessible pH range, because of the increasing repulsion between the charged macromolecule and hydroxonium ions with increasing degree of protonation. An aqueous poly(ethylenimine) solution reaches a maximum pH value of about 11.1.

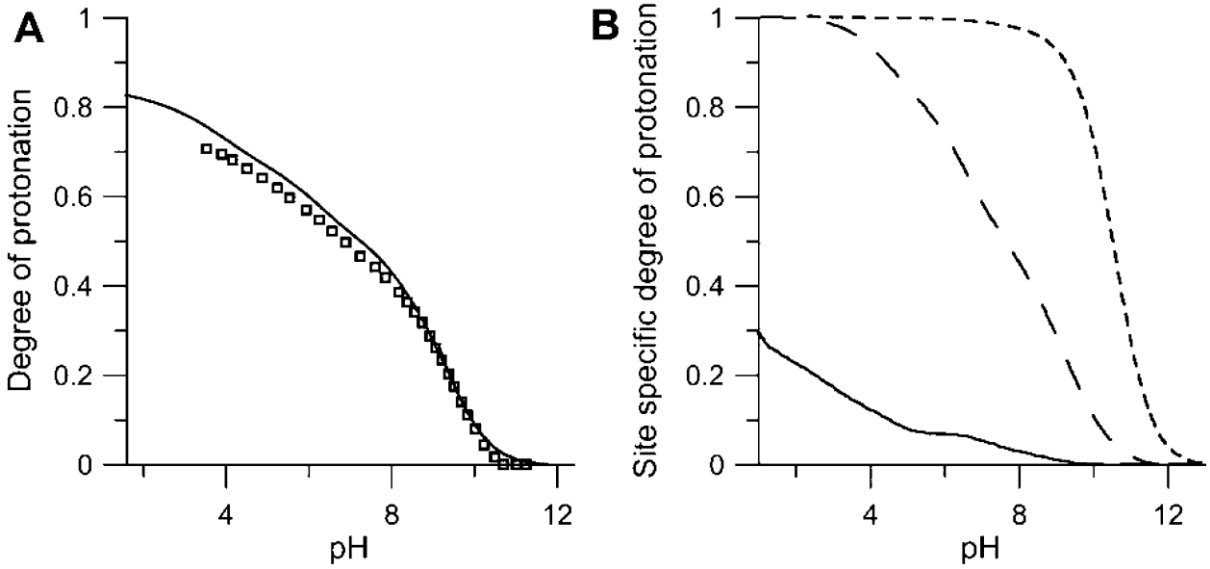

Figure 2-7a): Titration curves of hyperbranched poly(ethylenimine); squares: experimental data, line: theoretical predications, b) site-specific titration curves for primary (dashed line with short dashes), secondary (dashed line with long dashes) and tertiary amines (continuous line) (graphic taken from [22])

The nominal charge of a protonated poly(ethylenimine) molecule is given by the sum of charges of all protonated amino groups. The effective charge of a protonated poly(ethylenimine) molecule is the charge which acts effectively and is measurable. The effective charge is often much smaller than the nominal charge due the fact, that a part of the counterions enter the PEI macromolecule and become located in close vicinity to the cationic monomer units. This so-called “counterion condensation” [23] partially neutralize the

polyelectrolyte charge. The higher the degree of protonation of the polyelectrolyte is, the stronger becomes the interactions between the polyelectrolyte and its counterions and with it the counterion condensation, which lowers the effective charge.

In contrast to linear poly(ethylenimine), which elongates upon protonation with an increasing radius of gyration [24], it was proven by measuring the intrinsic viscosity [15] and performing small-angle neutron scattering [25] of aqueous solutions of hyperbranched poly-(ethylenimine) that the branched polymers do not change their conformation over a pH range of 2 < pH < 11. The hydrodynamic radius of a charged PEI molecule is only about 65% bigger than the one of the uncharged polymer in absence of salt and about 10% bigger in the presence of 0.1M sodium chloride [26].

2.2.4. Applications of hyperbranched poly(ethylenimine)

Poly(ethylenimine) is employed in a variety of commercial applications and is also found in recent researches. It was first applied technically as retention aid in paper production for improving the retention of fine materials during the paper formation [27] and as chelating agent to bind heavy metal ions in wastewater treatment [28]. PEI is employed for antibacterial coating in textiles [29] and as a base for anionic exchange resins [30]. It was recently investigated as transfection agent for gene delivery systems [31], as sorbent for carbon dioxide capture [32], and as cationic compound in multilayer assemblies [33].

2.3. Silica nanoparticles

The word “silica” is another name of the chemical compound silicon dioxide (SiO_2) [34]. Silica is found in nature as the mineral quartz. It is the main component of sand and the main ingredient of glass.

Fine particles of a size of one to several hundreds of nanometers are called nanoparticles. The word “nano” has his origin in the Greek word “nanos”, which means “dwarf”. One nanometer equals 10^{-9} meter = 0.000 000 001meter.

Silica nanoparticles are fine silicon dioxide particles in the range of one to several hundreds of nanometers.

2.3.1. Synthesis of silica nanoparticles

The most relevant synthesis of silica nanoparticles are the reverse microemulsion [35], the flame synthesis [36] and the sol-gel process [34]. The Stöber synthesis, a sol-gel process, is a well-established reaction to yield monodisperse spherical silica particles [37]. The particles are synthesized by hydrolysis (a) and condensation (b) of tetraalkoxysilanes, most commonly tetraethyl orthosilicate (TEOS), in a mixture of alcohol and water in presence of ammonia as a catalyst (see Figure 2-8).

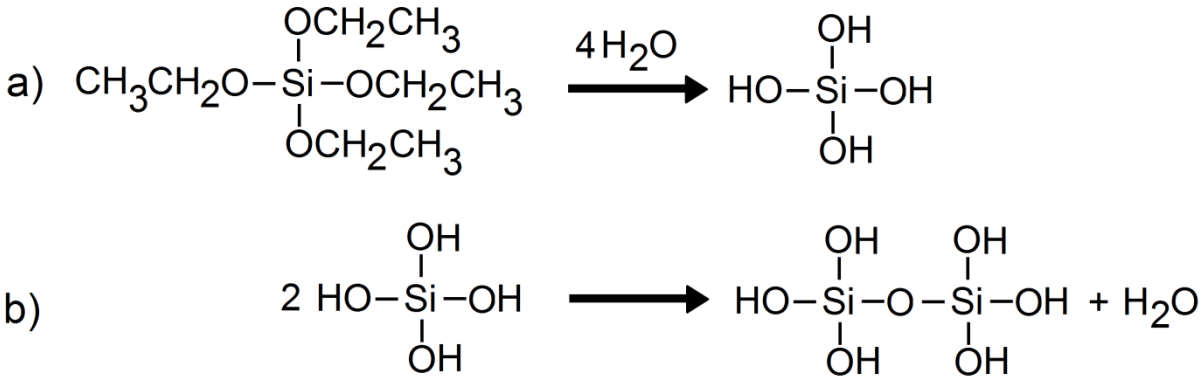

Figure 2-8: Stöber process; a) Hydrolysis; b) Condensation

The hydrolysis of TEOS in water can be catalyzed either by acid or by base. At an acidic pH, the hydrolysis is much faster than the polycondensation and gel structures are formed. At an alkaline pH, the hydrolysis is much slower than the polycondensation and spherical particles are produced as they are favored in the Stöber process. The average particle diameter can be varied between 50nm and 2µm depending on the used type of silicon alkoxide, the employed type of the alcohol, the ratio between reactants, catalyst, and solvent, as well as the reaction temperature [38,39]. The reaction is normally carried out at very low particle concentrations and has therefore a low mass yield.

2.3.2. Properties of silica nanoparticles

The surface of silica nanoparticles originating from Stöber-synthesis consists of siloxane groups, as well as free, geminal and vicinal silanols (see Figure 2-9) [40]. In aqueous solution all surface silicon atoms carry free hydroxyl groups. A fully hydroxylated silica surface on average contains 4.6 hydroxyl groups per nm² [40].

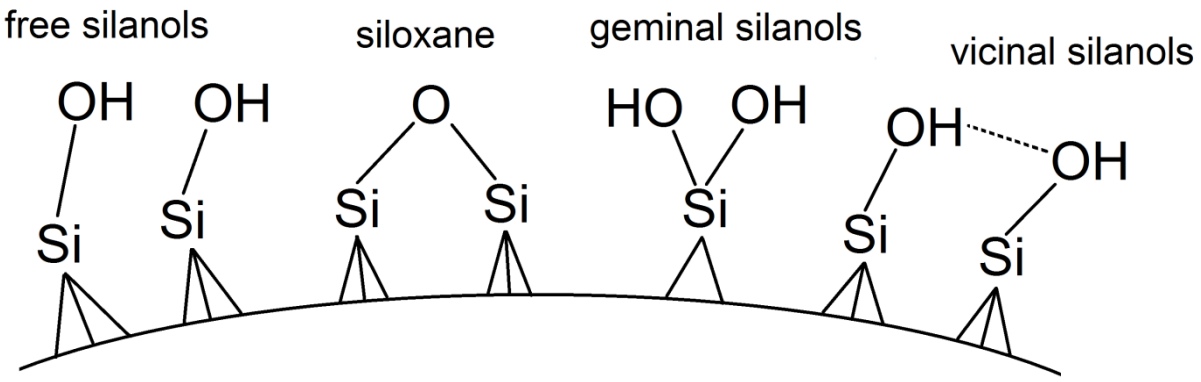

Figure 2-9: Siloxane, as well as free, geminal and vicinal silanols on the silica nanoparticle surface

Figure 2-10 shows the zeta potential of silica wafers determined by streaming potential measurements [42]. The zeta potential of the silica nanoparticles is slightly positive at low pH values, the isoelectric point occurs at pH values of around 2-4 depending on the specific material and its synthesis process [41], and above this pH the zeta potential reaches highly negative values. The potential decreases with an increase in ionic strength. Hence, under neutral conditions (pH = 7), silica surfaces are slightly negatively charged.

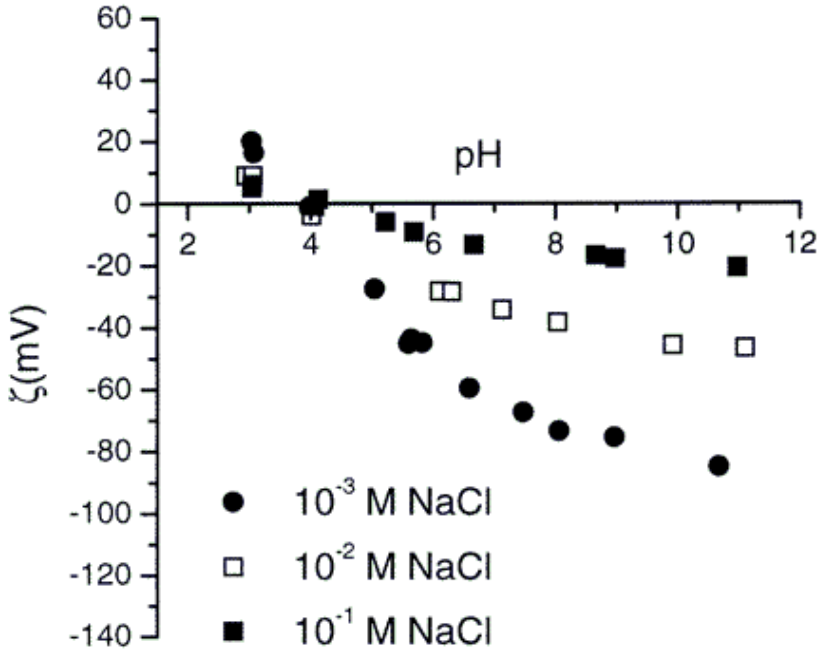

Figure 2-10: Zeta potential of a silica surface as a function of the solution pH for three different ionic strengths (Graphic taken from [42])

2.3.3. Applications of silica nanoparticles

Due to the precise and easy size control of silica nanoparticles they are widely applied in recent research, as well as in commercial technology. Silica nanoparticles are used, for example, in the biomedical field concerning drug delivery and drug release [43], in light-emitting devices [44], in photovoltaic applications [45], for heterogeneous nanocatalysis [46], and widely as additives in cosmetics and food [47].

2.4. Colloidal Stability

A colloid at least consists of two phases where one phase, called the “dispersed phase”, is dispersed within a second phase, the “dispersion medium” [48]. For example, a solid dispersed in a liquid is called “dispersion” (e.g. blood), a liquid dispersed in a liquid is called “emulsion” (e.g. milk), and a gas dispersed in a liquid is called “foam” (e.g. shaving cream). In the following text, the word “colloid” will refer to a solid dispersed in a liquid phase.

Colloids can only be stable in the presence of forces that impede the particle agglomeration caused by attractive Van-der-Waals interactions. One possibility is the presence of repulsive electric forces. The concept of the electric double layer developed by Helmholtz, remodeled by Gouy-Chapman, and revised by Stern deals with the arrangement of counterions at a charged surface in aqueous solution. The DLVO theory by Derjaguin, Landau, Verwey, and Overbeek describes the interaction potential between uniformly charged particles as the superposition of an electrostatic repulsive and an attractive van der Waals potential.

2.4.1. Electric double layer

The double layer theory, established in 1853 by Helmholtz [49], claims that a charged surface is covered by a layer of immobilized oppositely charged counterions (see Figure 2-11a). In 1910 Gouy [50] and in 1913 Chapman [51] assumed the thermal movement to disrupt the layer of immobile ions, and described the distribution of the counterions as a function of the distance to the surface (see Figure 2-11b). In 1924 Stern [52] combined the theory of Helmholtz and the one of Gouy and Chapman to the Stern model on assuming the presence of a fixed “Stern-layer” of oppositely charged counterions, followed by a Gouy-Chapman diffuse layer (see Figure 2-11c).

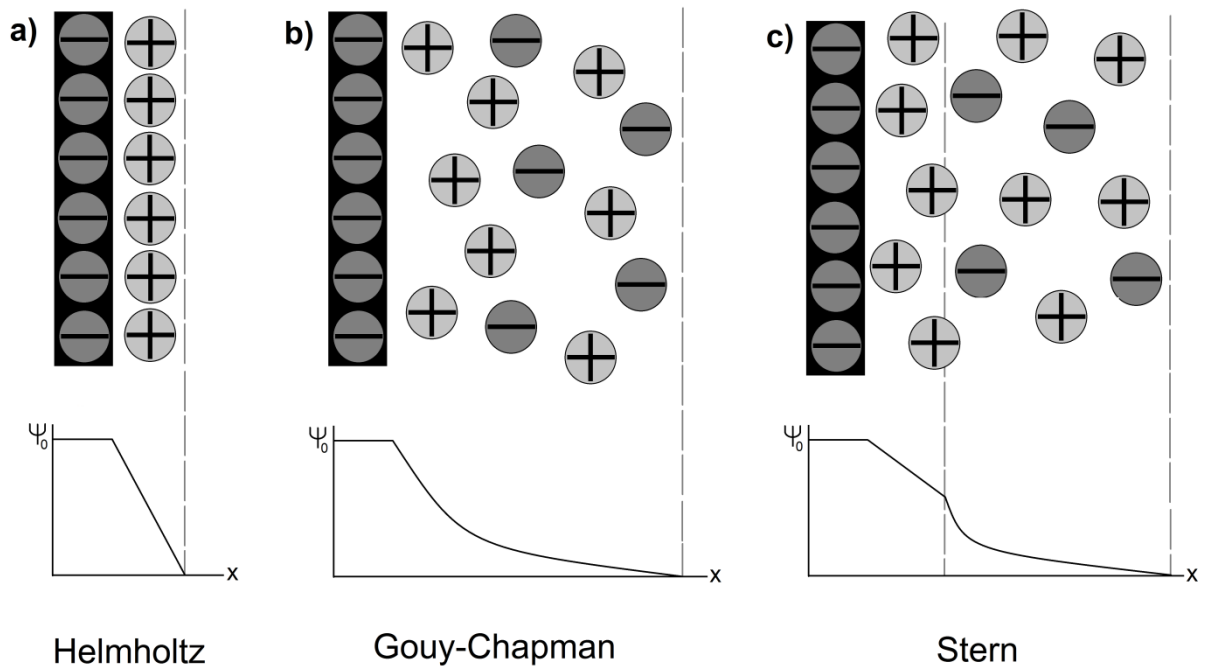

Figure 2-11: Sketch of the charged surface and the counterion distribution, as well as the trend of the surface potential as a function of the distance based on the theory of a) Helmholtz, b) Gouy-Chapman, and c) Stern

The Debye length is a characteristic value to describe the double layer thickness [48]. An approximation of the Debye length k^{-1} for diluted solutions ($I \leq 10^{-3}$mol/L) is given in Equation 2-1. In an aqueous solution for a monovalent salt at room temperature, the Debye length is inverse proportional to the square root of the ionic strength (see Equation 2-2). It equals about 3nm, 1nm, or 0.3nm in a sodium chloride solution of 0.01M, 0.1M, or 1M, respectively.

$$k^{-1}[\mathrm{nm}] = \sqrt{\frac{\varepsilon_r\ \varepsilon_0\ k_b\ T}{2\ N_A\ e^2\ I}} \qquad \textit{Equation 2-1}$$

$$k^{-1}[\mathrm{nm}] = \frac{0.304\ \mathrm{nm}}{\sqrt{I}} \left(\frac{\mathrm{mol}}{\mathrm{L}}\right)^{\frac{1}{2}} \qquad \textit{Equation 2-2}$$

with k^{-1}: Debye length; ε_r: permittivity of free space; ε_0: dielectric constant; k_b: Boltzmann constant; T: temperature; N_A: Avogadro number; e: elementary charge; I: ionic strength

2.4.2. DLVO theory

The DLVO theory is based on the works of Derjaguin and Landau in 1941 [53], and of Verwey and Overbeek in 1948 [54]. It describes the total interaction potential between two identical charged particles in solution as the superposition of an electrostatic repulsive potential and an attractive van der Waals potential as a function of the separation between the two particles (see Figure 2-12). Depending on the particles separation distance the DLVO-potential can be attractive or repulsive.

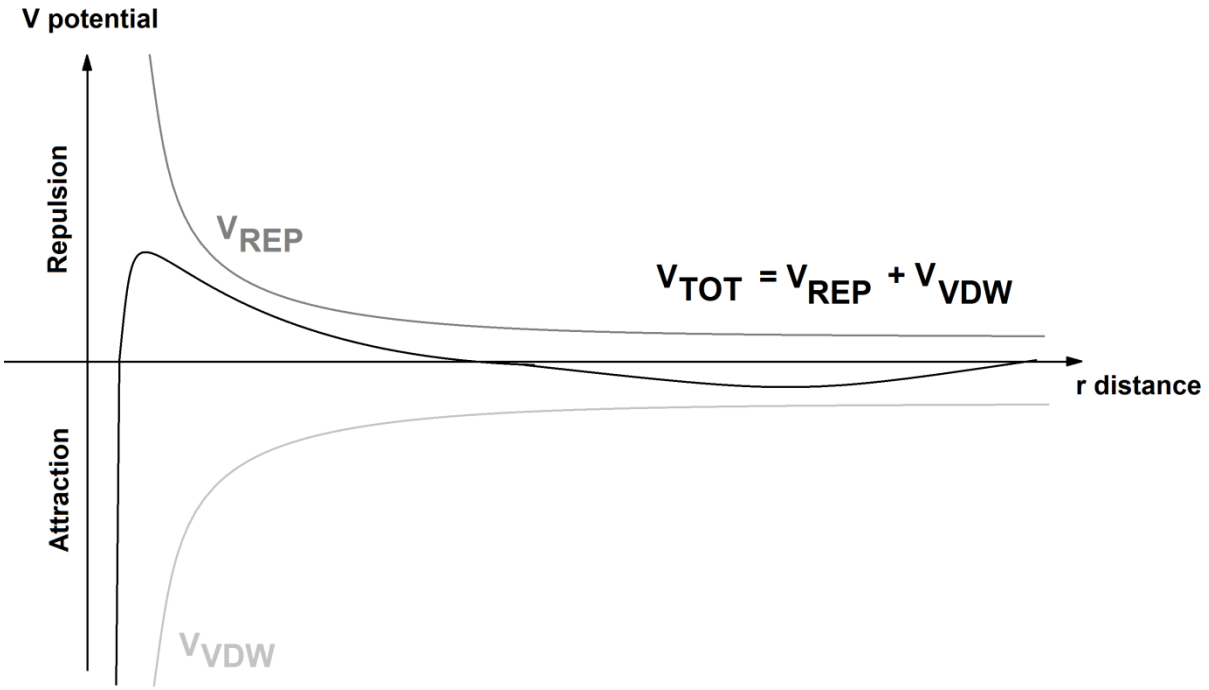

Figure 2-12: Repulsive, van der Waals and total interaction potential between two identical charged particles in solution as a function of the separation distance

A variation of the salt concentration influences the repulsive interaction, but not the attractive interaction between charged particles [48]. The DLVO theory predicts two aggregation regimes in dependence on the salt concentration: a slow aggregation regime at low salt concentrations and a fast aggregation regime at high salt concentrations. The transition is sharp and the transition concentration is called critical coagulation concentration (CCC).

$$CCC \sim \frac{1}{n^6} \qquad \textit{Equation 2-3}$$

with CCC: critical coagulation concentration; n: counterions valency

The ability of multivalent salt to coagulate particles as a function of the counterion valency is described by the empiric Schulze-Hardy rule (see Equation 2-3) [55,56] stating the critical coagulation concentration to be inverse proportional to the sixth power of the counterions valency.

2.5. Methods

Dynamic light scattering measurements can be employed to measure the size distribution of particles in solution. Electrophoretic mobility measurements are used to determine the electrophoretic mobility of a charged species in aqueous solution.

2.5.1. Dynamic light scattering

Dynamic light scattering (DLS), also known as quasi-elastic light scattering or photon correlation spectroscopy, is employed to determine the diffusion coefficient D of particles, polymers, micelles or proteins [57]. From D the hydrodynamic radius r_H of the particles can be calculated, sizes between several micro meters down to one nanometer can be detected.

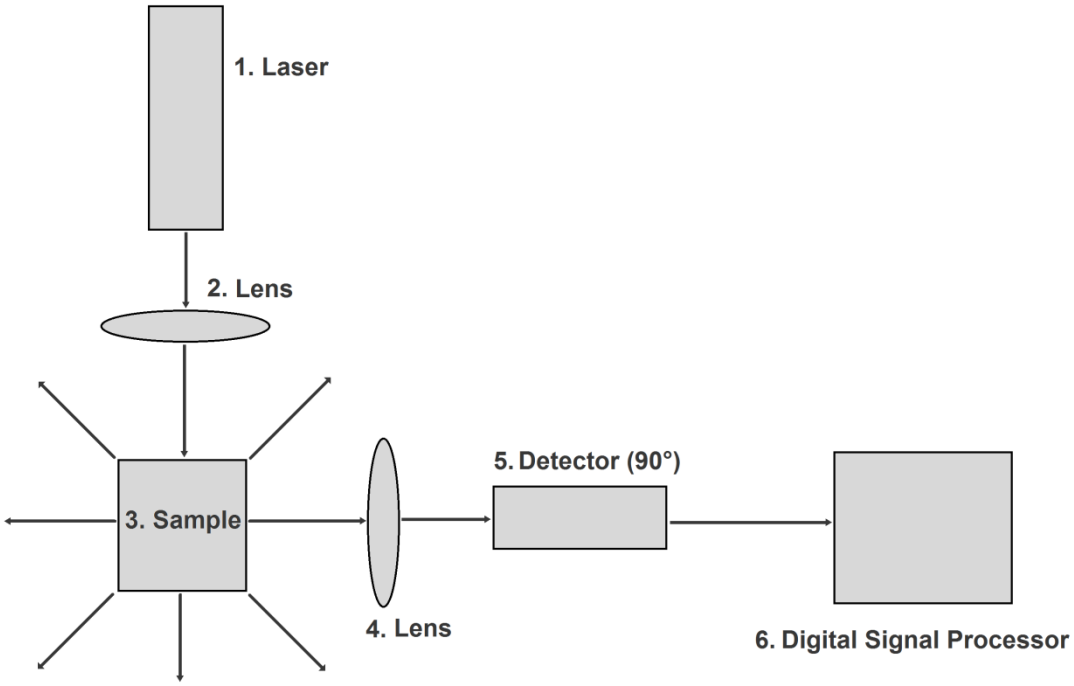

Figure 2-13: Dynamic light scattering measurement set-up

The dynamic light scattering set-up consists of at least six components (cf. Figure 2-13) [58]. A laser emits monochromatic light (1). The light is focused by a lens (2) and afterwards

illuminates the sample (3). Most of the light passes through the sample, but a part is scattered at all angles by the particles. The scattered light is again focused (4) and after this detected under one or several angles, in Figure 2-13 an angle of 90° is shown (5). The detected scattering intensity is passed to a digital signal processor (6).

Particles scatter light in all directions, if their diameter is small compared to the wavelength of the employed light (Rayleigh scattering). The particles in solution undergo Brownian motion, which is the random motion of particles in a medium, e.g. a liquid, resulting from their collision with the solvent molecules. In a small volume of the sample, the particle concentration fluctuates randomly. The rate of these fluctuations, i.e. the speed of which particles enter and leave the scattering volume, depend on the diffusion coefficient. The concentration fluctuations cause fluctuations in the scattering pattern due to constructive and destructive interferences. The time dependent intensity fluctuation I(t) is converted into the intensity correlation function g_2 (see Equation 2-4).

$$g_2(\tau) = \frac{\langle I(t)I(t+\tau)\rangle}{\langle I(t)^2\rangle} \qquad \textit{Equation 2-4}$$

with g_2: intensity correlation function; τ : delay time; I: intensity

The Siegert equation describes the relation between the measured intensity correlation function g_2 and the theoretical electric field correlation g_1 (see Equation 2-5).

$$g_2(\tau) = B\left[1 + \beta\,|g_1(\tau)|^2\right] \qquad \textit{Equation 2-5}$$

with g_2: intensity correlation function; τ: delay time; B: baseline; β: instrumental constant; g_1: electric field correlation

For a monodisperse sample the decay of electric field correlation g_1 as a function of time is exponential (see Equation 2-6). The decay constant (cf. Equation 2-7) depends on the diffusion coefficient and the scattering wave vector (defined in Equation 2-8).

$$g_1(\tau) = \exp^{-\Gamma\tau} \qquad \textit{Equation 2-6}$$

$$\Gamma = -D\,q^2 \qquad \textit{Equation 2-7}$$

$$q = \frac{4\,\pi\,n}{\lambda}\sin\left(\frac{\Theta}{2}\right) \qquad \textit{Equation 2-8}$$

with g_1: electric field correlation; τ : delay time; Γ: decay constant; D: diffusion coefficient; q: scattering wave vector; n: refractive index; λ: wavelength; Θ: angle between detector and incident beam

These mathematical descriptions allow determining the hydrodynamic radius from the measured intensity correlation function by employing the Stokes-Einstein-equation (cf. Equation 2-9). Note that the diameter measured by dynamic light scattering is the hydrodynamic radius r_H, which consists of the actual radius of the particle plus an additional surfactant layer adsorbed onto the surface.

$$D = \frac{k_b\,T}{6\,\pi\,\eta\,r_H} \qquad \textit{Equation 2-9}$$

with D: diffusion coefficient; k_b: Boltzmann constant; T: temperature; η: dynamic viscosity; r_H: hydrodynamic radius

If the sample is polydisperse, the autocorrelation function is the sum of the exponential decays of each species (cf. Equation 2-10).

$$g_1(\tau) = \int G(\Gamma)\exp^{-\Gamma\,\tau}\,d\Gamma \qquad \textit{Equation 2-10}$$

with g_1: electric field correlation; τ: delay time; G: distribution of decay rates; Γ: decay constant

To extract information about the size distribution from G(Γ) various mathematic methods can be used, most commonly the cumulant method or the contin algorithm [59]. Note that these methods are only valid for small τ-values and narrow G(Γ)-function.

2.5.2. Laser-Doppler-velocimetry

The electrophoresis describes the movement of charged particles in solution under the influence of an applied electric field [60,61]. The electrophoretic mobility characterizes this movement and is defined as the particle drift velocity divided by the applied electric field strength (see Equation 2-11). A negative electrophoretic mobility indicates a negative surface charge, whereas a positive electrophoretic mobility stands for a positive surface charge. The higher the magnitude of the electrophoretic mobility is, the higher is the surface charge.

$$\mu_e = \frac{v}{\mathrm{E}} \qquad \textit{Equation 2-11}$$

with μ_e: electrophoretic mobility; v: particle drift velocity; E: electric field strength

The electrophoretic mobility can be measured by Laser-Doppler-velocimetry [62]. Figure 2-14 shows the measurement setup. The laser (1) emits a beam, which is split into two parts by the beam splitter (2). The mirror (3) reflects the second beam and both beams are focused by the lens (4). The beam intersection lies inside of the sample (5), which contains a solution of charged particles. At the intersection the crossing beams form an interference pattern with a fringe spacing Λ (cf. Figure 2-15). An electric field is applied through the sample. The electric field forces charged particles to move and causes a particle flow through the sample. While the particles move through the interference pattern, they scatter the light in the regions of constructive interference and produce a scattering signal. The scattering signal is focused by the second lens (6) afterwards detected by the detector (7).

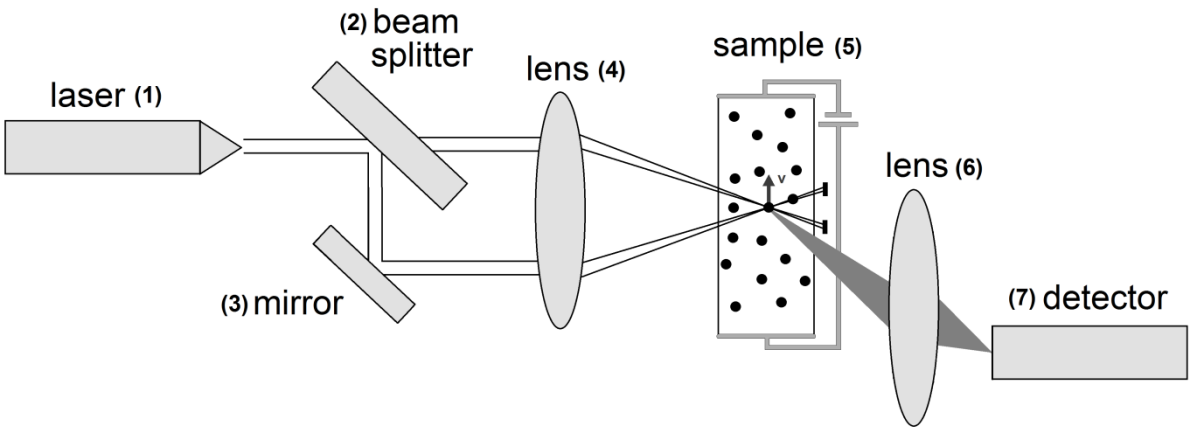

Figure 2-14: Electrophoretic mobility measurement set-up

The frequency of the scattering signal is shifted due to the Doppler effect [62]. The Doppler effect describes the change in the frequency, if the emitter or the receiver of a signal moves while the transmission of the signal, which means that the distance between emitter and receiver changes. The Doppler frequency shift f_D is the superposition of the Doppler frequency shifts from both beams, f_{D1} and f_{D2} (see Equation 2-12). The particle drift velocity is calculated from the measured Doppler frequency shift, the angle between the measured component and the flow, and the fringe spacing of the interference pattern (cf. Equation 2-13). Afterwards, the electrophoretic mobility is determined from particle drift velocity (see Equation 2-11).

$$f_D = |f_{D2} - f_{D1}| \qquad \textit{Equation 2-12}$$

$$|v| = \frac{f_D \cos(\beta)}{\Lambda} \qquad \textit{Equation 2-13}$$

with f_D: Doppler frequency shift; v: particle drift velocity; β: angle between the measured component and the flow; Λ: fringe spacing

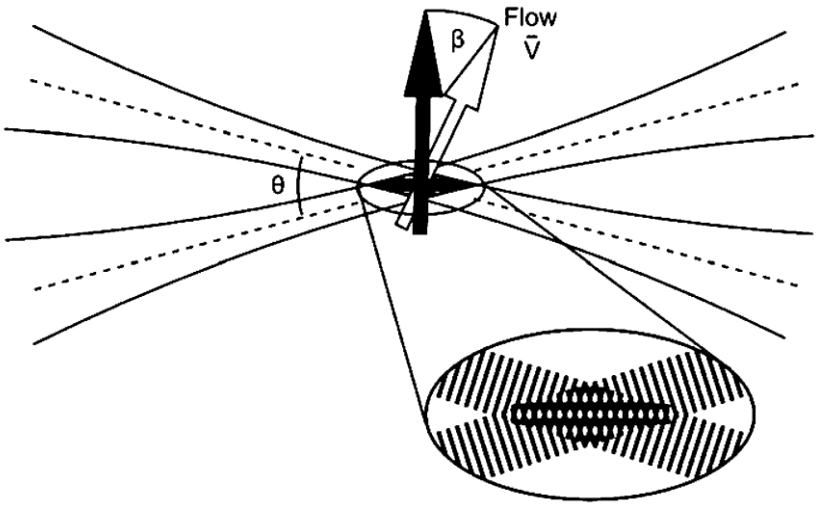

Figure 2-15: Doppler difference arrangement (picture taken from [62])

2.6. Charged polyelectrolytes adsorbed on oppositely charged particles

Upon addition of charged PEL to oppositely charged particles the particles start to agglomerate and are restabilized upon further addition. This behavior is observed for cationic

weak and strong PELs on negatively charged particles, as well as for anionic weak and strong PELs on positively charged particles [63,64,65].

2.6.1. Charge reversal

The charge reversal of a charged nanoparticle surface upon adsorption of oppositely charged PEL can be followed by electrophoretic measurements [66]. Figure 2-16a illustrates the electrophoretic mobility of amidine latex particles upon PSS adsorption (top) and of sulfate latex particles upon LPEI adsorption (bottom). The sulfate latex particles exhibit a highly negative surface charge and so a highly negative electrophoretic mobility. In this case, the electrostatic repulsion forces are stronger than the attractive van der Waal forces and the colloidal particles are stabilized.

By adding positively charged PEL to the solution, the PEL adsorb on the particle surfaces due to electrostatic attraction. The negative charge of the particle surface is reduced by the PEL charge, the electrophoretic mobility decreases. The repulsion between the particles is reduced, the attractive van der Waals forces exceed the repulsive forces and the particles start to agglomerate. The point, where the positive charge of the adsorbed PEL compensates the negative charge of the particle and the electrophoretic mobility is zero, is called isoelectric point (IEP). Further addition of the PEL increases the positive surface charge until the particles are stabilized again by repulsion forces and the electrophoretic mobility reaches a highly positive value. The charge reversal behavior, so-called overcharging happens due to the fact, that the adsorption of a PEL molecule only depends on the charge of the direct surrounding and not on the overall charge of the particle. The adsorption saturation point (ASP) is reached when the PEL cannot overcome the electrostatic barrier anymore and further adsorption becomes impeded. Beyond this point any excess of PEL remains dissolved in the solution. The same behavior of charge reversal and overcharging is found in Figure 2-16a) for positively charged amidine latex particles upon adsorption of the anionic PSS (top).

The stabilization of bare particles, the agglomeration of the weakly PEL covered particles, and the restabilization of the highly PEL covered particles can be explained only based on repulsive electrostatic forces and attractive van der Waals forces described by the DLVO theory.

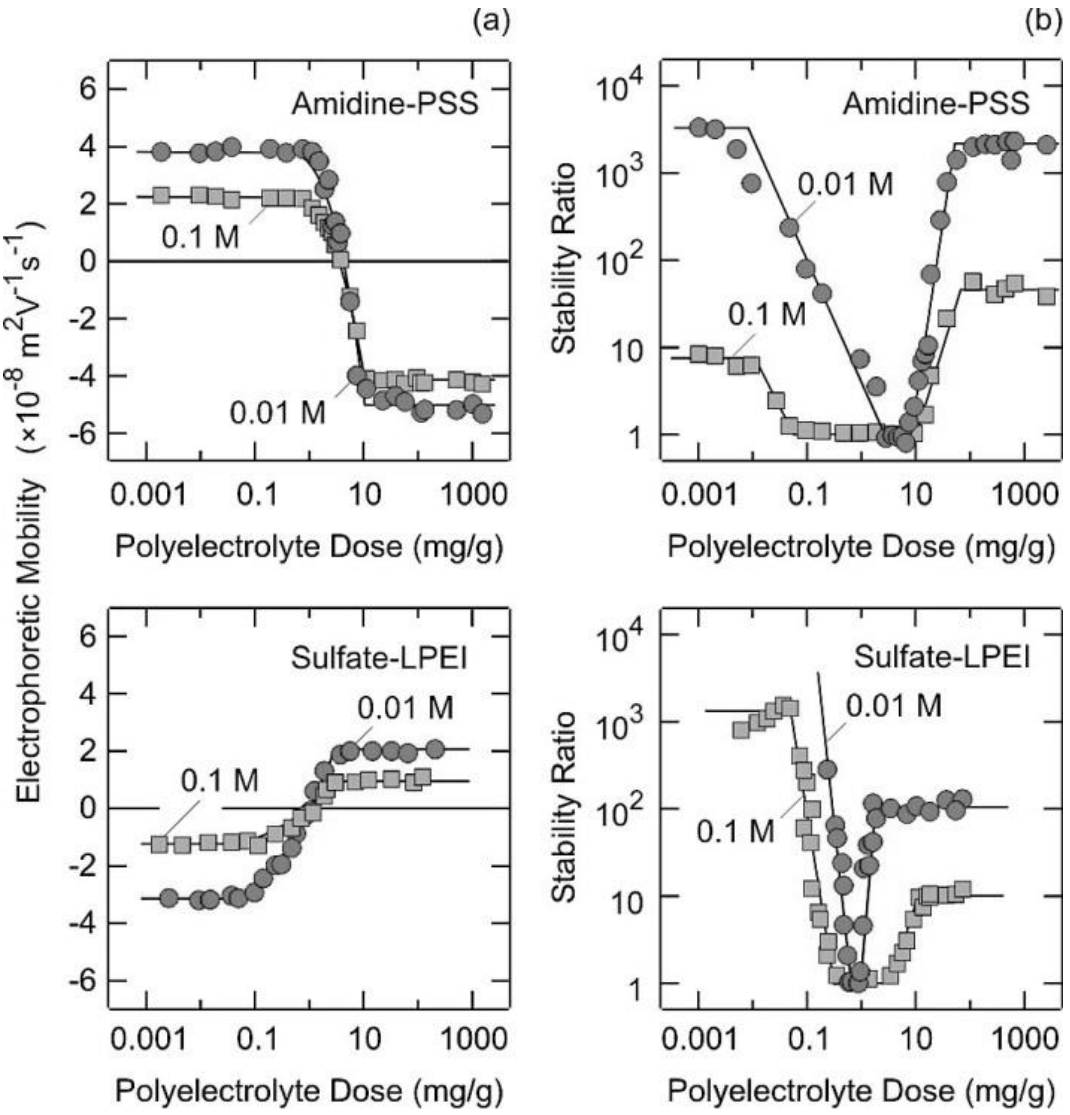

Figure 2-16: Electrophoretic mobility (a) and stability ratio (b) as a function of polyelectrolyte dose for amidine latex particles in the presence of PSS (top), for sulfate latex particles in the presence of LPEI (bottom) (Graphic taken from [64])

2.6.2. Particle Aggregation

The aggregation process of charged nanoparticles upon PEL adsorption can be followed by time-resolving light scattering, turbidity, single particle counting, or rheology [26,67,68,69]. Figure 2-16b) illustrates the stability ratio obtained by time-resolving light scattering of amidine latex particles upon PSS adsorption (top) and of sulfate latex particles upon LPEI adsorption (bottom). A stability ratio of unity indicates a fast aggregation and a high stability ratio shows a slow aggregation. In both shown examples of amidine latex particles in the presence of PSS and of sulfate latex particles in the presence of LPEI, the stability of the bare particles and the fully PEL covered particles is high and the aggregation rate very slow.

However, the stability of the partially PEL covered particles close to the IEP is slow and the aggregation rate very high.

2.6.3. Influence of ionic strength

As reported in Chapter 2.4.2., the DLVO theory predicts a decrease of the repulsive interaction between the charged particles with an increasing salt concentration [48]. A slow aggregation regime for low salt concentrations and a fast aggregation regime for high salt concentrations are expected.

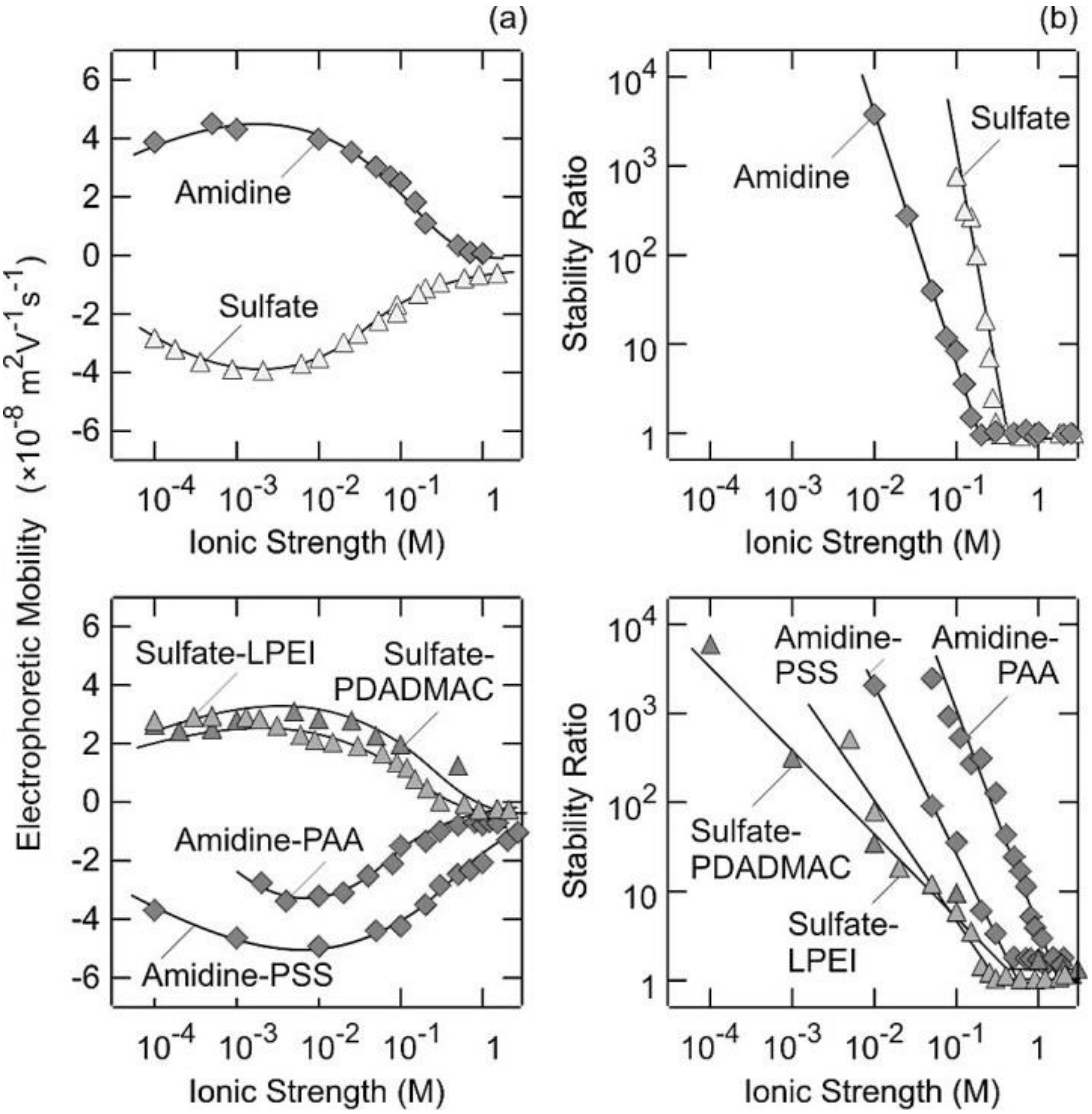

Figure 2-17: Electrophoretic mobility (a) and stability ratio (b) as a function of ionic strength of KCl for bare amidine latex particles and sulfate latex particles (top), for amidine latex particles in the presence of PSS and PAA, as well as for sulfate latex particles in the presence of LPEI and PDADMAC (bottom) (Graphic taken from [64])

Figure 2-17 shows the electrophoretic mobility (a) and stability ratio (b) as a function of ionic strength of KCl for bare amidine latex particles and bare sulfate latex particles (top). The magnitude of the electrophoretic mobility of the positively and negatively charged particles decreases upon salt addition and converge zero for high ionic strengths above 1M. The stability ratio of the positively and negatively charged particles decreases with an increasing ionic strength with a constant slope and reaches a constant value of unity for higher ionic strengths.

Figure 2-17 shows the electrophoretic mobility (a) and stability ratio (b) as a function of ionic strength of KCl for amidine latex particles in the presence of PSS and PAA, as well as for sulfate latex particles in the presence of LPEI and PDADMAC (bottom). Bare and fully PEL covered particles show the same behavior against salt addition [64], the magnitude of the electrophoretic mobility and the stability decrease. It can be concluded, that in both cases the stabilization is mainly due to electrostatic nature.

The transition between the destabilizating screening behavior of monovalent salt and the restabilization behavior of polyelectrolytes was tested with oligoamines [70]. The transition occurs for triethylenetetramine. However a second destabilization for high amounts of oligomers was found, that is absent for highmolecular PELs.

2.6.4. Charging ratio

The adsorption of PEL on oppositely charged surfaces is mostly “superstoichiometric” [71]. Superstoichiometric adsorption means the charge ratio (CR) to exceed one, implying that more than one charge per polymer is needed to compensate one charge of the surface. Reasons are that for a thicker adsorption layer not all charges of the PEL might contribute to the charge compensation and that adsorption is accompanied by counterion adsorption [23], which means that the effective charge of the PEL can be much lower than the nominal one. It was proven for dendritic PAMAM G10 on a silica wafer [72], that the effective charge was just 1% of the nominal charge. An increasing ionic strength leads to a higher screening of charges, which means a higher counterion adsorption and a lower effective charge.

2.6.5. Film morphology

The adsorbed mass and the film morphology are governed by the interaction between the PEL and the surface, the PEL and the solvent, as well as between different PEL molecules.

The adsorbed layer can be investigated by means of DLS, optical reflectivity, microbalances, and AFM [73,74,75]. The mass of adsorbed films of PELs on oppositely charged surfaces is typically below 2mg/m² [73]. The layer thickness is found to be below 10nm for different PELs; around 1-2nm at low ionic strengths and around 6-9nm at higher ionic strengths. The transition occurs between 0.01 and 0.05M of a monovalent salt. In the case of weakly charged PELs a homogeneous film is formed and if the PEL is highly charged, the strong repulsive forces lead to a heterogeneous film. The adsorbed mass increases with a decreasing PEL charge density, an increasing substrate charge density, or an increasing salt concentration.

2.6.6. Non-DLVO forces

The DLVO theory describes the interaction between charged particles against the addition of oppositely charged PELs quantitatively by the superposition of an electrostatic repulsive force and an attractive van der Waals force. Additional PEL-induced non-DLVO interactions were observed and are mostly attributed to bridging, patch-charge, steric, or depletion forces.

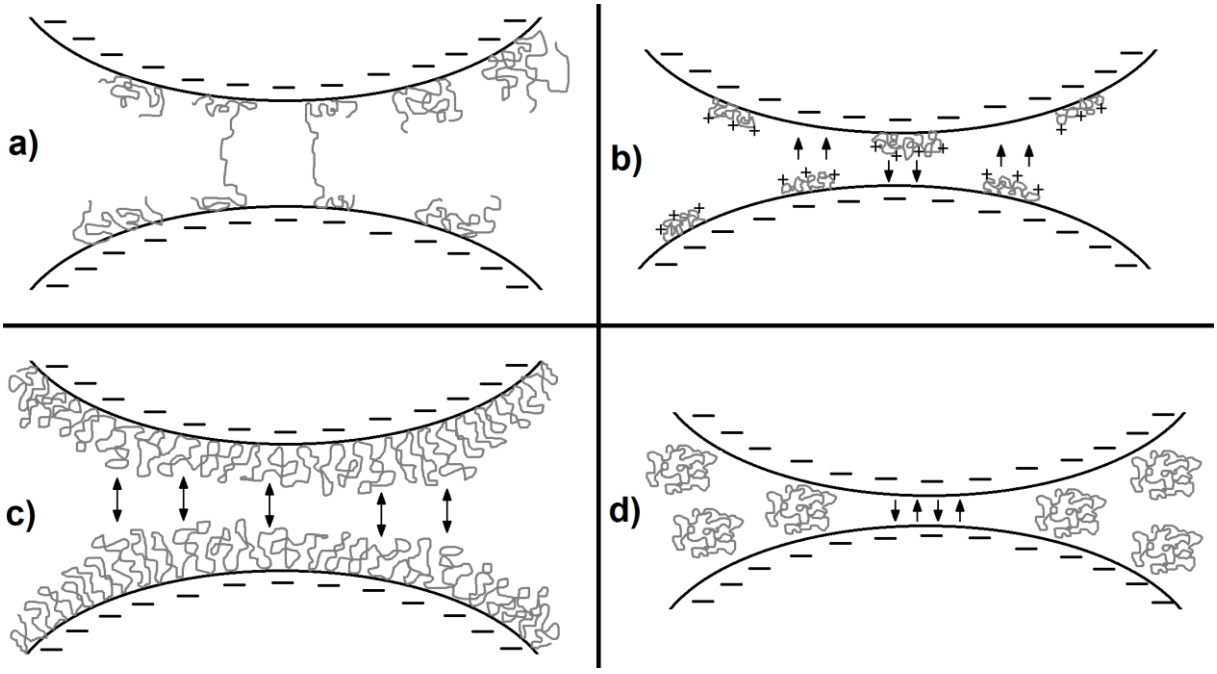

Figure 2-18: Non-DLVO interaction induced by polymers: a) bridging interaction, b) patch-charge interaction, c) steric interaction, d) depletion interaction

2.6.6.1. Bridging forces

Bridging occurs when a polymer molecule adsorbs on two or more particles simultaneously and holds them together physically (illustrated in Figure 2-18a) [76]. Bridging interaction

leads to additional non-electrostatic attractive forces and has been investigated by single molecule force spectroscopy [77]. Bridging occurs for partially polymer covered surfaces, where still enough of the surface is free to form bridges. The bridging model by La Mer [78] determines half covered surfaces as optimum conditions. Polymer bridging is most likely to be found for linear uncharged polymers and weakly charged PELs with a sufficient high length to overcome the separation distance between two particles [79]. These forces are not found with highly branched and dendritic structures or for highly charged PELs [75], because after adsorption on one surface their spatial extent in the solution is not large enough to form bridges.

2.6.6.2. Patch-Charge forces

Highly charged adsorbed PELs form compact, thin domains, called patches on the surface of oppositely charged particles (illustrated in Figure 2-18b) [75]. Charged PELs patches and oppositely charged patches of the uncovered particle surface result in a heterogeneous surface layer. Patches of opposite charge can induce attractive electrostatic forces between two particles, that can be detected by surface force technique [80] and AFM measurements [75]. Patch-charge-forces are likely to occur for partially PEL covered surfaces around the IEP and above, but vanish for fully PEL covered particles [81]. These forces increase with an increasing PEL charge density and molecular weight due to the increasing patch size [41]. The patch-charge-interaction cause an accelerated agglomeration, that become apparent by the widening of the stability plots in the fast aggregation regime and by the weaker dependence on the salt concentration in the slow aggregation regime [64,82].

2.6.6.3. Steric forces

When adsorbed polymers form dense layers with an extent larger than the double layer, and cannot interpenetrate each other, they can cause additional repulsive, non-electrostatic, steric forces (illustrated in Figure 2-18c) [83]. These forces are likely to be found for uncharged polymers and weakly charged PELs with a sufficient high molecular weight. Block-copolymers are known to enhance the stability of charged particles by steric stabilization [84], if they provide one block that is soluble in the media and one block that is insoluble in the media, but interact with the particle surface as an anchor block. If a polyelectrolyte is adsorbed to a charged particle surface, it can lead to an electrostatic, as well as to a steric stabilization, which is then called electrosteric stabilization [85].

2.6.6.4. Depletion forces

Depletion forces occur for charged particles in the presence of very high polymer concentrations, when there is free non-adsorbed polymer in the solution (illustrated in Figure 2-18d) [86]. If the gap between two particles is below the hydrodynamic radius of a free macromolecule, no polymer remains between the particles and a reservoir of free solvent is formed. This reservoir of free solvent is energetically unfavorable for a good solvent and an osmotic pressure difference between the gap and its surrounding solution arises, which leads to additional attractive forces between the particles and may result in aggregation. This process is called depletion flocculation [87]. If the free polymer concentration increases further, the solution becomes that concentrated that no reservoir of free solvent can be formed anymore, the particles are stabilized by the high free polymer concentration. This phenomenon is called “depletion stabilization” [88]. Depletion forces can be measured by AFM techniques [89] or by a hydrodynamic force balance [90]. These forces are found for bare particles, but are even more common for polymer covered, steric stabilized particles, where however theoretical predictions are more difficult [91]. They are well documented for systems involving neutral, non-adsorbing free polymers, but no systematic study has been performed yet concerning depletion forces arisen by high polyelectrolyte concentrations in oppositely charged particle dispersions [65]. The concentration, where depletion flocculation occurs, decreases with an increasing molecular mass of the polymer [92] and with an increasing salt concentration [93]. An increasing stability against depletion was found with an increasing molecular mass of an adsorbed steric layer [91].

2.7. Adsorption of poly(ethylenimine) on silica surfaces

The adsorption and charge reversal behavior of poly(ethylenimine) onto planar silica wafers and silica nanoparticles are confirmed widely in literature [26,41,42,69,80,94].

2.7.1. Influence of pH and ionic strength

PEI and silica develop charge contrariwise with a varying pH. PEI is highly positively charged at low pH values and its point of zero charge occurs at pH 10.8 [21,22]. Silica is highly negatively charged at high pH values and its point of zero charge occurs between 2 and 4 [41]. Due to the opposite pH-depended charge development of adsorbate and adsorbent the adsorption is highly influenced by the pH.

No adsorption between BPEI and silica nanoparticles was observed between pH 2 and 3.5 [26,41]. It is explained by the low surface charge of silica and the high charge density of PEI at this pH. This leads to a weak attraction between surface and polymer, as well as a strong repulsion between the polymer molecules. Above pH 3.5 the surface charge increases, reaches a maximum between pH 4 and 6, decreases, and reaches highly negative values at a pH around 12 [41]. Due to the hyperbranched structure of PEI and the high affinity between polymer and surface, the extent of charge reversal is very large compared to other cationic PELs [42]. The adsorbed amount increases with an increasing pH above 3 [26]. With an increasing pH, the surface charge of silica increases and the charge density of PEI decreases, which leads to an enhanced adsorption, whereat the overall positive charge of the system first increases and afterwards decreases. Flocculation occurs above pH 11. With an increasing amount of adsorbed PEI the IEP shifts to a higher pH value [41].

Desorption experiments were conducted for BPEI on silica wafers [94]. After an adsorption step at pH 9.7, the solvent was changed to fresh polymer free solutions with pH values of 9.7, 5.8, and 3.3, respectively. No desorption was observed for the solutions with a pH of 9.7 and 5.8, but for solution with a pH of 3.3 a fast desorption was observed. Adsorption of PEI on silica is irreversible at high and moderate pH values, however become highly reversible at very acidic conditions.

With an increasing ionic strength under a pH of 11, where PEI is positively charged, the salt screens the repulsion between polymer molecules and decreases the solution size of the polymer, which increases the adsorbed amount [26,42].

2.7.2. Film morphology

The adsorption behavior of BPEI on silica nanoparticles can be described by Langmuir equation and interpreted as monolayer formation [26]. Single hyperbranched PEI molecules were detected by AFM measurements on negatively charged mica surfaces [75]. The AFM images show heterogeneous monolayers of blob-like, separated, adsorbed molecules. The lateral dimension of the adsorbed molecule corresponds to the hydrodynamic radius measured by DLS. The molecule does not unfold upon adsorption. The degree of compression depends on the interaction between the molecule and the substrate. Typical values for the layer thickness are between 1 and 10nm. The charge density is adjusted through the PEI layer, so a higher amount of positive charge is located towards the nanoparticle surface [95].

The adsorbed amount and the layer thickness increase with a decreasing surface charge and with an increasing pH [42,96]. At higher pH values, where the PEI molecule is not charged, the surfaces gets more homogeneous and there is a tendency of the molecules to agglomerate on the silica surface similar to the behavior of uncharged polymers.

2.7.3. Non-DLVO forces

The mechanism of amine adsorption on silica surfaces was investigated for ethylene diamine with sum frequency generation spectroscopy (SFG) [97]. Ethylene diamine molecules are adsorbed to silica through protonation of one amino group and a $(H_2N(CH_2)_2NH_3)^+(O\text{-}SI)^-$ complex is formed. It was further proved that the degree of dissociation of silanol groups increases upon adsorption of cationic PEL [98].

Surface force measurements, as well as shear thickening measurements prove the occurrence of additional attractive non-DLVO forces between PEI covered silica wafers [80,81]. The forces increases with an increasing PEI concentration, reach a maximum and vanish at high polymer concentrations. Because of the thin layer thickness and the confirmed patch formation, the additional attractive non-DLVO forces are likely to arise from patch-charge interaction and not from bridging interaction [75]. The patch-charge forces increase with an increasing molecular weight, due to the increasing patch size [41].

At high pH values, the PEI layers get more homogeneous and the layer thickness increases, which leads to an additional contribution of steric forces [99].

2.8. Polymer-silica-nanocomposites

A polymer-nanocomposite is composed of a polymer matrix and an inorganic filler, which has at least one dimension in the nanometer size range [100]. Polymer-nanocomposites combine the properties of organic polymers, e.g. flexibility and processability, with the properties of inorganic materials, e.g. rigidity and thermal stability, and furthermore exhibit new special properties due to the increased interfacial area [101]. The first mass-produced polymer-nanocomposites were nanoparticle-toughened automobile tires [102] and clay-reinforced resin called bakelite [103] in the early 1900's. However, the research interest in polymer-nanocomposites started in 1990's after Toyota researchers found that the yield strength and tensile strength of nylon can be enhanced about five times by means of addition of mica [104,105].

Among the various polymer-nanocomposites, polymer-silica-nanocomposites are the most reported ones in literature [101]. They are used in diverse applications e.g. in coatings [106], flame retardant materials [107], or optical devices [108].

The most delicate task is to control the interfacial interaction between the nanoparticles and the polymer matrix, as well as its influence on the properties of the material [109]. The most employed method to enhance the compatibility between silica nanoparticles and polymers is the chemical or physical modification of the silica surface [101]. Physical modification is achieved by the adsorption of polar groups on the silica surface by electrostatic interactions. The most common used surfactants for silica surfaces are stearic acid [110], oleic acid [111], and cetyltrimethylammoniumbromid [112]. A disadvantage of physical modification with ionic surfactants is that the adsorption is reversible and because of this fragile against the variation of environmental conditions.

The idea of using a polymeric base, which contains quaternary ammonium groups, as well as diverse other functional groups with specific reactivity or compatibly, for surface coatings was described in a patent in 2006 [113]. A strong adherence should originate from a cooperative ionic interaction between the cationic ammonium groups of the polymer and the negative charge of the surface. Further modification by polymerization or coupling reactions allow the tuning of the chemical und physical properties of original surface. Successful applications of these so-called “quat-primer-polymers” were reported in literature. Hyperbranched poly(ethylenimine) bearing quaternary ammonium groups, was used as a dispersing agent for luminescent lanthanide phosphate nanoparticles [114]. Functionalized with quaternary carbonates and carbonate couplers, the BPEI enhances the interfacial shear strength between carbon fiber and an epoxy resin matrix [115]. Hyperbranched PEI modified with quaternary ammonium groups and PMMA chains was used as a dispersant to prepare carbon nanotubes-PMMA-composites [116].

[1] Dautzenberg, H.; Jaeger, W.; Kötz, J.; Philipp, B.; Seidel, C.; Stscherbina, D.; Polyelectrolytes, Chapter 1, pp. 1-9; Hanser, Munich, 1994

[2] Farinato, R.S.; Polyelectrolytes and Polyzwitterions, Chapter 9, pp. 153-168; ACS Symposium Series Vol. 937; American Chemical Society, 2006

[3] Schmitz, K. S.; Macro-ion Characterization, Chapter 1, pp. 1-22; ACS Symposium Series Vol. 548; American Chemical Society, 1993

[4] Bolto, B.; Gregory, J.; Water Research 2007, 41, 2301-2324

[5] Horn, D.; Linhart, F.; Paper Chemistry, Chapter 5, pp. 64-82; Chapman & Hall, London 1996

[6] Pincus, P.; Macromolecules 1991, 24, 2912-2919

[7] Ray, M.; Gupta, R.; Rousseau, D.; Nanotechnology and Functional Foods: Effective Delivery of Bioactive Ingredients, Chapter 11, pp. 175-190; Wiley-Blackwell, 2015

[8] Lochhead, R.Y.; Cosmetic Nanotechnology, Chapter 1, pp. 3-56; ACS Symposium Series Vol. 961; American Chemical Society, 2007

[9] Decher, G.; Science 1997, 277, 1232-1237

[10] Chluba, J.; Voegel, J.-C.; Decher, G.; Erbacher, P.; Schaaf, P.; Ogier, J.; Biomacromolecules 2001, 2, 800-805

[11] Zhu, Y.; Shi, J.; Shen, W.; Dong, X.; Feng, J.; Ruan, M.; Li, Y.; Angewandte Chemie 2005, 44, 5083-5087

[12] Fréchet, J.M.J.; Hawker, C.J.; Gitsov, I.; Leon, J.W.; Journal of Macromolecular Science, Part A 1996, 10, 1399-1425

[13] Yan, D.; Gao, C.; Frey, H.; Hyperbranched Polymers – Synthesis, Properties, and Applications, Chapter 1, pp. 1-22; John Wiley & Sons, Inc.; Hoboken, New Jersey 2011

[14] Kobayashi, S.; Progress in Polymer Science 1990, 15, 751-823

[15] Kobayashi, S.; Hiroishi, K.; Tokunoh, M.; Saegusa, T; Macromolecules 1987, 20, 1496-1500

[16] Lukovkin, G.M.; Pshezhetsky, V.S.; Murtazaeva, G.A.; European Polymer Journal 1973, 9, 559-565

[17] Antonietti, L.; Aymonier, C.; Schlotterbeck, U.; Garamus, V. M.; Maksimova, T.; Richtering, W.; Mecking, S.; Macromolecules 2005, 38, 5914-5920

[18] Krassusky, K.; Journal für Praktische Chemie 1907, 75, 238-247

[19] Hansson, J.; Svensk Kemisk Tidskrift 1948, 60, 183

[20] Rocher, N.M.; Frech, R.; Macromolecules 2005, 38, 10561‑10565

[21] Hostetler, R.E.; Swanson, J.W.; Journal of Polymer Sciene: Polymer Chemistry Edition 1974, 12, 29-43

[22] Koper, G.J.M.; Borkovec, M.; Polymer 2010, 51, 5649-5662

[23] Manning, G.S.; Journal of Chemical Physics 1969, 51, 924-933

[24] Choudhury, C. K.; Roy, S.; Soft Matter 2013, 9, 2269-2281

[25] Griffiths, P.C.; Paul, A.; Stilbs, P.; Petterson, E.; Macromolecules 2005, 38, 3539-3542

[26] Lindquist, G.M.; Stratton, R.A.; Journal of Colloid and Interface Science 1976, 55, 45-9

[27] Steuerle, U.; Feuerhake, R.; Aziridines; Ullmann's Encyclodedia of Industrial Chemistry; Wiley-VCH Verlag GmbH & Co, KGaA, Weinheim 2012

[28] Rivas, B.L.; Geckeler, K.E.; Advances in Polymer Science 1992, 102, 171-188

[29] Lin, J.; Qiu, S.; Lewis, K; Klibanov, A.M.; Biotechnology and Bioengineering 2003, 83, 168-172

[30] Mateo, C.; Abian, O.; Fernandez-Lafuente, R.; Guisan, J.M.; Biotechnology and Bioengineering, 2000, 68, 98-105

[31] Boussif, O.; Lezoulach F.; Zanta, M.A.; Mergny, M.D.; Scherman, D.; Demeneix, B.; Behr, J.P.; Proceedings of the National Academy of Sciences of the United States of America, 1995, 92, 7291-7301

[32] Ma, X.; Wang, X.; Song, C.; Journal of the American Chemical Society 2009, 131, 5777-5783

[33] Lvov, Y.; Katsuhiko, A.; Ichinose, I.; Kunitake, T.; Journal of the American Chemical Society 1995, 117, 6117-6123

[34] Iler, R.K.; The Chemistry of Silica, Chapter 1, pp. 1-115, John Wiley & Sons, 1979

[35] Yamauchi, H.; Ishikawa, T.; Kondo, Colloids and Surfaces 1989, 37, 71-80

[36] Kammler, H. K.; Mädler, L.; Pratsinis, S.E.; Chemical Engineering & Technology 2001, 24, 583–596

[37] Stöber, W.; Fink, A.; Journal of Colloid and Interface Science 1968, 26, 62-69

[38] Giesche, H.; Journal of the European Ceramic Society 1994, 14, 189-204

[39] Giesche, H.; Journal of the European Ceramic Society 1994, 14, 205-214

[40] Zhuravlev, L.T.; Colloids and Surfaces, Part A 2000, 173, 1-38

[41] Ong, B.C.; Leong, Y.K.; Chen S.B.; Journal of Colloid and Interface Science 2009, 337, 24-31

[42] Mészáros, R.; Thompson, L.; Bos, M; de Groot, P; Langmuir 2002, 18, 6164-6169

[43] Slowing, I.I.; Vivero-Escoto, J.L.; Wu, C.-W.; Lin, V.S.-Y.; Advanced Drug Delivery Reviews 2008, 60, 1278.1288

[44] Cheng, K.-Y.; Anthony, R.; Kortshagen, U.R.; Holmes, R.J.; Nano Letters 2011, 11, 1952-1956

[45] Conibeer, G.; Green, M.; Cho, E.-C.; König, D.; Cho, Y.-H.; Fangsuwannarak, T.; Scardera, G.; Pink, E.; Huang, Y.; Puzzer, T.; Huang, S.; Song, D.; Flynn, C.; Park, S.; Hao, X.; Mansfield, D.; Thin Solid Films 2008, 516, 6748-6756

[46] Kang, Z.; Tsang, C.H.A.; Wong, N.-B.; Zhang, Z.; Lee, S.-T.; Journal of the American Chemical Socierty 2007, 129, 12090-12091

[47] Chaaudhry, Q.; Groves, K.; Nanotechnologies in Food, Chapter 5, pp. 69-85; RSC Nanoscience & Nanotechnology No. 14; Royal Society of Chemistry, 2010

[48] Russel, W.B., Saville, D.A.; Schowalter, W. R. Colloidal Dispersions, Cambridge University Press, 1989

[49] Helmholtz, H.; Annalen der Physik 1853, 211-233

[50] Gouy, G.; Journal de Physique et le Radium 1910, 9, 457-468

[51] Chapman, D.L.; Philosophical Magazine 1913, 25, 475-481

[52] Stern, O.; Zeitschrift für Elektrochemie 1924, 30, 508-516

[53] Derjaguin, B.; Landau, L.; Acta Physico Chimica URSS 1941, 14, 633-662

[54] Verwey, E. J. W.; Overbeek, J. Th. G.; Theory of the stability of lyophobic colloids; Elsevier, Amsterdam, 1848

[55] Schulze, H.; Journal für Praktische Chemie 1882, 25, 431-452

[56] Hardy, W.B.; Zeitschrift für Physikalische Chemie 1900, 33, 385

[57] Berne, B.J.; Pecora, R.; Dynamic Light Scattering; Courier Dover Publications, New York, 2000

[58] Dynamic Light Scattering: An Introduction in 30 Minutes, Technical Note, Malvern Instruments Ltd

[59] Frisken, B.J.; Applied Optics 2001, 40, 4087-4091

[60] Delgado, A.V.; González-Caballero, F.; Hunter, R.J.; Koopal, L.K.; Lyklema, J.; Pure and Applied Chemistry 2005, 77, 1753-1805

[61] Zeta Potential: An Introduction in 30 Minutes, Technical Note, Malvern Instruments Ltd

[62] Charrett, T.O.H.; James, S.W.; Tatam, R.P.; Measurement Science and Technology 2012, 23, 032001-032033

[63] Gregory, J.; Journal of Colloid and Interface Science 1973, 42, 448-456

[64] Hierrezuelo, J.; Sadeghpour, A.; Szilagyi, I.; Vaccaro, A.; Borkovec, M.; Langmuir Letter 2010, 26, 15109-15111

[65] Szilagyi, I.; Trefalt, G.; Tiraferri, A.; Maroni, P.; Borkovec, M.; Soft Matter 2014, 10, 2479-2502

[66] Rehmet, R.; Killmann, E.; Colloid and Surfaces A 1999, 149, 323-328

[67] Holthoff, H.; Egelhaaf, S. U.; Borkovec, M.; Schurtenberger, P.; Sticher, H.; Langmuir 1996,12, 5541-5549

[68] Fernández-Barbero, A.; Schmitt, A.; Cabrerizo-Vílchez, M.; Martínez-García, R.; Physica A 1996, 230, 53-74

[69] Howe, A.M.; Wesley, R.D,; Bertrand, M.; Côte, M.; Leroy, J.; Langmuir 2006, 22, 4518-4525

[70] Szilagyi, I.; Polomska, A.; Citherlet, D.; Sadeghpour, A.; Borkovec, M.; Journal of Colloid and Interface Science 2013, 392, 34-41

[71] Kleimann, J.; Gehin-Delvel, C.; Auweter, H.; Borkovec, M.; Langmuir 2005, 21, 3688-3698

[72] Pericet-Camara, R.; Papastavrou, G.; Borkovec, M.; Macromolecules 2009, 42, 1749-1758

[73] Hierrezuelo, J.; Szilagyi, I.; Vaccaro, A.; Borkovec, M.; Macromolecules 2010, 43, 9108-9116

[74] Porus, M.; Maroni, P.; Borkovec, M.; Langmuir 2012, 28, 5642-5651

[75] Pfau, A.; Schrepp, W.; Horn, D.; Langmuir 1999, 15, 3219-3225

[76] Dickinson, E.; Eriksson, L.; Advances in Colloid and Interface Science 1991, 34, 1-29

[77] Kirwan, L.J.; Maroni, P.; Behrens, S.H.; Papastavrou, G.; Borkovec, M.; Journal of Physical Chemistry 2008, 112, 14609-14619

[78] La Mer, V.K.; Healy T.W.; Reviews of Pure and Applied Chemistry 1963, 13, 112-133

[79] Gregory, J.; Barany, S.; Advances in Colloid and Interface Science 2011, 169, 1-12

[80] Poptoshev, E.; Claesson, P.M.; Langmuir 2002, 18, 2590-2594

[81] Zhang, H.; Yuan, G.; Zhao, C.; Han, C.; Langmuir 2013, 29; 12110-12117

[82] Hierrezuelo, J.; Vaccaro, A.; Borkovec, M.; Journal of Colloid and Interface Science 2010, 347, 202-208

[83] Napper, D.H.; Journal of Colloid and Interface Science 1977, 58, 390-407

[84] Parsonage, E.; Tirrell, M.; Watanabe, H.; Nuzzo, R.G.; Macromolecules 1991, 24, 1987-1995

[85] Fritz, G.; Schädler, V.; Willenbacher, N.; Wagner, N.; Langmuir 2002, 18, 6381-6390

[86] Oosawa, F.; Asakura, A.; Journal of Chemical Physics 1954, 22, 1255

[87] Feigin, R.I.; Napper, D.H.; Journal of Colloid and Interface Science 1980, 74, 567-571

[88] Feigin, R.I.; Napper, D.H.; Journal of Colloid and Interface Science 1980, 75, 525-541

[89] Milling, A.J.; Kendall, K.; Langmuir 2000, 16, 5106-5115

[90] Piech, M.; Weronski, P.; Wu, Y.; Walz, J.Y.; Journal of Colloid and Interface Science 2002, 247, 327-341

[91] Seebergh, J.E.; Berg, J.C.; Langmuir 1994, 10, 454-463

[92] Li In-On, F.K.R.; Vincent, B.; Waite, F.A.; ACS Symposium Series 1975, 9, 165-172

[93] Sperry, P.R.; Hopfenberg, H.B.; Thomas N.L.; Journal of Colloid and Interface Science 1981, 82, 62-76

[94] Mészáros, R.; Varga, I.; Gilányi, T.; Langmuir 2004, 20, 5026-5029

[95] Böhmer, M.R; Evers, O.A; Scheutjens, J.M.H.M; Macromolecules 1990, 23, 2288-2301

[96] Schneider, M.; Brinkmann, M.; Möhwald, H.; Macromolecules 2003, 36, 9510-9518

[97] Xu, M.; Liu, D.; Allen, H.C.; Environmental Science & Technology 2006, 40, 1566-1572

[98] Shubin, V.; Linse, P.; Macromolecules 1997, 30, 5944-5952

[99] Claesson, P.M.; Paulson, O.E.H.; Blomberg, E.; Burns, N.L; Colloids and Surfaces A 1997, 123-124; 341-353

[100] Giannelis, E.P.; Advanced Materials 1996, 8, 29-35

[101] Zou, H.; Wu, S.; Shen, J.; Chemical Reviews 2008, 108, 3893-3957

[102] Goodyear, C.; Dinglers Polytechnisches Journal, 1856, 139, 376-390

[103] Baekeland, L.H.; Scientific American, Supplement 1909, 68, 322-3238

[104] Usuki, A.; Kojima, Y.; Kawasumi, M.; Okada, A.; Fukushima, Y.; Kurauchi, T.; Kamigaito, O.; Journal of Materials Research 1993, 8, 1179-1184

[105] Kojima, Y.; Usuki, A.; Kawasumi, M.; Okada, A.; Fukushima, Y.; Kurauchi, T.; Kamigaito, O.; Journal of Materials Research 1993, 8, 1185-1189

[106] Bauer, F.; Ernst, H.; Decker, U.; Findeisen, M.; Gläsel, H.J.; Langguth, H.; Hartmann, E.; Mehnert, R.; Peuker, C.; Macromolecular Chemistry and Physics 2001, 201, 2654-2659

[107] Liu, J.; Gao, Y.; Wang, F.D.; Wu, M.; Journal of Applied Polymer Science 2000, 75, 384-389

[108] Chang, C.C.; Chen, W.C.; Chemistry of Materials 2002, 14, 4242-4248

[109] Balazs, A.C.; Emrich, T.; Russell, T.P.; Science 2006, 314, 1107-1110

[110] Ahn, S.H.; Kim, S.H.; Lee, S.G.; Journal of Applied Polymer Science 2004, 94, 812-818

[111] Ding, X.; Zhao, J.; Liu, Y.; Zhang, H.; Wang, Z.; Materials Letters 2004, 58, 3126-3130

[112] Wu, T.M.; Chu, M.S.; Journal of Applied Polymer Science 2005, 98, 2058-2063

[113] Möller, M.; Beginn, U.; Keul, H.; Thomas, H.; European Patent Application, 060-07066 (to: DWI, RWTH Aachen e.V.), 03.04.2006 (EP 1710283A1)

[114] Komban, R.; Beckmann, R.; Rode, S.; Ichilmann, S.; Kühnle, A.; Beginn, U.; Haase, M.; Langmuir 2011, 27, 10174-10183

[115] Goel, V.; Beginn, U.; Mourran, A.; Möller, M., Macromolecules 2008, 41, 8187-8197

[116] Beckmann, R.; Beginn, U.; Journal of Polymer Science, Part A 2013, 51, 3700-3715

Chapter 3:

Experimental Part

3. Experimental Part

3.1. Methods

^{1}H-NMR- and ^{13}C-NMR-spectra were measured on a Bruker Avance III spectrometer, operated at 500MHz and 125MHz, respectively. Measurements were performed for samples of 90-110mg polymer solved in 0.5ml D_2O. Chemical Shifts are given in parts per million (ppm). The data analysis was done by means of TopSpin 2.1. software.

Elemental analysis of carbon, hydrogen and nitrogen content was performed by means of an Elementar vario MICRO cube instrument at the Institute of Chemistry of New Materials, University of Osnabrueck.

Fourier transform infrared (FTIR)-spectra were recorded by means of a Perkin Elmer Spectrum Two spectrometer equipped with an attenuated total reflection unit. The samples were placed on the ATR unit and measured in reflection. The measurements were performed for a frequency range from 4000 – 450 cm^{-1}. The data were analyzed by means of Spectrum Software Version 10.3.7.

Differential scanning calorimetry (DSC) was carried out with a Netzsch 204 F1 Phoenix thermal analyzer, equipped with a T-sensor and a Netzsch Intercooler. The instrument was calibrated against cyclohexane, tin and indium standards with a heating rate of 10K/min. Samples of 5 to 15 milligrams were weighed into a 25µL aluminium pan and sealed. The thermograms were recorded between -80°C and +50°C at heating and cooling rates of 10K/min. The data analysis was done by means of Netzsch Proteus software, version 5.0.

Ultraviolet/visible (UV/Vis)-absorption-spectra were performed with a Hewlett-Packard 8453 ultraviolet/visible diode-array spectrophotometer by Agilent. Spectra were recorded from 190 to 1100nm. As reference for dispersions the spectra of distilled water was used. The data were analyzed by means of ChemStation Software Rev. B.01.01.

Dynamic Light Scattering (DLS) measurements were performed with a Zetasizer nano S of Malvern Instruments fitted with a 633nm laser at 25°C. 1.3ml of the dispersion was measured in a PMMA cuvette. Three subsequent measurements have been combined to an average distribution.

Electrophoretic Measurements were carried out with a Zetasizer nano ZS (Model ZEN3600) of Malvern Instruments at 25°C with a 633nm laser. 0.8ml of the dispersion was measured in a DTS1070 cell. An average value was calculated from three subsequent measurements.

Transmission electron microscopy (TEM) images were taken with a JOEL JEM 2100 microscope using a LaB_6 cathode and an acceleration voltage of 200kV.

pH – values of solutions and dispersions were recorded with a compact, digital precision meter Multi 3420 provided by WTM with a SENTIX 940-3 pH – electrode by inserting the electrode into the solution or dispersion.

Ultrasound treatment for 10min using a Branson Sonifier 250 was conducted with dispersions after preparation. An output control level of three and a duty cycle of 50% were employed.

3.2. Materials

Table 3-1: Chemicals

Substance	Supplier	Characterization
Poly(ethylenimine) solution	Aldrich	Average M_n ~1,200 by GPC, average M_w ~1,300 by LS, 50wt% in H_2O
Poly(ethylenimine)	Aldrich	Average M_n ~10,000 by GPC, average M_w ~25,000 by LS
Poly(ethylenimine) solution	Aldrich	Average M_n ~60,000 by GPC, average M_w ~750,000 by LS, 50wt% in H_2O
Glycidyltrimethylammonium-chloride	Aldrich	90wt% in water (calc. based on dry substance)
Ludox TMA colloidal silica	Aldrich	34wt% suspension in water
Water	---	Deionized
Sodium chloride	Stockmeier	Solid, 99wt%

Substance	Supplier	Characterization
Hydrochloric acid	Aldrich	37wt% in water
Sodium hydroxide	Fluka	Pellets, 97wt%

3.3. Synthesis

Poly[ethylenimine-co-(ethylenimine-g-glycidyltrimethylammoniumchloride)] $\mathbf{PEI_{28}^{1Q}}$ (II)[1]: 0.9997g (0.0232mol) Poly(ethylenimine) (PEI) [X_n = 28] and 0.0352g (0.0002mol) glycidyl-trimethylammonium chloride ($quat_R$) were stirred in 25g H_2O for 24 hours at room temperature. The solvent was evaporated under reduced pressure at 60°C and afterwards the substance was dried for 24 hours in vacuum at 60°C. 1.0784g (104.2%) of a highly viscous oil was obtained.

The products (III) – (VII), (IX) – (XII) and (XIV) – (XVII) were synthesized according to the same procedure as mentioned above. Table 3-2 summarizes the employed amounts of poly(ethylenimine) (PEI), glycidyltrimethylammonium chloride ($quat_R$) and water as solvent, the degree of polymerization of the employed polymer, reaction time and yield. Unmodified poly(ethylenimine) with three different degrees of polymerization of 28 (I), 232 (VIII) and, 1393 (XIII) was employed.

Table 3-2: Used partially quaternized poyl(ethylenimine) derivatives

No	Polymer	X_n	m_{PEI} [g] (n_{PEI} [mol])	m_{quatR} [g] (n_{quatR} [mol])	m_{H2O} [g]	t [h]	yield [g(%)]
(I)	PEI_{28}	28	---	---	---	---	---
(II)	PEI_{28}^{1Q}	28	0.9997 (0.0232)	0.0352 (0.0002)	25	24	1.0784 (104.2)
(III)	PEI_{28}^{5Q}	28	1.0001 (0.0232)	0.1759 (0.0012)	25	24	1.2769 (108.6)

[1] The upper index gives the theoretical degree of quaternization q, the lower index gives the degree of polymerization X_n.

No	Polymer	X_n	m_{PEI} [g] (n_{PEI} [mol])	m_{quatR} [g] (n_{quatR} [mol])	m_{H2O} [g]	t [h]	yield [g(%)]
(IV)	PEI_{28}^{10Q}	28	1.0002 (0.0232)	0.3515 (0.0023)	25	24	1.4206 (105.1)
(V)	PEI_{28}^{20Q}	28	2.0001 (0.0464)	1.4074 (0.0093)	15	24	3.6597 (107.4)
(VI)	PEI_{28}^{50Q}	28	2.0000 (0.0464)	3.5181 (0.0232)	15	96	5.7102 (103.5)
(VII)	PEI_{28}^{100Q}	28	1.9999 (0.0464)	7.0358 (0.0464)	15	96	9.2499 (102.4)
(VIII)	PEI_{232}	232	---	---	---	---	---
(IX)	PEI_{232}^{10Q}	232	0.9998 (0.0232)	0.3520 (0.0023)	20	24	1.4221 (105.2)
(X)	PEI_{232}^{20Q}	232	2.0002 (0.0464)	1.4073 (0.0093)	15	96	3.5608 (104.5)
(XI)	PEI_{232}^{50Q}	232	2.0000 (0.0464)	3.5180 (0.0232)	15	96	5.6076 (101.6)
(XII)	PEI_{232}^{100Q}	232	2.0001 (0.0464)	7.0359 (0.0464)	15	96	9.2727 (102.6)
(XIII)	PEI_{1393}	1393	---	---	---	---	---
(XIV)	PEI_{1393}^{10Q}	1393	0.9999 (0.0232)	0.3518 (0.0023)	25	24	1.3787 (102.0)
(XV)	PEI_{1393}^{20Q}	1393	0.9999 (0.0232)	0.7041 (0.0046)	15	24	1.7415 (102.2)
(XVI)	PEI_{1393}^{50Q}	1393	1.9999 (0.0464)	3.5209 (0.0232)	25	96	5.6901 (103.1)
(XVII)	PEI_{1393}^{100Q}	1393	2.0002 (0.0464)	7.0411 (0.0464)	25	96	9.2199 (102.0)

PEI_{28}^{1Q} (II): ^{1}H-NMR (D_2O, δ [ppm]): 2.6 – 2.9 (4A + 4B + 2C), 3.3 – 3.4 (9F), 3.5 (2E), 4.4 (1D). ^{13}C-NMR (D_2O, δ [ppm]): 37.9 (b_1), 40.0 (b_2), 45.7 (b_3), 47.9 (b_4), 50.8 (b_5), 51.3 (b_6), 52.0 + 52.5 (b_x), 53.3 (b_7), 54.4 (F), 56.3 (b_8), 64.9 (D), 69.3 (E). IR (ATR, ν [cm^{-1}]): 3276.6, 2931.2, 2811.0, 1594.5, 1455.3, 1354.9, 1295.2, 1109.6, 1046.9, 907.3, 859.0, 760.6, 609.8. EA (found (calculated) [%]): C: 50.9 (55.7), H: 11.0 (11.7), N: 29.5 (32.3). T_G: -52.4°C

PEI_{28}^{5Q} (III): ^{1}H-NMR (D_2O, δ [ppm]): 2.6 – 2.8 (4A + 4B + 2C), 3.2 – 3.3 (9F), 3.4 – 3.5 (2E), 4.4 (1D). ^{13}C-NMR (D_2O, δ [ppm]): 38.0 (b_1), 40.0 (b_2), 45.7 (b_3), 47.8 (b_4), 50.8 (b_5), 51.2 (b_6), 52.1 (b_x), 53.3 (b_7), 54.3 (F), 56.2 (b_8), 63.7 + 64.2 + 64.9 + 66.5 (D), 68.3 + 69.3 (E). IR (ATR, v [cm^{-1}]): 3268.7, 2933.4, 2813.4, 1593.6, 1455.7, 1357.7, 1297.1, 1106.6, 1047.8, 916.6, 862.3, 759.0, 572.3. EA (found (calculated) [%]): C: 49.9 (55.5), H: 10.3 (11.6), N: 26.8 (31.6). T_G: -39.6°C

PEI_{28}^{10Q} (IV): ^{1}H-NMR (D_2O, δ [ppm]): 2.5 – 2.8 (4A + 4B + 2C + 4G + 2H), 3.2 – 3.3 (9F + 18K), 3.3 (1I), 3.4 – 3.5 (2E + 4J), 3.6 (2L), 4.3 – 4.4 (1D + 1M). ^{13}C-NMR (D_2O, δ [ppm]): 38.0 (b_1), 40.0 (b_2), 45.7 (b_3), 47.8 (b_4), 50.8 (b_5), 51.3 (b_6), 52.5 (b_x), 53.3 (b_7), 54.4 (F + K), 56.2 (b_8), 63.7 + 64.2 + 64.9 + 66.5 (D + M), 68.4 + 69.4 (E + J). IR (ATR, v [cm^{-1}]): 3267.7, 2935.4, 2819.6, 1595.3, 1461.0, 1355.4, 1298.5, 1105.0, 1050.0, 963.6, 917.9, 866.8, 757.5, 566.2. EA (found (calculated) [%]): C: 46.5 (55.1), H: 10.5 (11.5), N: 23.3 (30.7). T_G: -32.0°C

PEI_{28}^{20Q} (V): ^{1}H-NMR (D_2O, δ [ppm]): 2.6 – 2.8 (4A + 4B + 2C + 4G + 2H), 3.2 – 3.3 (9F + 18K), 3.3 (1I), 3.4 – 3.5 (2E + 4J), 3.6 (2L), 4.3 – 4.4 (1D + 1M). ^{13}C-NMR (D_2O, δ [ppm]): 38.0 (b_1), 40.0 (b_2), 45.7 (b_3), 47.8 (b_4), 50.7 (b_5), 51.2 (b_6), 52.1 (b_x), 53.3 (b_7), 54.4 (F + K), 56.1 (b_8), 63.7 + 64.2 + 64.8 + 66.5 (D + M), 68.4 + 69.3 (E + J). IR (ATR, v [cm^{-1}]): 3257.6, 3021.5, 2935.8, 2821.5, 1595.1, 1475.5, 1355.8, 1298.1, 1102.4, 1053.8, 964.8, 917.9, 868.6, 758.2, 547.7. EA (found (calculated) [%]): C: 47.2 (54.5), H: 10.0 (11.3), N: 21.1 (28.9). T_G: -17.3°C

PEI_{28}^{50Q} (VI): ^{1}H-NMR (D_2O, δ [ppm]): 2.7 – 2.9 (4A + 4B + 2C + 4G + 2H), 3.3 – 3.4 (9F + 18K), 3.4 (1I), 3.5 – 3.6 (2E + 4J), 3.7 (2L), 4.4 – 4.5 (1D + 1M). ^{13}C-NMR (D_2O, δ [ppm]): 37.9 (b_1), 39.8 (b_2), 45.8 (b_3), 47.8 (b_4), 51.4 (b_6), 52.6 (b_x), 53.3 (b_7), 54.4 (F + K), 58.5 (C + H), 62.2 (I), 63.8 + 64.2 + 64.9 + 66.5 (D + M), 68.3 + 69.3 (E + J), 73.3 (L). IR (ATR, v [cm^{-1}]): 3736.7, 3235.4, 3012.6, 2935.8, 2819.3, 1574.0, 1477.9, 1358.8, 1294.0, 1214.8, 1098.9, 965.8, 918.5, 870.8, 759.0, 564.1, 455.5. EA (found (calculated) [%]): C: 47.7 (52.6), H: 10.5 (10.8), N: 17.1 (23.5). T_G: -4.1°C

PEI_{28}^{100Q} (VII): ^{1}H-NMR (D_2O, δ [ppm]): 2.6 – 2.9 (4A + 4B + 2C + 4G + 2H), 3.2 – 3.3 (9F + 18K), 3.3 (1I), 3.4 – 3.5 (2E + 4J), 3.6 (2L), 4.3 – 4.4 (1D + 1M). ^{13}C-NMR (D_2O, δ [ppm]): 45.9 (b_3), 51.7 (b_6), 52.6 (b_x), 53.4 (b_7), 54.5 (F + K), 57.9 + 58.2 + 58.6 + 58.9 (C + H), 62.2 (I), 63.8 + 64.3 + 64.9 + 66.6 (D + M), 67.8 + 68.4 + 69.3 (E + J), 73.0 + 73.3 (L). IR (ATR, v [cm^{-1}]): 3239.7, 3013.9, 2945.5, 2825.3, 1643.0, 1478.5, 1344.9, 1292.3, 1214.7, 1096.1,

964.4, 918.7, 872.7, 756.1, 491.3. EA (found (calculated) [%]): C: 46.2 (49.4), H: 9.8 (9.8), N: 13.6 (14.4). T_G: 32.2°C

PEI_{232}^{10Q} (IX): ^{1}H-NMR (D_2O, δ [ppm]): 2.5 – 2.8 (4A + 4B + 2C + 4G + 2H), 3.2 – 3.3 (9F + 18K), 3.3 (1I), 3.3 – 3.4 (2E + 4J), 3.6 (2L), 4.2 – 4.4 (1D + 1M). ^{13}C-NMR (D_2O, δ [ppm]): 38.0 (b_1), 40.0 (b_2), 45.8 (b_3), 47.9 (b_4), 50.8 (b_5), 51.2 (b_6), 52.5 (b_x), 53.3 (b_7), 54.3 (F + K), 56.2 (b_8), 63.7 + 64.1 + 64.8 + 66.5 (D + M), 68.4 + 69.4 (E + J). IR (ATR, v [cm^{-1}]): 3070.0, 2937.8, 2822.7, 2232.3, 1649.1, 1597.5, 1462.7, 1354.0, 1298.2, 1105.3, 1049.2, 963.3, 917.6, 867.9, 755.5, 555.5. EA (found (calculated) [%]): C: 44.6 (55.1), H: 10.5 (11.5), N: 21.5 (30.7). T_G: -32.0°C

PEI_{232}^{20Q} (X): ^{1}H-NMR (D_2O, δ [ppm]): 2.6 – 2.8 (4A + 4B + 2C + 4G + 2H), 3.2 – 3.3 (9F + 18K), 3.3 (1I), 3.4 – 3.5 (2E + 4J), 3.6 (2L), 4.3 – 4.4 (1D + 1M). ^{13}C-NMR (D_2O, δ [ppm]): 38.0 (b_1), 40.0 (b_2), 45.7 (b_3), 47.9 (b_4), 50.7 (b_5), 51.3 (b_6), 52.5 (b_x), 53.3 (b_7), 54.4 (F + K), 56.1 (b_8), 58.4 (C + H), 62.4 (I), 63.8 + 64.2 + 64.9 + 66.6 (D + M), 68.4 + 69.3 (E + J), 73.3 (L). IR (ATR, v [cm^{-1}]): 3265.0, 3027.2, 2938.7, 2826.2, 2155.7, 1645.9, 1581.6, 1475.5, 1354.3, 1299.1, 1217.0, 1102.6, 1054.7, 964.4, 869.1, 527.7. EA (found (calculated) [%]): C: 43.7 (54.5), H: 10.4 (11.3), N: 18.7 (28.9). T_G: -25.8°C

PEI_{232}^{50Q} (XI): ^{1}H-NMR (D_2O, δ [ppm]): 2.6 – 2.9 (44A + 4B + 2C + 4G + 2H), 3.2 – 3.3 (9F + 18K + 1I), 3.4 – 3.5 (2E + 4J), 3.6 (2L), 4.3 – 4.4 (1D + 1M). ^{13}C-NMR (D_2O, δ [ppm]): 45.8 (b_3), 47.9 (b_4), 51.5 (b_6), 52.6 (b_x), 53.2 (b_7), 54.3 (F + K), 58.3 (C + H), 62.3 (I), 63.8 + 64.2 + 64.9 + 66.6 (D + M), 66.6 + 67.9 + 68.4 + 69.3 (E + J), 73.4 (L). IR (ATR, v [cm^{-1}]): 3246.1, 3016.7, 2941.0, 2823.7, 2114.4, 1645.1, 1477.6, 1347.2, 1293.2, 1215.1, 1098.0, 1058.8, 965.0, 918.3, 870.9, 758.1, 509.5. EA (found (calculated) [%]): C: 46.4 (52.6), H: 10.1 (10.8), N: 15.9 (23.5). T_G: -2.5°C

PEI_{232}^{100Q} (XII): ^{1}H-NMR (D_2O, δ [ppm]): 2.6 – 2.9 (4A + 4B + 2C + 4G + 2H), 3.2 – 3.4 (9F + 18K + 1I), 3.4 – 3.6 (2E + 4J), 3.6 (2L), 4.3 – 4.5 (1D + 1M). ^{13}C-NMR (D_2O, δ [ppm]): 46.0 (b_3), 51.4 (b_6), 51.8 (b_x), 52.8 (b_7), 54.5 (F + K), 57.7 + 58.7 (C + H), 62.2 (I), 63.8 + 64.3 + 65.1 + 66.5 (D + M), 67.9 + 68.4 + 69.0 (E + J), 73.4 (L). IR (ATR, v [cm^{-1}]): 3242.6, 3015.9, 2948.0, 2827.1, 2115.1, 1640.1, 1478.1, 1417.3, 1344.6, 1292.0, 1245.1, 1214.4, 1143.0, 1095.9, 1057.1, 963.9, 938.0, 918.6, 872.4, 754.5, 490.7. EA (found (calculated) [%]): C: 45.8 (49.4), H: 9.7 (9.8), N: 13.1 (14.4). T_G: 23.7°C

PEI_{1393}^{10Q} (XIV): ^{1}H-NMR (D_2O, δ [ppm]): 2.5 – 2.8 (4A + 4B + 2C + 4G + 2H), 3.2 – 3.3 (9F + 18K), 3.3 (1I), 3.4 – 3.5 (2E + 4J), 3.6 (2L), 4.3 – 4.4 (1D + 1M). ^{13}C-NMR (D_2O, δ [ppm]): 37.9 (b_1), 40.0 (b_2), 45.9 (b_3), 47.9 (b_4), 50.7 (b_5), 51.2 (b_6), 52.0 (b_x), 53.3 (b_7), 54.4 (F + K), 56.0 (b_8), 63.8 + 64.3 + 64.8 + 66.6 (D + M), 68.0 + 68.4 + 69.2 (E + J). IR (ATR, ν [cm^{-1}]): 3263.0, 2935.8, 2815.1, 2151.4, 1586.5, 1460.9, 1353.3, 1298.0, 1104.2, 1048.4, 964.1, 917.9, 866.2, 759.1, 555.2. EA (found (calculated) [%]): C: 48.2 (55.1), H: 11.0 (11.5), N: 23.5 (30.7). T_G: -26.2°C

PEI_{1393}^{20Q} (XV): ^{1}H-NMR (D_2O, δ [ppm]): 2.6 – 2.8 (4A + 4B + 2C + 4G + 2H), 3.2 – 3.3 (9F + 18K), 3.3 (1I), 3.4 – 3.5 (2E + 4J), 3.6 (2L), 4.3 – 4.4 (1D + 1M). ^{13}C-NMR (D_2O, δ [ppm]): 37.9 (b_1), 39.9 (b_2), 45.8 (b_3), 47.9 (b_4), 50.5 (b_5), 51.3 (b_6), 52.5 (b_x), 53.2 (b_7), 54.4 (F + K), 55.8 (b_8), 58.4 (C + H), 62.3 (I), 63.8 + 64.1 + 64.9 + 66.6 (D + M), 67.9 + 67.9 + 68.5 + 69.4 (E + J), 73.4 (L). IR (ATR, ν [cm^{-1}]): 3261.7, 3022.2, 2938.0, 2821.3, 1643.8, 1584.2, 1475.7, 1355.3, 1297.7, 1102.5, 1054.3, 964.8, 918.05, 869.7, 758.5, 558.4. EA (found (calculated) [%]): C: 48.4 (54.5), H: 10.4 (11.3), N: 20.8 (28.9). T_G: -14.6°C

PEI_{1393}^{50Q} (XVI): ^{1}H-NMR (D_2O, δ [ppm]): 2.6 – 2.9 (4A + 4B + 2C + 4G + 2H), 3.2 – 3.3 (9F + 18K + 1I), 3.4 – 3.5 (2E + 4J), 3.6 (2L), 4.3 – 4.4 (1D + 1M). ^{13}C-NMR (D_2O, δ [ppm]): 45.9 (b_3), 47.9 (b_4), 51.6 (b_6), 52.7 (b_x), 53.1 (b_7), 54.4 (F + K), 58.4 (C + H), 62.3 (I), 63.8 + 64.3 +64.9 + 66.6 (D + M), 67.9 + 68.4 + 69.4 (E + J), 73.3 (L). IR (ATR, ν [cm^{-1}]): 3244.8, 3015.5, 2940.0, 2821.2, 1642.1, 1566.9, 1477.6, 1347.9, 1293.2, 1215.2, 1098.0, 1058.9, 965.1, 938.5, 918.3, 871.2, 758.1, 510.5. EA (found (calculated) [%]): C: 47.3 (52.6), H: 10.4 (10.8), N: 16.4 (23.5). T_G: 9.3°C

PEI_{1393}^{100Q} (XVII): ^{1}H-NMR (D_2O, δ [ppm]): 2.6 – 2.9 (4A + 4B + 2C + 4G + 2H), 3.2 – 3.4 (9F + 18K + 1I), 3.5 – 3.6 (2E + 4J), 3.7 (2L), 4.3 – 4.5 (1D + 1M). ^{13}C-NMR (D_2O, δ [ppm]): 46.0 (b_3), 51.4 (b_6), 51.8 (b_x), 52.7 (b_7), 54.6 (F + K), 57.8 + 58.7 (C + H), 62.3 (I), 63.8 + 64.4 + 65.0 + 66.6 (D + M), 67.9 + 68.4 + 69.3 (E + J), 73.4 (L). IR (ATR, ν [cm^{-1}]): 3243.6, 3015.7, 2947.2, 2826.8, 2111.0, 1642.7, 1478.1, 1417.3, 1344.8, 1291.9, 1245.3, 1214.3, 1143.1, 1096.0, 1057.0, 964.1, 938.4, 918.6, 872.9, 755.4, 495.0. EA (found (calculated) [%]): C: 47.2 (49.4), H: 10.1 (9.8), N: 13.6 (14.4). T_G: 32.9°C

3.4. Solutions of amino-quat-primer polymers

P(XIII)-001: 0.0010g PEI_{1393} was dissolved in 9.9991g water in a 20ml glass vessel. The total mass of the sample was 10.0001g.

The samples P(XIII)-002 – P(XIII)-009, P(XIV)-001 – P(XIV)-009, P(XV)-001 – P(XV)-009, P(XVI)-001 – P(XVI)-009 and P(XVII)-001 – P(XVII)-009 were prepared according to the same procedures as mentioned above. Table 3-3 summarizes the employed mass of polymer and water, as well as the resulting total mass. The notation of the solutions of polymer in water is given by “P” followed by the Roman numeral of the used poly(ethylenimine) derivative and a consecutively number.

Table 3-3: Polymer solutions in water

Polymer	Sample	m_P [g]	m_{H2O} [g]	m_{tot} [g]
PEI_{1393}	P(XIII)-001	0.0010	9.9991	10.0001
	P(XIII)-002	0.0050	9.9943	9.9993
	P(XIII)-003	0.0100	9.9896	9.9995
	P(XIII)-004	0.0499	9.9501	9.9999
	P(XIII)-005	0.0999	9.8998	9.9997
	P(XIII)-006	0.2501	9.7509	10.0010
	P(XIII)-007	0.0010	9.9999	10.0009
	P(XIII)-008	0.0010	9.9999	10.0009
	P(XIII)-009	0.0010	9.9984	9.9994
$\mathrm{PEI}_{1393}^{10Q}$	P(XIV)-001	0.0010	9.9989	9.9999
	P(XIV)-002	0.0050	9.9940	9.9990
	P(XIV)-003	0.0101	9.9904	10.0005
	P(XIV)-004	0.0500	9.9500	10.0000
	P(XIV)-005	0.0996	9.8994	9.9990
	P(XIV)-006	0.2496	9.7503	9.9999
	P(XIV)-007	0.0010	10.0000	10.0010
	P(XIV)-008	0.0010	9.9994	10.0004
	P(XIV)-009	0.0010	10.0003	10.0013
$\mathrm{PEI}_{1393}^{20Q}$	P(XV)-001	0.0010	9.9987	9.9997
	P(XV)-002	0.0050	9.9944	9.9994
	P(XV)-003	0.0098	9.9905	10.0003

Polymer	Sample	m_P [g]	m_{H2O} [g]	m_{tot} [g]
	P(XV)-004	0.0504	9.9501	10.0005
	P(XV)-005	0.1005	9.9003	10.0008
	P(XV)-006	0.2496	9.7506	10.0002
	P(XV)-007	0.0010	9.9984	9.9994
	P(XV)-008	0.0010	9.9990	10.0000
	P(XV)-009	0.0010	9.9987	9.9997
PEI_{1393}^{50Q}	P(XVI)-001	0.0010	9.9992	10.0002
	P(XVI)-002	0.0050	9.9948	9.9998
	P(XVI)-003	0.0100	9.9899	9.9999
	P(XVI)-004	0.0502	9.9506	10.0008
	P(XVI)-005	0.1004	9.9001	10.0005
	P(XVI)-006	0.2503	9.7508	10.0011
	P(XVI)-007	0.0010	9.9982	9.9992
	P(XVI)-008	0.0010	9.9982	9.9992
	P(XVI)-009	0.0010	10.0008	10.0018
PEI_{1393}^{100Q}	P(XVII)-001	0.0010	9.9995	10.0005
	P(XVII)-002	0.0050	9.9950	10.0000
	P(XVII)-003	0.0102	9.9894	9.9996
	P(XVII)-004	0.0497	9.9508	10.0005
	P(XVII)-005	0.1001	9.8997	9.9998
	P(XVII)-006	0.2497	9.7504	10.0001
	P(XVII)-007	0.0010	9.9981	9.9991
	P(XVII)-008	0.0010	10.0002	10.0012
	P(XVII)-009	0.0010	9.9994	10.0004

P(XIII)-010: 0.0004g PEI_{1393} and 0.0003g sodium chloride were dissolved in 2.9995g water in a 5ml glass vessel. The total mass of the sample was 3.0002g.

The samples P(XIII)-011 – P(XIII)-012, P(XIV)-010 – P(XIV)-012, P(XV)-010 – P(XV)-012, P(XVI)-010 – P(XVI)-012 and P(XVII)-010 – P(XVII)-012 were prepared according to the same procedures as mentioned above. Table 3-4 summarizes the employed mass of polymer, sodium chloride and water, as well as the resulting total mass.

Table 3-4: Polymer solutions in water with added sodium chloride

Polymer	Sample	m_P [g]	m_{NaCl} [g]	m_{H2O} [g]	m_{tot} [g]
PEI_{1393}	P(XIII)-010	0.0004	0.0003	2.9995	3.0002
	P(XIII)-011	0.0009	0.0003	3.0003	3.0015
	P(XIII)-012	0.0017	0.0003	2.9986	3.0006
PEI_{1393}^{10Q}	P(XIV)-010	0.0006	0.0003	2.9988	2.9997
	P(XIV)-011	0.0012	0.0003	2.9984	2.9999
	P(XIV)-012	0.0023	0.0003	2.9978	3.0004
PEI_{1393}^{20Q}	P(XV)-010	0.0007	0.0003	2.9993	3.0003
	P(XV)-011	0.0015	0.0003	2.9996	3.0014
	P(XV)-012	0.0029	0.0003	2.9975	3.0007
PEI_{1393}^{50Q}	P(XVI)-010	0.0012	0.0003	2.9976	2.9991
	P(XVI)-011	0.0024	0.0003	2.9969	2.9996
	P(XVI)-012	0.0048	0.0003	2.9957	3.0008
PEI_{1393}^{100Q}	P(XVII)-010	0.0020	0.0003	2.9995	3.0018
	P(XVII)-011	0.0039	0.0003	2.9952	2.9994
	P(XVII)-012	0.0078	0.0003	2.9925	3.0006

P(XIII)-013: 0.0010g PEI_{1393} and 0.0002g sodium chloride were dissolved in 3.9992g deuterium oxide in a 5ml glass vessel. The total mass of the sample was 4.0004g.

The samples P(XIV)-013, P(XV)-013, P(XVI)-013, P(XVII)-013 and P(XVII)-014 were prepared according to the same procedures as mentioned above. Table 3-5 summarizes the employed mass of polymer, sodium chloride and deuterium oxide, as well as the resulting total mass.

Table 3-5: Polymer solutions in deuterium oxide

Polymer	Sample	m_P [g]	m_{NaCl} [g]	m_{D2O} [g]	m_{tot} [g]
PEI_{1393}	P(XIII)-013	0.0010	0.0002	3.9992	4.0004
PEI_{1393}^{10Q}	P(XIV)-013	0.0014	0.0002	3.9992	4.0008
PEI_{1393}^{20Q}	P(XV)-013	0.0018	0.0002	3.9991	4.0011

Polymer	Sample	m_P [g]	m_{NaCl} [g]	m_{D2O} [g]	m_{tot} [g]
PEI_{1393}^{50Q}	P(XVI)-013	0.0029	0.0002	3.9978	4.0009
PEI_{1393}^{100Q}	P(XVII)-013	0.0047	0.0002	3.9950	3.9999
	P(XVII)-014	0.0047	0.0002	3.9952	4.0001

3.5. Silica-nanoparticle-dispersions

001: 0.1471g Ludox TMA (0.0500g silica nanoparticles) and 9.9498g water were added into a 20ml glass vessel. The total mass of the sample was 9.9998g.

The samples 002 – 014 were prepared according to the same procedure as mentioned above. Table 3-6 summarizes the employed mass of Ludox TMA, silica nanoparticles, water and the resulting total mass. The notation of the dispersions of pure silica nanoparticles in water is given by a consecutively number.

Table 3-6: Dispersions of silica nanoparticles in water

Dispersion	$m_{LudoxTMA}$ [g]	m_{NP} [g]	m_{H2O} [g]	m_{tot} [g]
001	0.1471	0.0500	9.8527	9.9998
002	0.0291	0.0099	9.9704	9.9995
003	0.0150	0.0051	9.9857	10.0007
004	0.0029	0.0010	9.9971	10.0000
005	0.0014	0.00049	9.9988	10.0002
006	0.00032	0.00011	10.0002	10.0005
007	0.00015	0.000050	9.9994	9.9995
008	0.000026	0.000009	9.9996	9.9996
009	0.1476	0.0502	9.8519	9.9995
010	0.1468	0.0499	9.8528	9.9996
011	0.1467	0.0499	9.8528	9.9995
012	0.1467	0.0499	9.8527	9.9994
013	0.1476	0.0502	9.8524	10.0000
014	0.1470	0.0500	9.8532	10.0002

015: 0.1470g Ludox TMA (0.0500g silica nanoparticles), 0.9997g of a 0.1M hydrochloric acid solution, 0.1005g of a 1M sodium chloride solution and 8.7527g water were added into a 20ml glass vessel. The total mass of the sample was 9.9999g.

The samples 016 – 025 were prepared according to the same procedure as mentioned above. Table 3-7 summarizes the employed mass of Ludox TMA, silica nanoparticles, the concentration and mass of the acidic / basic solution, concentration and mass of the sodium chloride solution, the mass of water and the resulting total mass.

Table 3-7: Dispersions of silica nanoparticles in water with added acid or base

Dispersion	$m_{LudoxTMA}$ [g]	m_{NP} [g]	c_{PH} [mol/L]	m_{PH} [g]	C_{NaCl} [mol/L]	m_{NaCl} [g]	m_{H2O} [g]	m_{tot} [g]
015	0.1470	0.0500	0.1M HCl	0.9997	1.0000	0.1005	8.7527	9.9999
016	0.1468	0.0499	0.1M HCl	0.0996	1.0000	0.1003	9.6526	9.9993
017	0.1473	0.0501	0.01M HCl	0.2002	1.0000	0.1004	9.5524	10.0003
018	0.1470	0.0500	0.001M HCl	0.9998	1.0000	0.0997	8.7527	9.9992
019	0.1469	0.0499	0.001M HCl	0.6996	1.0000	0.1007	9.0528	10.0000
020	0.1476	0.0502	---	---	1.0000	0.1005	9.7534	10.0015
021	0.1468	0.0499	0.001M NaOH	0.0998	1.0000	0.0999	9.6528	9.9993
022	0.1477	0.0502	0.001M NaOH	0.4012	1.0000	0.0997	9.3530	10.0016
023	0.1469	0.0499	0.001M NaOH	1.4998	1.0000	0.1006	8.2531	10.0004
024	0.1478	0.0503	0.01M NaOH	0.4008	1.0000	0.1000	9.3524	10.0010
025	0.1471	0.0500	0.01M NaOH	2.5003	1.0000	0.1004	7.2526	10.0004

3.6. Silica-nanoparticles-dispersion containing amino-quat-primer polymers

(XVII)-011: 0.1478g Ludox TMA (containing 0.0503g silica nanoparticles), an amount of a stock solution, which corresponds to 0.2521g poly(ethylenimine) and a mass of 9.6016g water were added into a 20ml glass vessel. The total mass of the sample was 10.0015g. The sample was dispersed by means of a Branson Sonifier 250 with an output control level of three and a duty cycle of 50% for 10min.

The dispersions (I)-001 – (I)-019, (II)-001 – (II)-010, (III)-001 – (III)-010, (IV)-001 – (IV)-015, (V)-001 – (V)-012, (VI)-001 – (VI)-014, (VII)-001 – (VII)-014, (VIII)-001 – (VIII)-010, (IX)-001 – (IX)-022, (X)-001 – (X)-015, (XI)-001 – (XI)-015, (XII)-001 – (XII)-015, (XIII)-001 – (XIII)-014, (XIV)-001 – (XIV)-012, (XV)-001 – (XV)-011, (XVI)-001 – (XVI)-027 and (XVII)-001 – (XVII)-010 were prepared according to the same procedure as mentioned above. The notation of the dispersions is given by the Roman numeral of the used poly(ethylenimine) derivative followed by a consecutively number for different dispersions for one polymer. Table 3-8 summarizes the employed mass of Ludox TMA, silica nanoparticles, polymer, water and the resulting total mass.

Table 3-8: Dispersions of silica nanoparticles and quaternized poly(ethylenimine) derivatives

Polymer	Dispersion	$m_{LudoxTMA}$ [g]	m_{NP} [g]	m_{P} [g]	m_{H2O} [g]	m_{tot} [g]
PEI_{28}	(I)-001	0.1465	0.0498	0.000005	9.8528	9.9993
	(I)-002	0.1471	0.0500	0.000036	9.8458	9.9929
	(I)-003	0.1470	0.0500	0.000050	9.8534	10.0004
	(I)-004	0.1475	0.0502	0.000072	9.8566	10.0042
	(I)-005	0.1469	0.0499	0.00011	9.8588	10.0058
	(I)-006	0.1470	0.0500	0.00018	9.8533	10.0005
	(I)-007	0.1470	0.0500	0.00027	9.8555	10.0028
	(I)-008	0.1469	0.0499	0.00036	9.8531	10.0004
	(I)-009	0.1479	0.0503	0.00049	9.8445	9.9929
	(I)-010	0.1474	0.0501	0.0011	9.8530	10.0015
	(I)-011	0.1474	0.0501	0.0024	9.8514	10.0012
	(I)-012	0.1469	0.0499	0.0051	9.8522	10.0042
	(I)-013	0.1483	0.0504	0.0125	9.8450	10.0058

Polymer	Dispersion	$m_{LudoxTMA}$ [g]	m_{NP} [g]	m_{P} [g]	m_{H2O} [g]	m_{tot} [g]
	(I)-014	0.1473	0.0501	0.0250	9.8282	10.0005
	(I)-015	0.1470	0.0500	0.0500	9.8058	10.0028
	(I)-016	0.1476	0.0502	0.1250	9.7278	10.0004
	(I)-017	0.1469	0.0499	0.5000	9.3523	9.9992
	(I)-018	0.1475	0.0502	0.7499	9.1047	10.0021
	(I)-019	0.1470	0.0500	1.0001	8.8546	10.0017
PEI_{28}^{1Q}	(II)-001	0.1469	0.0499	0.000005	9.8549	10.0018
	(II)-002	0.1472	0.0500	0.00005	9.8529	10.0001
	(II)-003	0.1469	0.0499	0.00011	9.8538	10.0008
	(II)-004	0.1468	0.0499	0.00024	9.8525	9.9995
	(II)-005	0.1466	0.0498	0.00050	9.8534	10.0005
	(II)-006	0.1465	0.0498	0.0011	9.8534	10.0010
	(II)-007	0.1470	0.0500	0.0024	9.8489	9.9983
	(II)-008	0.1476	0.0502	0.0050	9.8493	10.0019
	(II)-009	0.1474	0.0501	0.0500	9.8026	10.0000
	(II)-010	0.1475	0.0502	0.4999	9.3534	10.0008
PEI_{28}^{5Q}	(III)-001	0.1479	0.0503	0.000005	9.8533	10.0012
	(III)-002	0.1467	0.0499	0.00005	9.8524	9.9991
	(III)-003	0.1467	0.0499	0.00011	9.8521	9.9989
	(III)-004	0.1468	0.0499	0.00024	9.8546	10.0016
	(III)-005	0.1467	0.0499	0.00050	9.8523	9.9995
	(III)-006	0.1473	0.0501	0.0011	9.8507	9.9991
	(III)-007	0.1478	0.0503	0.0023	9.8502	10.0003
	(III)-008	0.1479	0.0503	0.0050	9.8489	10.0018
	(III)-009	0.1468	0.0499	0.0500	9.8102	10.0070
	(III)-010	0.1466	0.0498	0.4998	9.3531	9.9995
PEI_{28}^{10Q}	(IV)-001	0.1466	0.0498	0.000005	9.8525	9.9991
	(IV)-002	0.1470	0.0500	0.00005	9.8518	9.9988
	(IV)-003	0.1467	0.0499	0.00010	9.8548	10.0016
	(IV)-004	0.1475	0.0502	0.00015	9.8561	10.0037
	(IV)-005	0.1474	0.0501	0.00024	9.8522	9.9998
	(IV)-006	0.1470	0.0500	0.00036	9.8544	10.0018
	(IV)-007	0.1469	0.0499	0.00048	9.8540	10.0014
	(IV)-008	0.1472	0.0500	0.0011	9.8509	9.9992

Polymer	Dispersion	$m_{LudoxTMA}$ [g]	m_{NP} [g]	m_{P} [g]	m_{H2O} [g]	m_{tot} [g]
	(IV)-009	0.1468	0.0499	0.0024	9.8506	9.9998
	(IV)-010	0.1474	0.0501	0.0050	9.8490	10.0014
	(IV)-011	0.1472	0.0500	0.0124	9.8480	10.0076
	(IV)-012	0.1471	0.0500	0.0248	9.8292	10.0011
	(IV)-013	0.1471	0.0500	0.0497	9.8041	10.0009
	(IV)-014	0.1473	0.0501	0.1226	9.7119	9.9818
	(IV)-015	0.1468	0.0499	0.4994	9.3541	10.0003
	(V)-001	0.1469	0.0499	0.000005	9.8530	9.9999
	(V)-002	0.1467	0.0499	0.00005	9.8618	10.0086
	(V)-003	0.1475	0.0502	0.00011	9.8522	9.9998
	(V)-004	0.1476	0.0502	0.00024	9.8533	10.0011
	(V)-005	0.1465	0.0498	0.00050	9.8526	9.9996
PEI_{28}^{20Q}	(V)-006	0.1475	0.0502	0.0011	9.8533	10.0019
	(V)-007	0.1473	0.0501	0.0024	9.8513	10.0010
	(V)-008	0.1478	0.0503	0.0051	9.8613	10.0142
	(V)-009	0.1470	0.0500	0.0110	9.8426	10.0006
	(V)-010	0.1478	0.0503	0.0235	9.8284	9.9997
	(V)-011	0.1470	0.0500	0.0500	9.8017	9.9987
	(V)-012	0.1465	0.0498	0.5000	9.3532	9.9997
	(VI)-001	0.1466	0.0498	0.000005	9.8524	9.9990
	(VI)-002	0.1476	0.0502	0.00005	9.8543	10.0019
	(VI)-003	0.1467	0.0499	0.00010	9.8541	10.0009
	(VI)-004	0.1468	0.0499	0.00020	9.8522	9.9992
	(VI)-005	0.1468	0.0499	0.00030	9.8517	9.9988
	(VI)-006	0.1467	0.0499	0.00050	9.8575	10.0047
PEI_{28}^{50Q}	(VI)-007	0.1472	0.0500	0.00074	9.8511	9.9990
	(VI)-008	0.1469	0.0499	0.00100	9.8509	9.9988
	(VI)-009	0.1472	0.0500	0.0023	9.8490	9.9985
	(VI)-010	0.1466	0.0498	0.0050	9.8547	10.0063
	(VI)-011	0.1471	0.0500	0.0127	9.8392	9.9990
	(VI)-012	0.1469	0.0499	0.0237	9.8299	10.0005
	(VI)-013	0.1470	0.0500	0.0500	9.8098	10.0068
	(VI)-014	0.1474	0.0501	0.4998	9.3528	10.0000
PEI_{28}^{100Q}	(VII)-001	0.1465	0.0498	0.000005	9.8518	9.9983

Polymer	Dispersion	$m_{LudoxTMA}$ [g]	m_{NP} [g]	m_{P} [g]	m_{H2O} [g]	m_{tot} [g]
	(VII)-002	0.1473	0.0501	0.00005	9.8523	9.9997
	(VII)-003	0.1468	0.0499	0.00016	9.8521	9.9991
	(VII)-004	0.1467	0.0499	0.00032	9.8520	9.9990
	(VII)-005	0.1471	0.0500	0.00051	9.8547	10.0023
	(VII)-006	0.1470	0.0500	0.00082	9.8563	10.0041
	(VII)-007	0.1473	0.0501	0.0012	9.8518	10.0003
	(VII)-008	0.1467	0.0499	0.0016	9.8513	9.9996
	(VII)-009	0.1475	0.0502	0.0024	9.8512	10.0011
	(VII)-010	0.1466	0.0498	0.0050	9.8478	9.9994
	(VII)-011	0.1468	0.0499	0.0110	9.8417	9.9995
	(VII)-012	0.1475	0.0502	0.0237	9.8307	10.0019
	(VII)-013	0.1472	0.0500	0.0500	9.8029	10.0001
	(VII)-014	0.1466	0.0498	0.5004	9.3524	9.9994
PEI_{232}	(VIII)-001	0.1471	0.0500	0.00003	9.8525	9.9996
	(VIII)-002	0.1472	0.0500	0.00017	9.8524	9.9998
	(VIII)-003	0.1466	0.0498	0.00050	9.8492	9.9963
	(VIII)-004	0.1477	0.0502	0.0017	9.8516	10.001
	(VIII)-005	0.1474	0.0501	0.0050	9.8496	10.002
	(VIII)-006	0.1465	0.0498	0.0126	9.8425	10.0016
	(VIII)-007	0.1467	0.0499	0.0250	9.8230	9.9947
	(VIII)-008	0.1466	0.0498	0.0501	9.8004	9.9971
	(VIII)-009	0.1468	0.0499	0.1260	9.7370	10.0098
	(VIII)-010	0.1469	0.0499	0.2938	9.5589	9.9996
PEI_{232}^{10Q}	(IX)-001	0.1471	0.0500	0.000005	9.8523	9.9994
	(IX)-002	0.1471	0.0500	0.00005	9.8518	9.9989
	(IX)-003	0.1475	0.0502	0.00013	9.8531	10.0007
	(IX)-004	0.1467	0.0499	0.00025	9.8532	10.0002
	(IX)-005	0.1466	0.0498	0.00038	9.8542	10.0012
	(IX)-006	0.1468	0.0499	0.00050	9.8532	10.0005
	(IX)-007	0.1468	0.0499	0.0015	9.8556	10.0039
	(IX)-008	0.1477	0.0502	0.0025	9.8505	10.0007
	(IX)-009	0.1467	0.0499	0.0038	9.8509	10.0014
	(IX)-010	0.1476	0.0502	0.0050	9.8481	10.0007
	(IX)-011	0.1472	0.0500	0.0075	9.8451	9.9998

Polymer	Dispersion	$m_{LudoxTMA}$ [g]	m_{NP} [g]	m_{P} [g]	m_{H2O} [g]	m_{tot} [g]
	(IX)-012	0.1474	0.0501	0.0100	9.8422	9.9996
	(IX)-013	0.1474	0.0501	0.0125	9.8408	10.0007
	(IX)-014	0.1468	0.0499	0.0150	9.8396	10.0014
	(IX)-015	0.1475	0.0502	0.0200	9.8332	10.0007
	(IX)-016	0.1476	0.0502	0.0250	9.8282	10.0008
	(IX)-017	0.1465	0.0498	0.0375	9.8151	9.9991
	(IX)-018	0.1470	0.0500	0.0501	9.8074	10.0045
	(IX)-019	0.1466	0.0498	0.1253	9.7371	10.0090
	(IX)-020	0.1470	0.0500	0.2502	9.6053	10.0025
	(IX)-021	0.1465	0.0498	0.3760	9.4866	10.0091
	(IX)-022	0.1471	0.0500	0.5005	9.3576	10.0052
PEI_{232}^{20Q}	(X)-001	0.1468	0.0499	0.00005	9.8525	9.9994
	(X)-002	0.1471	0.0500	0.00009	9.8537	10.0009
	(X)-003	0.1473	0.0501	0.00016	9.8533	10.0008
	(X)-004	0.1478	0.0503	0.00028	9.8540	10.0021
	(X)-005	0.1470	0.0500	0.00050	9.8535	10.0010
	(X)-006	0.1478	0.0503	0.00089	9.8522	10.0009
	(X)-007	0.1467	0.0499	0.0016	9.8524	10.0007
	(X)-008	0.1467	0.0499	0.0028	9.8501	9.9996
	(X)-009	0.1478	0.0503	0.0050	9.8461	9.9989
	(X)-010	0.1475	0.0502	0.0089	9.8441	10.0005
	(X)-011	0.1474	0.0501	0.0159	9.8373	10.0006
	(X)-012	0.1472	0.0500	0.0283	9.8267	10.0022
	(X)-013	0.1476	0.0502	0.0501	9.8021	9.9998
	(X)-014	0.1472	0.0500	0.0891	9.7639	10.0002
	(X)-015	0.1478	0.0503	0.1584	9.6947	10.0009
PEI_{232}^{50Q}	(XI)-001	0.1469	0.0499	0.00008	9.8535	10.0005
	(XI)-002	0.1470	0.0500	0.00014	9.8529	10.0000
	(XI)-003	0.1475	0.0502	0.00026	9.8536	10.0014
	(XI)-004	0.1468	0.0499	0.00046	9.8522	9.9995
	(XI)-005	0.1478	0.0503	0.00081	9.8535	10.0021
	(XI)-006	0.1469	0.0499	0.0014	9.8522	10.0005
	(XI)-007	0.1476	0.0502	0.0026	9.8501	10.0003
	(XI)-008	0.1477	0.0502	0.0046	9.8477	10.0000

Polymer	Dispersion	$m_{LudoxTMA}$ [g]	m_{NP} [g]	m_{P} [g]	m_{H2O} [g]	m_{tot} [g]
	(XI)-009	0.1474	0.0501	0.0081	9.8450	10.0005
	(XI)-010	0.1469	0.0499	0.0145	9.8389	10.0003
	(XI)-011	0.1478	0.0503	0.0257	9.8281	10.0016
	(XI)-012	0.1473	0.0501	0.0456	9.8078	10.0007
	(XI)-013	0.1472	0.0500	0.0811	9.7725	10.0008
	(XI)-014	0.1478	0.0503	0.1452	9.7075	10.0005
	(XI)-015	0.1475	0.0502	0.2565	9.5960	10.0000
PEI_{232}^{100Q}	(XII)-001	0.1477	0.0502	0.00013	9.8531	10.0009
	(XII)-002	0.1469	0.0499	0.00024	9.8534	10.0005
	(XII)-003	0.1474	0.0501	0.00042	9.8536	10.0014
	(XII)-004	0.1478	0.0503	0.00075	9.8536	10.0021
	(XII)-005	0.1476	0.0502	0.0013	9.8532	10.0021
	(XII)-006	0.1478	0.0503	0.0024	9.8510	10.0012
	(XII)-007	0.1476	0.0502	0.0042	9.8506	10.0024
	(XII)-008	0.1478	0.0503	0.0075	9.8457	10.001
	(XII)-009	0.1475	0.0502	0.0133	9.8389	9.9997
	(XII)-010	0.1470	0.0500	0.0236	9.8304	10.001
	(XII)-011	0.1477	0.0502	0.0421	9.8110	10.0008
	(XII)-012	0.1478	0.0503	0.0746	9.7790	10.0014
	(XII)-013	0.1475	0.0502	0.1332	9.7201	10.0008
	(XII)-014	0.1477	0.0502	0.2360	9.6179	10.0016
	(XII)-015	0.1478	0.0503	0.4198	9.4338	10.0014
PEI_{1393}	(XIII)-001	0.1468	0.0499	0.00018	9.8532	10.0002
	(XIII)-002	0.1475	0.0502	0.00049	9.8582	10.0062
	(XIII)-003	0.1471	0.0500	0.0010	9.8531	10.0012
	(XIII)-004	0.1466	0.0498	0.0018	9.8517	10.0001
	(XIII)-005	0.1483	0.0504	0.0050	9.8628	10.0161
	(XIII)-006	0.1481	0.0504	0.0125	9.8403	10.0009
	(XIII)-007	0.1478	0.0503	0.0250	9.8290	10.0018
	(XIII)-008	0.1477	0.0502	0.0500	9.8085	10.0062
	(XIII)-009	0.1470	0.0500	0.1251	9.7282	10.0003
	(XIII)-010	0.1476	0.0502	0.0035	9.8506	10.0017
	(XIII)-011	0.1474	0.0501	0.0035	9.8503	10.0012
	(XIII)-012	0.1473	0.0501	0.0035	9.8493	10.0001

Polymer	Dispersion	$m_{LudoxTMA}$ [g]	m_{NP} [g]	m_{P} [g]	m_{H2O} [g]	m_{tot} [g]
	(XIII)-013	0.1469	0.0499	0.0035	9.8500	10.0004
	(XIII)-014	0.1472	0.0500	0.0035	9.8502	10.0009
PEI_{1393}^{10Q}	(XIV)-001	0.1466	0.0498	0.00024	9.8535	10.0003
	(XIV)-002	0.1472	0.0500	0.00047	9.8538	10.0015
	(XIV)-003	0.1475	0.0502	0.00077	9.8526	10.0009
	(XIV)-004	0.1473	0.0501	0.0013	9.8527	10.0013
	(XIV)-005	0.1472	0.0500	0.0030	9.8489	9.9991
	(XIV)-006	0.1474	0.0501	0.0050	9.8480	10.0004
	(XIV)-007	0.1468	0.0499	0.0124	9.8434	10.0026
	(XIV)-008	0.1475	0.0502	0.0248	9.8372	10.0095
	(XIV)-009	0.1472	0.0500	0.0495	9.8023	9.9990
	(XIV)-010	0.1476	0.0502	0.1262	9.7394	10.0132
	(XIV)-011	0.1472	0.0500	0.0762	9.7771	10.0005
	(XIV)-012	0.1475	0.0502	0.2383	9.6146	10.0004
PEI_{1393}^{20Q}	(XV)-001	0.1474	0.0501	0.0003	9.8534	10.0011
	(XV)-002	0.1476	0.0502	0.0006	9.8528	10.0010
	(XV)-003	0.1466	0.0498	0.0010	9.8526	10.0002
	(XV)-004	0.1474	0.0501	0.0017	9.8514	10.0005
	(XV)-005	0.1475	0.0502	0.0030	9.8515	10.0020
	(XV)-006	0.1466	0.0498	0.0060	9.8462	9.9988
	(XV)-007	0.1476	0.0502	0.0095	9.8452	10.0023
	(XV)-008	0.1477	0.0502	0.0169	9.8381	10.0027
	(XV)-009	0.1473	0.0501	0.0300	9.8250	10.0023
	(XV)-010	0.1469	0.0499	0.0598	9.7916	9.9983
	(XV)-011	0.1465	0.0498	0.0949	9.7574	9.9988
PEI_{1393}^{50Q}	(XVI)-001	0.1468	0.0499	0.00049	9.8526	9.9999
	(XVI)-002	0.1467	0.0499	0.0010	9.8513	9.9990
	(XVI)-003	0.1470	0.0500	0.0015	9.8510	9.9995
	(XVI)-004	0.1475	0.0502	0.0027	9.8509	10.0011
	(XVI)-005	0.1474	0.0501	0.0049	9.8494	10.0017
	(XVI)-006	0.1473	0.0501	0.0097	9.8443	10.0013
	(XVI)-007	0.1470	0.0500	0.0154	9.8386	10.0010
	(XVI)-008	0.1476	0.0502	0.0274	9.8262	10.0012
	(XVI)-009	0.1474	0.0501	0.0487	9.8061	10.0022

Polymer	Dispersion	$m_{LudoxTMA}$ [g]	m_{NP} [g]	m_{P} [g]	m_{H2O} [g]	m_{tot} [g]
	(XVI)-010	0.1476	0.0502	0.0973	9.7551	10.0000
	(XVI)-011	0.1471	0.0500	0.1541	9.7006	10.0018
	(XVI)-012	0.1469	0.0499	0.2563	9.5963	9.9995
	(XVI)-013	0.1477	0.0502	0.5018	9.3516	10.0011
	(XVI)-014	0.1468	0.0499	0.0005	9.8530	10.0003
	(XVI)-015	0.1467	0.0499	0.0015	9.8510	9.9992
	(XVI)-016	0.1473	0.0501	0.0049	9.8491	10.0013
	(XVI)-017	0.1470	0.0500	0.0154	9.8390	10.0014
	(XVI)-018	0.1476	0.0502	0.0487	9.8038	10.0001
	(XVI)-019	0.1469	0.0499	0.0015	9.8529	10.0013
	(XVI)-020	0.1468	0.0499	0.0016	9.8528	10.0012
	(XVI)-021	0.1473	0.0501	0.0049	9.8494	10.0016
	(XVI)-022	0.1467	0.0499	0.0049	9.8494	10.0010
	(XVI)-023	0.1478	0.0503	0.0097	9.8444	10.0019
	(XVI)-024	0.1476	0.0502	0.0097	9.8440	10.0013
	(XVI)-025	0.1475	0.0502	0.0097	9.8434	10.0006
	(XVI)-026	0.1469	0.0499	0.0097	9.8443	10.0009
	(XVI)-027	0.1477	0.0502	0.0097	9.8436	10.0010
PEI_{1393}^{100Q}	(XVII)-001	0.1465	0.0498	0.00082	9.8509	9.9982
	(XVII)-002	0.1468	0.0499	0.0016	9.8528	10.0012
	(XVII)-003	0.1475	0.0502	0.0025	9.8525	10.0025
	(XVII)-004	0.1467	0.0499	0.0045	9.8496	10.0008
	(XVII)-005	0.1466	0.0498	0.0081	9.8441	9.9988
	(XVII)-006	0.1473	0.0501	0.0160	9.8377	10.0010
	(XVII)-007	0.1473	0.0501	0.0255	9.8295	10.0023
	(XVII)-008	0.1478	0.0503	0.0453	9.8078	10.0009
	(XVII)-009	0.1475	0.0502	0.0806	9.7717	9.9998
	(XVII)-010	0.1470	0.0500	0.1595	9.6933	9.9998
	(XVII)-011	0.1478	0.0503	0.2521	9.6016	10.0015

(XIII)-015: 0.1474g Ludox TMA (containing 0.0501g silica nanoparticles), an amount of a stock solution, which corresponds to 0.0035g PEI_{1393} and a mass of 9.6700g water were added into a 20ml glass vessel. The sample was dispersed by means of a Branson Sonifier 250 with an output control level of three and a duty cycle of 50% for 10min. After dispersing

0.1798g of a 0.01M sodium hydroxide solution was added. The total mass of the sample was 10.0007g.

The dispersions (XIII)-016 – (XVII)-020 and (XVI)-028 – (XVI)-033 were prepared according to the same procedure as mentioned above. Table 3-9 summarizes the employed mass of Ludox TMA, silica nanoparticles, polymer, the concentration and mass of the acidic / basic solution, the mass of water and the resulting total mass.

Table 3-9: Dispersions of silica nanoparticles and quaternized poly(ethylenimine) derivatives with added acid or base

Polymer	Dispersion	$m_{LudoxTMA}$ [g]	m_{NP} [g]	m_{P} [g]	c_{PH} [mol/L]	m_{PH} [g]	m_{H2O} [g]	m_{tot} [g]
PEI_{1393}	(XIII)-015	0.1474	0.0501	0.0035	0.01M NaOH	0.1798	9.6700	10.0007
	(XIII)-016	0.1478	0.0503	0.0035	0.01M NaOH	0.0498	9.7995	10.0006
	(XIII)-017	0.1475	0.0502	0.0035	0.1M HCl	0.1004	9.7502	10.0016
	(XIII)-018	0.1472	0.0500	0.0035	0.1M HCl	0.2002	9.6491	10.0000
	(XIII)-019	0.1475	0.0502	0.0035	0.1M HCl	0.2999	9.5497	10.0006
	(XIII)-020	0.1477	0.0502	0.0035	0.1M HCl	0.4199	9.4294	10.0005
PEI_{1393}^{50Q}	(XVI)-028	0.1478	0.0503	0.0097	0.01M NaOH	0.4998	9.3444	10.0017
	(XVI)-029	0.1473	0.0501	0.0097	0.01M NaOH	0.2409	9.6031	10.0010
	(XVI)-030	0.1475	0.0502	0.0097	0.01M NaOH	0.0798	9.7635	10.0005
	(XVI)-031	0.1470	0.0500	0.0097	0.1M HCl	0.0406	9.8043	10.0016
	(XVI)-032	0.1478	0.0503	0.0097	0.1M HCl	0.1800	9.6648	10.0023
	(XVI)-033	0.1476	0.0502	0.0097	0.1M HCl	0.2804	9.5642	10.0019

(XIII)-034: 0.1474g Ludox TMA (containing 0.0501g silica nanoparticles), 0.0098g PEI_{1393}^{50Q}, 0.0001g sodium chloride and a mass of 9.8423g water were added into a 20ml glass vessel. The total mass of the sample was 9.9995g. The sample was dispersed by means of a Branson Sonifier 250 with an output control level of three and a duty cycle of 50% for 10min.

The dispersions (XIII)-035 – (XIII)-041 were prepared according to the same procedure as mentioned above. Table 3-10 summarizes the employed mass of Ludox TMA, silica nanoparticles, polymer, the concentration and mass of the sodium chloride solution, the mass of water and the resulting total mass.

Table 3-10: Dispersions of silica nanoparticles and quaternized poly(ethylenimine) derivatives with added sodium chloride

Polymer	Dispersion	$m_{LudoxTMA}$ [g]	m_{NP} [g]	m_{P} [g]	m_{NaCl} [g]	m_{H2O} [g]	m_{tot} [g]
PEI_{1393}^{50Q}	(XVI)-034	0.1474	0.0501	0.0098	0.0001	9.8423	9.9995
	(XVI)-035	0.1469	0.0499	0.0098	0.0006	9.8426	9.9998
	(XVI)-036	0.1477	0.0502	0.0098	0.0058	9.8375	10.0008
	(XVI)-037	0.1478	0.0503	0.0097	0.0117	9.8322	10.0014
	(XVI)-038	0.1474	0.0501	0.0097	0.0234	9.8206	10.0011
	(XVI)-039	0.1469	0.0499	0.0097	0.0351	9.8088	10.0004
	(XVI)-040	0.1470	0.0500	0.0097	0.0468	9.7973	10.0008
	(XVI)-041	0.1476	0.0502	0.0098	0.0584	9.7852	10.0010

Chapter 4:

Synthesis and characterization of amino-quat-primer polymers

4. Synthesis and characterization of amino-quat-primer polymers

The charge density of poly(ethylenimine) can be controlled by introducing covalently fixed positive charges into the polymers. Partially quaternized poly(ethylenimine) derivatives, so-called amino-quat-primer polymers, with degrees of polymerization of X_n = 28, 232 and 1393, as well as degrees of quaternization of q = 1, 5, 10, 20, 50 and 100% were synthesized. The structure of the products was proved by ^{1}H- and ^{13}C-NMR-spectroscopy and the degree of quaternization was confirmed by ^{1}H-NMR-spectroscopy and elemental analysis. The theoretical molecular weights and the diameters of the synthesized derivatives were calculated. Their thermal behavior, as well as their solubility in a variety of solvents was investigated. The pH of polymer-water-solutions was measured, and the degree of protonation was determined by titrations. Furthermore the electrophoretic mobility of polymer molecules in polymer-water-solutions was measured. The effective charge of the macromolecules was investigated by a combination of DOSY-NMR-spectroscopy and electrophoretic measurements. The size of the polymer molecules was investigated by dynamic light scattering, as well as DOSY-NMR-measurements and compared with the theoretical values.

4.1. Synthesis

Technical poly(ethylenimine) exhibits a hyperbranched structure and contains terminal, linear and dendritic units in a ratio of approximately 25:50:25 (cf. literature review, Chapter 2.2.1.) [1]. The terminal units consist of primary -, the linear units of secondary - and the dendritic units of tertiary amino groups. A primary - bears two protons, a secondary - one proton and a tertiary amino group no protons. For poly(ethylenimine) consisting of 25% amino groups with two protons, 50% amino groups with one proton and 25% amino groups without any protons, on average every amino group bears one proton.

Poly(ethylenimine) (PEI) and glycidyltrimethylammonium chloride ($quat_R$) were stirred in water for 24 hours at room temperature. The solvent was evaporated under reduced pressure at 60°C and afterwards the substance was dried for 24 hours in vacuum at 60°C (cf. experimental part, Chapter 3.3.). Because of the high hydrophilicity of the partially quaternized poly(ethylenimine) derivatives, the gained highly viscous oils could not be obtained free of water. A reaction between PEI and $quat_R$ was expected to proceed via a ring opening addition of a nitrogen atom of the polymer to the oxirane ring (cf. literature review,

Chapter 2.2.2.) [2]. Figure 4-1 shows the reaction scheme of a linear subunit of PEI with $quat_R$ to yield in a partially quaternized poly(ethylenimine) (PEI^{qQ}). The unmodified poly(ethylenimine) unit contains two chemically equivalent carbon atoms named “A”. The quaternized poly(ethylenimine) subunit consists of four additional kinds of carbon atoms, named “C” – “F”, beside the backbone atoms termed “B”.

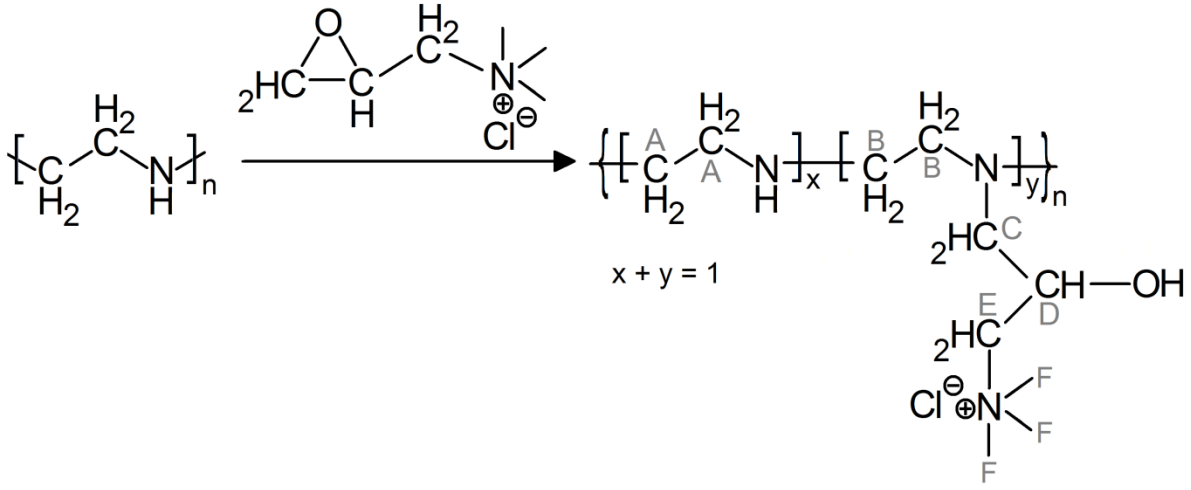

Figure 4-1: Reaction of a linear repetition unit of poly(ethylenimine) to form a quaternized poly(ethylenimine) subunit by addition of glycidyltrimethylammonium chloride ($quat_R$)

The degree of quaternization q is defined as the ratio between the number of quaternized ethylenimine units per macromolecule and the number average degree of polymerization (see Equation 4-1). Concerning the experimental conditions, the degree of quaternization is given by the ratio between the amount of substance of glycidyltrimethylammonium chloride ($quat_R$) and the amount of substance of ethylenimine units.

$$q = \frac{n_{N+}}{X_n} = \frac{n_{QuatR}}{n_{PEI}} \qquad \textit{Equation 4-1}$$

with q: degree of quaternization; n_{N+} : number of quaternized ethylenimine units per macromolecule; X_n : number average degree of polymerization; n_{QuatR} : amount of substance of glycidyltrimethylammonium chloride; n_{PEI} : amount of substance of ethylenimine units

4.2. Qualitative structure analysis

The structure of the synthesized, partially quaternized poly(ethylenimine) derivatives was investigated by means of ^{1}H- and ^{13}C-NMR-spectroscopy, comparing the spectra of the educt poly(ethylenimine) (PEI) with the spectra of the products.

4.2.1. ^{1}H-NMR-spectroscopy

Figure 4-2 shows the ^{1}H-NMR-spectra of a) $\mathrm{PEI}_{28}^{100\mathrm{Q}}$ (VII), b) $\mathrm{PEI}_{28}^{10\mathrm{Q}}$ (IV) and c) PEI_{28} (I). The ^{1}H-NMR-spectrum of PEI_{28} (I) exhibits a group of mutually overlapping broad signals between 2.5 and 2.8ppm, which arise from the methylene protons A in the backbone (see Figure 4-1).

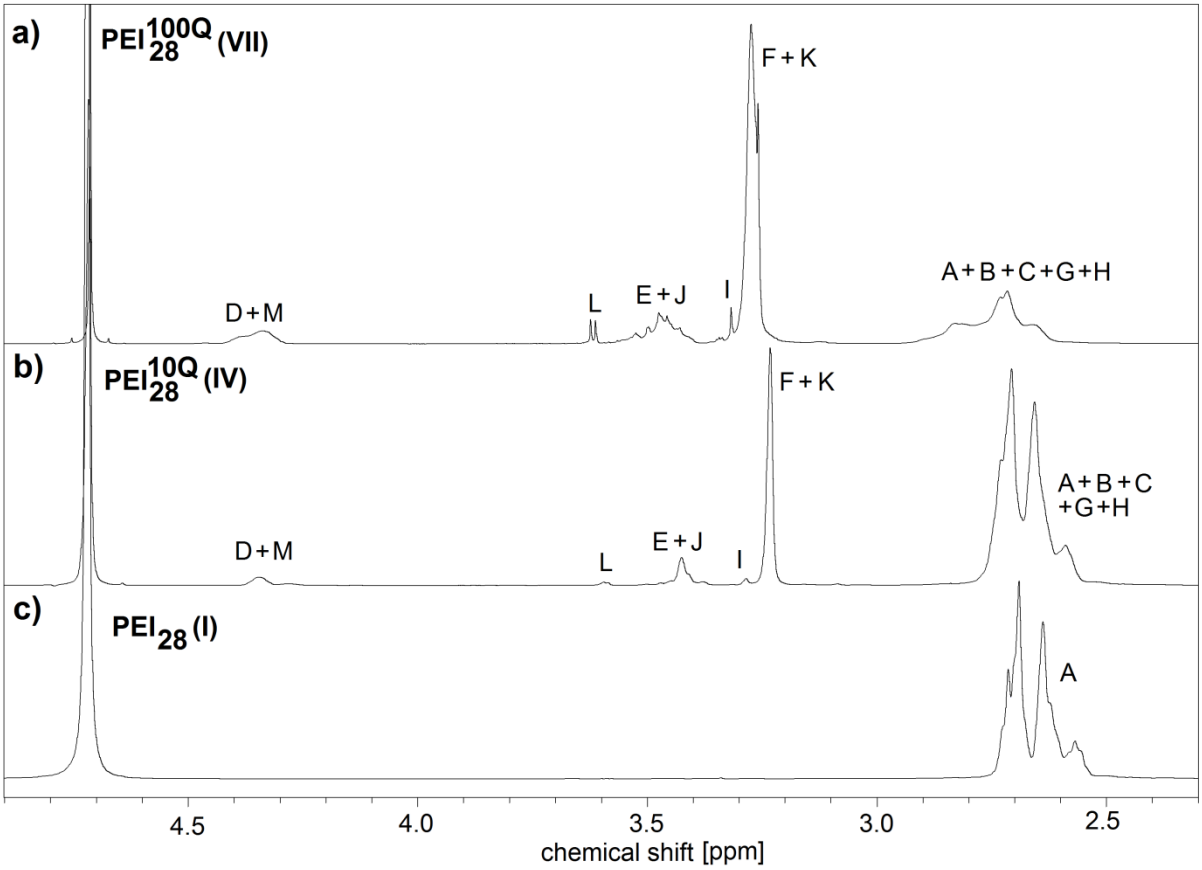

Figure 4-2: ^{1}H-NMR-spectra of a) PEI_{28}^{100Q} (VII), b) PEI_{28}^{10Q} (IV) and c) PEI_{28} (I); denotation of protons according to Figure 4-4a)

The ^{1}H-NMR-spectrum of $\mathrm{PEI}_{28}^{10\mathrm{Q}}$ (IV) also shows this broad signal group between 2.5 and 2.8ppm caused by the backbone methylene protons (A+B+G) and the α-backbone ammonium bonded-methylene protons (C+H). Additionally a new signal between 3.2 and 3.3ppm appears, arising from the methyl protons of the ammonium groups (F+K). The peak

between 3.4 and 3.5ppm is caused by the α-ammonium bonded-methylene protons (E+J). A signal between 4.3 and 4.4ppm originates from the hydroxyl-bonded methine protons (D+M). Additionally to the named signals, two further peaks are found at 3.3ppm (I) and 3.6ppm (L) in the ^{1}H-NMR-spectrum of $\mathrm{PEI}_{28}^{10\mathrm{Q}}$ (IV) that cannot be correlated to the structural elements shown in Figure 4-1, but should occur on mono-addition of glycidyltrimethylammonium chloride to the backbone nitrogen atom of poly(ethylenimine). The “excess” signals (I and L) of $\mathrm{PEI}_{28}^{10\mathrm{Q}}$ (IV) and $\mathrm{PEI}_{28}^{100\mathrm{Q}}$ (VII) occur at the same chemical shift, however, the integrals are different and related to the varied degree of quaternization.

Proton-NMR-spectroscopy of $\mathrm{PEI}^{\mathrm{qQ}}$ is of limited help in structure elucidation because of the strongly overlapping of the broad signals. ^{13}C-NMR-spectroscopy is better suited, since the range of chemical shift of ^{13}C atoms is much larger than that of ^{1}H atoms. Hence, ^{13}C-NMR-spectroscopy allows distinguishing the signals of linear, dendritic and terminal ethylenimine repetition groups [3].

4.2.2. ^{13}C-NMR-spectroscopy

Figure 4-3a) shows the five possible combinations of neighboring the terminal, linear and dendritic amino groups giving rise to eight different carbon atom signals (b_1 – b_8). The denotations b_1 – b_8 denote the backbone carbon atoms within the five types of repetition units. Between a terminal and a dendritic unit (td, see Figure 4-3a), the carbon atom next to the terminal group is labeled b_1 and the one next to the dendritic unit is named b_8. Between a linear and a dendritic unit (ld), the carbon atom next to the linear group is labeled b_3 and the one next to the dendritic unit is named b_7. Between a terminal and a linear unit (tl), the carbon atom next to the terminal group is labeled b_2 and the one next to the linear unit is named b_5. Between two linear units (ll), the carbon atoms are labeled b_4 and between two dendritic units (dd), the carbon atoms are labeled b_6.

Figure 4-3 shows the ^{13}C-NMR-spectra of b) $\mathrm{PEI}_{28}^{100\mathrm{Q}}$ (VII), c) $\mathrm{PEI}_{28}^{10\mathrm{Q}}$ (IV) and d) PEI_{28} (I). The ^{13}C-NMR-spectra of PEI_{28} (I) consists of eight signals, that correspond to the eight different kind of backbone carbon atoms identified in Figure 4-3a) [3].

The ^{13}C-NMR-spectra of $\mathrm{PEI}_{28}^{10\mathrm{Q}}$ (IV) (Figure 4-3c) shows additional signals compared to the spectra of pure poly(ethylenimine) (Figure 4-3d), caused by the presence of the 2-hydroxypropylammonium side groups. A peak at 52.5ppm (b_x) arises from carbon atoms in the backbone, which are bonded to a nitrogen atom that reacted with quat_R. At 54.4ppm the

signal of the methyl groups of quaternary ammonium groups (F+K) appears. A signal at 64.2ppm is caused by the hydroxyl-bonded methine carbon atom (D+M) and a peak at 69.4ppm originates from the α-ammonium bonded-methylene carbon atom (E+J). In this spectrum no signal emerges, which corresponds to the α-backbone ammonium bonded-methylene carbon atom (C+H). Between 63.7 and 68.4ppm four signals of weak intensities appear which do not correspond to the expected structural elements shown in Figure 4-1.

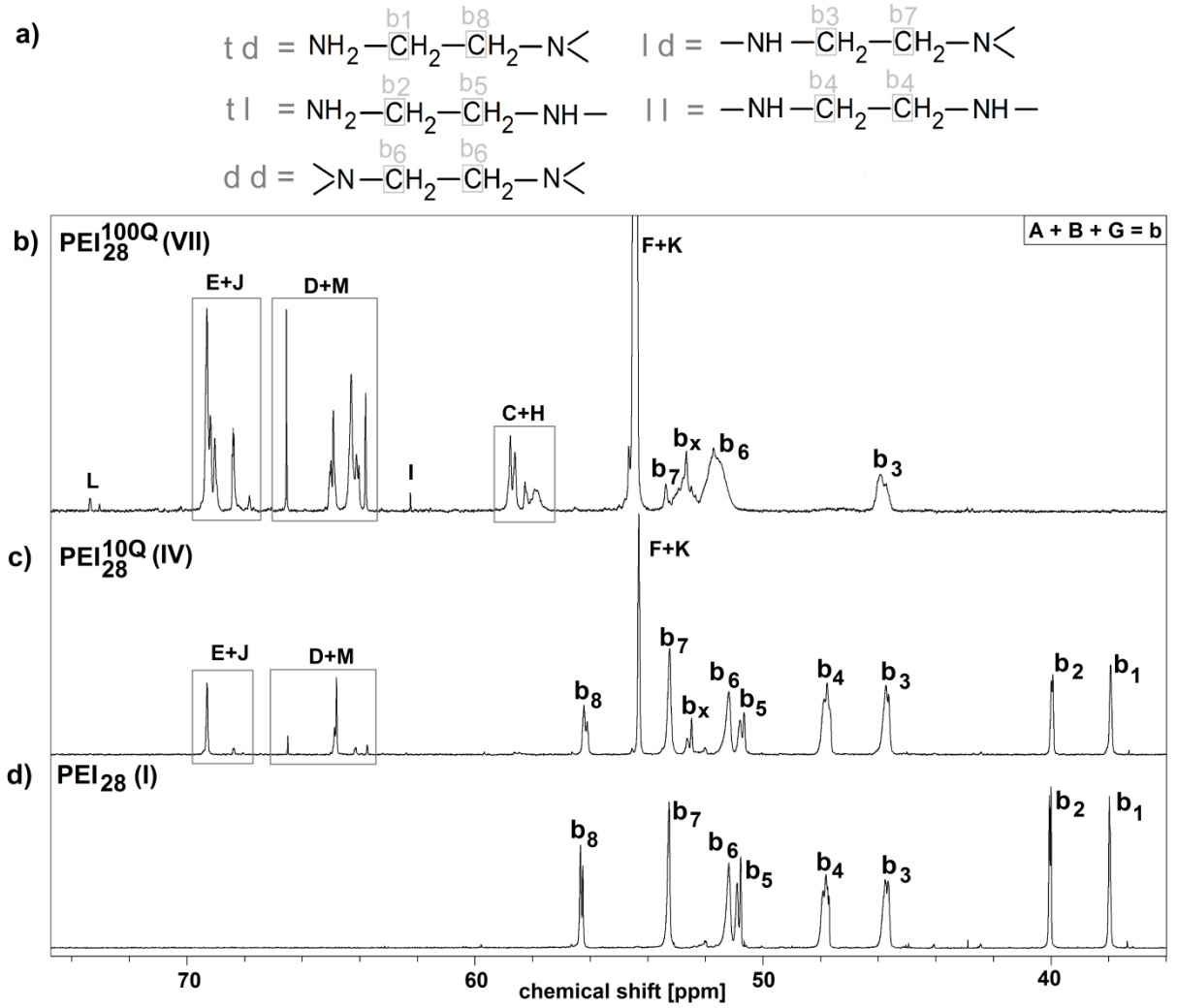

Figure 4-3a): Possible combinations of neighboring terminal, linear and dendritic amino groups, b) ^{13}C-NMR-spectra of PEI_{28}^{100Q} (VII), c) ^{13}C-NMR-spectra of PEI_{28}^{10Q} (IV) and d) ^{13}C-NMR-spectra of PEI_{28} (I); denotation of carbon atoms A – M according to Figure 4-4a); denotation of backbone carbon atoms b according to Figure 4-3a)

In the ^{13}C-NMR-spectra of PEI_{28}^{100Q} (VII) (Figure 4-3b), the signals b_1, b_2, b_4, b_5 and b_8 of the backbone carbon atoms of the td, tl and ll repetition units do not occur, only the signals b_3, b_6, b_7 of the ld and dd repetition units and the additional peak b_x by carbon atoms in the

backbone, which are bonded to a nitrogen atom, that reacted with $quat_R$, appear. The explanation is, that the additional peaks are caused by carbon atoms of terminal and linear groups, and with an increasing degree of quaternization, more and more terminal and linear groups are further reacted with $quat_R$ and their position in the ^{13}C-NMR-spectra is shifted. The signals of the hydroxyl-bonded methine carbon atom (D+M), of the α-ammonium bonded-methylene carbon atom (E+J), as well as of the methyl groups of the quaternary ammonium groups (F+K) occur in the ^{13}C-NMR-spectra of $\mathrm{PEI}_{28}^{100\mathrm{Q}}$ (VII) in the same regions as of $\mathrm{PEI}_{28}^{10\mathrm{Q}}$ (IV) (Figure 4-3c). The signal at 58.9ppm is caused by the α-backbone ammonium bonded-methylene carbon atom (C+H).

Additionally to the named signals, two peaks at 62.2 and 73.3ppm emerge in the ^{13}C-NMR-spectrum of $\mathrm{PEI}_{28}^{100\mathrm{Q}}$ (VII) that cannot be correlated to the structural elements shown in Figure 4-1. Furthermore, five additional signals between 63.8 and 68.4ppm occur in this spectrum with comparable intensities as the signals caused by the hydroxyl-bonded methine carbon atom (D+M) and the α-ammonium bonded-methylene carbon atom (E+J).

In the ^{1}H- and ^{13}C-NMR-spectra of partially quaternized poly(ethylenimine) derivatives signals occur which do not correspond to the structural elements of the mono-addition of glycidyltrimethylammonium chloride to the backbone nitrogen atom of poly(ethylenimine) shown in Figure 4-1. It is concluded, that additional structural elements must occur, which cause the additional peaks in the spectra. Two possible side reactions are (i) the addition of $quat_R$ to tertiary amino groups of poly(ethylenimine) resulting in additional quaternary ammonium groups (Figure 4-4b) and (ii) the addition of $quat_R$ to hydroxyl groups of prior formed 2-hydroxypropylammonium side groups (Figure 4-4a).

The addition of $quat_R$ to tertiary amino groups of poly(ethylenimine) would lead to symmetrically substituted quaternary ammonium groups in the polymer backbone. The resonances in the ^{1}H-NMR-spectra of each of the α-ammonium bonded-methylene protons (O+Q) are expected to appear in the same range of chemical shift and one additional peak should emerge due to the hydroxyl-bonded methane protons (P). The expected signals in the ^{1}H-NMR-spectra of partially quaternized poly(ethylenimine) for the occurrence of the addition of $quat_R$ to tertiary amino groups of poly(ethylenimine) do not match with the actually found signals (see Figure 4-3b). Furthermore, the reactivity of epoxides towards tertiary alkylamines is nearly zero for nitrogen atoms bound to longer chains like they occur in poly(ethylenimine) (cf. literature review, Chapter 2.2.2.) [4]. Based on these facts, the addition of $quat_R$ to tertiary amino groups is excluded.

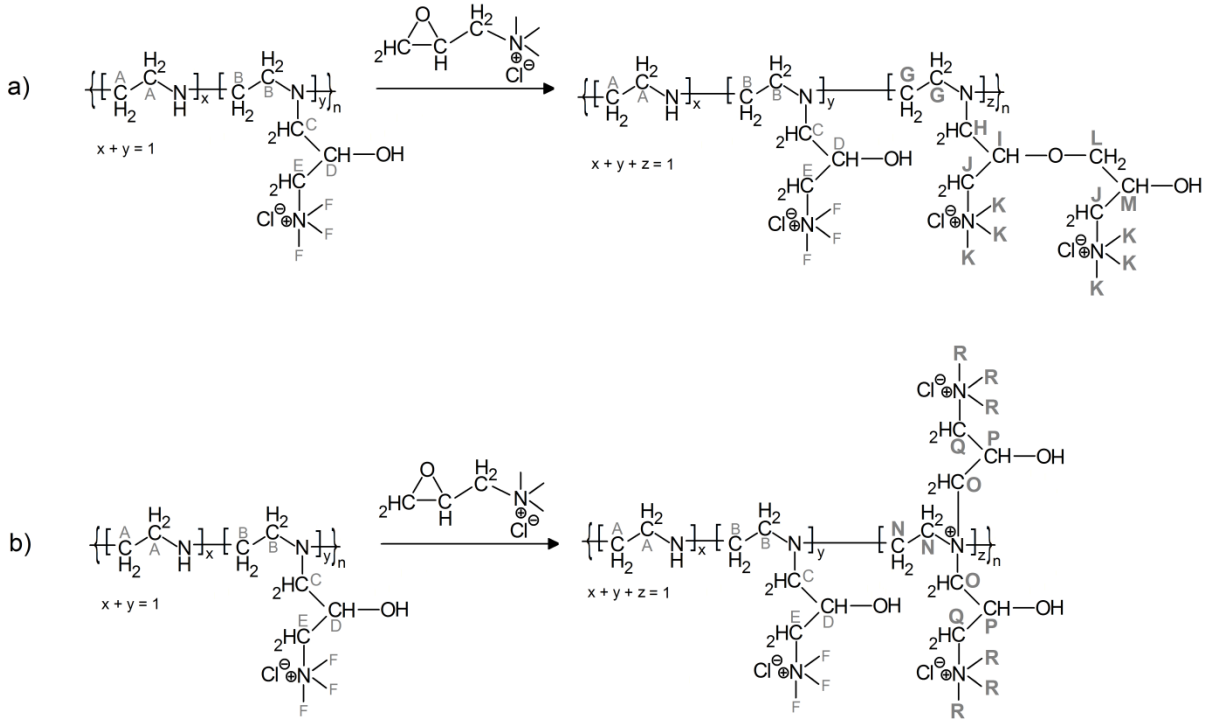

Figure 4-4: Possible side reactions during the addition of glycidyltrimethylammonium chloride to poly-(ethylenimine); a) Addition of quat$_R$ to hydroxyl groups of prior formed 2-hydroxypropylammonium side groups; b) Addition of quat$_R$ to tertiary amino groups of poly(ethylenimine)

The addition of quat$_R$ to hydroxyl groups of prior formed 2-hydroxypropylammonium side groups leads to an etherfication and to two additional resonances in the ^{1}H-NMR-spectra caused by the α-oxygen bonded-methylene (L) and α-oxygen bonded-methine protons (I). The occurrence of the two additional signals in the ^{1}H-NMR-spectra of $\mathrm{PEI}\,{}^{100\mathrm{Q}}_{28}$ (VII) (Figure 4-3b) is in agreement with the expected structural elements for the addition of quat$_R$ to hydroxyl groups of prior formed 2-hydroxypropylammonium side groups. Moreover, the ratio of the integrals between the signals corresponding to the α-oxygen bonded-methylene (L) and the α-oxygen bonded-methine protons (I) are roughly two to one as expected (more details will be given in Chapter 4.3.1.).

The two peaks emerging at 62.2 and 73.3ppm in the ^{13}C-NMR-spectra of $\mathrm{PEI}\,{}^{100\mathrm{Q}}_{28}$ (VII) can be assigned to the α-oxygen bonded-methylene (L) and α-oxygen bonded-methine carbon atoms (I). The splitting of the signal of the α-ammonium bonded-methylene carbon atom (E+J) into a group of three peaks, and of the signals of the hydroxyl-bonded methine carbon atom (D+M), as well as of the α-backbone ammonium bonded-methylene carbon atom (C+H) into four peaks, respectively, is caused by the increasing variety of chemical environment by

the occurrence of the addition of $quat_R$ by etherfication. The appearance of the signals b_C and b_G in the ^{13}C-NMR-spectra of $\mathrm{PEI}_{28}^{100\mathrm{Q}}$ (VII) prove, that even for a nominal conversion of 100%, there are still secondary amino groups left in the polymer, that have not reacted with $quat_R$.

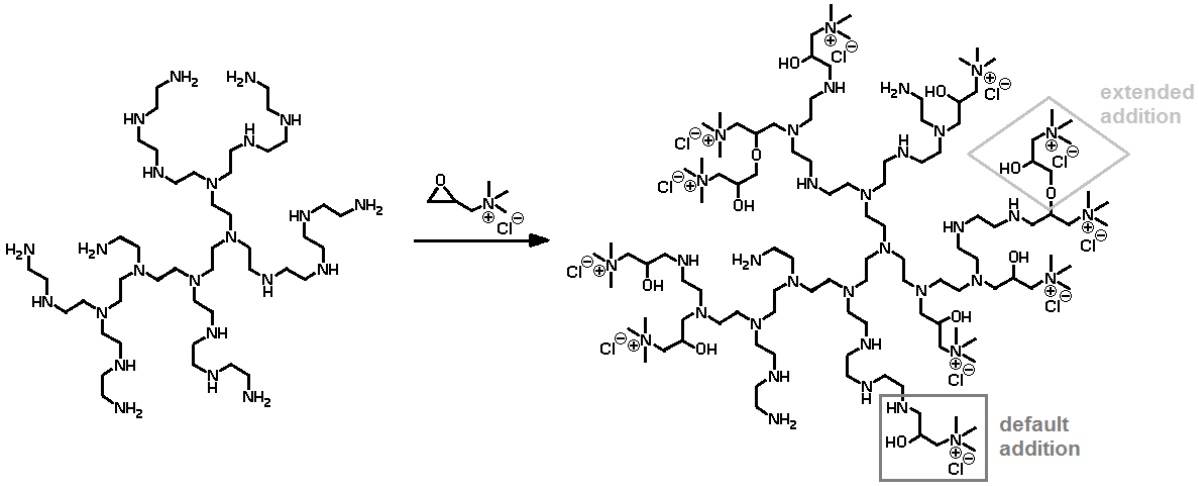

Figure 4-5: Reaction of poly(ethylenimine) with $quat_R$ to partially quaternized poly(ethylenimine)

By comparing the expected signals in the ^{1}H- and ^{13}C-NMR-spectra of partially quaternized poly(ethylenimine) derivatives with the actual found ones, the occurrence of the addition of $quat_R$ to tertiary amino groups of poly(ethylenimine) was ruled out and the emerging of the addition of $quat_R$ to hydroxyl groups of prior formed 2-hydroxypropylammonium side groups was confirmed. Figure 4-5 shows exemplary the expected occurring structural elements for the addition of $quat_R$ to poly(ethylenimine), where the main reaction is the addition of $quat_R$ to primary and secondary amino groups of PEI (labeled as default addition) and a side reaction occurs, where $quat_R$ is added to hydroxyl groups of prior formed 2-hydroxypropylammonium side groups (labeled as extended addition).

In Summary, the structure of the synthesized, partially quaternized poly(ethylenimine) derivatives was confirmed by means of ^{1}H- and ^{13}C-NMR-spectroscopy. All appearing signals were assigned to structural elements of the compounds (cf. Figure 4-5).

4.3. Quantitative composition analysis

The degree of quaternization q has been defined as the ratio between the number of quaternized ethylenimine units per macromolecule and the number average degree of polymerization (cf. Chapter 4.1., Equation 4-1). It has been determined of all synthesized

amino-quat-primer polymers from the ^{1}H-NMR-spectra and from the results of the elementary analysis.

4.3.1. ^{1}H-NMR-spectroscopy

Figure 4-6 depicts a ^{1}H-NMR-spectrum of $\mathrm{PEI}_{28}^{100\mathrm{Q}}$ (VII), indicating the integration regions A_1 – A_3 required for the quantitative analysis. Due to the strong overlap of the broad signals it was not possible to obtain the amount of a structure element from individual signals. Instead an equation system had to be set up and solved for each sample. The area A_1 equals the area of two protons L of the subunit z in Figure 4-4. The area of one proton of subunit z is named H_z (see Equation 4-2). Area A_2 contains the signals of 19 protons K+I of the subunit z and nine protons F of the subunit y. The area of one proton of subunit y is named H_y (see Equation 4-3). The area A_3 is caused by six protons of subunit y (B+C), six protons of the subunit z (G+H) and four protons A of the unmodified subunit x. The area of one proton of subunit x is named is named H_x (see Equation 4-4). The calculations of the molar fraction y_{nmr} and z_{nmr}, as well as the resulting degree of quaternization q_{nmr} are shown in Equation 4-5, Equation 4-6 and Equation 4-7 and their results are listed in Table 4-1 in Chapter 4.3.3., column 4 – 6. The results will be discussed in section 4.3.3. together with the evaluation of elemental analysis data to allow for an easy comparison.

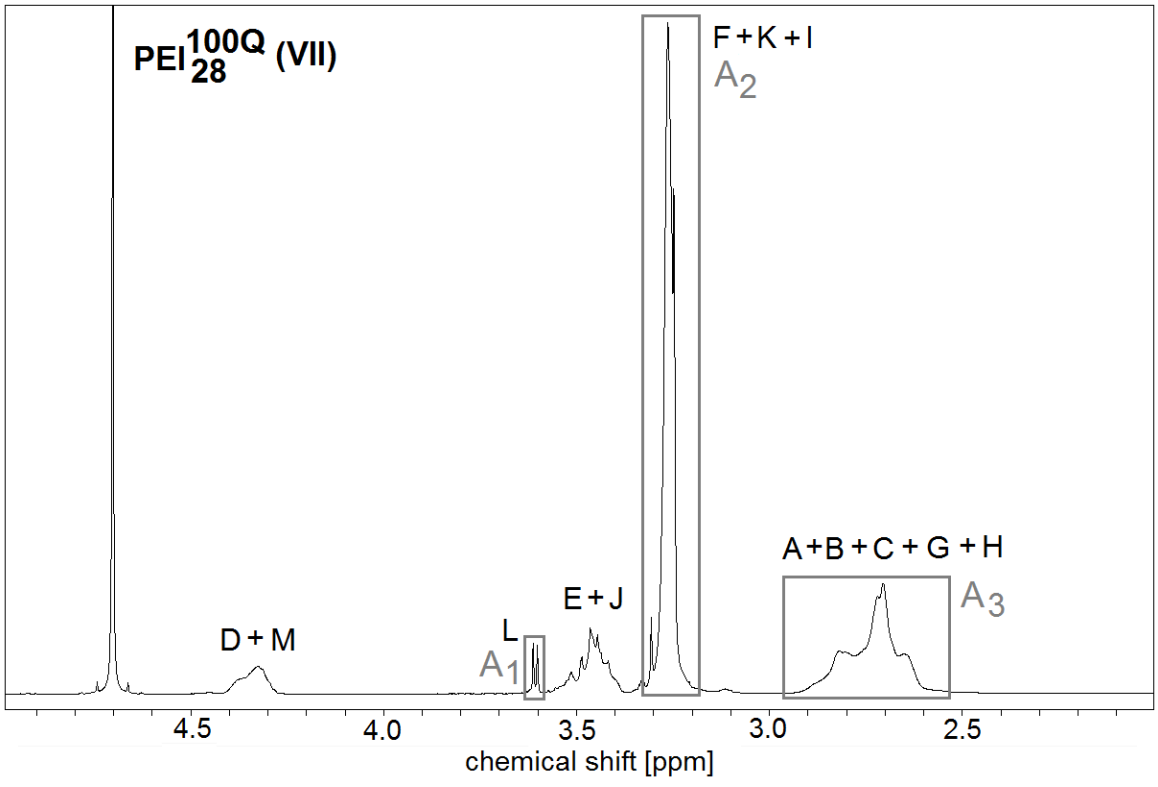

Figure 4-6: ^{1}H-NMR-spectra of PEI_{28}^{100Q} (VII) with marked integration regions

$$H_z = \left(\frac{A_1}{2}\right) \qquad \textit{Equation 4-2}$$

$$H_y = \left(\frac{A_2 - 19\,H_z}{9}\right) \qquad \textit{Equation 4-3}$$

$$H_x = \left(\frac{A_3 - 6\,H_y - 6\,H_z}{4}\right) \qquad \textit{Equation 4-4}$$

$$y_{nmr} = \frac{H_y}{H_x + H_y + H_z} \qquad \textit{Equation 4-5}$$

$$z_{nmr} = \frac{H_z}{H_x + H_y + H_z} \qquad \textit{Equation 4-6}$$

$$q_{nmr} = y + 2\,z \qquad \textit{Equation 4-7}$$

with q_{nmr}: degree of quaternization from ^{1}H-NMR-spectroscopy; H_x: area of a proton of subunit x; H_y: area of a proton of subunit y; H_z: area of a proton of subunit z; y_{nmr}: molar fraction of occurring mono-quaternized subunits y; z_{nmr}: molar fraction of occurring double-quaternized subunits z; A_1, A_2 and A_3: integrals marked in Figure 4-6

4.3.2. Elemental analysis

Referring to the thesis of Beckmann [5] the composition of the PEI^Q polymers can be calculated from the carbon to nitrogen ratio. Elemental analysis only yields the mass ratios between the occurring elements, hence the appearance of etherification and the ratio between the amount of subunits y and z cannot be revealed. The percentage of nitrogen in a partially quaternized poly(ethylenimine) of a structure as shown in Figure 4-5 is given by Equation 4-8. The repetition unit of unmodified poly(ethylenimine) contains one, and the quaternized poly(ethylenimine) subunit contains two nitrogen atoms (Equation 4-9). The simplified equation for the percentage of nitrogen in a partially quaternized poly(ethylenimine) is given by Equation 4-10.

$$p_N = q \cdot p_N(PEI^Q) + (1 - q) \cdot p_N(PEI) \qquad \textit{Equation 4-8}$$

$$p_N = q \cdot A_N \cdot 2 + (1 - q) \cdot A_N \cdot 1 \qquad \textit{Equation 4-9}$$

$$p_N = A_N + q \cdot A_N \qquad \textit{Equation 4-10}$$

with p_N: percentage of nitrogen ;A_N: atomic weight of nitrogen

The percentage of carbon in a partially quaternized poly(ethylenimine) is given by Equation 4-11. The poly(ethylenimine) repetition unit contains two carbon atoms, while a quaternized poly(ethylenimine) subunit consists of eight carbon atoms (Equation 4-12). The simplified equation for the percentage of carbon in a partially quaternized poly(ethylenimine) is given by Equation 4-13.

$$p_C = q \cdot p_C(PEI^Q) + (1 - q) \cdot p_C(PEI) \qquad \textit{Equation 4-11}$$

$$p_C = q \cdot A_C \cdot 8 + (1 - q) \cdot A_C \cdot 1 \qquad \textit{Equation 4-12}$$

$$p_C = 2 \cdot A_C + 6q \cdot A_C \qquad \textit{Equation 4-13}$$

with p_C: percentage of carbon; A_C: atomic weight of carbon

The ratio of carbon to nitrogen is given by Equation 4-14. Resolving this equation to the degree of quaternization q, results in Equation 4-15. The results of the calculation of the degree of quaternization q_{EA} from the data of the elemental analysis are listed in Table 4-1 in Chapter 4.3.3., column 7.

$$\frac{p_C}{p_N} = \frac{2 \cdot A_C + 6q \cdot A_C}{A_N + q \cdot A_N} \qquad \textit{Equation 4-14}$$

$$q = \frac{A_N \cdot p_C - 2\ A_C \cdot p_N}{6\ A_C \cdot p_N - A_N \cdot p_C} \qquad \textit{Equation 4-15}$$

with A_N: atomic weight of nitrogen, A_C: atomic weight of carbon, p_N: percentage of nitrogen, p_C: percentage of carbon

4.3.3. Comparison of ^{1}H-NMR- and elemental analysis results

The degree of quaternization (q_{nmr}), as well as the molar fractions of mono- (y_{nmr}) and double-substituted (z_{nmr}) repetition units of the partially quaternized poly(ethylenimine) derivatives has been determined from the ^{1}H-NMR-spectra. Furthermore, the degree of quaternization (q_{EA}) was alternatively determined from the results of the elementary analysis. The results are listed in Table 4-1.

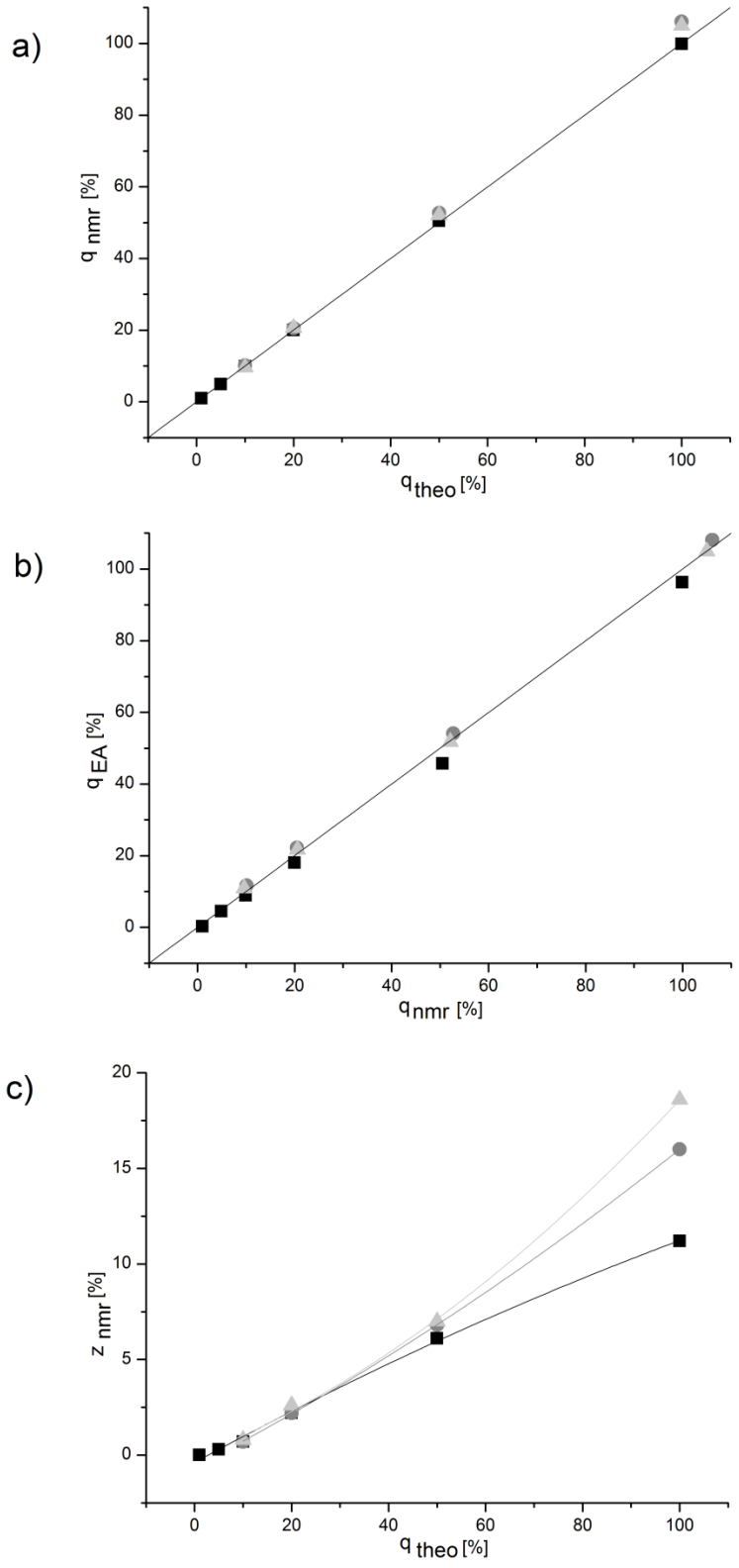

Figure 4-7a): Calculated degree of quaternization from ^{1}H-NMR-spectroscopy (q_{nmr}) as a function of theoretical values (q_{THEO}); b) Calculated degree of quaternization from elemental analysis (q_{EA}) as a function of calculated values from ^{1}H-NMR-spectroscopy (q_{nmr}); c) Molar fractions of double-substituted repetition units (z_{nmr}) as a function of theoretical values (q_{THEO}); black dots: PEI_{28}^{qQ}, dark grey circles: PEI_{232}^{qQ}, light grey triangles: PEI_{1393}^{qQ}

Table 4-1: Degree of quaternization q of the amino-quat-primer derivatives: theoretical values (q_{THEO}),calculated values from ^{1}H-NMR-spectroscopy (q_{nmr}), elemental analysis (q_{EA}), and molar fractions of mono- (y_{nmr}) and double-substituted (z_{nmr}) repetition units

No.	Polymer	q_{theo} [%]	y_{nmr} [%]	z_{nmr} [%]	q_{nmr} [%]	q_{EA} [%]
(II)	PEI_{28}^{1Q}	1	1.0	0.0	1.0	0.3
(III)	PEI_{28}^{5Q}	5	4.3	0.3	4.9	4.5
(IV)	PEI_{28}^{10Q}	10	8.5	0.7	9.9	8.9
(V)	PEI_{28}^{20Q}	20	15.7	2.2	20.0	18.0
(VI)	PEI_{28}^{50Q}	50	38.4	6.1	50.5	45.7
(VII)	PEI_{28}^{100Q}	100	77.6	11.2	99.9	96.3
(IX)	PEI_{232}^{10Q}	10	8.7	0.7	10.1	11.7
(X)	PEI_{232}^{20Q}	20	16.0	2.2	20.5	22.2
(XI)	PEI_{232}^{50Q}	50	39.1	6.8	52.7	54.1
(XII)	PEI_{232}^{100Q}	100	74.2	16.0	106.1	108.1
(XIV)	PEI_{1393}^{10Q}	10	8.0	0.8	9.6	10.9
(XV)	PEI_{1393}^{20Q}	20	15.4	2.6	20.6	21.7
(XVI)	PEI_{1393}^{50Q}	50	38.2	7.0	52.1	51.8
(XVII)	PEI_{1393}^{100Q}	100	67.7	18.6	105.0	104.9

The theoretical values q_{theo} (column 3, Table 4-1) are the targeted values as determined by the experimentally used monomer unit to quat ratios.

Figure 4-7a) depicts the from ^{1}H-NMR-spectroscopy calculated values of the degree of quaternization (q_{nmr}) as a function of theoretical values (q_{THEO}). The black curve indicates the ideal case of identical values of the theoretical and calculated values. The calculated values are in very good agreement with the theoretical values. The deviation of the calculated

values from the theoretical values is smaller than one percent for all investigated samples except the four samples with the degree of quaternization of $q_{THEO} \geq 50\%$ and $X_n \geq 232$, where the deviation ranges between 2.1 and 6.1 percent.

Figure 4-7b) illustrates the relation of q as obtained from the elemental analysis (q_{EA}) and from ^{1}H-NMR-spectroscopy (q_{nmr}). The black line indicates the ideal case of identical values of the calculated values from the ^{1}H-NMR-spectroscopy and the one from the elemental analysis. Both analysis methods are in very good agreement with the theoretical values based on the experimental conditions. The deviation of the calculated values from the elemental analysis to the calculated values from the ^{1}H-NMR-spectroscopy is smaller than two percent for all investigated samples except the two samples with the degree of quaternization of $q_{THEO} \geq 50\%$ and $X_n = 28$, where the deviation still is below five percent.

Figure 4-7c) shows the molar fraction of double-substituted repetition units (z_{nmr}) calculated from the ^{1}H-NMR-spectroscopy as a function of theoretical values (q_{THEO}). The three curves connect the values for each degree of polymerization. The molar fraction of double-substituted repetition units increases with an increasing theoretical degree of quaternization for all three degrees of polymerization. With the highest investigated degree of quaternization of q = 100%, z_{nmr} with the highest degree of polymerization $X_n = 1393$ is significant larger than with the intermediate and the lowest degree of polymerization ($X_n = 28$, $z_{nmr} = 11.2\%$; $X_n = 232$, $z_{nmr} = 16.0\%$; $X_n = 1393$, $z_{nmr} = 18.6\%$). This can be explained by the limited accessibility of the amino group protons in the inner part of the polymer. This effect should be larger at higher degrees of polymerization and at higher degrees of quaternization.

The degree of quaternization of all synthesized, partially quaternized poly(ethylenimine) derivatives was determined by means of ^{1}H-NMR-spectroscopy, as well as elemental analysis and the results are in reasonable agreement with the theoretical values. For this reason in the subsequent text, the theoretical values of the degrees of quaternization q_{THEO} ($q_{THEO} \approx q_{nmr} \approx q_{EA}$) will be used simplified as q.

4.4. Theoretical molecular weights and diameters

The theoretical values of the number average molecular weight of the synthesized partially quaternized poly(ethylenimine) derivatives can be calculated based on the degree of quaternization and the degree of polymerization of each derivative employing Equation 4-16 (values listed in Table 4-2, column 3). The volume of a single molecule of the partially quaternized poly(ethylenimine) derivatives can be determined from the molecular weight of

the polymer and its density (see Equation 4-17; values listed in Table 4-2, column 4). To estimate its diameter, the polymer molecule is assumed to be a sphere, which is a good assumption for hyperbranched polymers [6]. The diameter of a sphere as a function of its volume is given in Equation 4-18. The calculated theoretical values of the diameter of a single molecule of the polymers PEI_{28} (I) – $\mathrm{PEI}_{1393}^{100\mathrm{Q}}$ (XVII) are listed in Table 4-2, column 5.

$$\mathrm{M_{theo}} = \left(\mathrm{M_{EI}} + \frac{\mathrm{q}}{100} \cdot \mathrm{M_{quatR}}\right) \cdot \mathrm{X_n} \qquad \textit{Equation 4-16}$$

$$\mathrm{V_{theo}} = \frac{\mathrm{M_{theo}}}{\mathrm{N_A} \cdot \rho_{\mathrm{PEI}}} \qquad \textit{Equation 4-17}$$

$$\mathrm{d_{theo}} = 2\mathrm{r_{theo}} = 2 \cdot \sqrt[3]{\frac{3 \cdot \mathrm{V_{theo}}}{4 \cdot \pi}} \qquad \textit{Equation 4-18}$$

with $\mathrm{M_{theo}}$: theoretical molecular weight; M_{EI}: molecular weight of a ethylenimine subunit ($\mathrm{M_{EI}} = 43.069\ \frac{\mathrm{g}}{\mathrm{mol}}$); q: degree of quaternization; M_{quatR}: molecular weight of $quat_R$ ($\mathrm{M_{quatR}} = 151.63\ \frac{\mathrm{g}}{\mathrm{mol}}$); X_n: degree of polymerization; V_{theo}: theoretical volume; N_A: Avogadro constant; ρ_{PEI}: densitiy of PEI ($\rho = 1.03 * 10^6\ g/m^3$ [7]); d_{theo}: theoretical diameter; r_{theo}: theoretical radius

Table 4-2: Theoretical values of the molecular weight, the volume and diameter of single molecules of the polymers PEI_{28} (I) – PEI_{1393}^{100Q} (XVII)

No.	Polymer	$M_{N\_theo}^{PEI^Q}$ [kg/mol]	V_{theo} [m^3]	d_{theo} [nm]
(I)	PEI_{28}	1.20	$1.93*10^{-27}$	1.55
(II)	$\mathrm{PEI}_{28}^{1\mathrm{Q}}$	1.25	$2.01*10^{-27}$	1.57
(III)	$\mathrm{PEI}_{28}^{5\mathrm{Q}}$	1.42	$2.29*10^{-27}$	1.63
(IV)	$\mathrm{PEI}_{28}^{10\mathrm{Q}}$	1.63	$2.63*10^{-27}$	1.71
(V)	$\mathrm{PEI}_{28}^{20\mathrm{Q}}$	2.06	$3.31*10^{-27}$	1.85
(VI)	$\mathrm{PEI}_{28}^{50\mathrm{Q}}$	3.33	$5.37*10^{-27}$	2.17
(VII)	$\mathrm{PEI}_{28}^{100\mathrm{Q}}$	5.45	$8.79*10^{-27}$	2.56

No.	Polymer	$M_{N\_theo}^{PEI^Q}$ [kg/mol]	V_{theo} [m^3]	d_{theo} [nm]
(IX)	PEI_{232}	10.00	$1.61*10^{-26}$	3.13
(IX)	PEI_{232}^{10Q}	13.51	$2.18*10^{-26}$	3.46
(X)	PEI_{232}^{20Q}	17.03	$2.75*10^{-26}$	3.74
(XI)	PEI_{232}^{50Q}	27.58	$4.45*10^{-26}$	4.40
(XII)	$\mathrm{PEI}_{232}^{100Q}$	45.17	$7.28*10^{-26}$	5.18
(XIII)	PEI_{1393}	60.00	$9.67*10^{-26}$	5.70
(XIV)	$\mathrm{PEI}_{1393}^{10Q}$	81.12	$1.31*10^{-25}$	6.30
(XV)	$\mathrm{PEI}_{1393}^{20Q}$	102.24	$1.65*10^{-25}$	6.80
(XVI)	$\mathrm{PEI}_{1393}^{50Q}$	165.61	$2.67*10^{-25}$	7.99
(XVII)	$\mathrm{PEI}_{1393}^{100Q}$	271.22	$4.37*10^{-25}$	9.42

The theoretical values of the molecular weight, volume and diameter increase with an increasing degree of polymerization X_n, as well as with an increasing degree of quaternization q. The theoretical diameter of $\mathrm{PEI}_{1393}^{100Q}$ (XVII), the substance with the highest degree of polymerization and the highest degree of quaternization (d_{theo} = 9.4nm), is about six times larger than the one of PEI_{28} (I), the substance with the lowest degree of polymerization and without quaternization (d_{theo} = 1.6nm).

4.5. Thermal characterization

The thermal behavior of the partially, quaternized poly(ethylenimine) derivatives was investigated by means of differential scanning calorimetry. Three heating and two cooling curves were recorded between -80°C and +50°C with heating and cooling rates of 10K/min. Figure 4-8 illustrates exemplary the thermograms of the second heating for the derivatives PEI_{1393}^{qQ} ((XIV) – (XVII)) depicted with a y-axis offset. All curves for all four different degrees of quaternization exhibit a glass transition point. With an increasing degree of quaternization, the temperature T_G of the glass transition is shifted to higher values and the temperature range ΔT_G of the glass transition increases. An increase of the width of the glass transition area complicates the determination of the glass transition point and leads to higher

uncertainties. Moreover, for the both derivatives with the highest degrees of quaternization (q = 50, 100%), there might be two glass transition points in the curve. Nevertheless, one glass transition point as the turning point of the whole temperature range of the transition was determined as an average temperature.

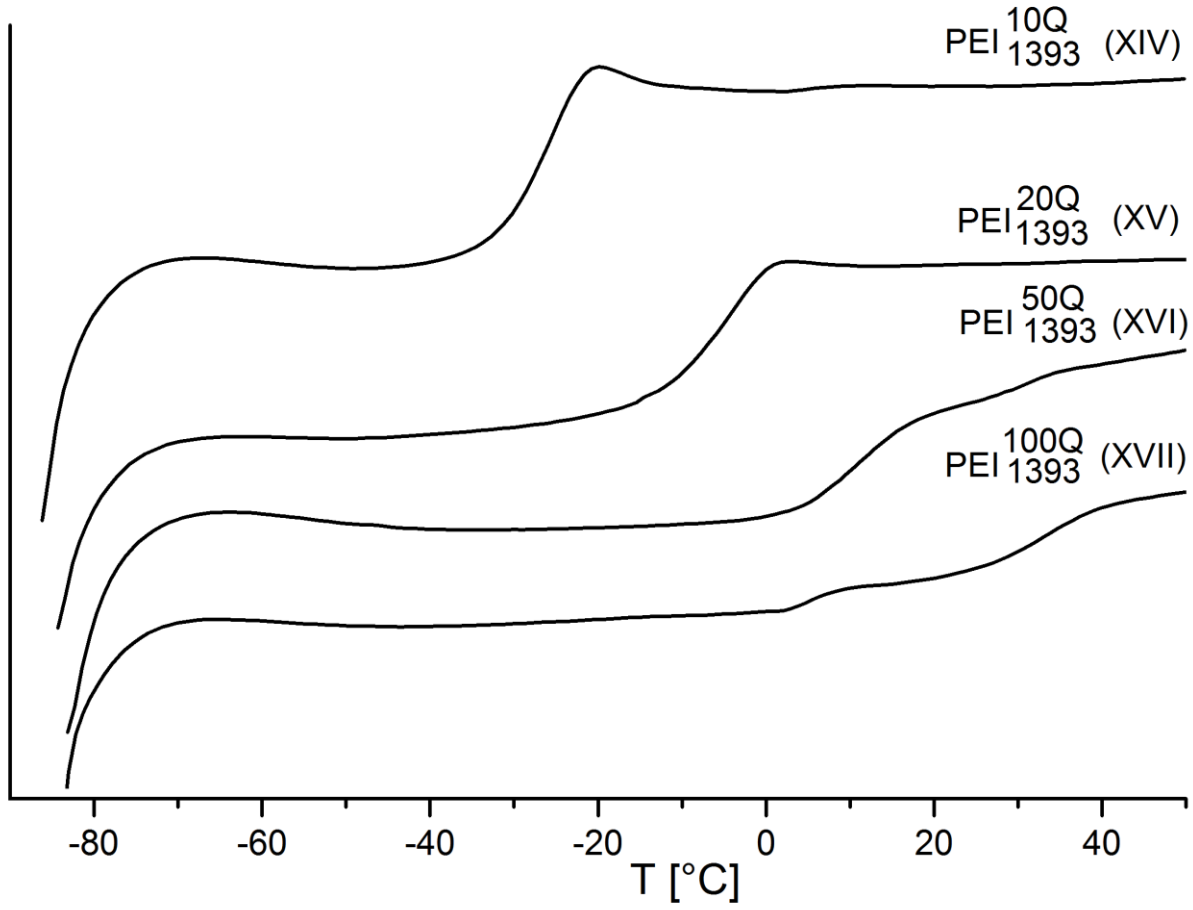

Figure 4-8: Thermograms of the second heating for the partially, quaternized poly(ethylenimine) derivatives PEI_{1393}^{qQ} ((XIV) – (XVII))

Figure 4-9 shows the glass transition temperature T_G as a function of the degree of quaternization for all three degrees of polymerization. The general trend of T_G as a function of q is independent of X_n, since T_g increases with increasing degree of quaternization from -52.1°C for PEI_{28} (I) to 32.2°C for $\mathrm{PEI}_{28}^{100\mathrm{Q}}$ (VII) (cf. experimental part, Chapter 3.3.). Despite the high discrepancies between the glass transition temperatures for a given degree of quaternization and different degrees of polymerization, which can be explained by the difficulties of the determination from the broad signals in the thermograms, the glass transition temperature is assumed to be independent of the degree of polymerization for the investigated samples.

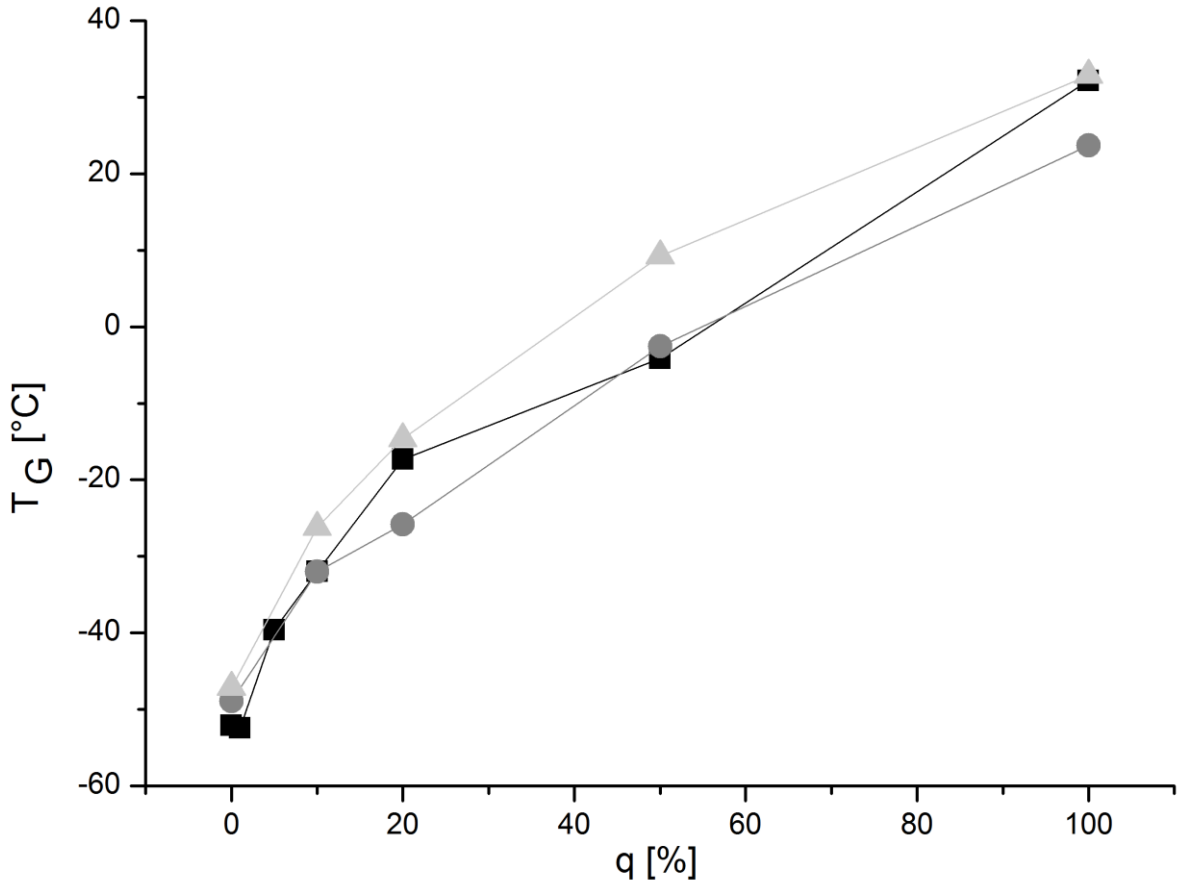

Figure 4-9: Glass temperatures determined from the second heating as a function of the degree of quaternization for the partially, quaternized poly(ethylenimine) derivatives $PEI_{X_n}^{qQ}$ ***((I) – (XVII); black squares:*** PEI_{28}^{qQ} ***, dark grey circles:*** PEI_{232}^{qQ}***, light grey triangles:*** PEI_{1393}^{qQ}

4.6. Solubility

Table 4-3 summarizes the solubility of the partially quaternized poly(ethylenimine) derivatives in ten different solvents. 10-12mg of the substances was mixed with 1ml of a solvent, the samples were placed on a rocking plate for 24 hours at room temperature, and afterwards the solubility was judged. Dimethylformamide, water, methanol, ethanol, acetone, ethyl acetate, chloroform, tetrahydrofuran, toluene and petroleum ether were employed as solvents. The solubility in the ten employed solvents was found to be the same for all synthesized, partially quaternized poly(ethylenimine) derivatives. They are soluble in protic polar solvents like water, methanol and ethanol, but insoluble in all other investigated solvents.

Table 4-3: Solubility of partially quaternized poly(ethylenimine) derivatives (RT; 10-12mg substance in 1ml solvent)

polymer	DMF	H_2O	MeOH	EtOH	Ac	EA	$CHCl_3$	THF	Tol	PE
$PEI_{x_n}^{qQ}$	---	X	X	X	---	---	---	---	---	---

q: degree of quaternization (q = 1, 5, 10, 20, 50, 100%); X_n: degree of polymerization (X_n=28,232,1393); X: soluble, ---: insoluble, DMF: dimethylformamide; H_2O: water; MeOH: methanol; EtOH: ethanol; Ac: acetone; EA: ethyl acetate; $CHCl_3$: chloroform; THF: tetrahydrofuran; Tol: toluene; PE: petroleum ether

4.7. pH of polymer-water-solutions

The pH of solutions of partially quaternized poly(ethylenimine) derivatives in water was measured as a function of the polymer concentration c_p. The results are illustrated in Figure 4-10 (values listed in Table I-1, Appendix).

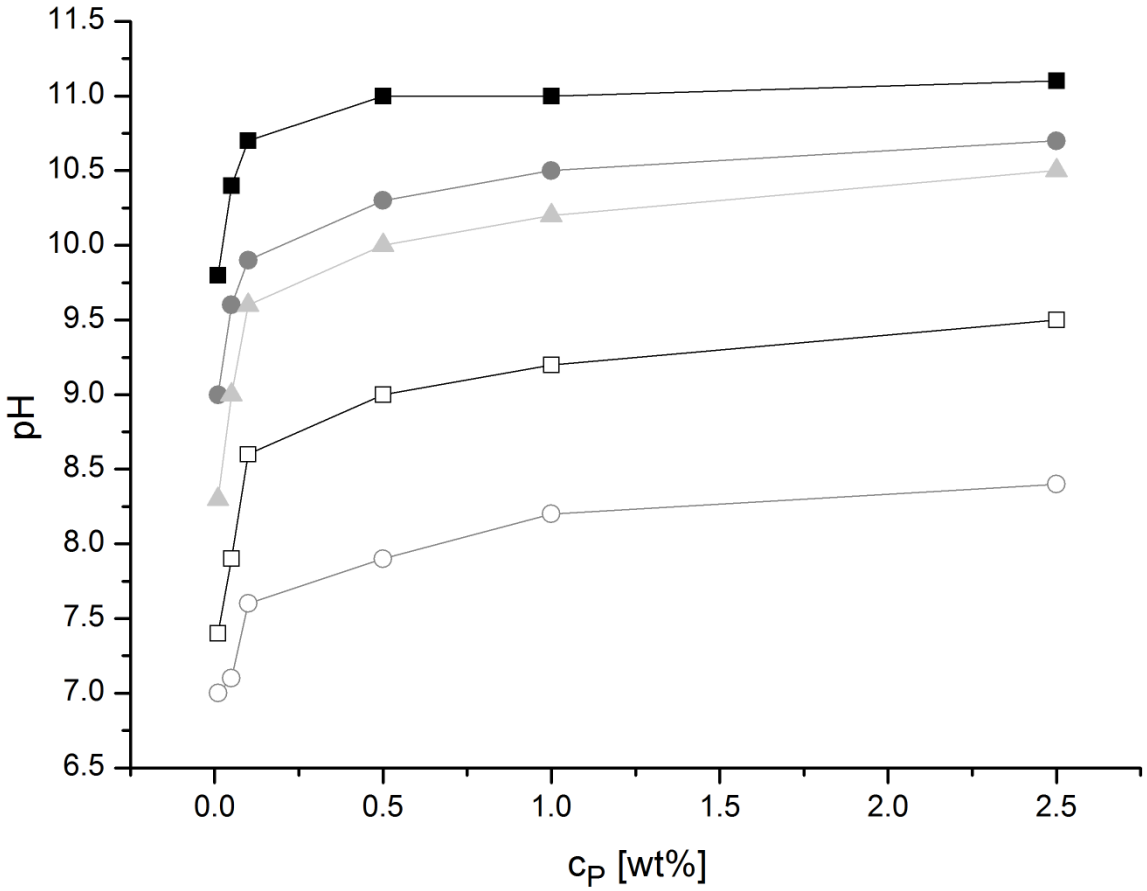

Figure 4-10: pH of polymer-water-solutions as a function of polymer concentration c_P for the five polymers with the highest degree of polymerization PEI_{1393} (XIII) – PEI_{1393}^{100Q} (XVII); filled back squares: PEI_{1393} (XIII), filled dark grey circles: PEI_{1393}^{10Q} (XIV), filled light grey triangles: PEI_{1393}^{20Q} (XV), empty black squares: PEI_{1393}^{50Q} (XVI), empty dark grey circles: PEI_{1393}^{100Q} (XVII)

Six samples of each of the five polymers with the same degree of polymerization (X_n = 1393), but different degrees of quaternization (q = 0, 10, 20, 50 and 100%) were employed (PEI_{1393}(XIII) – $\mathrm{PEI}_{1393}^{100\mathrm{Q}}$(XVII)). The general trend of the solution pH for all investigated polymers as a function of the polymer concentration is similar. The pH increases rapidly at small polymer concentrations (c_P < 0.1wt%) and afterwards converges to a plateau value. The pure poly(ethylenimine) reaches the plateau value at a smaller polymer concentration than the partially quaternized derivatives. Figure 4-11 depicts the pH value at a polymer concentration of 2.5wt% (= plateau value) as a function of the degree of quaternization for the five polymers with the highest degree of polymerization. The decrease of the pH with an increasing degree of quaternization is linear with a slope of $\mathrm{m} = -0.027\ \frac{1}{\%}$. All polymer-water-solutions exhibit an alkaline pH, which increases with an increasing polymer concentration and a decreasing degree of quaternization.

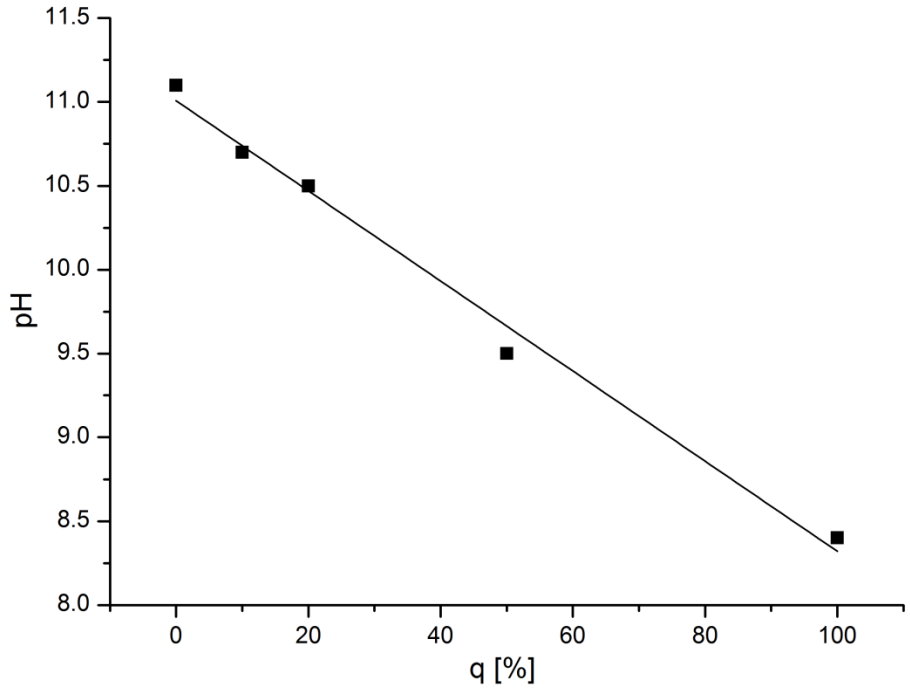

Figure 4-11: pH value at a polymer concentration of 2.5wt% as a function of the degree of quaternization for the polymers with the highest degree of polymerization PEI_{1393} (XIII) – PEI_{1393}^{100Q} (XVII)

4.8. Degree of protonation

The pH change of polymer-water-solutions on addition of acid or base was investigated to determine the polymers degree of protonation depending on their different degrees of quaternization. Three polymer solutions of each of the five polymers with the highest degree

of polymerization PEI_{1393} (XIII) – $\mathrm{PEI}_{1393}^{100\mathrm{Q}}$ (XVII) have been prepared. Each solution had a total mass of 10g, and contained 0.01wt% polymer. One solution of each polymer was titrated with 0.01M HCl, 0.001M HCl, and with 0.001M NaOH in water (see Table I-2, Appendix). The measured values of the pH were noted for a known added volume of the titrant. From the added volume and the known concentration of the titrant, the amount of added protons or hydroxide ions has been determined (see Equation 4-19 or Equation 4-20 respectively).

$$\mathrm{n}\,(\mathrm{H}^+)[\mathrm{mol}] = \mathrm{C}_{\mathrm{H}+}\left[\frac{\mathrm{mol}}{\mathrm{L}}\right] \cdot \mathrm{V}_{\mathrm{H}+}\,[\mathrm{L}] \qquad \textit{Equation 4-19}$$

$$\mathrm{n}\,(\mathrm{OH}^-)[\mathrm{mol}] = \mathrm{C}_{\mathrm{OH}-}\left[\frac{\mathrm{mol}}{\mathrm{L}}\right] \cdot \mathrm{V}_{\mathrm{OH}-}\,[\mathrm{L}] \qquad \textit{Equation 4-20}$$

with $n(H^+)$: amount of added protons; C_{H+}: concentration of the acidic solution; V_{H+}: added volume of the acidic solution; $n(OH^-)$: amount of added hydroxide ions; C_{OH-}: concentration of the alkaline solution; V_{OH-}: added volume of the alkaline solution

The results of the three titrations of each polymer solution were put together to one plot. Figure 4-12 shows the pH of a polymer-water-solution as a function of the added proton or hydroxide ion concentration for the five polymers PEI_{1393}(XIII) – $\mathrm{PEI}_{1393}^{100\mathrm{Q}}$ (XVII) and pure water as a reference. The starting pH of the titrations, the pH of the polymer solutions of 0.01wt% was 9.8, 9.0, 8.3, 7.4 and 7.0, respectively for the polymers with a degree of quaternization of 0, 10, 20, 50 and 100% (values listed in Table I-1, Appendix). Under addition of protons the pH of the polymer solutions decreases slower than the one of the reference. The polymer has the effect of a buffer, it can be protonated and because of this the polymer solution retains a higher pH compared to water. The decrease is stronger for the partially quaternized polymers than for the pure polymer, which means that at a given amount of protons the pH of the partially quaternized polymer solutions is lower than for the pure poly(ethylenimine). This can be explained by the higher amount of primary and secondary amino groups of the pure polymer, which are protonated faster than tertiary amino groups [8]. Between a pH of 3 and 4, this sequence changes and at a given amount of protons the pH for the pure poly(ethylenimine) is lower than for the partially quaternized derivatives. It is assumed that a rearrangement of the chloride counterions may happen, so that more counterions are condensated to the polyion and less quaternary amino groups contribute to the effective charge, which might allow a further protonation of the amino groups.

On addition of hydroxide ions the pH of the polymer solutions increases slower than for the reference. The polymers are protonated in a polymer-water-solution. With increasing the pH, protons are released from the polymer, which results in a smaller pH in comparison with pure water. The increase is stronger for the partially quaternized polymers than for the pure polymer, which means that at a given amount of hydroxide ions the pH for the partially quaternized polymers is higher than for the pure poly(ethylenimine). The reason for this is again the higher amount of primary and secondary amino groups in the pure polymer.

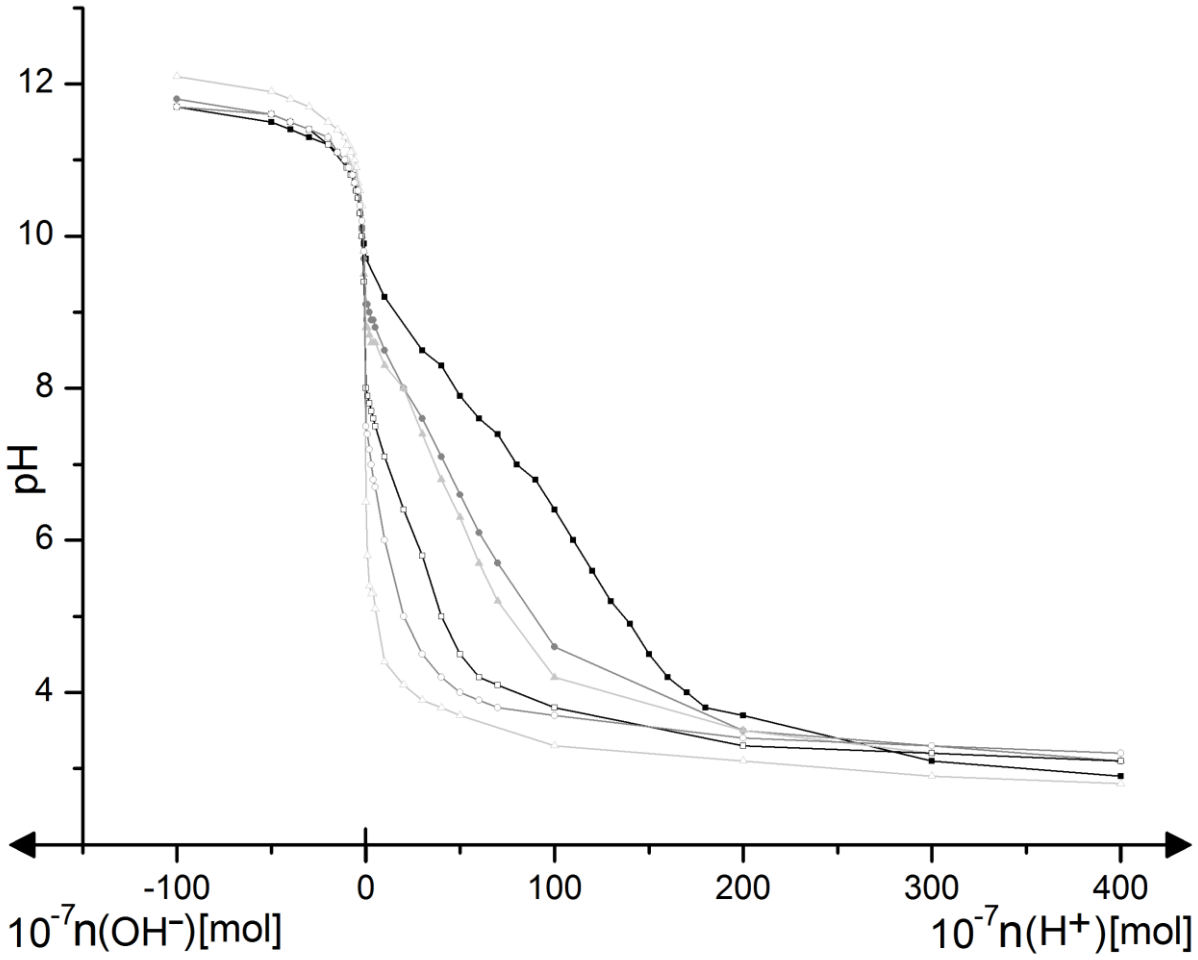

Figure 4-12: pH as a function of proton / hydroxide ion concentration for polymer solutions of PEI_{1393} (XIII) – PEI_{1393}^{100Q} (XVII) and pure water; filled back squares: PEI_{1393} (XIII), filled dark grey circles: PEI_{1393}^{10Q} (XIV), filled light grey triangles: PEI_{1393}^{20Q} (XV), empty black squares: PEI_{1393}^{50Q} (XVI), empty dark grey circles: PEI_{1393}^{100Q} (XVII); empty light grey triangles: water

The proton or hydroxide ion concentration for each polymer solution was determined graphically in 0.5 pH-steps between pH 5 and the particular starting pH out of Figure 4-12.

To remove the effect of water in the polymer solutions the values of $n(H^+)_{H2O}$ for each pH was subtracted from the values of the polymer solution $n(H^+)_{PS}$ resulting in $n(H^+)_P$ the amount of protons on the polymer molecules (see Equation 4-21).

$$n(H^+)_P = n(H^+)_{PS} - n(H^+)_{H2O} \qquad \textit{Equation 4-21}$$

with $n(H^+)_P$: amount of protons on the polymer molecules; $n(H^+)_{PS}$: amount of protons in the polymer solution, $n(H^+)_{H2O}$: amount of protons in the reference

The degree of protonation α (see Equation 4-22) is defined as the ratio between the number of protons per number of polymer molecules per degree of polymerization. It can be derived from the amount of protons on the polymer molecules $n(H^+)_P$.

$$\alpha = \frac{N(H^+)}{N_p \cdot X_n} = \frac{n(H^+)_P \cdot M_{SU}}{m_{tot}} \qquad \textit{Equation 4-22}$$

with α: degree of protonation; $N(H^+)$: number of protons; N_P: number of polymer molecules; X_n: degree of polymerization; $n(H^+)_P$: amount of protons on the polymer molecules; M_{SU}: molecular mass of the subunit; m_{tot}: total mass of the sample (prior to titration)

Figure 4-13 shows the degree of protonation α as a function of pH for the polymers PEI_{1393} (XIII) – PEI_{1393}^{100Q} (XVII) (values listed in Table I-3, Appendix). Note that the polymers are already slightly protonated in the polymer-water-solution without any addition of acid. The illustrated values of the degree of protonation show the increase of the degree of protonation from the polymer-water-solution under addition of acid. At a pH of around 10, all investigated partially quaternized poly(ethylenimine) derivatives exhibit a degree of protonation of zero, i.e. they are not protonated. For more acidic conditions the polymers get further positively charged. The charge of pure poly(ethylenimine) roughly grows linearly between pH 10 to pH 5 up to α = 0.56. The partially quaternized poly(ethylenimine) derivatives did not develop further charges over a broader pH range. The start of the protonation is shifted to a smaller pH value with an increasing degree of quaternization. The slope of the increase of the degree of protonation as a function of the pH is almost equal for all investigates polymers and therefore independent of the degree of quaternization.

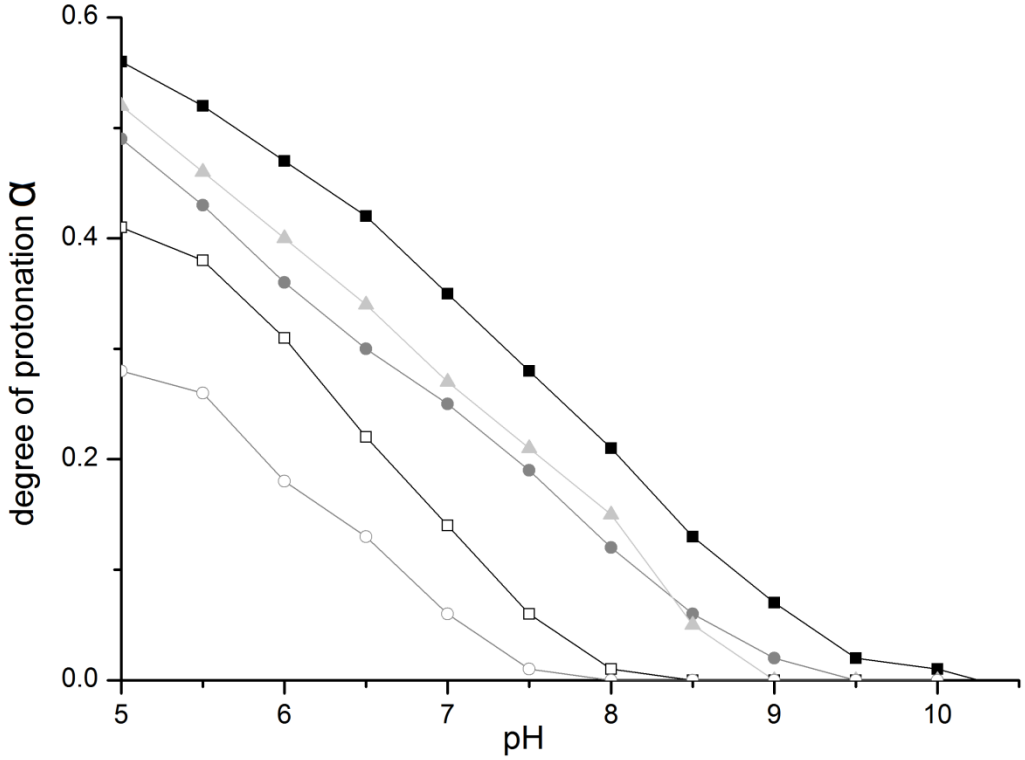

Figure 4-13: Degree of protonation α as a function of pH for the polymers PEI_{1393} (XIII) – PEI_{1393}^{100Q} (XVII); filled back squares: PEI_{1393} (XIII), filled dark grey circles: PEI_{1393}^{10Q} (XIV), filled light grey triangles: PEI_{1393}^{20Q} (XV), empty black squares: PEI_{1393}^{50Q} (XVI), empty dark grey circles: PEI_{1393}^{100Q} (XVII)

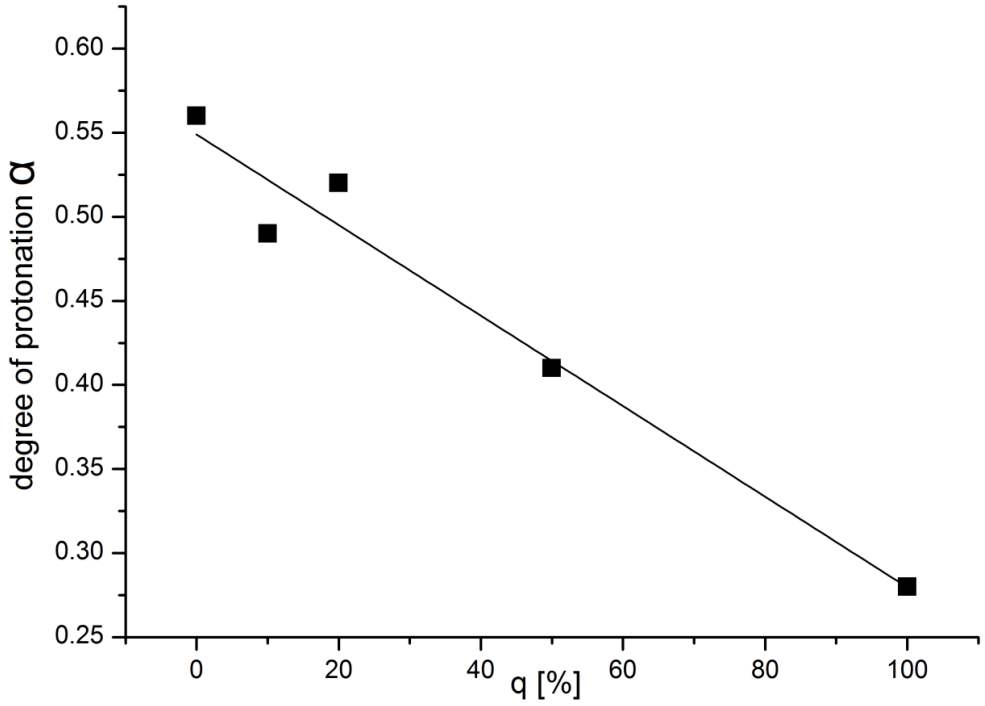

Figure 4-14: Degree of protonation at pH 5 as a function of the degree of quaternization for the polymers PEI_{1393} (XIII) – PEI_{1393}^{100Q} (XVII)

Figure 4-14 illustrates the degree of protonation at pH 5 as a function of the degree of quaternization for the polymers PEI_{1393} (XIII) – $\mathrm{PEI}_{1393}^{100\mathrm{Q}}$ (XVII). The degree of protonation decreases linearly with a slope of $\mathrm{m} = -0.0027\ \frac{1}{\%}$ with an increasing degree of quaternization.

The quaternization of poly(ethylenimine) results in a weaker protonation of the polymer and therefore leads to a more stable amount of charge against pH variation. The reason for this is the higher amount of primary and secondary amino groups of less quaternized polymers. Primary amino groups protonate faster than secondary amino groups and secondary amino groups fast than tertiary amino groups (cf. literature review, Chapter 2.2.3.) [8].

4.9. Electrophoretic mobility

The electrophoretic mobility of solutions of the partially quaternized poly(ethylenimine) derivatives PEI_{1393} (XIII) – $\mathrm{PEI}_{1393}^{100\mathrm{Q}}$ (XVII) in water was measured for three different molar polymer concentrations c_P = 3.33mM, 6.66mM and 13.33mM at a constant salt concentration of 0.1mM sodium chloride by means of Laser-Doppler-velocimetry (cf. literature review, Chapter 2.5.2.).

Figure 4-15 illustrates the macromolecule's electrophoretic mobility as a function of the degree of quaternization (values listed in Table I-4, Appendix). Over all there appears a trend that the values of the electrophoretic mobility increase with an increasing degree of quaternization from 0 until 50%. The electrophoretic mobility of $\mathrm{PEI}_{1393}^{100\mathrm{Q}}$ (XVII), however, is notably smaller than the one of $\mathrm{PEI}_{1393}^{50\mathrm{Q}}$(XVI). Based on the fact, that $\mathrm{PEI}_{1393}^{100\mathrm{Q}}$ (XVII) bears formally twice the amount of fixed, introduced positive charges on the polymer than $\mathrm{PEI}_{1393}^{50\mathrm{Q}}$(XVI), an increase of the electrophoretic mobility with an increasing degree of quaternization was expected, which is not found experimentally. Further investigations to explain this trend will be presented later. The discrepancy between the measured values for one polymer for the three different molar concentrations is so big that they do not fit together in their standard deviations. However, there is no trend for all investigated polymers that either the higher or the lower molecular concentration results in higher values of the electrophoretic mobility.

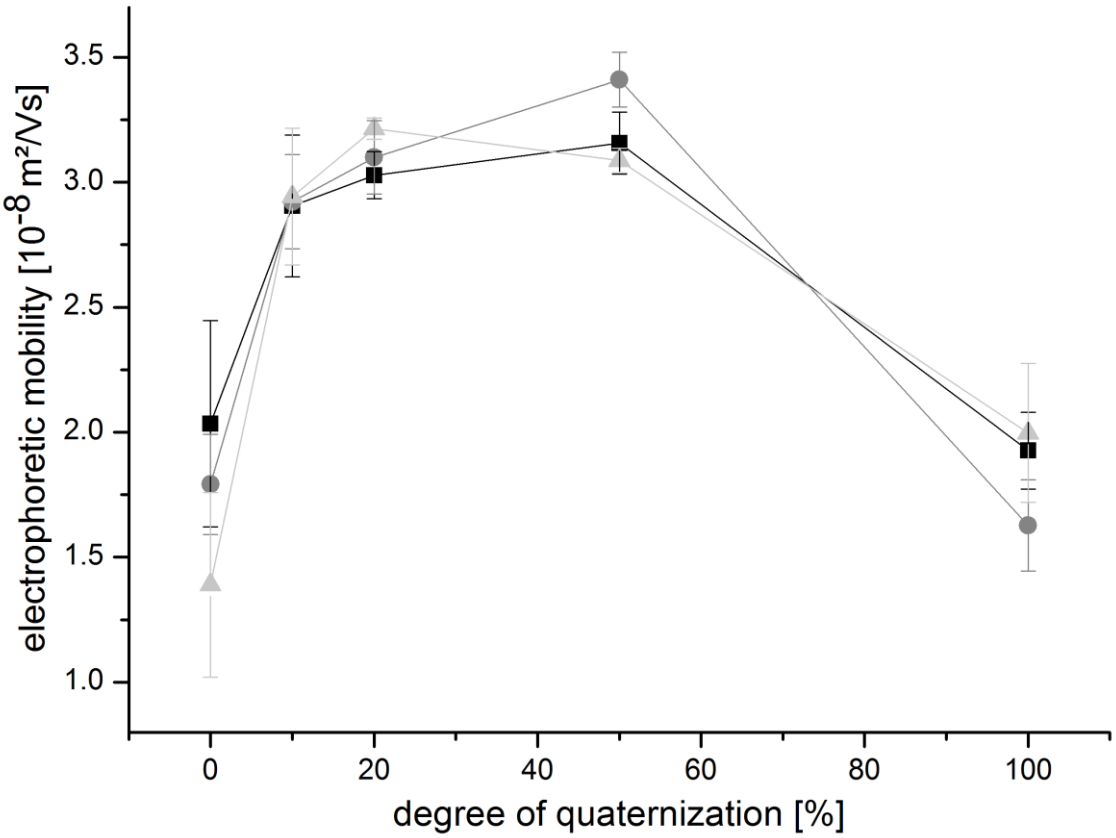

Figure 4-15: Electrophoretic mobility of partially quaternized poly(ethylenimine) derivatives PEI_{1393} (XIII) – PEI_{1393}^{100Q} (XVII) as a function of the degree of quaternization for three different molar concentration; black squares: c_p = 3.33mM, dark grey circles : c_p = 6.66mM; light grey triangles: c_p = 13.33mM

4.10. Effective charge

Poly(ethylenimine) was partially modified with glycidyltrimethylammonium chloride ($quat_R$) to exhibit fixed positive charges. The number of fixed positive charges n_{c+} of one polymer molecule is assigned by the product of its degree of polymerization X_n and its degree of quaternization q divided by 100 (see Equation 4-23). The number of fixed positive charges n_{c+} for each synthesized, partially quaternized poly(ethylenimine) derivative PEI_{28} (I) – $\mathrm{PEI}_{1393}^{100\mathrm{Q}}$ (XVII) is listed in Table 4-4, Column 5. Because of the much higher degree of polymerization, one molecule of the polymer $\mathrm{PEI}_{1393}^{100\mathrm{Q}}$ (VII) exhibits fifty times more fixed positive charges than one molecule of the polymer $\mathrm{PEI}_{28}^{100\mathrm{Q}}$ (I) with the same degree of quaternization q.

$$n_{c+} = \frac{X_n \cdot q}{100}$$ ***Equation 4-23***

with n_{c+}: number of fixed positive charges; X_n: degree of polymerization; q: degree of quaternization

Table 4-4: degree of polymerization X_n, degree of quaternization q and number of fixed positive charges n_{c+} for PEI_{28}(I) – PEI_{1393}^{100Q} (XVII)

No.	Polymer	X_n	q [%]	n_{c+}
(II)	PEI_{28}^{1Q}	28	1	0.3
(III)	PEI_{28}^{5Q}	28	5	1.4
(IV)	PEI_{28}^{10Q}	28	10	2.8
(V)	PEI_{28}^{20Q}	28	20	5.6
(VI)	PEI_{28}^{50Q}	28	50	14.0
(VII)	PEI_{28}^{100Q}	28	100	28.0
(IX)	PEI_{232}^{10Q}	232	10	23.2
(X)	PEI_{232}^{20Q}	232	20	46.4
(XI)	PEI_{232}^{50Q}	232	50	116.0
(XII)	PEI_{232}^{100Q}	232	100	232.0
(XIV)	PEI_{1393}^{10Q}	1393	10	139.3
(XV)	PEI_{1393}^{20Q}	1393	20	278.6
(XVI)	PEI_{1393}^{50Q}	1393	50	696.5
(XVII)	PEI_{1393}^{100Q}	1393	100	1393.0

As shown in Figure 4-13 in Chapter 4.8., the partially quaternized poly(ethylenimine) derivatives are protonated under acidic conditions and so the amino groups carry positive charges in dependency on the pH. In comparison, the degree of protonation of pure

poly(ethylenimine) is higher than of the quaternized polymers at the same pH. The nominal charge of the partially quaternized poly(ethylenimine) derivatives is the sum of the fixed positive charges n_{c+} and the charges by protonation n_{H+} (see Equation 4-24).

$$n_+ = n_{c+} + n_{H+}$$ ***Equation 4-24***

with n_+: nominal charge; n_{c+}: number of fixed positive charges; n_{H+}: number of charges by protonation

It is known that the effective charge n_{eff} of highly charged polymer molecules can be much smaller than the nominal charge n_+ [9]. A reason for this can be counterion condensation, which means that a part of the counterions are located closely to the polyion (= "condesated"), which lowers the effective charge density [10]. The effective charge is determined as the charge of one polymer molecule that is influenced by the outer electrical field. To determine the effective charge of a polyelectrolyte a combination of the results of DOSY-NMR and electrophoretic measurements can be employed [11]. In an electrophoresis experiment, there is a force balance between the force of the electrical field F_{el} (see Equation 4-25) and the one of the hydrodynamic friction F_f (see Equation 4-26). From this force balance, the effective charge n_{eff} can be determined (see Equation 4-27).

$$F_{el} = E \cdot e \cdot n_{eff}$$ ***Equation 4-25***

$$F_f = \frac{v \cdot k_B \cdot T}{D}$$ ***Equation 4-26***

$$n_{eff} = \frac{\mu_e \cdot k_B \cdot T}{e \cdot D}$$ ***Equation 4-27***

with F_{el}: electrical field force; E: electric field strength; e: elementary charge; n_{eff}: effective charge; F_f: hydrodynamic friction force; v: velocity; k_B: Boltzmann constant; T: temperature; D: diffusion coefficient; μ_e: electrophoretic mobility

Table 4-5: Measured diffusion coefficient and electrophoretic mobility, calculated effective charge, calculated ratio between effective charge and nominal charge for the samples of the polymers PEI_{1393} (XIII) – PEI_{1393}^{100Q} (XVII) at a molar concentration of 1.65mM and a salt concentration of 0.001M sodium chloride in deuterium oxide

Polymer	Sample	D [10^{-11}m²/s]	μ_e [10^{-8}m²/Vs]	n_{eff}	$\frac{n_{eff}}{n_{c+}}$
PEI_{1393}	P(XIII)-013	4.73	1.607±0.169	8.7	---
PEI_{1393}^{10Q}	P(XIV)-013	5.16	2.335±0.203	11.6	0.08
PEI_{1393}^{20Q}	P(XV)-013	4.59	2.379±0.108	13.3	0.05
PEI_{1393}^{50Q}	P(XVI)-013	4.79	2.762±0.151	14.8	0.02
PEI_{1393}^{100Q}	P(XVII)-013	5.89	2.347±0.206	10.2	0.01
	P(XVII)-014	6.31	2.471±0.256	10.1	0.01

For each polymer PEI_{1393} (XIII) – PEI_{1393}^{100Q} (XVII) a solution with a molar concentration of 1.65mM and a salt concentration of 0.001M sodium chloride in deuterium oxide was produced. The diffusion coefficient (D) was measured by means of DOSY-NMR-spectroscopy. The electrophoretic mobility (μ_e) was determined by means of laser-doppler-velocimetry. The effective charge (n_{eff}), as well as the ratio between the effective charge and the number of fixed positive charges ($\frac{n_{eff}}{n_{c+}}$) were calculated. The results are summarized in Table 4-5.

Figure 4-16 shows the ^{1}H-DOSY-NMR-spectrum of PEI_{1393}^{10Q} (XIV) measured in deuterium oxide with a molar concentration of 1.65mM and a salt concentration of 0.001M sodium chloride. The ^{1}H-DOSY-signals of PEI_{1393}^{10Q} (XIV) are very broad. The signal in the ^{1}H-NMR-spectrum between 3.2 and 3.3ppm, that corresponds to the protons F and K (see Figure 4-4a), which belong to the quaternized side chains of the polymer exhibits a very broad ^{1}H-DOSY-signal from -log(D) = 10.41 until 9.92. The signal between δ = 2.5 and 2.8ppm of the ^{1}H-NMR-spectrum, which corresponds to the protons bonded to the carbon atoms A+B+C+G+H (see Figure 4-4a), show a negative logarithmic diffusion coefficient between 10.43 and 10.15. The diffusion range of the signal of the side chain protons is broader compared to the signal of the backbone protons, because the side chains of the polymers

reach further in solution than their backbone. The diffusion coefficient D of the polymer molecule was defined as the average value of the backbone signal (see grey horizontal line in Figure 4-16). In the case of $\mathrm{PEI}_{1393}^{10\mathrm{Q}}$ (XIV) an average value of the logarithmic diffusion coefficient of -log(D) = 10.287 was determined (see Table 4-5, column 3). The diffusion coefficients measured for the five polymers are all in the same magnitude differing about maximum 30%, but do not show a clear trend with an increasing degree of quaternization.

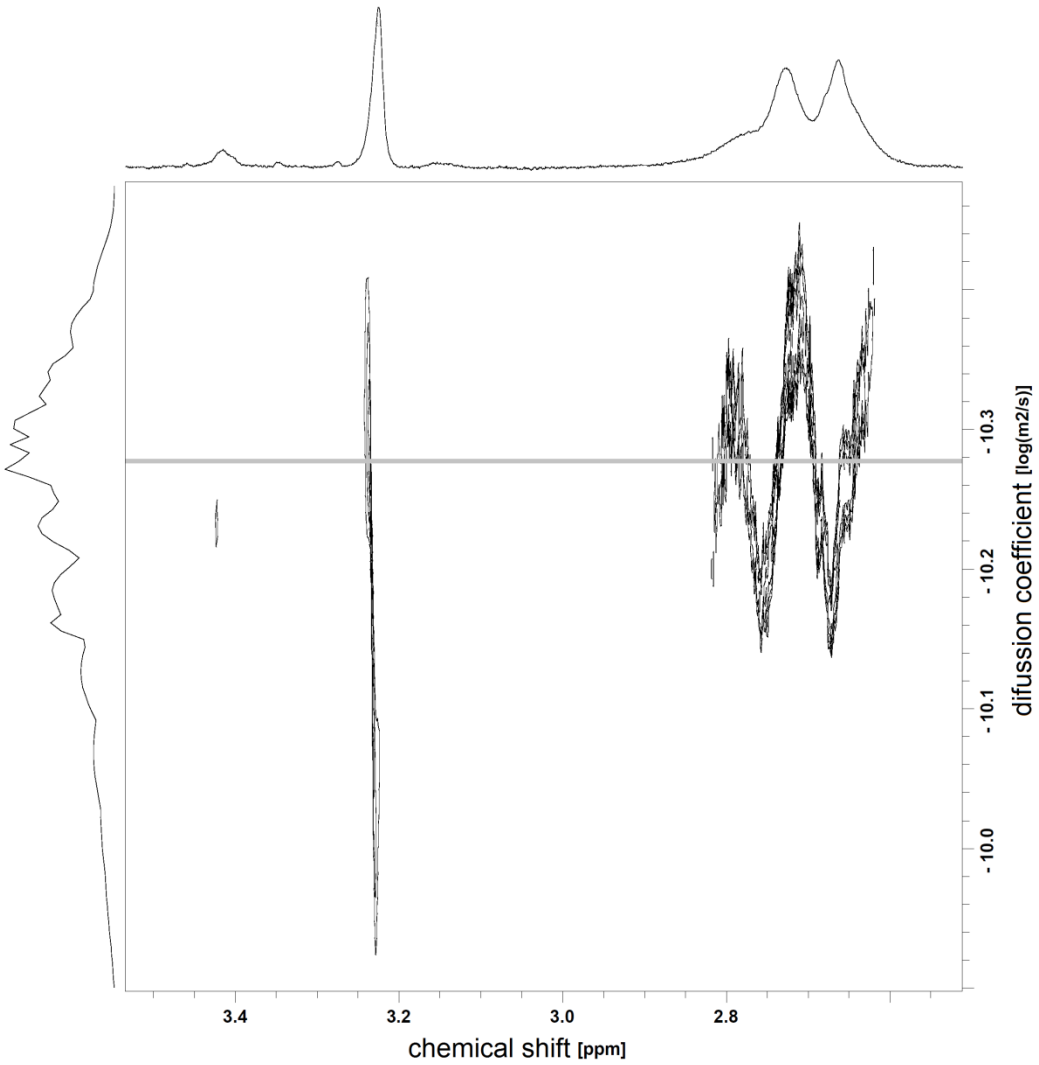

Figure 4-16: ^{1}H-DOSY-NMR-spectrum of P(XIV)-013 (PEI_{1393}^{10Q}(XIV))

The electrophoretic mobilities (see Table 4-5, column 4) of the polymer solutions in deuterium oxide show the same trend as for the investigated samples in water in Chapter 4.9. The value of the electrophoretic mobility increases from PEI_{1393} (XIII) to $\mathrm{PEI}_{1393}^{50\mathrm{Q}}$ (XVI), however the value decreases again from $\mathrm{PEI}_{1393}^{50\mathrm{Q}}$ (XVI) to $\mathrm{PEI}_{1393}^{100\mathrm{Q}}$ (XVII). Two samples of

PEI_{1393}^{100Q} (XVII) were investigated to confirm this result. These results contradict the expectation that the electrophoretic mobility increases with increasing degree of quaternization.

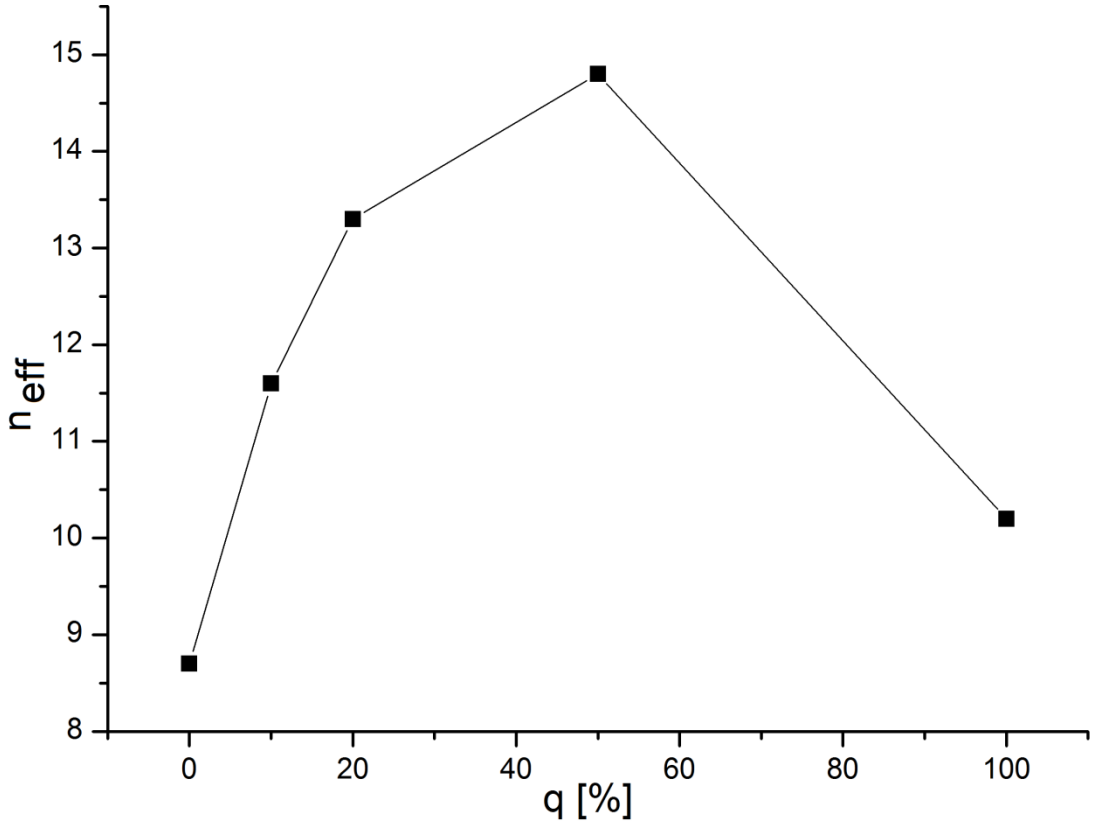

Figure 4-17: Effective charge of PEI_{1393}^{qQ} (XIII) – (XVII) in deuterium oxide solutions as a function of the degree of quaternization with c_P = 1.65mM and c_{NaCl} = 0.001M

Figure 4-17 illustrates the effective charge as a function of the degree of quaternization for the amino-quat-primer polymer PEI_{1393} (XIII) – PEI_{1393}^{100Q} (XVII) in solutions with a molar concentration of 1.65mM and a salt concentration of 0.001M sodium chloride in deuterium oxide. The effective charge develops with the same trend as the measured electrophoretic mobility and is therefore also contradictory to the expectations. The value increases from PEI_{1393} (XIII) to PEI_{1393}^{50Q} (XVI), however decreases again from PEI_{1393}^{50Q} (XVI) to PEI_{1393}^{100Q} (XVII).

The values of the ratios between the effective charge n_{eff} and the number of fixed positive charges n_{c+} are very small (see Table 4-5, column 6). The effective charge varies between one and eight percent of the number of fixed positive charges for PEI_{1393}^{10Q} (XIV) – PEI_{1393}^{100Q}

(XVII), whereas the ratio decreases with an increasing degree of quaternization. The small values of the effective charge indicate that the biggest fraction of the fixed positive charges on the polymer molecules are condensated to their counterions and do not contribute to the effective charge of the polymer as expected. The fraction of condensated charge, which does not contribute to the effective charge, increases with an increasing degree of quaternization, due to an upper limit of free charge per volume in the polymer due to charge repulsion.

A weak point of the employed method of the effective charge determination is the lack of an applied electrical field strength while measuring the diffusion coefficient in the DOSY-NMR. It is known that diffusion coefficients can sufficiently depend on an external field strength [12]. The calculations presented here were, however, performed under the assumption that the difference of the diffusion coefficient with and without an applied electrical field can be neglected, which will definitively hold true in the limiting case of E→0.

4.11. Size determination

The diameters of the synthesized partially quaternized poly(ethylenimine) derivatives were determined theoretically in Chapter 4.4., and also from the diffusions coefficients of ^{1}H-DOSY-NMR measurements employing the Stokes-Einstein-equation, as well as from dynamic light scattering (DLS) measurements.

4.11.1. Dynamic Light Scattering

The size distribution of the amino-quat-primer polymers in aqueous solution was investigated by means of dynamic light scattering (cf. literature review, Chapter 2.5.1.). Figure 4-18 shows exemplary the size distribution measured by DLS of $\mathrm{PEI}_{1393}^{100\mathrm{Q}}$ (XVII) with log (m_p) = -2 and sodium chloride concentrations of a) 0.1M; b) 0.01M and c) 0.001M. The average molecule diameter determined at a sodium chloride concentration of c_{NaCl} = 0.1M is 9.27±6.72nm (see Figure 4-18a), of c_{NaCl} = 0.01M 10.02±4.82nm (see Figure 4-18b) and of c_{NaCl} = 0.001M 13.29±8.73nm (see Figure 4-18c).

Dynamic light scattering measurements work ideally only with monodisperse samples. [13] If a size distribution is very broad, the results become more defective and less reliable. The standard deviations of the size distributions shown in Figure 4-18 range between roughly 50 and 75% of the mean diameters. The polydispersity of the employed poly(ethylenimine) derivatives increase with an increasing molecular weight from 1.1 of $\mathrm{M_n} = 1{,}200\ \frac{\mathrm{g}}{\mathrm{mol}}$, to

2.5 of $M_n = 10{,}000 \frac{g}{mol}$, to 12.5 of $M_n = 60{,}000 \frac{g}{mol}$ (cf. experimental part, Chapter 3.2.). High polydispersities like of the polymers with the intermediate and highest degree of polymerization lead to broad size distributions, which complicates the size determination by means of DLS.

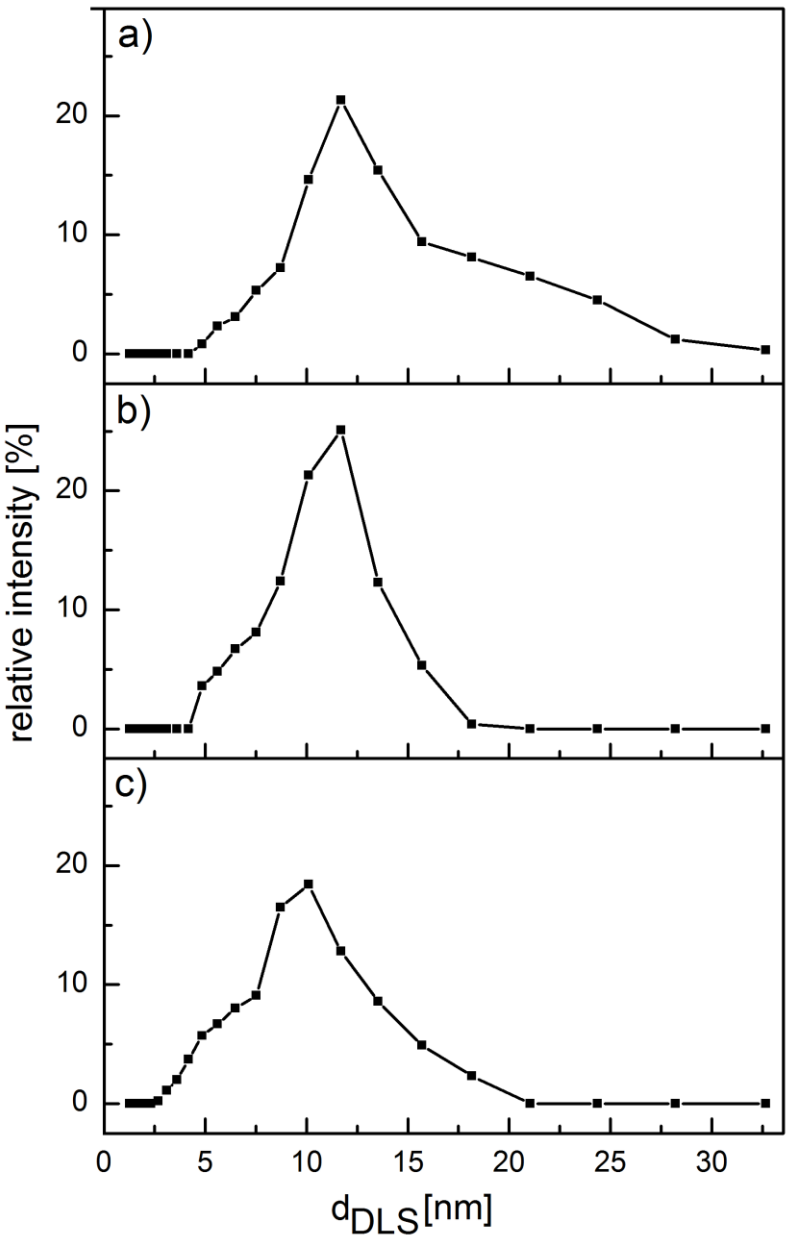

Figure 4-18: Size distributions determined by dynamic light scattering for PEI_{1393}^{100Q} (XVII) with log (m_p) = -2 and sodium chloride concentrations of a) 0.1M; b) 0.01M and c) 0.001M

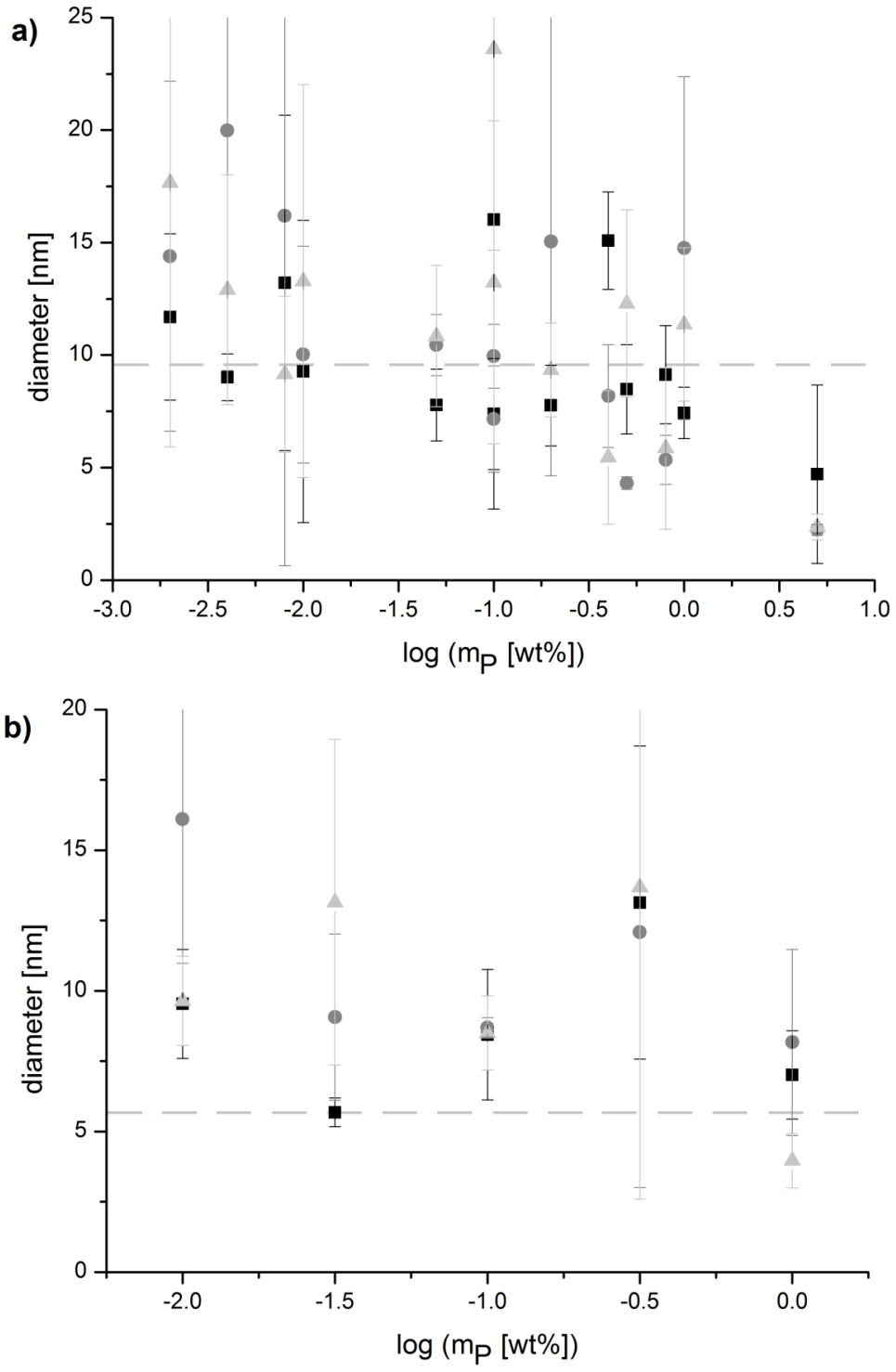

Figure 4-19: Diameter measured by dynamic light scattering as a function of logarithmic mass percentage for a) PEI_{1393} (XIII) and b) PEI_{1393}^{100Q} (XVII) in solution for three different salt concentrations of sodium chloride (black squares: 0.1M; dark grey squares: 0.01M; light grey triangles: 0.001M). The dark grey dashed lines indicate the theoretical values

A systematic investigation on the diameter was performed by means of DLS measurements using different polymer concentrations between 0.001 and 5wt%, as well as three different salt concentrations of 0.1M, 0.01M, and 0.001M of sodium chloride. The measurements were conducted with the two polymers PEI_{1393} (XIII) and $\mathrm{PEI}_{1393}^{100\mathrm{Q}}$ (XVII), i.e. one without quaternization and one with a degree of quaternization of 100%. The results are depicted in Figure 4-19a) and b). The diameters measured at one fixed polymer mass concentration, but with three different salt concentrations strongly differ. There is no trend that higher or lower salt concentrations may result in smaller diameters. Very high polymer mass concentrations (5wt%) result in small diameters. The explanation of this could be a multiscattering occurring for high concentrations [13], which leads to false smaller results. For all other investigated polymer mass concentration, there exists no trend of the diameter in dependence on the concentration. The measurement of $\mathrm{PEI}_{1393}^{100\mathrm{Q}}$ (XVII) (see Figure 4-19b) leads to similar results. No trend in the development of the diameter is recognizable in dependence on the polymer mass concentration or the salt concentration. Note again, as before also for these DLS measurements the standard deviations of the obtained diameters are very large, in the same order as the measured values.

Sodium chloride was added to the polymer solutions to screen the Coulomb interactions between the polymer molecules. Therefore the ionic strength of the added sodium chloride should have the same magnitude as the ionic strength of the polymer solution. The ionic strength depends on the molar concentration and charge number of the ions (see Equation 4-28). For sodium chloride, a monovalent salt, the ionic strength equals the salt concentration. For the polymer solutions it is assumed that the ionic strength can be calculated based on the effective charge of the polymer. The ionic strength is calculated exemplary of a 1wt% solution of $\mathrm{PEI}_{1393}^{100\mathrm{Q}}$ (XVII). The calculated effective charge $\mathrm{n_{eff}} \approx 10$ (cf. Chapter 4.10., Table 4-5, Column 6) is employed for this calculation as the charge number of the polymer. The molar polymer concentration of the solution is $\mathrm{c_p} = 3.69 * 10^{-5}\ \frac{\mathrm{mol}}{\mathrm{L}}$ (cf. Equation 4-29). The calculated ionic strength of a 1wt% solution of $\mathrm{PEI}_{1393}^{100\mathrm{Q}}$ (XVII) is $\mathrm{I_p}\ (\mathrm{PEI}_{1393}^{100\mathrm{Q}}) = 0.019\ \frac{\mathrm{mol}}{\mathrm{L}}$ (cf. Equation 4-30) and therefore smaller than the highest employed salt concentration, however, larger than the both lowest salt concentrations. It is concluded, that for the calculated ionic strength of the polymer solution, a screening of the coulomb interactions between the polymer molecules is expected at least with the highest employed salt concentration ($\mathrm{c_{Nacl}} = 0.1\mathrm{M}$) and that the determined diameters were measured in absence of coulomb interactions between the polymer molecules.

$$I_p = \frac{1}{2} \cdot \sum_i c_i \cdot z_i^2$$ ***Equation 4-28***

$$c_p = \frac{c_m}{M_n} = \frac{10\,\frac{g}{L}}{271.22 \cdot 10^3\,\frac{g}{mol}} = 3.69 \cdot 10^{-5}\,\frac{mol}{L}$$ ***Equation 4-29***

$$I_p\left(PEI_{1393}^{100Q}\right) = \frac{1}{2} \cdot (10^2 \cdot 3.69 \cdot 10^{-5} + 1^2 \cdot 3.69 \cdot 10^{-5}) = 0.019\,\frac{mol}{L}$$ ***Equation 4-30***

with I_p: ionic strength of the polymer solution; c_i: molar concentration of the ionic species i; z_i: charge number of the ionic species i; c_p: molar polymer concentration; c_m: mass polymer concentration; M_n: molecular weight of PEI_{1393}^{100Q}

Larger values of the diameter measured by DLS than the theoretical values could be expected, because the hydrodynamic radius is measured be means of DLS [13]. To investigate if larger diameters are obtained by DLS measurements due to an increase of the diameter by inclusion of water molecules in the polymer molecule, the percentage of water content for an increased diameter is calculated. Equation 4-31 and Equation 4-32 show the calculation of the volume of the polymer and the increased volume of an assumed sphere. The percentage of water content can be derived from the volume difference (cf. Equation 4-33). Table 4-6 lists the water contents for the two polymers PEI_{1393} (XIII) and PEI_{1393}^{100Q} (XVII) for an increased radius of 1.5 and two times of the theoretical value. An increase of the theoretical radius of 1.5 and two times leads to a water content of 70.4% and 87.5%, respectively. These high values make clear, that the cause of a two times larger diameter determined by DOSY measurement and a three times larger diameter determined by DLS measurement for PEI_{1393} (XIII) is not the inclusion of water in the polymer.

$$V_p = \frac{4}{3} \cdot \pi \cdot r_p^3$$ ***Equation 4-31***

$$V_{tot} = \frac{4}{3} \cdot \pi \cdot r_{tot}^3$$ ***Equation 4-32***

$$\emptyset_{H2O} = \left(1 - \frac{V_p}{V_{tot}}\right) \cdot 100$$ ***Equation 4-33***

with V_p: polymer volume; r_p: polymer radius; V_{tot}: total volume; r_{tot}: total radius; $\emptyset_{H2O}$: volume fraction of water

Table 4-6: Theoretical radii of polymers and water content for increased radii

Polymer	r_{theo} [nm]	r_{tot} [nm]	$\emptyset_{H2O}$ [%]
PEI_{1393}	2.85	$1.5r_{theo}$ = 4.28	70.4
	2.85	$2.0r_{theo}$ = 5.70	87.5
PEI_{1393}^{100Q}	4.71	$1.5r_{theo}$ = 7.07	70.4
	4.71	$2.0r_{theo}$ = 9.42	87.5

4.11.2. Comparison of DLS and DOSY results

The theoretically calculated diameters of the partially quaternized poly(ethylenimine) are compared with determined values from DOSY and DLS measurements (cf. Table 4-7).

Table 4-7: Theoretical diameters and calculated values from DOSY measurements and from DLS measurements for the samples of the polymers PEI_{1393} (XIII) – PEI_{1393}^{100Q} (XVII) at a molar concentration of 1.65mM and a salt concentration of 0.001M sodium chloride in deuterium oxide

Polymer	Sample	d_{THEO} [nm]	d_{DOSY} [nm]	d_{DLS} [nm]
PEI_{1393}	P(XIII)-013	5.70	11.77	17.47±15.86
PEI_{1393}^{10Q}	P(XIV)-013	6.30	10.79	12.72±8.82
PEI_{1393}^{20Q}	P(XV)-013	6.80	12.13	15.63±10.00
PEI_{1393}^{50Q}	P(XVI)-013	7.99	11.62	12.72±5.55
PEI_{1393}^{100Q}	P(XVII)-013	9.42	9.45	7.28±2.74
	P(XVII)-014	9.42	8.82	8.05±5.26

Figure 4-20 shows the measured diameter of dissolved PEI_{1393}^{qQ} (XIII) – (XVII) as a function of the degree of quaternization. The black squares indicate the theoretical values of single macromolecules, the dark grey circles show the values obtained from DOSY measurements, while the light grey triangles depict the values calculated from DLS measurements. Note that the results from the DLS measurements are shown without their large standard deviations, which are in the same order as the measured values.

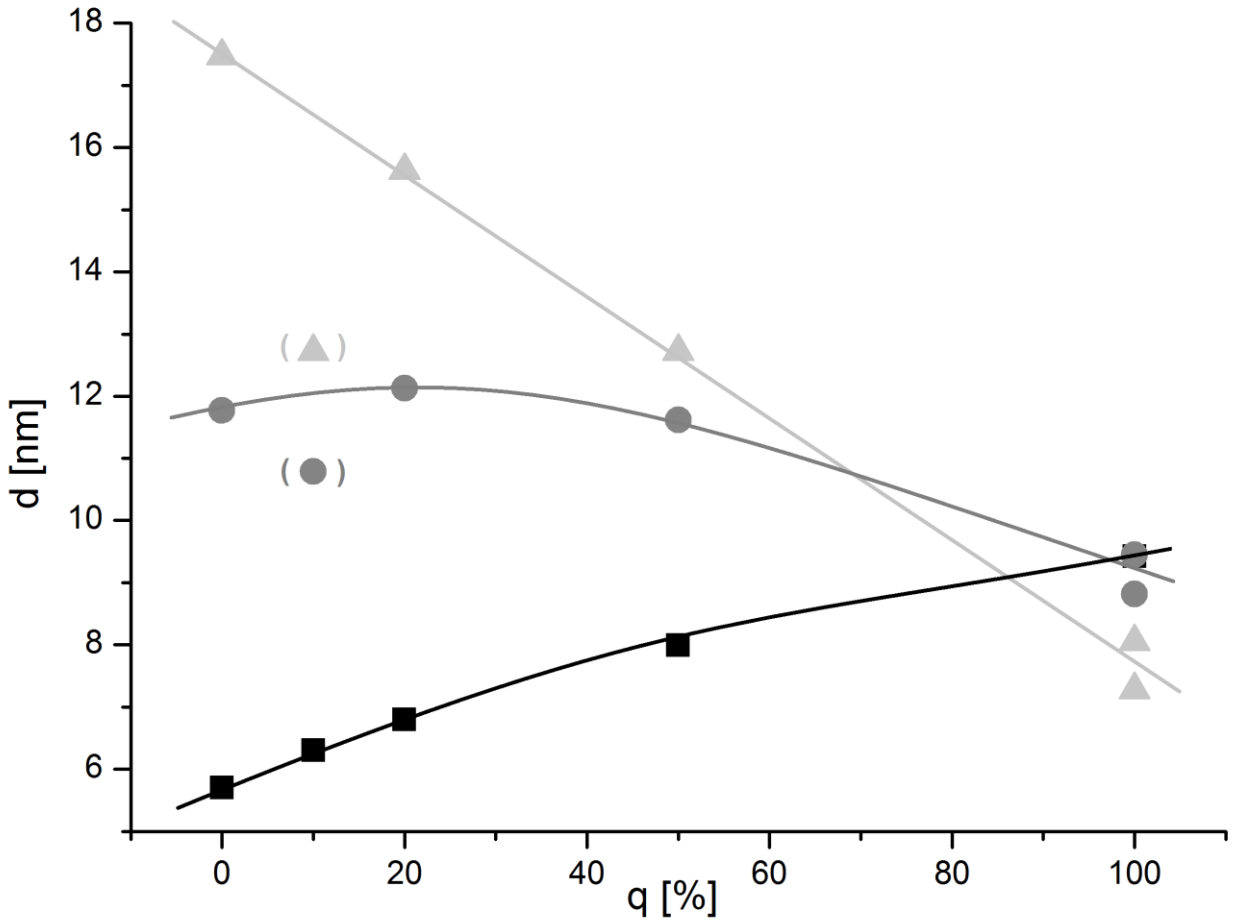

Figure 4-20: Molecule diameter of PEI_{1393}^{qQ} (XIII) – (XVII) as a function of the degree of quaternization; black square: theoretical values, dark grey circles: calculated values from DOSY measurements, light grey triangles: calculated values from DLS measurements (c_P = 1.65mM, c_{NACl} = 1mM, T = 25°C, D_2O)

The theoretical values of the diameters increase with an increasing degree of quaternization about 65% from PEI_{1393} (XIII) to $\mathrm{PEI}_{1393}^{100\mathrm{Q}}$ (XVII). In contrast to this, the measured values from the DOSY and DLS measurements decrease with an increasing degree of quaternization. For the derivatives with q ≤ 50%, the determined values from the DLS measurements are bigger than the ones from the DOSY measurements, whereas the results for q = 100% are contrary to this. For PEI_{1393} (XIII) the determined diameter from the DOSY measurements is around two times and the one from the DLS measurements around three times larger than the theoretical value. However, for $\mathrm{PEI}_{1393}^{100\mathrm{Q}}$ (XVII) the theoretical diameter and the value obtained from the DOSY measurement are nearly identical and the value from the DLS measurement is around 20% smaller than the theoretical value. The results from both measurement methods are in good agreement with the theoretical values with highly charged poly(ethylenimine) derivatives, whereas big discrepancies between the measured values and

the theoretical values occur with non- and weakly charged poly(ethylenimine) derivatives. It is concluded that with the highly charged amino-quat-primer polymer (q = 100%), single molecules are detected by DLS and electrophoretic mobility measurements. In contrast to this, structures with higher diameters are detected with non- and weakly charged derivatives, which leads to the assumption that association of molecules occur in solution. This finding might explain the unexpected low values of the electrophoretic mobility and the effective charge of the highly charged amino-quat-primer polymer (q = 100%).

An exact size determination of the partially quaternized poly(ethylenimine) derivatives was difficult. The measured values of derivatives with low degrees of quaternization obtained by DLS and DOSY measurements lead to larger results than the theoretical values. Reasons for this can be difficulties in the measurement performance due to broad molecular weight distributions of the employed polymers and due to possible interactions between single polymer molecules. Nevertheless, the measured values range in the same order as the theoretical values (up to three times) and therefore lead to the conclusion that the theoretical values are a reasonable assumption of the macromolecule diameters.

4.12. Conclusion

Fourteen partially quaternized poly(ethylenimine) derivatives with three different degrees of polymerization (X_n = 28, 232, 1393) and a degree of quaternization q between 1 and 100% were synthesized. The structure of the products was confirmed by ^{1}H- and ^{13}C-NMR-spectroscopy. The degree of quaternization was calculated from ^{1}H-NMR-spectra, as well as elemental analysis and was found to be in reasonable agreement with the theoretical values based on the experimental conditions. Their thermal behavior, as well as their solubility in a variety of solvents was examined.

The pH of polymer-water-solutions was measured. It was found, that all polymer-water-solution exhibit an alkaline pH, which increases with an increasing polymer concentration and a decreasing degree of quaternization. The degree of protonation was determined from titrations of polymer-water-solutions against acid and base. For acidic conditions the polymers get further positively charged. At a special acidic pH, the charge by protonation of a weakly quaternized polymer is always higher than of the strongly quaternized polymers. The quaternization of poly(ethylenimine) results in a weaker protonation of the polymer and leads to a more stable amount of charge against pH variation.

The electrophoretic mobility of polymer-water-solutions increases with an increasing degree of quaternization from 0 until 50%, however the value for q = 100% is notably smaller than the one for q = 50%, which was found to be in contrast to the expectation of an increasing electrophoretic mobility with an increasing degree of quaternization. The effective charge was investigated by a combination of DOSY-NMR-spectroscopy and electrophoretic measurements. It is for all polymers significantly smaller than the number of fixed positive charges as assumed due to ion condensation. Similar to the electrophoretic mobility, the effective charge increases with an increasing degree of quaternization from 0 to 50%, but the value for the polymer with q = 100% is smaller than the one for 50%.

The size of amino-quat-primer polymers was determined by means of DLS and DOSY measurements and compared with theoretical calculated values. The sizes of derivatives with low degrees of quaternization obtained by DLS and DOSY measurements lead to larger results (up to three times) than the theoretical values. Nevertheless, the measured values range in the same order as the theoretical values and therefore it is concluded that the theoretical values are a reasonable assumption of the diameters. Reasons for the discrepancies can be due to broad molecular weight distributions of the polymers and due to possible association of polymer molecules. With this finding all measured values of the diffusion coefficient, the electrophoretic mobility and the diameter, as well as the derived effective charge have to be considered with additional carefulness, because they might not be the true values of single molecules, but the average values of all occurring structures in the sample. This could explain the unexpected small values of the electrophoretic mobility and the effective charge of the derivative with the highest degree of quaternization.

The structure and composition of fourteen partially quaternized poly(ethylenimine) derivatives was confirmed and their charging behavior upon variation of concentration, pH and salt concentration was investigated.

[1] Kobayashi, S.; Hiroishi, K.; Tokunoh, M.; Saegusa, T; Macromolecules 1987, 20, 1496-1500

[2] Komban, R.; Beckmann, R.; Rode, S.; Ichilmann, S.; Kühnle, A.; Beginn, U.; Haase, M.; Langmuir 2011, 27, 10174-10183

[3] Lukovkin, G.M.; Pshezhetsky, V.S.; Murtazaeva, G.A.; European Polymer Journal 1973, 9, 559-565

[4] Hansson, J.; Svensk Kemisk Tidskrift 1948, 60, 183

[5] Beckmann, R.; Dissertation “Quat-Primer” Polymers as Dispersants for Nanoparticles, Osnabrueck 2012, p.73

[6] Griffiths, P.C.; Paul, A.; Stilbs, P.; Petterson, E.; Macromolecules 2005, 38, 3539-3542

[7] Supplier information: Aldrich – poly(ethylenimine), average Mn ~10,000

[8] Koper; G.J.M.; Borkovec, M.; Polymer 2010, 51, 5649 - 5662

[9] Pericet-Camara, R.; Papastavrou, G.; Borkovec, M.; Macromolecules 2009, 42, 1749-1758

[10] Manning, G.S.; Journal of Chemical Physics 1969, 51, 924-933

[11] Böhme, U.; Scheler, U.; Macromolecular Chemistry and Physics 2007, 208, 2254-2257

[12] Weingaertner. H.; Holz, M.; Annual Reports on the Progress of Chemistry Section C 2002, 98, 121–155

[13] Berne, B.J.; Pecora, R.; Dynamic Light Scattering; Courier Dover Publications, New York, 2000

Chapter 5:

Silica-nanoparticle-dispersions containing amino-quat-primer polymers

5. Silica-nanoparticle-dispersions containing amino-quat-primer polymers

Silica-nanoparticle-dispersions were prepared in the presence of partially quaternized poly(ethylenimine) derivatives, whose synthesis and characterization was described in Chapter 4. First, the bare nanoparticles were investigated concerning their size and charging behavior. Afterwards the preparation process is described. The terms “mass ratio” and “number ratio” of the dispersions are introduced. The prepared dispersions were judged optically and were analyzed by means of UV/Vis-absorption measurements.

5.1. Characterization of silica nanoparticles (Ludox TMA)

Silica nanoparticles were supplied as an aqueous dispersion called “Ludox TMA”, which contains 34wt% silica nanoparticles in water. For having a better insight in the interaction between the nanoparticles and the polymers, first the size and the surface charge of the non-modified silica nanoparticles as a function of pH were investigated.

5.1.1. Size determination

The size of the dispersed silica nanoparticles was investigated by means of dynamic light scattering (cf. literature review, Chapter 2.5.1.) and transmission electron microscopy. To determine the diameter of the nanoparticles by dynamic light scattering, the Ludox TMA dispersion was diluted with water and measured. Table 5-1 summarizes the performed measurements of the samples 001 – 008, the used concentrations of silica nanoparticles and the obtained particle diameters with their standard deviation. In Figure 5-1 the particle size distributions of five exemplary measurements at different silica nanoparticle concentrations are illustrated. With a decreasing particle concentration the measured diameter increased. If the particle concentration is very high, e.g. in the case of samples 001 – 003, multiscattering occurs, which falsifies the resulting diameters. If the particle concentration is very small, e.g. in the case of sample 008, smaller particles are not detected by the device and the resulting average diameter is too large. For nanoparticle concentrations between 0.0005 (sample 007) and 0.01wt% (sample 004), the diameter was constant between 29.8 and 34.6nm. These values fit well together in the range of their standard deviation. It was hence concluded that dynamic light scattering must be performed with silica nanoparticle concentrations of about 0.005wt%.

Table 5-1: Nanoparticle content, and particle diameters with their standard deviation of the dispersions 001 – 008

sample	nanoparticle content [wt%]	diameter [nm]
001	0.5	5.93 ± 2.19
002	0.1	16.69 ± 5.22
003	0.05	24.40 ± 6.41
004	0.01	29.75 ± 6.81
005	0.005	32.15 ± 5.72
006	0.001	34.58 ± 7.39
007	0.0005	30.36 ± 5.68
008	0.0001	44.79 ± 7.21

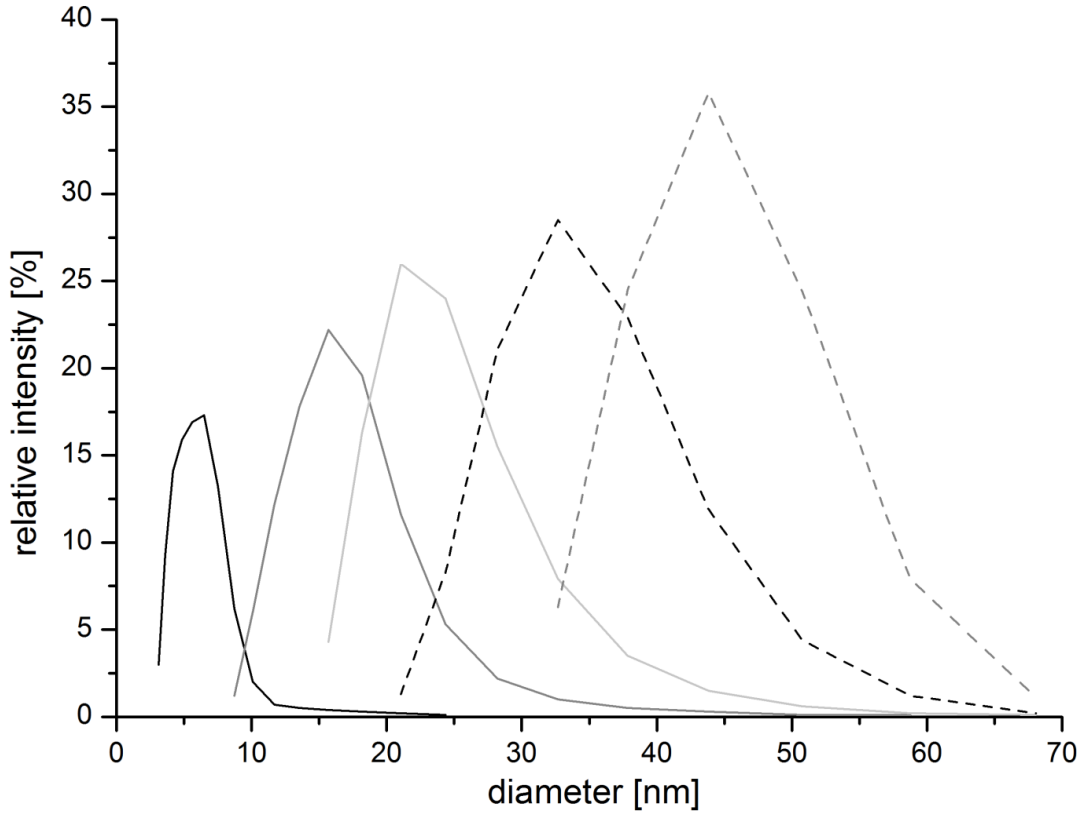

Figure 5-1: Size distribution measured by dynamic light scattering for different concentrations of nanoparticle content; black line: 0.5wt%, dark grey line: 0.1wt%, light grey line: 0.05wt%, dashed black line: 0.001wt%; dashed dark grey line: 0.0001wt%

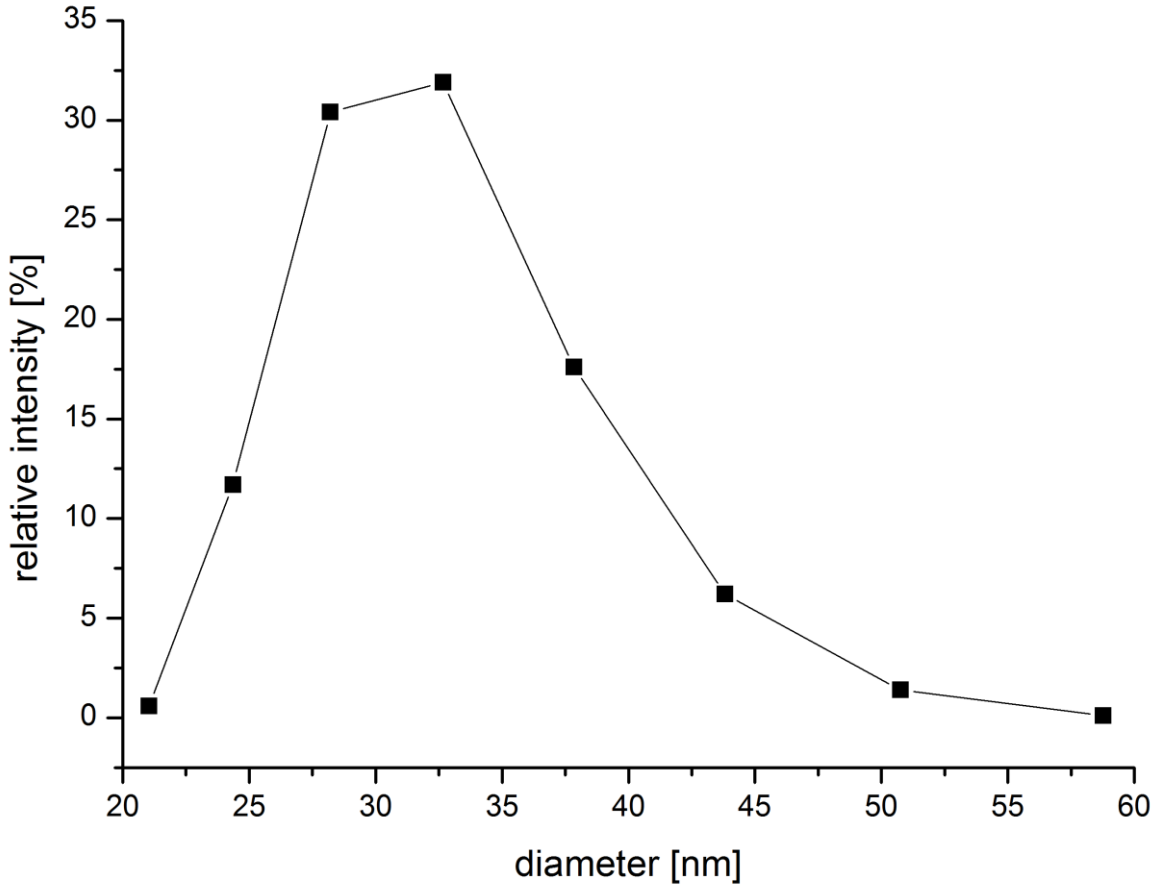

Figure 5-2: Size distribution of silica nanoparticles (0.005wt%, sample 005) by dynamic light scattering with $d_{average}$ = 32.15±5.72nm

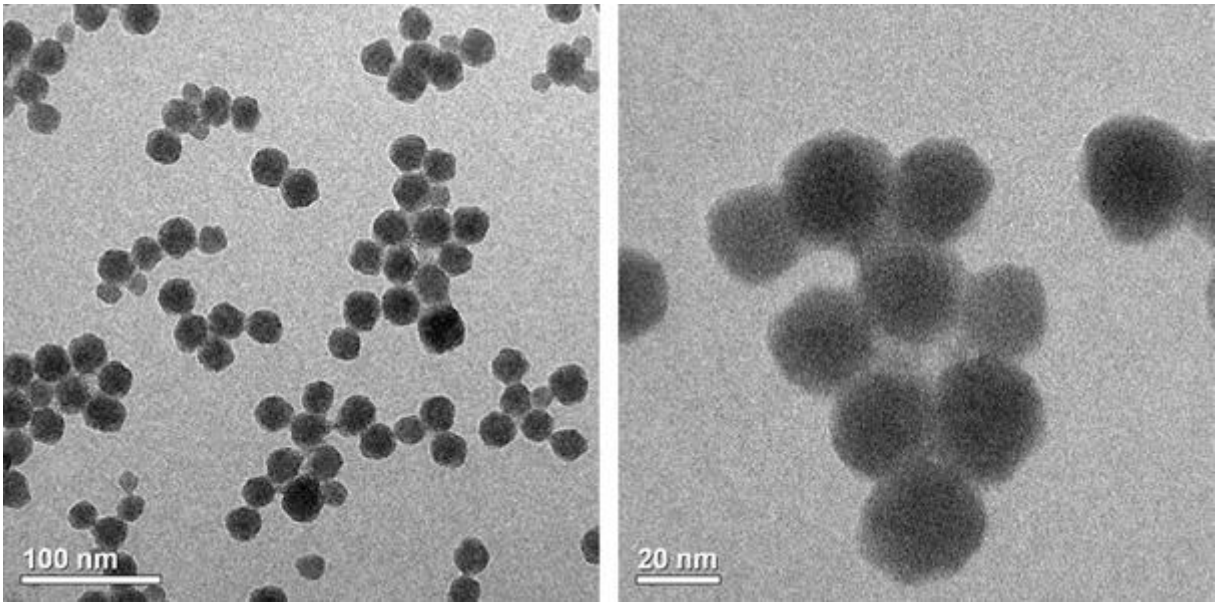

Figure 5-3: Images of silica nanoparticles (0.0001wt%, sample 008) by transmission electron microscopy

Figure 5-2 shows the size distribution measured by dynamic light scattering of the silica nanoparticles at a concentration of 0.005wt% (sample 005), the average diameter is 32.15 ± 5.72nm, which well agrees to the manufacturer information ($d_{TMA} \approx 30nm$).

To verify the results by the dynamic light scattering, transmission electron microscopy was performed (see Figure 5-3) with sample 008. The size of the particles in Figure 5-3 was investigated by means of an analytical graphic program. The size of 18 particles was investigated and an average diameter of 23.72 ± 2.97nm was determined. It is known from literature, that the nanoparticle size determined by transmission electron microscopy results in smaller values compared to diameters determined by dynamic light scattering [1]. During the following work a diameter of the silica nanoparticles of d=30 ± 5nm will be assumed.

5.1.2. Protonation and deprotonation behavior

Six dispersions of silica nanoparticles in water with a nanoparticle content of 0.5wt% (samples 009 – 014) were titrated against different acidic and basic solutions (see Table I-5, Appendix). The measured values of the pH were noted for a known added volume of the acidic or basic solution. Form the added volume and the concentration of the acidic or basic solution the amount of added protons or hydroxide ions was determined (see Equation 4-19 and Equation 4-20 in Chapter 4.8.)

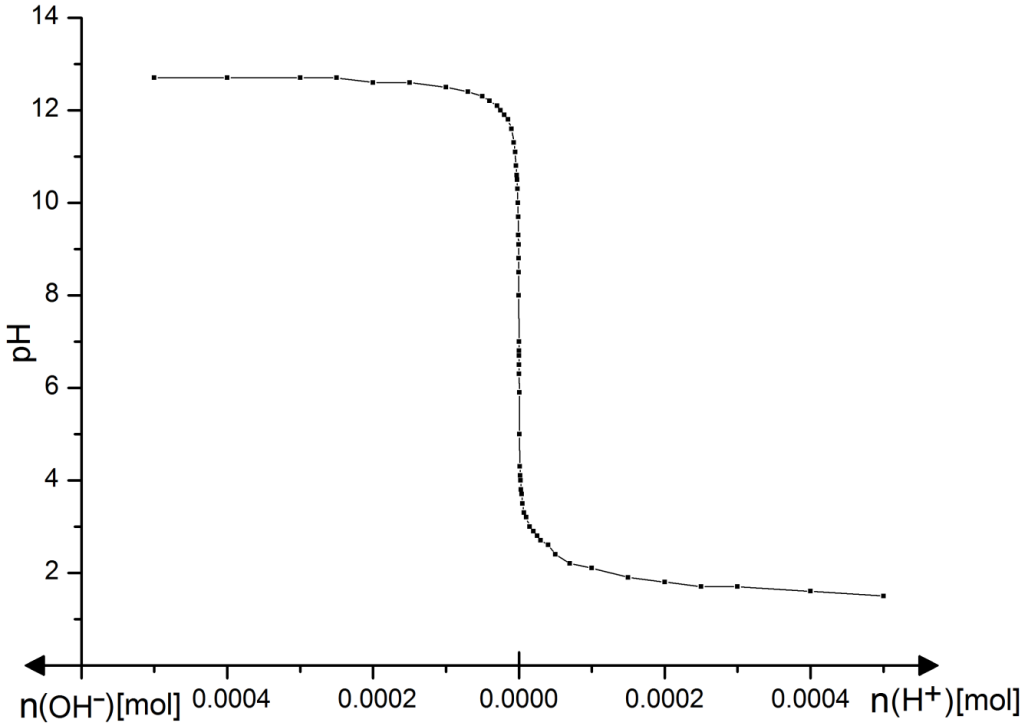

Figure 5-4: Titration of silica nanoparticles: pH as a function of the amount of protons or hydroxide ions

Figure 5-4 illustrates the superposition of the six titration curves of the silica nanoparticle solutions against acid and base, the pH as a function of the amount of protons or the amount of hydroxide ions is shown. The pH of a dispersion of 0.5wt% silica nanoparticles in water is 7. The pH decreases rapidly against addition of acid and afterwards converge to a plateau value of around 1.7. The pH increases rapidly against addition of base and afterwards converge to a plateau value of around 12.8.

From the data of Figure 5-4 the amount of protons or hydroxide ions in the silica solution was determined between pH 5 and 11 in steps of one pH-unit. The results are illustrated in Figure 5-5, the pH of pure water against the amount of added protons, and hydroxide ions was shown in Figure 4-12 in Chapter 4.8.

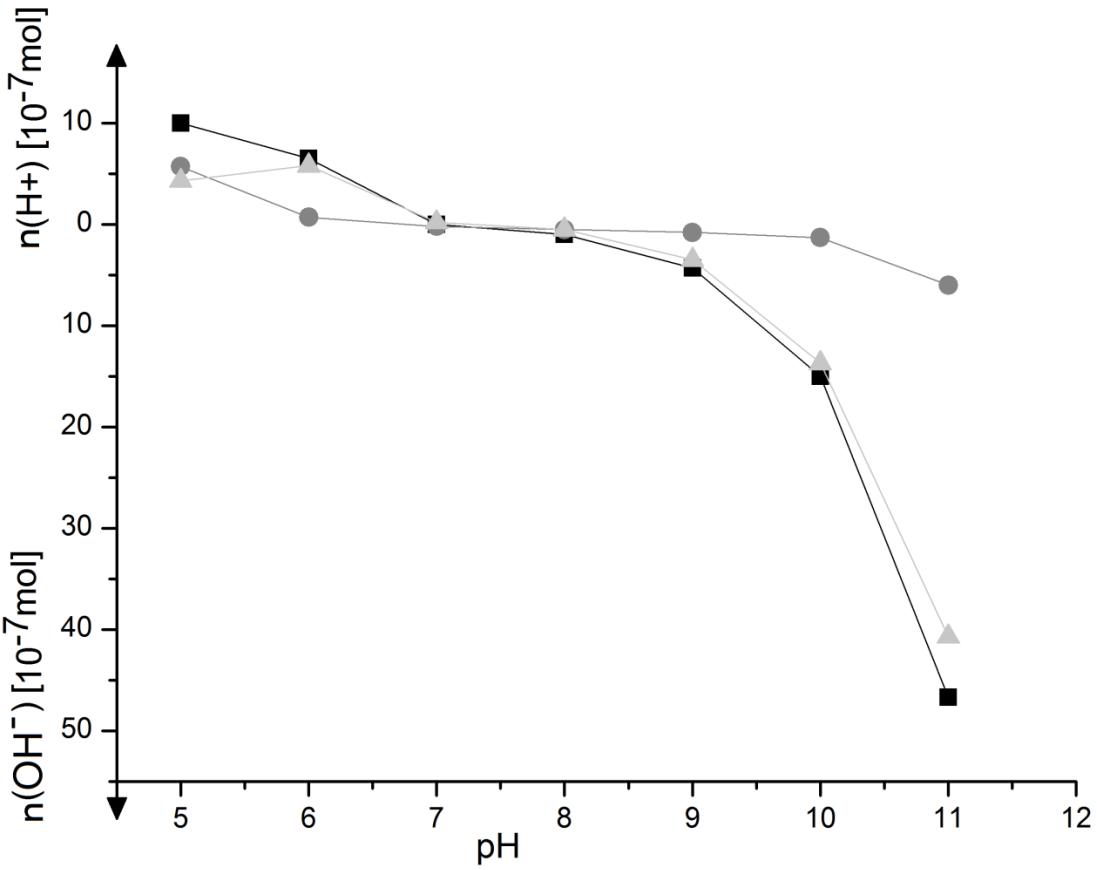

Figure 5-5: Amount of protons or hydroxide ions as a function of the pH for the silica-nanoparticle-dispersion (black squares), water (dark grey circles) and silica surfaces (light grey triangles)

To remove the effect of water in the silica nanoparticle solution the amount of protons or hydroxide ions of water (dark grey circles in Figure 5-5) at each pH-value were subtracted

from the ion content of the silica nanoparticle solution (black dots in Figure 5-5) to result in the amount of protons or hydroxide ions on the silica surfaces (light grey triangles in Figure 5-5). The amount of protons and hydroxide ions in water between a pH of 5 and 11 varies just slightly, each between 0 and $5*10^{-7}$mol, whereas the amount of protons in the silica solution is around $10*10^{-7}$ mol at pH 5 and the amount of hydroxide ions is around $47*10^{-7}$mol at pH 11. From the measured amount of protons or hydroxide ions on the silica surfaces, the number of protonated (Equation 5-1) and deprotonated (Equation 5-2) hydroxyl groups on the silica surface of one nanoparticle can be calculated.

$$\frac{N(OH_2^+)}{N_{np}} = n(H^+) \cdot \frac{N_A \cdot \rho \cdot \pi \cdot d_{np}^3}{6 \cdot m_{np}} = n(H^+) \cdot 3.405 \cdot 10^8 \qquad \textit{Equation 5-1}$$

$$\frac{N(O^-)}{N_{np}} = n(OH^-) \cdot \frac{N_A \cdot \rho \cdot \pi \cdot d_{np}^3}{6 \cdot m_{np}} = n(OH^-) \cdot 3.405 \cdot 10^8 \qquad \textit{Equation 5-2}$$

with $N(OH_2^+)$: number of protonated hydroxyl groups; $N(O^-)$: number of deprotonated hydroxyl groups; N_{np}: number of nanoparticles; $n(H^+)$: amount of protons; $n(OH^-)$: amount of hydroxide ions; N_A: Avogadro-constant; ρ: density of silica (ρ = 2,000,000 g/m³ [2]); d_{np}: diameter of a nanoparticle (d_{np} = 30±5nm (compare Chapter 5.1.1.)); m_{np}: mass of nanoparticles (m_{np} ≈ 0.05g)

Table 5-2: Number of protonated or deprotonated hydroxyl groups on a silica surface of one nanoparticle as a function of the pH

pH	$\frac{N(O^-)}{N_{np}}$	$\frac{N(OH_2^+)}{N_{np}}$
5	---	146
6	---	198
7	---	7
8	17	---
9	119	---
10	467	---
11	1386	---

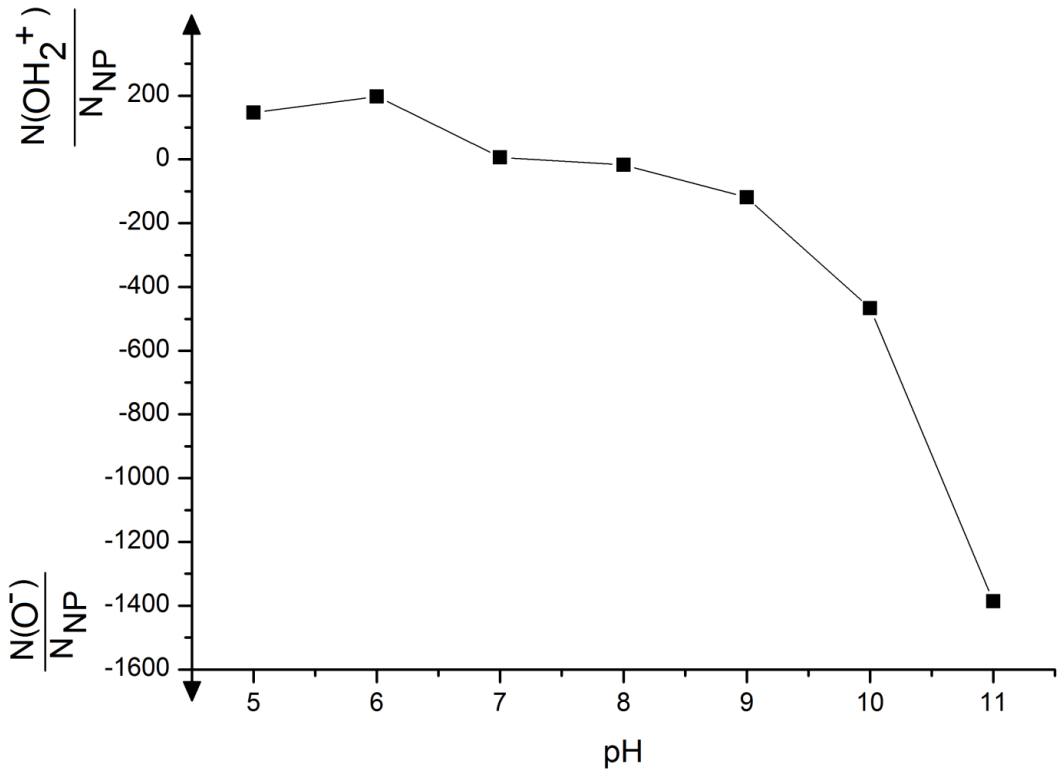

Figure 5-6: Number of protonated and deprotonated hydroxyl groups per nanoparticle as a function of the dispersion pH

Figure 5-6 illustrates the number of protonated and deprotonated hydroxyl groups on the surface of one silica nanoparticle as a function of the dispersion pH (values listed in Table 5-2). At a pH of 7 the silica surface is essentially electrically neutral, i.e. it carries nearly no protonated or deprotonated hydroxyl groups. When the pH is lowered to 5 and 6, the surface exhibits a small number (up to 200) of protonated hydroxyl groups ($\sigma_S \approx 0.07$ O^+H_2 / nm²). For a basic pH between 8 and 11 the number of deprotonated hydroxyl groups increases slightly, but between pH 10 and 11 strongly and reaches a number of nearly 1400 deprotonated hydroxyl groups per nanoparticle at pH 11 ($\sigma_S \approx 0.5$ O^- / nm²).

5.1.3. Particle surface charge

The electrophoretic mobility of silica nanoparticles in aqueous solutions at different pH values was investigated by means of laser-Doppler-velocimetry (cf. literature review, Chapter 2.5.2.). Eleven samples of silica-water-dispersions each with a total mass of 10g, and a nanoparticle content of 0.5wt% have been prepared under variation of the content of acid or base. (Samples 015 – 025). The pH of the samples 015 – 025 and their electrophoretic mobility were determined, the obtained values are listed in Table I-6, Appendix.

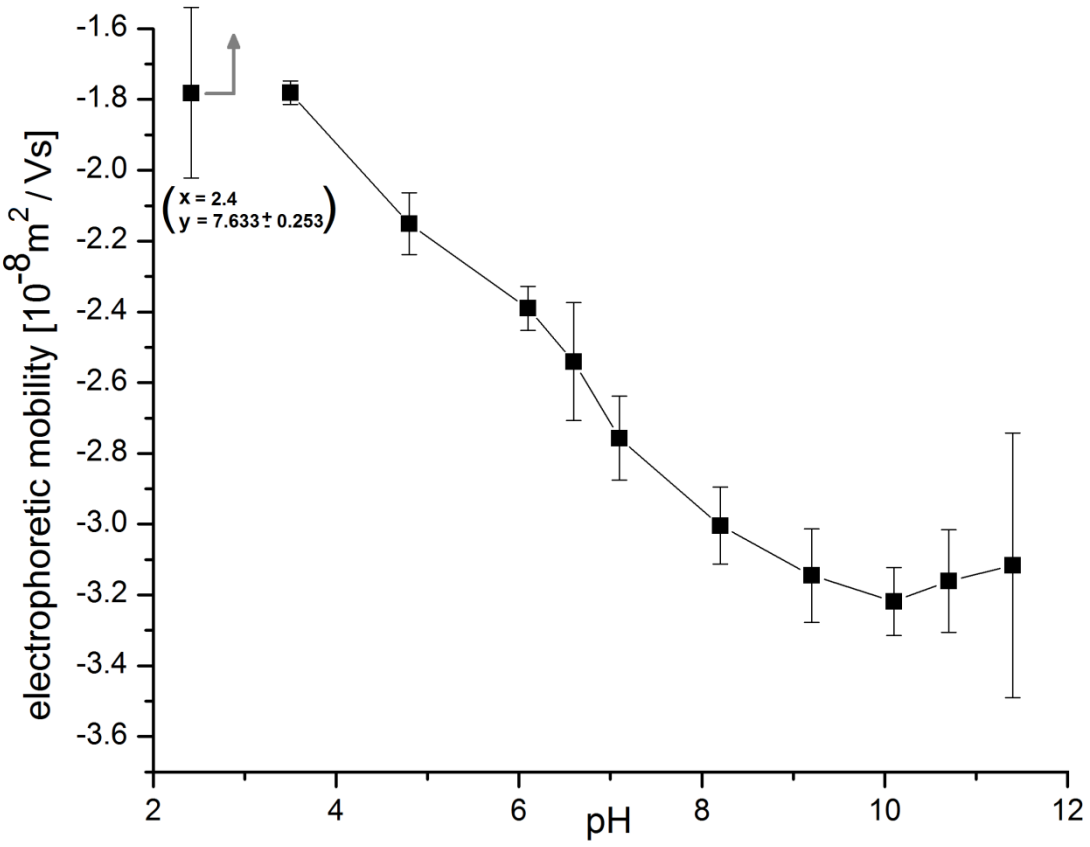

Figure 5-7: Electrophoretic mobility as a function of pH for solution with 0.5wt% silica nanoparticles

The electrophoretic mobility of the silica particles as a function of the dispersions pH between 2.4 and 11.4 is shown in Figure 5-7. Note that because of the highly positive value of the electrophoretic mobility of the dispersion with a dispersion pH of 2.4, this point is only indicated in the graph and the electrophoretic mobility is shown on the y-axis between -3.7 and $-1.6*10^{-8}$ m²/Vs. By making a linear regression between the measured electrophoretic mobility of samples 015 (pH = 2.4, $\mu_e = 7.633*10^{-8}$ m²/Vs) and 016 (pH = 3.5, $\mu_e = -1.781*10^{-8}$ m²/Vs) the isoelectric point (IEP) was determined to be located at pH 3.0. The values of the electrophoretic mobility between a pH of 3.5 and 11.4 are negative. The absolute value of the electrophoretic mobility increases for a pH of 3.5 until a pH of 9.2. The measured electrophoretic mobilities of the samples 022 – 025 with pH-values between 9.2 and 11.4 fluctuate between -3.22 and -3.12 $*10^{-8}$m²/Vs. The standard deviation of μ_e of sample 025 increased massively compared to the other samples, which indicated difficulties in the determination of the electrophoretic mobility at very high pH values.

5.1.4. Summarized properties

The dispersion “Ludox TMA” contains 34wt% silica nanoparticles in water. The size of the silica nanoparticles was investigated by dynamic light scattering and transmission electron microscopy. An average diameter of 30 ± 5nm was determined.

The number of protonated or deprotonated hydroxyl groups on the silica surface, i.e. the particles surface charge, as a function of the pH was determined by means of titration. At a pH of 7 the surface is electrically neutral. Under acidic conditions (pH 5-7), the surface gets slightly protonated (i.e. positively charged), and at basic conditions (pH 7-12) the number of deprotonated groups increases strongly with an increasing pH, making the particles negatively charged.

The electrophoretic mobility of silica-water-dispersions was measured as a function of pH. At pH 2 the electrophoretic mobility is highly positive, the isoelectric point is located at pH 3 and for a pH between 3 and 12 the electrophoretic mobility decreases with an increasing pH to highly negative values.

5.2. Dispersion preparation

Aqueous dispersions of silica nanoparticles were prepared in the presence of increasing amounts of partially quaternized poly(ethylenimine) derivatives ($\mathrm{PEI}_{\mathrm{X_n}}^{\mathrm{qQ}}$, cf. Chapter 4). The polymers differ in their degree of polymerization, and their degree of quaternization.

An amount of silica nanoparticles, which corresponds to 0.5wt% of the dispersions total mass was added into a 20ml glass vessel. Polymer stock solutions (0.1, 0.01, 0.001 and 0.0001wt% of $\mathrm{PEI}_{\mathrm{X_n}}^{\mathrm{qQ}}$) were prepared from the respective poly(ethylenimine) derivative and the required amount of this stock solution was added to the glass vessel. Water was added until the total mass of the sample was 10g. The samples were treated for 10min with ultrasound using a Branson Sonifier 250 (see Figure 5-8). An output control level of three and a duty cycle of 50% were used (cf. Experimental Part, Chapter 3.1.).

Figure 5-8: Branson Sonifier 250 (parameters: time; duty cycle; output control) with an ultrasound horn probe (5mm diameter, 15.5cm length)

5.3. Definition of the mass ratio and subunit ratio

To compare dispersions prepared in the presence of different polymer derivatives the mass ratio r_m between the mass of the polymer and the mass of the nanoparticles, as well as the subunit ratio r_u between the number of polymer repetition units, and the number of nanoparticles are introduced.

The number of nanoparticles per sample can be calculated from the quotient of the total mass of nanoparticles and the mass of a single nanoparticle (Equation 5-3). Equation 5-4 shows the mass of one nanoparticle as a function of its density and its diameter under the assumption, that the nanoparticles are of spherical shape. Inserting Equation 5-4 in Equation 5-3 results in Equation 5-5.

$$N_{np} = \frac{m_{np}^{tot}}{m_{np}} \qquad \textit{Equation 5-3}$$

$$m_{np} = V_{np} \cdot \rho_{np} = \frac{1}{6} \cdot \pi \cdot d_{np}^3 \cdot \rho_{np} \qquad \textit{Equation 5-4}$$

$$N_{np} = \frac{6 \cdot m_{np}^{tot}}{\rho_{np} \cdot \pi \cdot d_{np}^3} \qquad \textit{Equation 5-5}$$

with N_{np}: total number of nanoparticles, m_{np}^{tot}: total mass of nanoparticles, m_{np}: mass of a single nanoparticle, V_{np}: volume of a single nanoparticle, ρ_{np}: density of nanoparticles, d_{np}: diameter of a single nanoparticle

The number of polymer molecules per sample can be calculated from the quotient of the total mass of polymer in the dispersion and the mass of a single polymer molecule (Equation 5-6). Equation 5-7 shows the mass of one polymer molecule as a function of its degree of polymerization and the molecular weight of one monomer unit. Equation 5-8 gives the total number of repetition units as the product of the total number of polymer molecules and the degree of polymerization. Inserting Equation 5-6 and Equation 5-7 in Equation 5-8 results in Equation 5-9.

$$N_p = \frac{m_p^{tot}}{m_p} \qquad \textit{Equation 5-6}$$

$$m_p = \frac{X_n \cdot M_u}{N_A} \qquad \textit{Equation 5-7}$$

$$N_u = N_p \cdot X_n \qquad \textit{Equation 5-8}$$

$$N_u = \frac{m_p^{tot} \cdot N_A}{M_u} \qquad \textit{Equation 5-9}$$

with N_p : total number of polymer molecules, m_p^{tot}: total mass of polymer molecules, m_p: mass of a single polymer molecule; X_n: degree of polymerization, M_u: molecular weight of a single subunit of a polymer molecule, N_A: Avogadro-constant, N_U: total number of polymer subunits

The mass ratio r_m of polymer to nanoparticles of each dispersion is defined as the quotient of the used mass of polymer, and the used mass of nanoparticles (Equation 5-10). For sake of comparability of dispersions obtained with polymers that differ in degree of polymerization, and degree of quaternization the subunit ratio r_u will be preferred. The subunit ratio r_u gives the number of polymer repetition units per nanoparticle (Equation 5-11). Because the range of both the number ratios span over many orders of magnitude, the logarithmic mass ratio log r_m and the logarithmic subunit ratio log r_u were used. Note that here the logarithm to the base of 10 is named "log" ($\log_{10} \equiv \log$). In the special case of Ludox TMA nanoparticles, with a diameter of 30±5nm (see Chapter 5.1.) and an assumed density of $\rho_{NP} = 2 * 10^6 \frac{g}{m^3}$[2], the subunit ratio r_u is proportional to the mass ratio r_m (Equation 5-12) and the proportionality constant k just depends on the molecular weight of the subunit of the used macromolecule (Equation 5-13).

$$r_m = \frac{m_p^{tot}}{m_{np}^{tot}} \qquad \textit{Equation 5-10}$$

$$r_u = \frac{N_u}{N_{np}} \qquad \textit{Equation 5-11}$$

$$r_u = k \cdot r_m \qquad \textit{Equation 5-12}$$

$$k = \frac{N_A \cdot \pi \cdot d_{np}^3 \cdot \rho_{np}}{6 \cdot M_u} = 1.703 \cdot 10^7 \frac{g}{mol} \cdot M_u^{-1} \qquad \textit{Equation 5-13}$$

with r_m = polymer : particle mass ratio, m_p^{tot} = total mass of polymer, m_{np}^{tot} = total mass of nanoparticles, r_u = polymer subunit : particle number ratio, N_u = total number of polymer subunits, N_{np} = total number of nanoparticles, k = proportionality constant, N_A= Avogadro constant, d_{np} = nanoparticle diameter, ρ_{np} = nanoparticle density, M_u = molecular weight of one polymer subunit

The calculated logarithmic mass ratios and logarithmic subunit ratios of the prepared silica dispersions in the presence of amino-quat-primer polymers are detailed in Table I-7, column 3 and 4, Appendix.

5.4. Optical Investigations

Pictures of the dispersions were taken directly subsequent, and 24 hours after ultrasound treatment. Figure 5-9 shows pictures of the dispersions of the silica nanoparticles in

presence of the unmodified poly(ethylenimine) with a degree of polymerization of 1393, PEI_{1393} (XIII) with a logarithmic subunit ratio between 3.15 – 6.00 (samples (XIII)-001 – (XIII)-009) a) directly after dispersing and b) after 24 hours after dispersing. All samples consisted of one phase directly after dispersing. The samples (XIII)-001 and (XIII)-005 – (XIII)-009 are just slightly milky and translucent. While dispersions (XIII)-002 – (XIII)-004 had a strong white color and were opaque. After 24 hours of standing at ambient conditions the appearance of the dispersions (XIII)-001 and (XIII)-005 – (XIII)-009 did not change at all. An obvious change has taken place with the samples (XIII)-002 – (XIII)-004 that exhibited sedimentation of agglomerated particles. Two phases, a completely clear and transparent upper phase, as well as a white and opaque bottom phase can be seen.

Figure 5-9: Dispersions (XIII)-001 – (XIII)-009 a) directly after dispersing and b) 24 hours after dispersing (log r_u = 3.15, 3.59, 3.89, 4.15, 4.59, 4.99, 5.29, 5.59 and 6.00)

All samples that remain clear to translucent over the first 24 hours after the ultrasound treatment without exhibiting precipitation, will be addressed as “dispersion” in the subsequent text (compare samples (XIII)-001 and (XIII)-005 – (XIII)-009 in Figure 5-9). If a sample completely, or even partly precipitated, or if a sample became highly opaque, the term “precipitated” will be used (compare (XIII)-002 – (XIII)-004 in Figure 5-9). The results from the optical judgment of the dispersions are listed in Table 5-3, column 6 (cutout of Table I-7, Appendix).

Table 5-3: Logarithmic mass and number ratio, the absorbance at 400nm and optical judgment for silica dispersions in presence of partially quaternized poly(ethylenimine) derivatives, exemplary for (XIII)-001 – (XIII)-009; cutout of Table I-7, Appendix)

Polymer	Dispersion	log r_m	log r_u	A_{400nm}	Optical judgment
PEI_{1393}	(XIII)-001	-2.45	3.15	0.28	D
	(XIII)-002	-2.01	3.59	1.73	P
	(XIII)-003	-1.70	3.89	1.78	P
	(XIII)-004	-1.44	4.15	1.49	P
	(XIII)-005	-1.00	4.59	0.55	D
	(XIII)-006	-0.61	4.99	0.62	D
	(XIII)-007	-0.30	5.29	0.59	D
	(XIII)-008	0.00	5.59	0.67	D
	(XIII)-009	0.40	6.00	0.63	D

(D: dispersion; P: precipitation)

5.5. UV/Vis-absorption measurements

UV/Vis-absorption spectra were measured 24 hours after the ultrasound treatment was performed. Note that every sample was treated with a Vortexer to stir up the agglomerates prior to the absorption measurements. The agglomerates were found to remain in solution for about the 2min required to perform the measurement. The spectra were recorded over a wavelength range from 190 to 1100nm. In the performed UV/Vis-absorption measurements of the silica dispersions, only a slight absorption of UV light occurred, so that the occurrence of light scattering could be investigated.

Figure 5-10 shows four UV/Vis-absorption spectra, one of 0.5wt% silica nanoparticles in water (sample 001), and three samples containing 0.5wt% silica nanoparticles plus an increasing amount of PEI_{1393} (XIII) (samples (XIII)-001 (log r_u = 3.15), (XIII)-003 (log r_u = 3.89), and (XIII)-005 (log r_u = 4.59)).

The samples 001, (XIII)-001 and (XIII)-005 do not absorb light at wavelengths above 800nm. The absorption of the sample (XIII)-003 shows a broad absorption band ranging from 500nm to the highest measured wavelength of 1100nm. Towards a smaller wavelength from 500 to 200nm the absorbance increases due to light scattering [3]. The magnitude of absorbance at a wavelength below 500nm was correlated to the magnitude of turbidity. Comparing the

spectra, and the optical appearance of the dispersions revealed that the latter can be well correlated to A_{400}, i.e. the absorbance measured at λ=400nm, allowing to compare the turbidity of dispersions. The chosen wavelength has also been used by other authors [4], who demonstrated that increasing A_{400} values indicate more turbid systems. The values of the measured absorbance at 400nm of the silica dispersions in the presence of partially amino-quat-primer derivatives are summarized in Table I-7, column 5, Appendix and a cutout of the relevant samples for Chapter 5.4. and Chapter 5.5. is shown in Table 5-3.

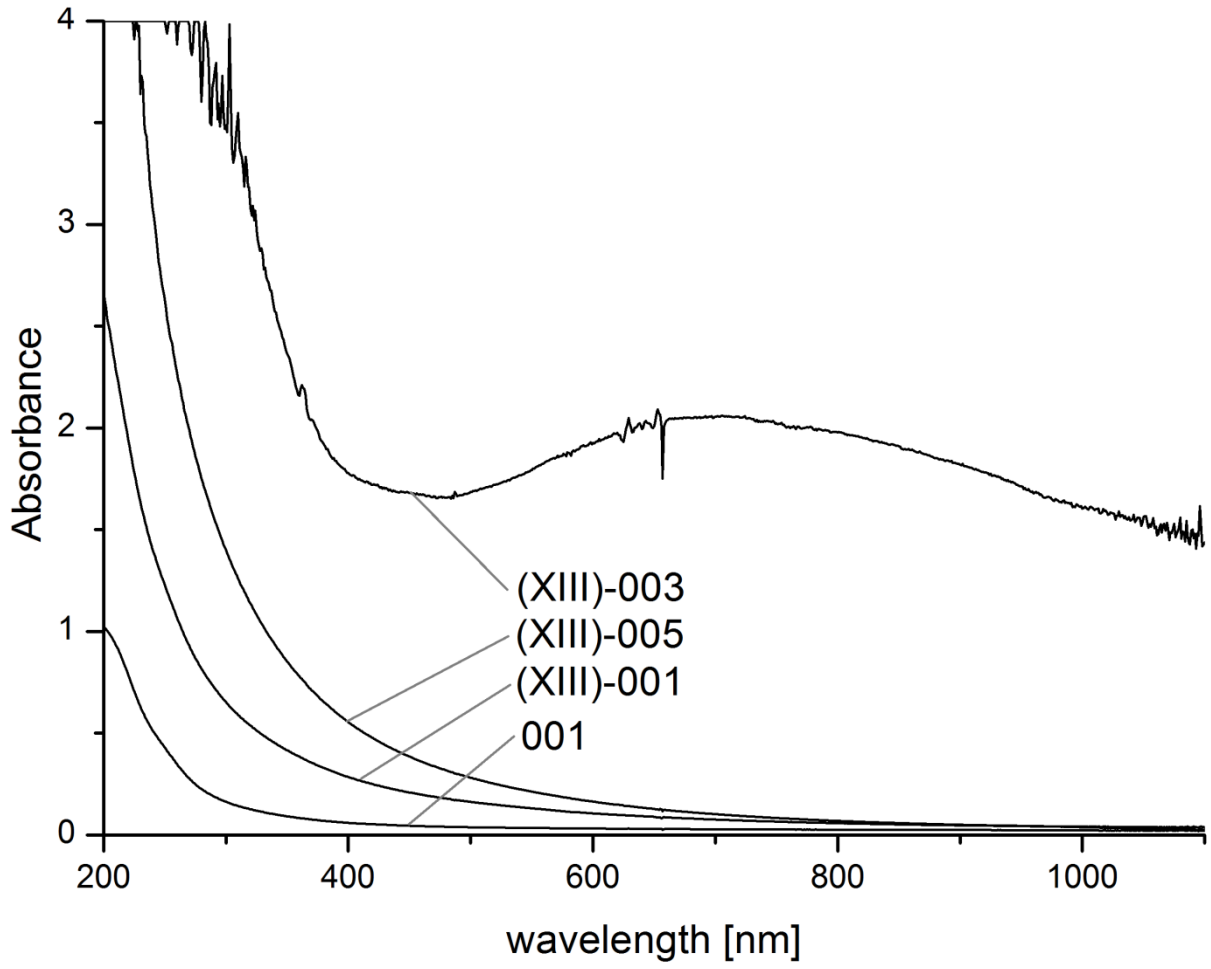

Figure 5-10: UV/Vis-absorption spectra of the dispersions 001, (XIII)-001 (log r_u = 3.15), (XIII)-003 (log r_u = 3.89) and (XIII)-005 (log r_u = 4.59); (0.5wt% silica, T = 25°C)

5.5.1. Reproducibility

To investigate on the reproducibility of the production of the dispersions one stable, (XVI)-005, and one non-stable dispersion composition, (XVI)-003, were chosen and the production and the UV/Vis-absorption measurements were repeated twice for each of the samples.

Figure 5-11a) shows the absorbance as a function of the wavelength of the dispersion (XVI)-005, as well as its replications (XVI)-019 and (XVI)-020, while Figure 5-11b) illustrates respective measurements with samples (XVI)-003, (XVI)-021 and (XVI)-022.

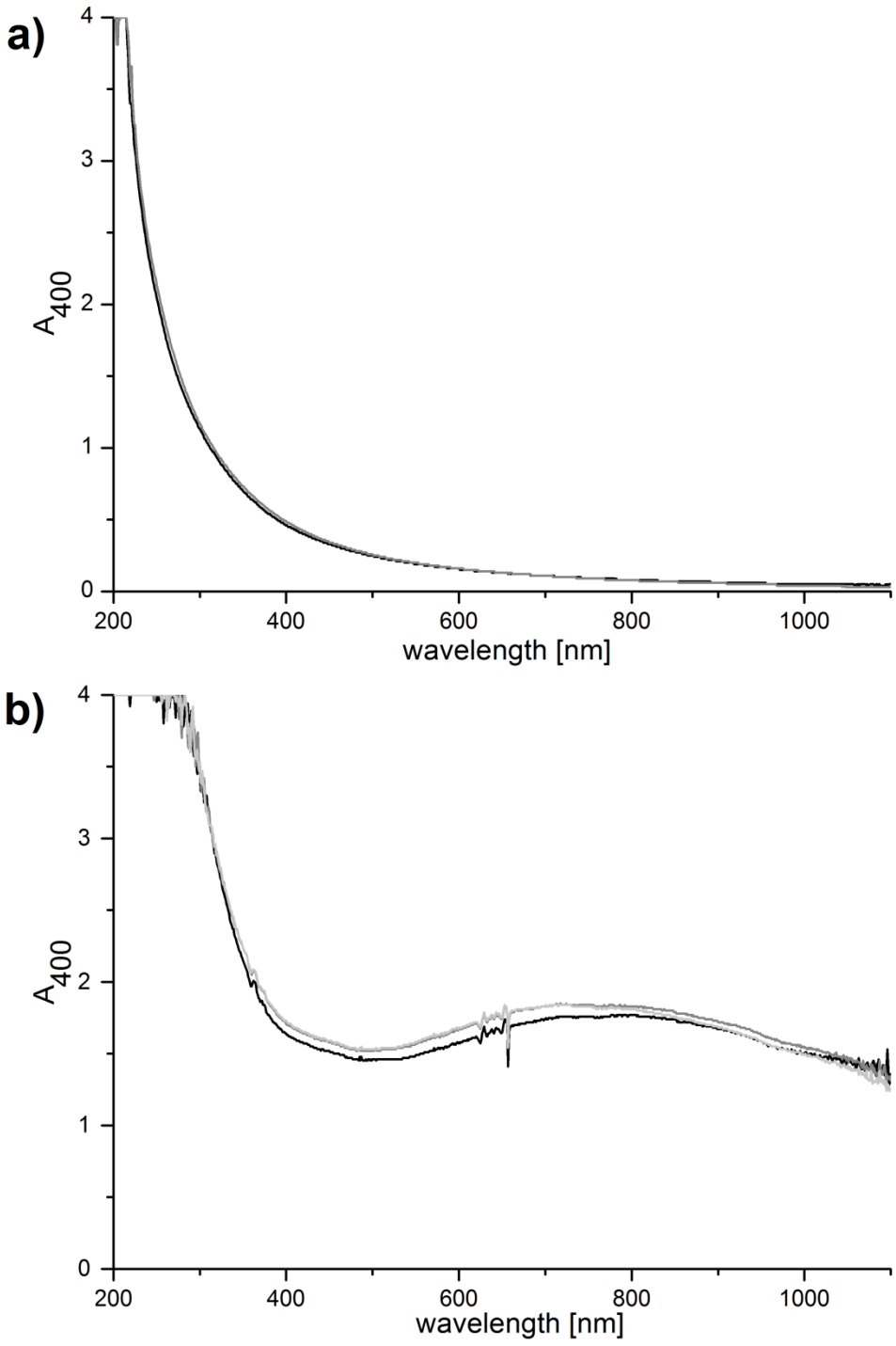

Figure 5-11a): UV/Vis-absorption spectra of the dispersions (XVI)-005 (black line), (XVI)-019 (dark grey line) and (XVI)-020 (light grey) (log r_u = 4.15), b) UV/Vis-absorption spectra for the dispersions (XVI)-003 (black line), (XVI)-021 (dark grey line) and (XVI)-022 (light grey line) (log r_u = 3.65); (0.5wt% silica, T = 25°C)

The absorbances at 400nm of the stable sample (XVI)-005, and its replications differ only about 6.5% (ΔA_{400} < 0.03). The A_{400}-values of the non-stable sample compositions were of similar reproducibility (ΔA_{400} < 0.09, eqv. 5.5%). It can be concluded, that the production of the dispersions and the absorption measurements give well reproducible results.

5.5.2. Influence of ultrasound treatment

To investigate on the influence of the process of sonication on the stability of the dispersions, samples of the same composition, one time after ultrasound treatment and one time without further treatment are compared. Samples were prepared with a logarithmic subunit ratio of log r_u = 3.15, 3.65, 4.14, 4.64 and 5.14 without further treatment after producing, (XVI)-014 – (XVI)-018, and with ultrasound treatment, (XVI)-001, (XVI)-003, (XVI)-005, (XVI)-007 and (XVI)-009.

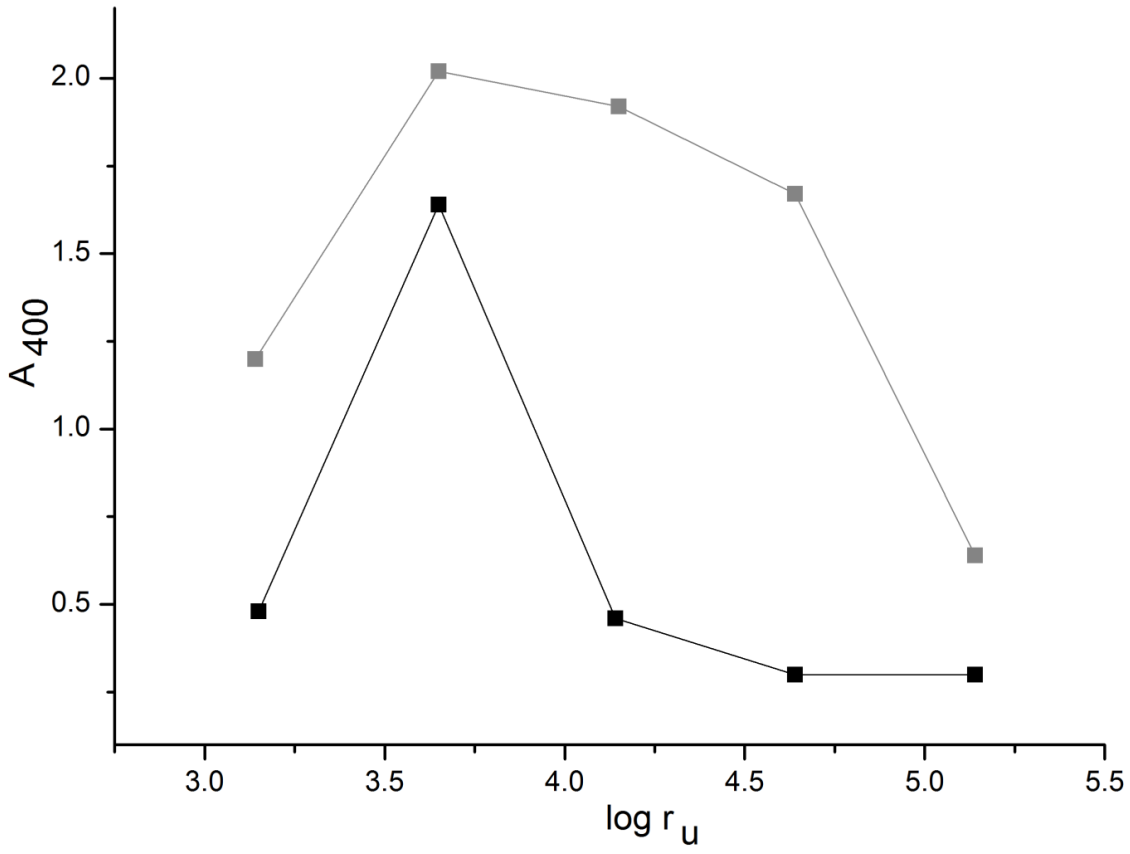

Figure 5-12: Absorbance at 400nm as a function of logarithmic subunit ratio of silica dispersions containing PEI_{1393}^{50Q} (XVI); black dots: after ultrasound treatment, grey dots: without further treatment; (0.5wt% silica; log r_u = 3.15, 3.65, 4.14, 4.64 and 5.14; T = 25°C)

Figure 5-12 illustrates the absorbance at 400nm as a function of the logarithmic subunit ratio of the dispersions of silica nanoparticles in the presence of $\mathrm{PEI}_{1393}^{50\mathrm{Q}}$ (XVI). Black squares stand for samples after ultrasound treatment and grey squares for samples without further treatment. The values of absorbance at 400nm are in all cases much higher for the samples without sonication than for the samples with sonication. It can be concluded that the process of sonication strongly enhances the stability of dispersions made from quaternized poly(ethylenimine) derivatives and silica nanoparticles. A possible explanation could be that the energy introduced to the system by ultrasound sonication is sufficiently large to break the physical connections between the silica surface and the quaternary ammonium groups of the polymers. This possibly gives the polymer the opportunity to rearrange its conformation, to wrap around single nanoparticles and to avoid agglomeration.

5.5.3. Absorbance at 400nm

Plots of A_{400} versus the logarithmic subunit ratio log r_u of dispersions prepared with amino-quat-primer derivatives of a uniform degree of polymerization, but different degrees of quaternization are shown in Figure 5-13 for X_n = 28 (samples: (I)-001 – 019, (II)-001 – 010, (III)-001 – 010, (IV)-001 – 015, (V)-001 – 012, (VI)-001 – 014, (VII)-001 – 014), in Figure 5-14 for X_n = 232 (samples: (VIII)-001 – 010, (IX)-001 – 022, (X)-001 – 015, (XI)-001 – 015, (XII)-001 – 015),and in Figure 5-15 for X_n = 1393 (samples: (XIII)-001 – 009, (XIV)-001 – 012, (XV)-001 – 011, (XVI)-001 – 013, (XVII)-001 – 011).

In Figure 5-13g) the graph of PEI_{28} (I) (q = 0%) starts with a low absorbance between 0.09 and 0.25 for the first eight dispersions (log r_u = 1.60 – 3.45). The following eight samples (log r_u = 3.59 – 5.99) show a high absorbance between 1.41 and 1.93, whereas the absorbance of the last three samples (log r_u = 6.60 – 6.90) come back to a low absorbance of around 0.1. The graphs for the polymers $\mathrm{PEI}_{28}^{1\mathrm{Q}}$ (II) and $\mathrm{PEI}_{28}^{5\mathrm{Q}}$ (III) in Figure 5-13f) and e) start with a low absorbance, followed by an increase and afterwards stay at a constant high value. For the partially quaternized poly(ethylenimine) derivatives with a degree of quaternization of q ≥ 10% (IV) – (VII) (Figure 5-13a) – d) the graphs consist of a low absorbance at the start followed by an increase, a decrease, and a slight increase. The start of the first increase of the absorbance is shifted to a lower number ratio with a higher degree of quaternization.

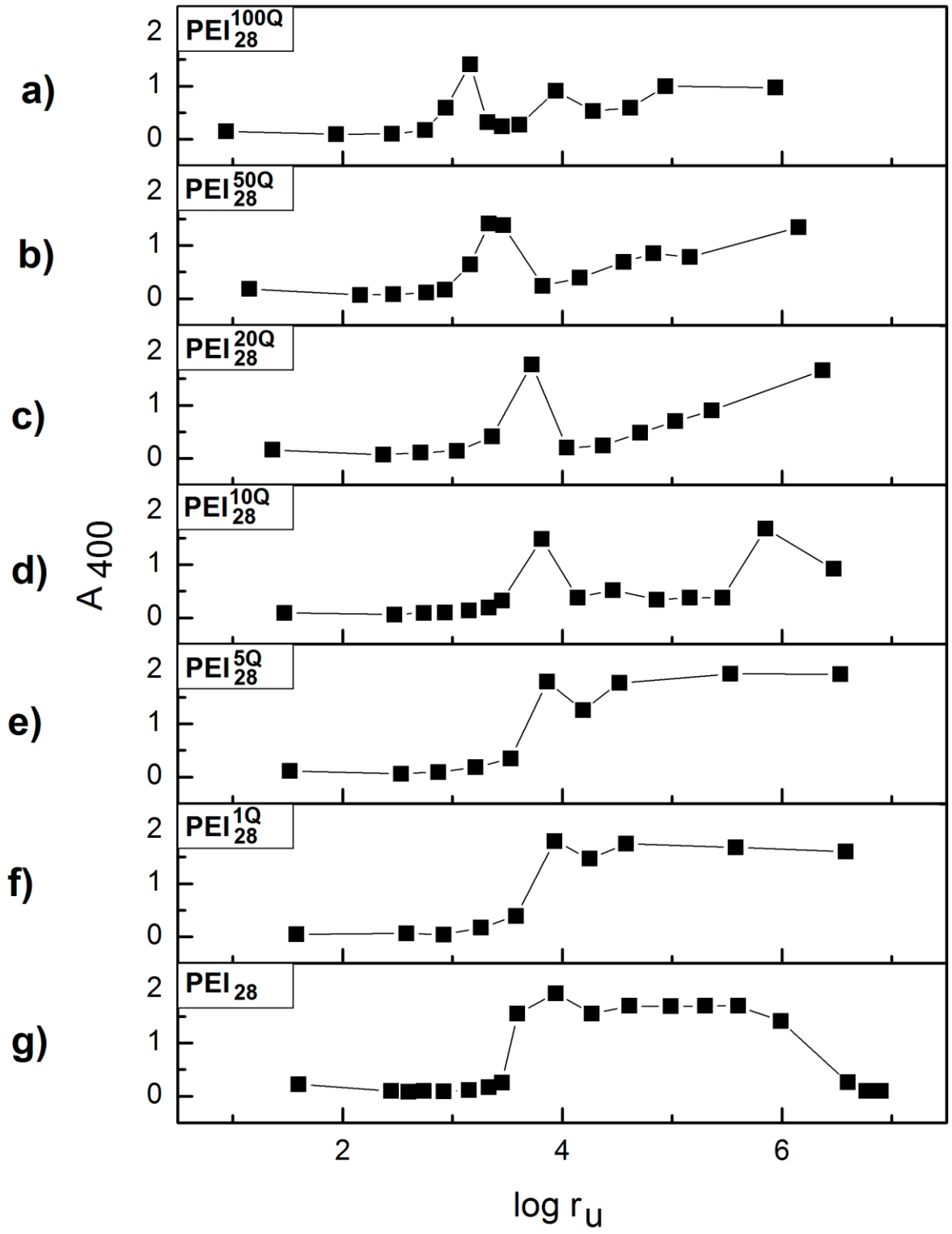

Figure 5-13: Absorbance at 400nm as a function of the logarithmic subunit ratio of silica dispersions containing the PEI_{28}^{qQ} polymers with the lowest degree of polymerization (I) – (VII); samples: (I)-001 – 019, (II)-001 – 010, (III)-001 – 010, (IV)-001 – 015, (V)-001 – 012, (VI)-001 – 014, (VII)-001 – 014; 0.5wt% silica, T = 25°C

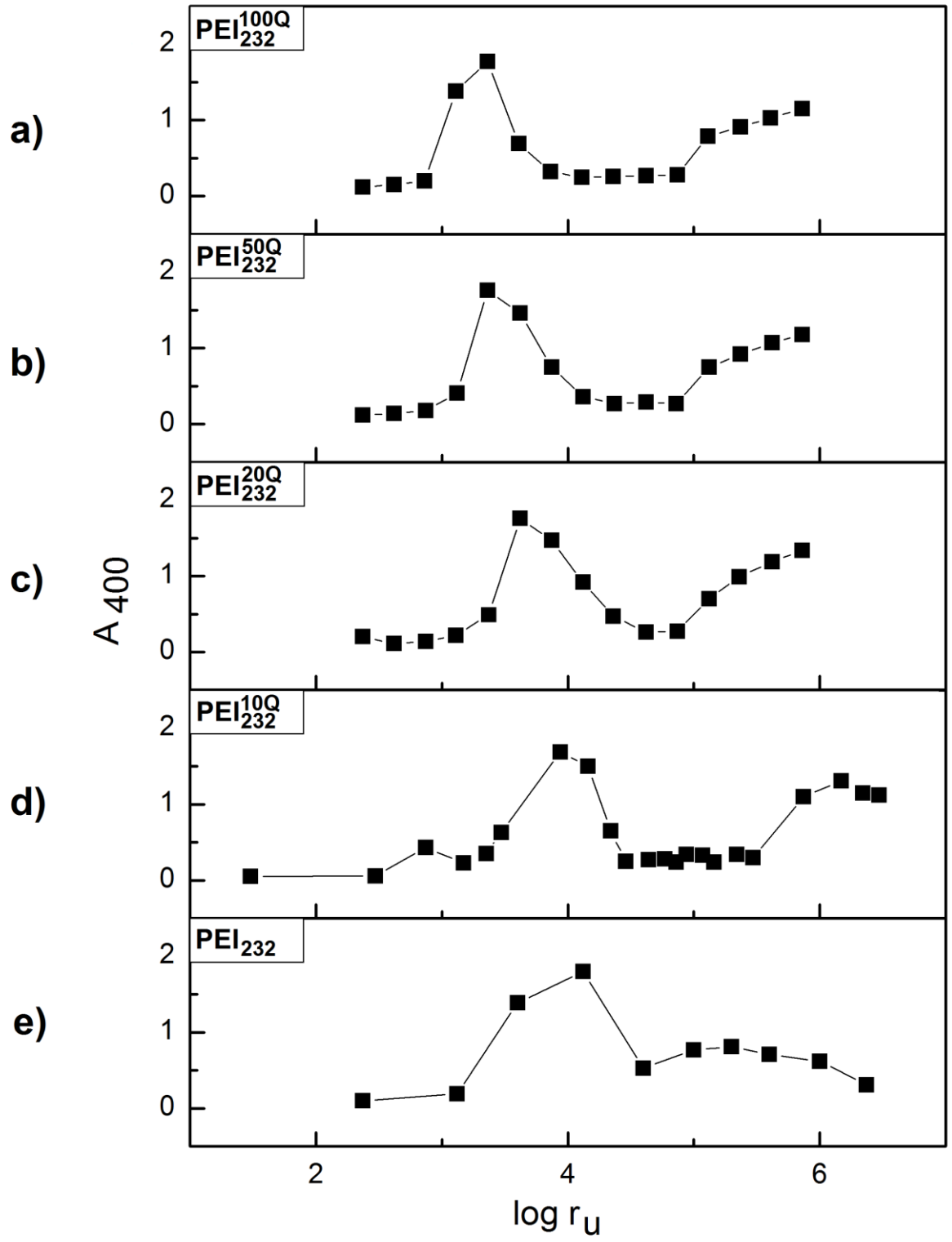

Figure 5-14: Absorbance at 400nm as a function of the logarithmic subunit ratio of silica dispersions containing the PEI_{232}^{qQ} polymers with the medium degree of polymerization (VIII) – (XII); samples: (VIII)-001 – 010, (IX)-001 – 022, (X)-001 – 015, (XI)-001 – 015, (XII)-001 – 015; 0.5wt% silica, T = 25°C

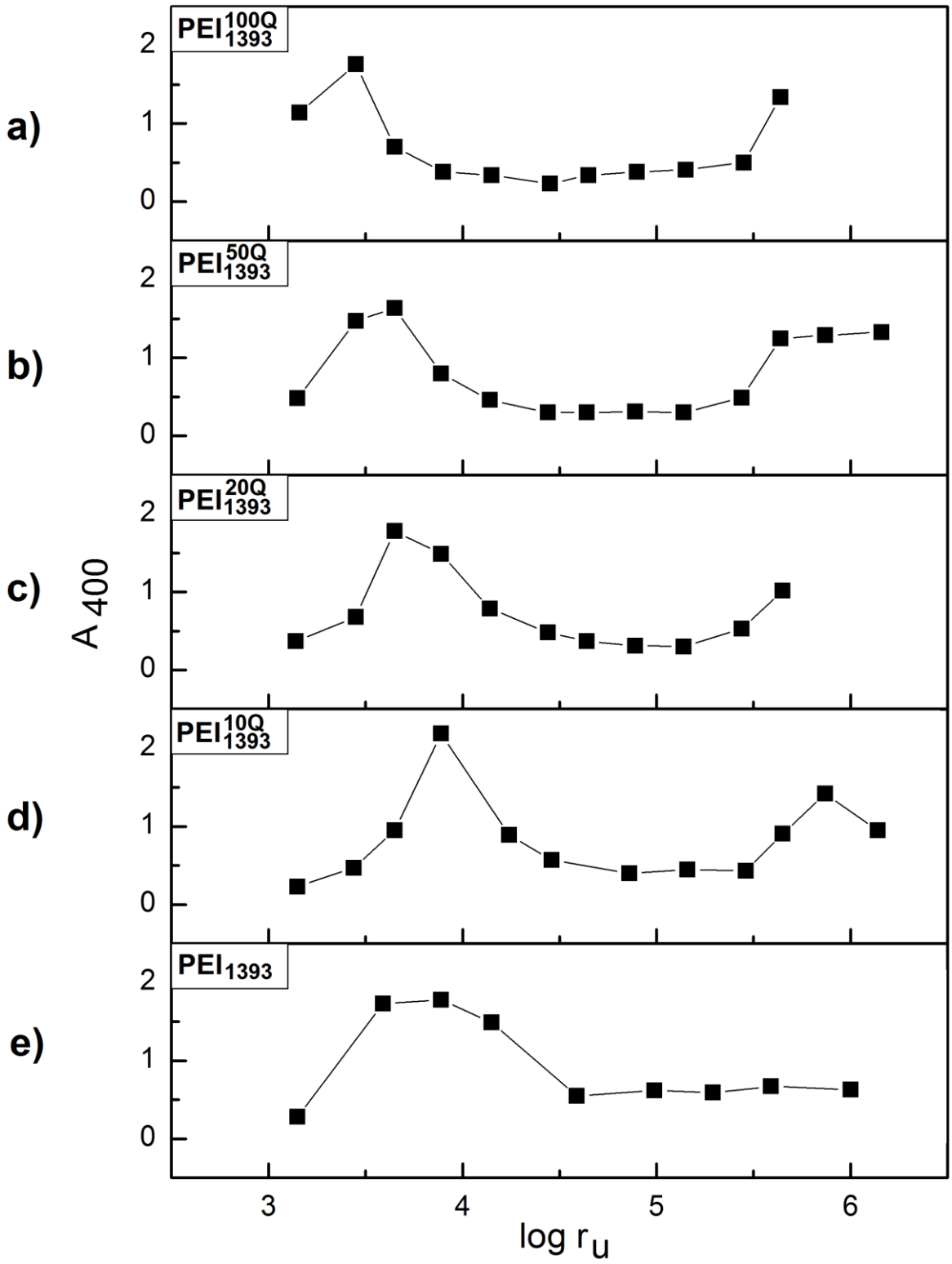

Figure 5-15: Absorbance at 400nm as a function of the logarithmic subunit ratio of silica dispersions containing the PEI_{1393}^{qQ} polymers with the highest degree of polymerization (XIII) – (XVII); samples: (XIII)-001 – 009, (XIV)-001 – 012, (XV)-001 – 011, (XVI)-001 – 013, (XVII)-001 – 011; 0.5wt% silica, T = 25°C

The graphs of the dispersions containing partially quaternized derivatives $\mathrm{PEI}_{232}^{\mathrm{qQ}}$ (IX) – (XII) with q ≥10 % (Figure 5-14a) – e) exhibit a low absorbance at the start followed by an increase, a decrease, a constant low value and a slight increase with growing log r_u. In contrast to this, in the graph of the dispersions with pure poly(ethylenimine) PEI_{232} (VIII) no final increase occurs. Also with the intermediate degree of polymerization (X_n = 232) the start of the first increase is shifted to a lower number ratio with an increasing degree of quaternization.

The graphs in Figure 5-15 of silica dispersions containing the derivatives of the highest degree of polymerization $\mathrm{PEI}_{1393}^{\mathrm{qQ}}$ (XIII) – (XVII) show the same trend as the polymers with the intermediate degree of polymerization, except from the difference that with the derivative $\mathrm{PEI}_{1393}^{100\mathrm{Q}}$ (XVII), the graph starts with a high value virtually “in the middle of the increase” without an occurring earlier low absorbance region.

5.6. Conclusion

The preparation and the optical investigation methods of silica dispersions in the presence of partially quaternized poly(ethylenimine) derivatives were discussed.

First the non-treated silica nanoparticles were characterized. Their size was determined to 30 ± 5 nm by means of dynamic light scattering and transmission electron microscopy. It was confirmed by titration and electrophoretic measurements that the particles carry slightly positive charge at low pH values and are highly negative charged at high pH values.

Silica-polymer-dispersions were prepared by means of sonication.

The terms “mass ratio” and “subunit ratio” between the mass of polymer and particles, as well as between the number of polymer subunits and the number of particles were introduced to compare dispersions prepared with macromolecules differing in the degree of polymerization X_n and in the degrees of quaternization q.

Prepared dispersions were optically judged as “dispersion” or as “precipitated” after 24 hours after the ultrasound treatment.

UV/Vis-absorption measurements were conducted and a correlation between the absorption value at 400nm and the turbidity of the sample was identified. The more turbid a dispersion

is, the higher the absorption at 400nm becomes. The turbidity of a dispersion may be correlated to particle agglomeration. The more unstable a dispersion is, the more turbid it becomes. The reproducibility of the absorption measurements was proved and the strong stabilization of the sonication during the dispersion preparation was confirmed.

Further characterization of the silica dispersions containing partially quaternized poly(ethylenimine) derivatives prepared in this chapter will be presented in Chapter 6.

[1] Berne, B.J.; Pecora, R.; Dynamic Light Scattering; Courier Dover Publications, New York, 2000

[2] Khlebtsov, B.N.; Kanadeev, V.A.; Khlebtsov, N.G.; Langmuir 2008, 24, 8964-8970

[3] Chong, C.S.; Colbow, K.; Biochimica et Biophysica Acta 1976, 436, 260-282

[4] Metin, C.O.; Lake, L.W.; Miranda, C.R.; Nguyen, Q.P.; Journal of Nanoparticle Research 2011, 13, 839-850

Chapter 6:

Stability of silica-nanoparticle-dispersions containing amino-quat-primer polymers

6. Stability of silica-nanoparticle-dispersions containing amino-quat-primer polymers

The stability of the silica-nanoparticle-dispersions (prepared in Chapter 5) containing partially quaternized poly(ethylenimine) derivatives (characterized in Chapter 4) was investigated in dependence on the subunit ratio r_u (defined in Chapter 5.3.) between the total number of polymer subunits and the total number of silica nanoparticles, the degree of polymerization X_n and the degree of quaternization q of the employed derivatives, as well as the pH and the salt concentration of the solution. The particle surface charge was investigated by means of laser-Doppler-velocimetry (cf. literature review, Chapter 2.5.2.), the dispersions turbidity was determined by means of absorption measurements at a fixed wavelength of 400nm (see Chapter 5.5.), and the dispersion pH was measured.

6.1. Dispersion stability

The combined results from the optical judgment (Chapter 5.4.) and the UV/Vis-absorption measurements (Chapter 5.5) of the silica dispersions containing amino-quat-primer polymers were used to construct “stability maps” to separately judge the influence of the degree of quaternization q and the degree of polymerization X_n on the dispersion stability.

6.1.1. Construction of stability maps

The “stability maps” were generated for each degree of polymerization (X_n = 28, 232 and 1393) of the added amino-quat-primer polymer, where the degree of quaternization q is shown as a function of the logarithmic subunit ratio log r_u (see Chapter 6.1.2., Figure 6-2a) – c) and for each degree of quaternization (q = 0, 10, 20, 50 and 100%), where the logarithmic degree of polymerization log X_n is shown as a function of the logarithmic subunit ratio log r_u (see Chapter 6.1.3., Figure 6-3a) – e). The construction of the “stability maps” will be explained exemplary for silica dispersions containing $\mathrm{PEI}_{1393}^{50\mathrm{Q}}$ (XVI), i.e. the polymer derivative with the highest degree of polymerization (X_n = 1393) and a degree of quaternization of q = 50%. Figure 6-1a) shows the picture of the dispersions (XVI)-001 – (XVI)-013 with $\mathrm{PEI}_{1393}^{50\mathrm{Q}}$ (XVI) 24 hours after dispersing. The samples (XVI)-001 and (XVI)-004 – (XVI)-013 consist of one continuous phase, whereas the dispersions (XVI)-002 and (XVI)-003 consist of two phases, one upper clear phase and a bottom white one. The samples (XVI)-004 – (XVI)-013 differ optically in their translucence.

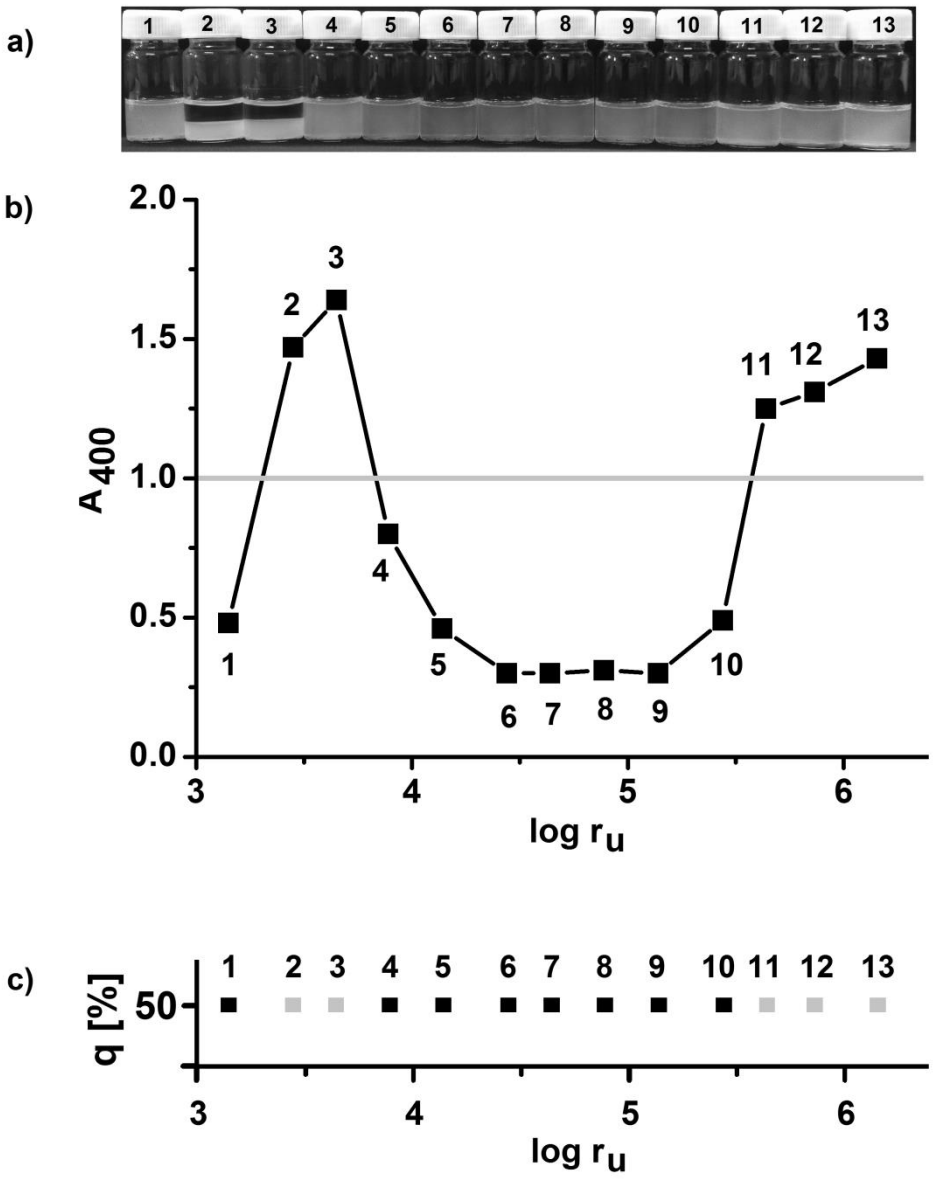

Figure 6-1a) Picture of the dispersions (XVI)-001 – (XVI)-013 24 hours after dispersing; b) Absorbance at 400nm of the dispersions (XVI)-001 – (XVI)-013; c) Constructed row for PEI_{60}^{50Q} (XVI) of the stability map of silica / PEI_{1393}^{qQ} –dispersion; black dots: dispersion, grey dots: precipitation

Figure 6-1b) illustrates the absorbance at 400nm of the samples (XVI)-001 – (XVI)-013 as a function of the logarithmic subunit ratio. Dispersions with value of A_{400} < 1 are defined as stable and samples with a value of A_{400} > 1 as unstable. The limiting value of A_{400} separating stable and non-stable dispersions depends on the degree of polymerization of the used polymer. The limiting values are A_{400} = 0.39 for X_n = 28, A_{400} = 0.91 for X_n = 232, and A_{400} = 1.00 for X_n = 1393. The distinction between dispersion and precipitated sample based on the value of A_{400} (cf. Table I-7, column 5, Appendix) is in agreement with the optical judgment (cf. Table I-7, column 6, Appendix) within an error limit of 0.03 of the absorbance for all samples that were employed to construct the stability maps. Figure 6-1c) illustrates the construction of

a horizontal line within the stability map of the system silica / PEI_{1393}^{qQ}. Black dots indicate stable dispersions and grey dots stand for precipitated samples, according to the optical investigations.

6.1.2. Influence of the degree of quaternization on the dispersion stability

To investigate the influence of the degree of quaternization on the stability of silica nanoparticles in the presence of partially quaternized poly(ethylenimine) derivatives, three stability maps, each for a constant degree of polymerization (X_n = 28, 232 and 1393) were constructed (see Figure 6-2a)-c). The dark grey plains were constructed to guide the eyes showing areas of stability. In the stability map of dispersions containing PEI_{1393}^{qQ} (XIII) – (XVII) (q = 0 – 100%, Figure 6-2a), four different regimes can be distinguished, namely two areas of stability (D_I and D_{II}) and two areas of instability (P_I and P_{II}), which occur alternatingly. With unmodified PEI_{1393} (XIII) (q = 0%) the area P_I is broad compared to the quaternized derivatives (q > 0%) and the area P_{II}, the second area of instability, does not exist in the investigated r_u range. The area P_I, the first area of instability becomes located at smaller subunit ratios with an increasing degree of quaternization q. With highly quaternized PEI_{1393}^{100Q} (XVII) (q = 100%), the first area of stability D_I is not present in the investigated range, and is speculated to appear at log r_u < 3. The subunit ratio where the area P_{II} starts is independent of the degree of quaternization of q ≥ 20%.

The stability map of the dispersions prepared in the presence of derivatives with the intermediate degree of polymerization (X_n = 232) PEI_{232}^{qQ} (VIII) – (XII) (Figure 6-2b) shows a similar shape as the one with polymers with the highest degree of polymerization (Figure 6-2a), four different stability regions (D_I, P_I, D_{II}, and P_{II}) can be found. Similar to the case of the dispersions with the polymers with the highest degree of polymerization, the row for the unmodified derivative PEI_{232} (VIII) does not exhibit a second area of instability at log r_u < 6.4. Similar to Figure 6-2a) the first area of instability P_I is shifted to a smaller subunit ratio with an increasing degree of quaternization of q ≥ 20%, and the subunit ratio where the area P_{II}, the second area of instability, starts, is independent of the degree of quaternization.

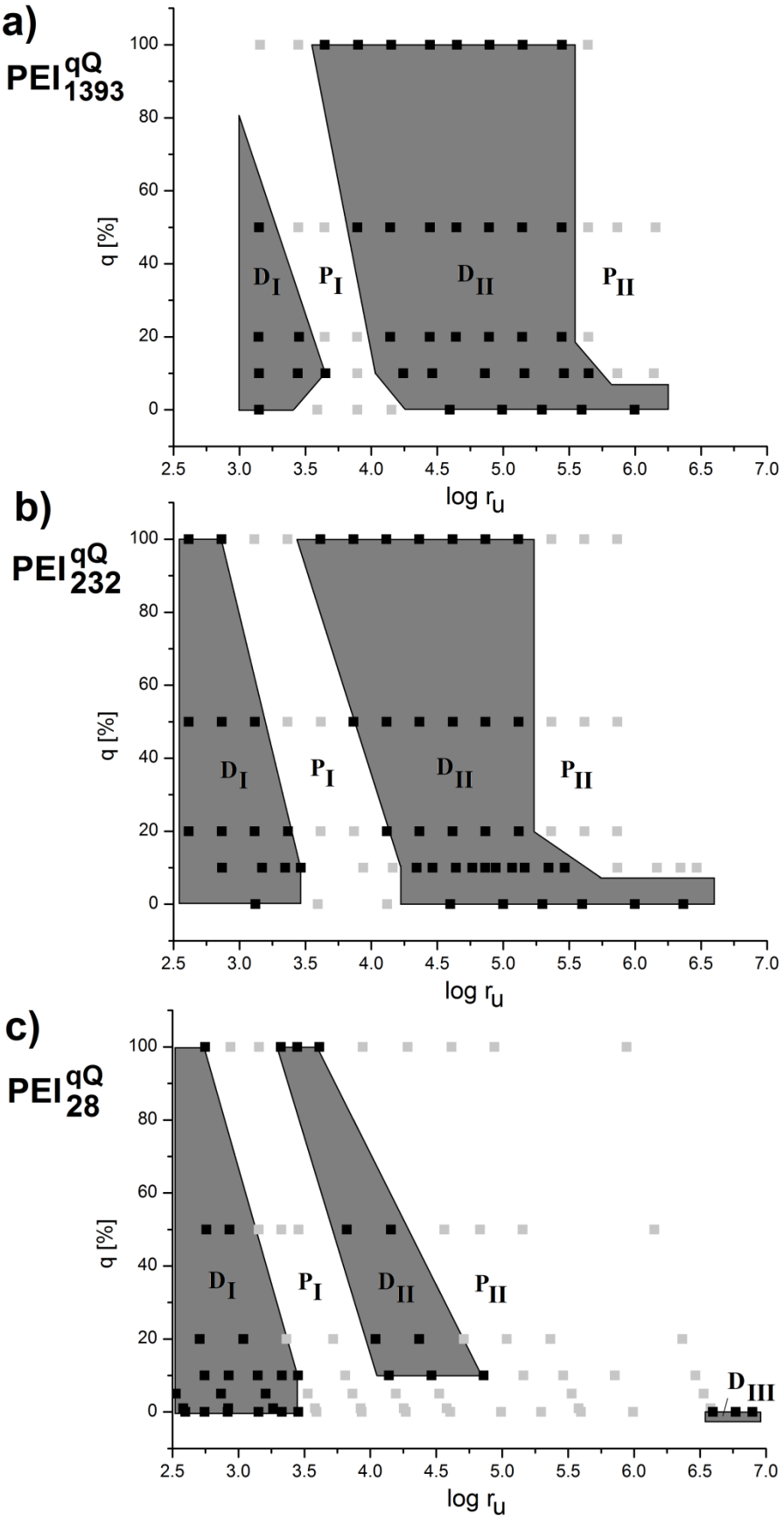

Figure 6-2: Stability maps of silica / $PEI_{X_n}^{qQ}$ –dispersions, degree of quaternization against logarithmic subunit ratio; black dots: stable dispersions, grey dots: precipitated samples

Figure 6-2c) shows the stability map obtained with the PEI^{Q}-dispersants with a lowest degree of polymerization (X_n = 28) PEI_{28}^{qQ} (I) – (VII). With derivatives of a degree of quaternization below 10%, the areas D_{II} and P_{II} do not occur in the investigated range of log r_u. Similar as with derivatives with the both higher degrees of polymerization, the first area of instability, area P_I, is also with X_n = 28 shifted to a smaller subunit ratio with an increasing degree of quaternization of q ≥ 10%. In contrast to the higher degrees of polymerization, the subunit ratio, where the area P_{II}, the second area of instability, starts, decreases with an increasing degree of quaternization for q ≥ 10%. A special feature in this diagram is the emergence of a new region of stability (area D_{III}) exclusively to be found with PEI_{28} (I), the derivative with the lowest degree of polymerization without any quaternization at very high subunit ratios of log r_u > 6.5.

The three stability maps in Figure 6-2 illustrate the influence of the degree of quaternization on the stability of silica nanoparticles in the presence of partially quaternized poly(ethylenimine) derivatives. In all three stability maps for the different degrees of polymerization, two areas of stability (D_I and D_{II}) and two areas of instability (P_I and P_{II}) occur alternatingly. Only for a minimum degree of quaternization of q ≥ 10%, there is found a restabilization and redestabilization behavior indicated by the areas D_{II} and P_{II} for the lowest degree of polymerization (Figure 6-2c), and a redestabilization behavior indicated by area P_{II} for the intermediate (Figure 6-2b) and the highest degree of polymerization (Figure 6-2a). With an increasing degree of quaternization (q ≥ 10%) the location of area P_I and the start of area D_{II} are shifted to lower subunit ratios for all degrees of polymerization. With the intermediate and the highest degree of polymerization the start of area P_{II} seems to be independent of the degree of quaternization at q ≥ 20%, and the extent of area D_{II} increases with a growing degree of quaternization. In contrast to this the extent of area D_{II} decreases with an increasing degree of quaternization for the lowest degree of polymerization.

6.1.3. Influence of the degree of polymerization on the dispersion stability

To investigate the influence of the degree of polymerization on the stability of silica nanoparticles dispersions containing amino-quat-primer polymers, five stability maps, each for a constant degree of quaternization (q = 0, 10, 20, 50 and 100%) were constructed.

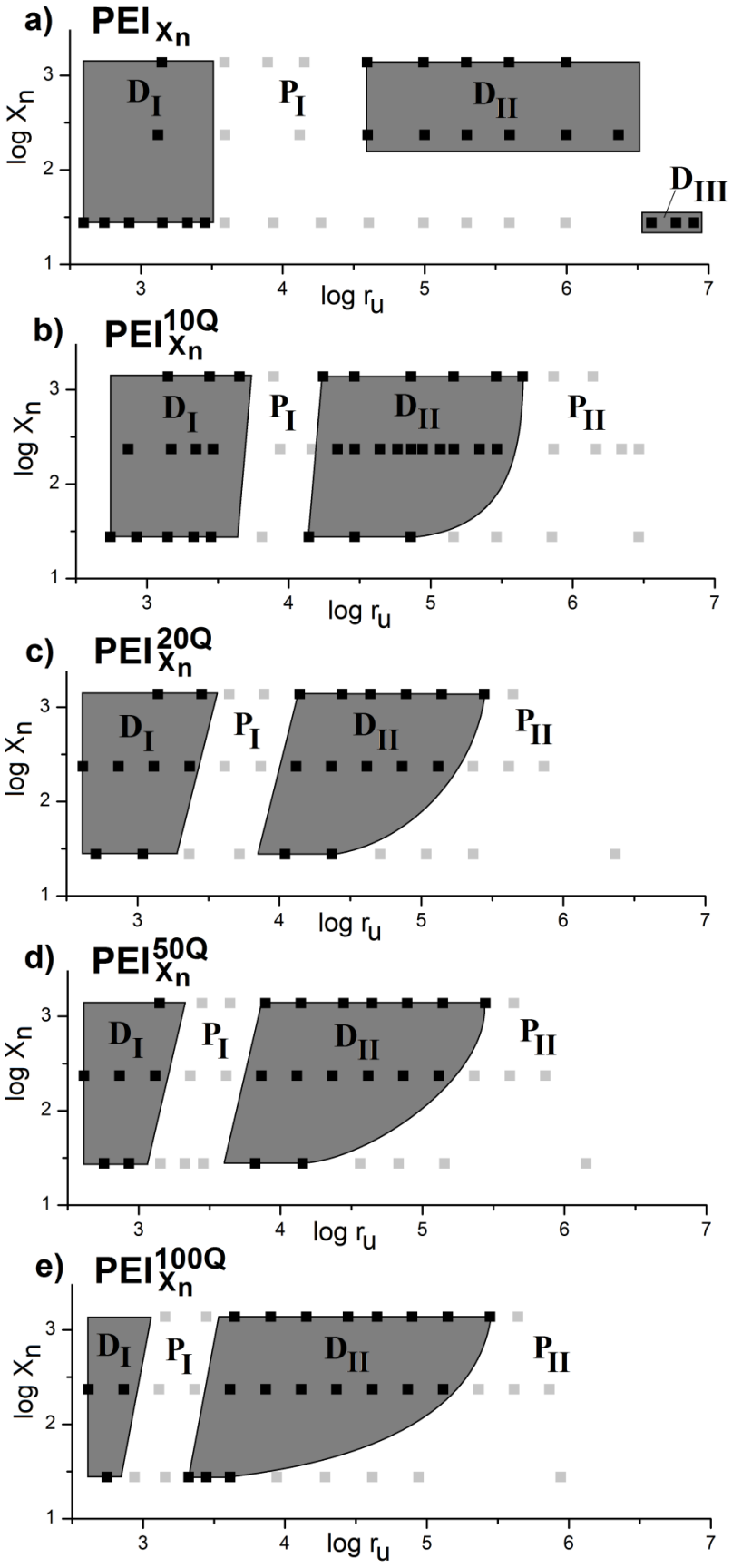

Figure 6-3: Stability maps of silica / $PEI_{X_n}^{qQ}$ –dispersions, logarithmic degree of polymerization against logarithmic subunit ratio; black dots: stable dispersions, grey dots: precipitated samples

Figure 6-3 depicts the stability maps of dispersions containing a) PEI_{X_n}, b) $PEI_{X_n}^{10Q}$, c) $PEI_{X_n}^{20Q}$, d) $PEI_{X_n}^{50Q}$, and e) $PEI_{X_n}^{100Q}$. The logarithmic degree of polymerization is plotted versus the logarithmic subunit ratio log r_u. As in the stability maps shown in Figure 6-2 in Chapter 6.1.2., the black dots indicate stable dispersions and the grey dots stand for samples, where precipitation occurred. The dark grey plains were constructed to guide the eyes and should show areas of stability.

In the stability map of the unmodified derivatives (Figure 6-3a), the first area of instability P_I starts at a subunit ratio of log $r_u \approx 3.5$ independently of the degree of polymerization. For the intermediate and the highest degree of polymerization, the second area of stability D_{II} starts at the same subunit ratio and is still present for the highest investigated subunit ratios. With the lowest degree of polymerization the areas P_{II} and D_{II} do not occur, but the area D_{III} emerges.

The shape of the occurring stability regimes D_I, P_I, D_{II} and P_{II} is similar in the stability maps with a degree of quaternization of q ≥ 10% (Figure 6-3b) – e). The location of the first area of instability P_I is shifted to a higher subunit ratio with an increasing degree of polymerization. The extent of the area D_{II} increases with an increasing degree of polymerization, however the extent does not increase linearly. It is much smaller with the lowest degree of polymerization compared to the larger ones, whereas it increases just slightly from the intermediate to the highest degree of polymerization.

6.2. Dispersion pH

The change of the dispersions pH was investigated upon addition of the quaternized poly(ethylenimine) derivatives. The pH values of two series of dispersions, prepared in the presence of an amino-quat-primer polymer with (i) a constant degree of polymerization of X_n = 1393, and (ii) a constant degree of quaternization of q = 50% was measured.

6.2.1. Influence of the degree of quaternization on the dispersion pH

The pH-values of all silica-nanoparticle-dispersions containing the amino-quat-primer polymers with X_n = 1393, PEI_{1393}^{qQ} (XIII) – (XVII), were measured (values listed in Table I-8, column 3, Appendix).

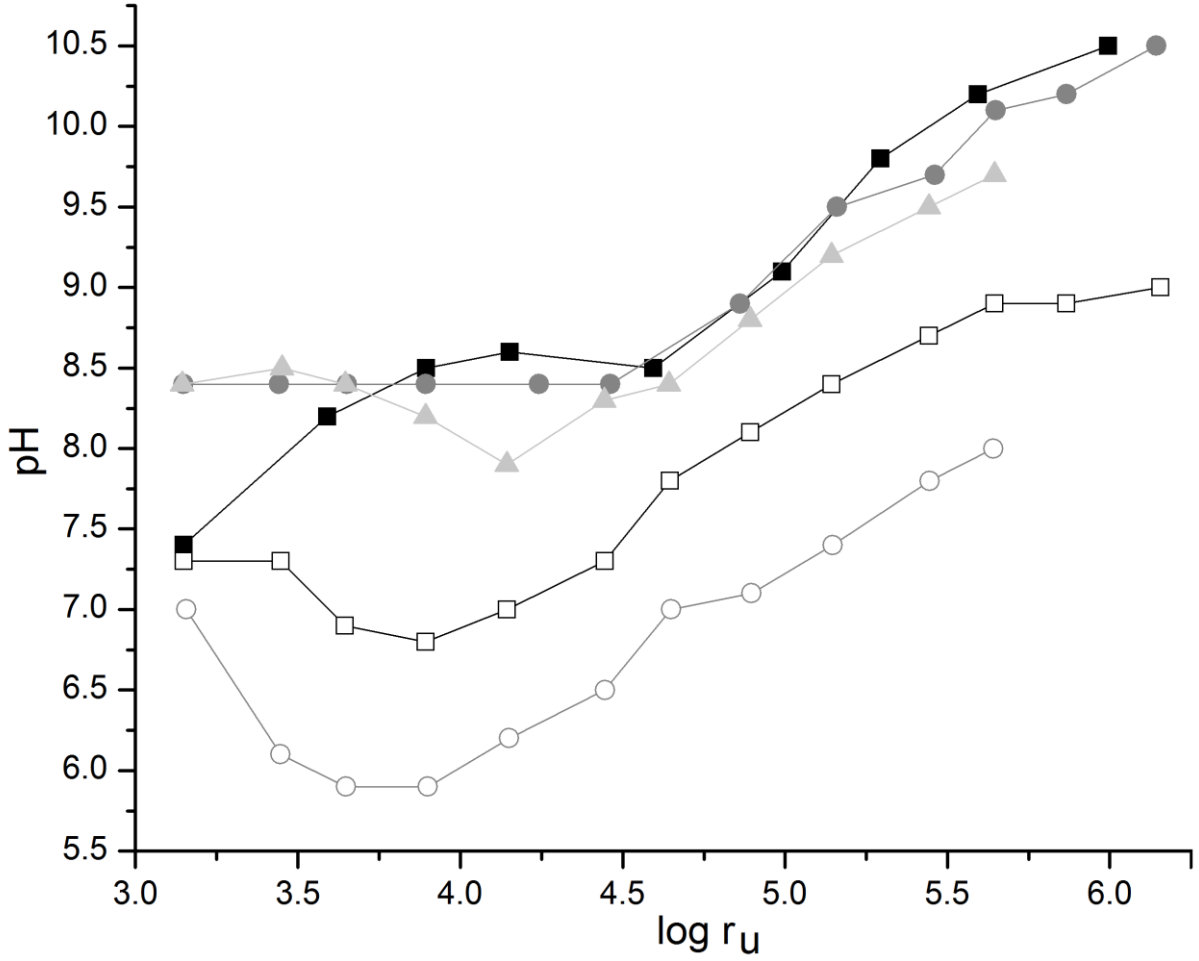

Figure 6-4: pH values of silica / PEI_{1393}^{qQ} –dispersions as a function of the logarithmic subunit ratio log r_u; filled back squares: PEI_{1393} (XIII), filled dark grey circles: PEI_{1393}^{10Q} (XIV), filled light grey triangles: PEI_{1393}^{20Q} (XV), empty black squares: PEI_{1393}^{50Q} (XVI), empty dark grey circles: PEI_{1393}^{100Q} (XVII)

The plots of the dispersion pH against the logarithmic subunit ratio of all five investigated partially quaternized poly(ethylenimine) derivatives in Figure 6-4 can be split into two parts with respect to their slope. In the first part (log r_u < 4.5) the slope depends on the degree of quaternization of the used polymer. The higher the degree of quaternization, the smaller becomes the slope. The pH of the dispersions prepared in the presence of the non-quaternized poly(ethylenimine) PEI_{1393} (XIII) increase between log r_u from 3.15 to 4.59 with a decreasing slope. The pH of the dispersions with PEI_{1393}^{10Q} (XIV) is constant at log r_u = 3.15 – 4.46, and in presence of the highly quaternized polymers with q ≥ 20% (XV) – (VII) the pH value decreases until log r_u = 4.14 for q = 20% and until log r_u = 3.90 for q = 50%, as well as 100%. In the second part (log r_u > 4.5) the pH increases fairly constant, independent of the degree of quaternization.

6.2.2. Influence of the degree of polymerization on the dispersion pH

Figure 6-5 illustrates the dispersion pH as a function of the logarithmic subunit ratio of dispersions prepared in the presence of partially quaternized poly(ethylenimine) derivatives with a constant degree of quaternization of q = 50% (values listed in Table I-8, column 3, Appendix).

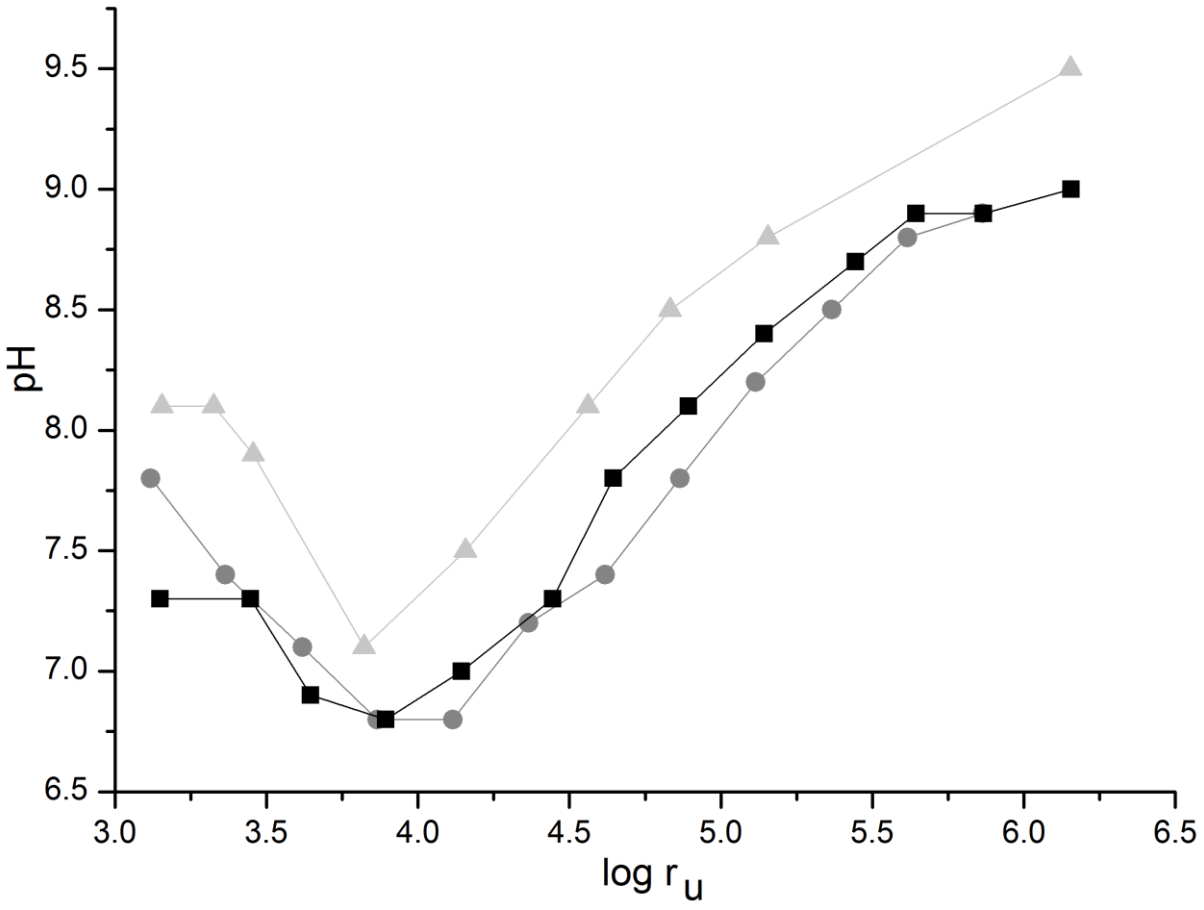

Figure 6-5: pH values of silica /$PEI_{X_n}^{50Q}$ –dispersions as a function of the logarithmic subunit ratio; back squares: PEI_{28}^{50Q} (VI), dark grey circles: PEI_{232}^{50Q} (XI), light grey triangles: PEI_{1393}^{50Q} (XVI)

The curves can be divided into two parts concerning their slope. In the first part (log r_u < 4.2) the slope is negative, and in the second part positive. The slope of both parts, as well as the position of the reversal point are very similar of all three curves in the presence of the three polymers with different degrees of polymerization. The curves for both higher degrees of polymerization overlap, but the curve for the lowest degree of polymerization is shifted to higher pH values about an interval of 0.5.

6.2.3. Deprotonation of the silica surface

It was shown in Chapter 4.7. that the pH of solutions of amino-quat-primer polymers in water is always basic, and increases with increasing polymer concentration, and with decreasing the degree of quaternization. A constant increase of the pH upon addition of polymer to the dispersion like it appears after the change of the slope of the curves for all polymers can be explained by the basicity of the polymers. The slope of the curves before the change happens, is smaller than after the change for PEI_{1393} (XIII), equals zero for $\mathrm{PEI}_{1393}^{10\mathrm{Q}}$ (XIV) and is even negative for the polymers with q ≥ 20%.

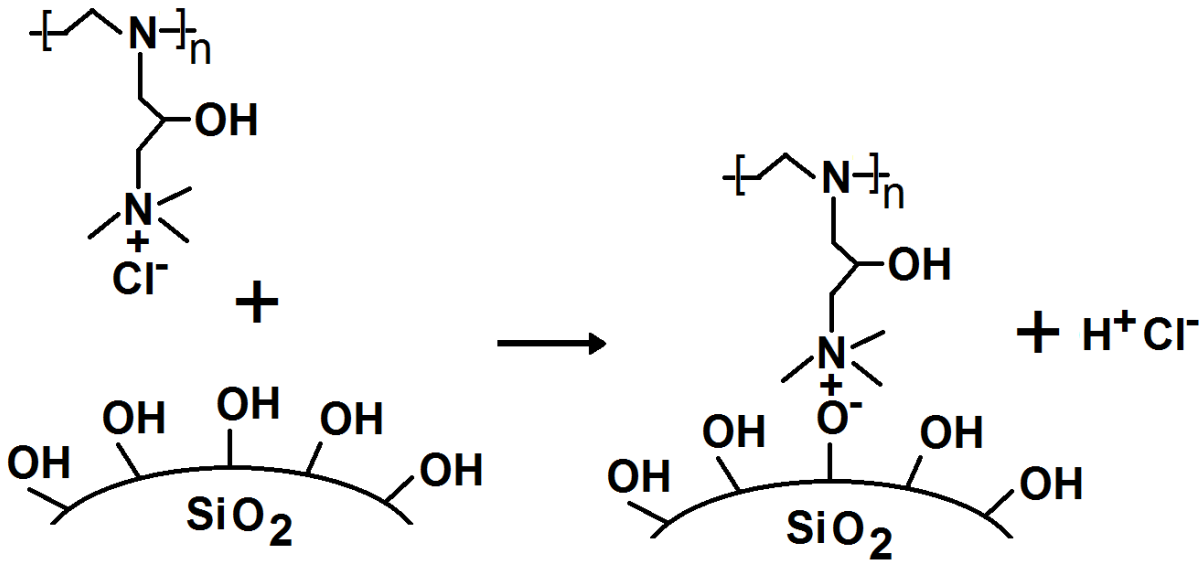

Figure 6-6: Adsorption of a partially quaternized poly(ethylenimine) derivative to the silica surface upon release of hydrochloric acid

The pH of the neutral nanoparticle-dispersion decreases upon addition of a basic polymer solution, due to a release of chloride counterions from the quaternized groups of the polymer and of protons from the silica surfaces upon the adsorption of the partially quaternized poly(ethylenimine) to the nanoparticle surface (see Figure 6-6). This means, that the charge interaction between polymer and nanoparticle is strong enough to deprotonate the surface of the silica nanoparticles. The release of hydrochloric acid into the solution then lowers the solution pH.

6.3. Particle surface charge

Electrophoretic measurements (cf. literature review, Chapter 2.5.2.) were performed with dispersions of silica nanoparticles prepared in the presence of the partially quaternized poly(ethylenimine) derivatives with a constant degree of polymerization and a varying degree

of quaternization (X_n = 1393; q = 0, 10, 20, 50 and 100%), as well as with a constant degree of quaternization and a varying degree of polymerization (q = 50%, X_n = 28, 232 and 1393).

6.3.1. Influence of the degree of quaternization on the particle surface charge

Figure 6-7 shows the electrophoretic mobility μ_e of the silica / $\mathrm{PEI}_{1393}^{\mathrm{qQ}}$ -particles as a function of the logarithmic subunit ratio log r_u (values listed in Table I-8, column 4, Appendix). Note, that the electrophoretic mobility of the bare silica nanoparticles was μ_e = -4.094*10^{-8} m²/Vs.

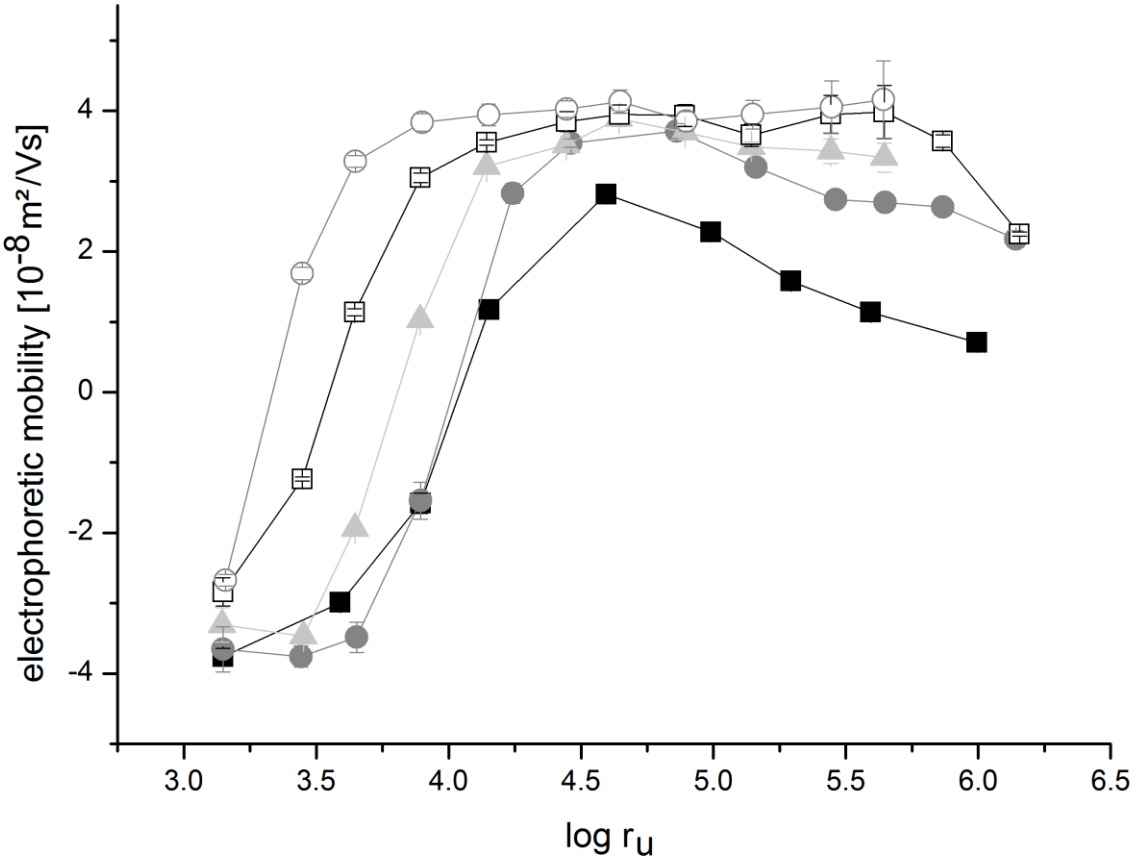

Figure 6-7: Electrophoretic mobility of silica / PEI_{1393}^{qQ} –dispersions as a function of the logarithmic subunit ratio; filled back squares: PEI_{1393} (XIII), filled dark grey circles: PEI_{1393}^{10Q} (XIV), filled light grey triangles: PEI_{1393}^{20Q} (XV), empty black squares: PEI_{1393}^{50Q} (XVI), empty dark grey circles: PEI_{1393}^{100Q} (XVII)

The general trend of the electrophoretic mobility is similar for all investigated polymers with the highest degree of polymerization. The graph starts at a highly negative value of the μ_e between -3.761*10^{-8} m²/Vs with q = 0% and -2.675*10^{-8} m²/Vs with q = 100% at log r_u = 3.15. With an increasing subunit ratio, the magnitude of the negative electrophoretic mobility values decreases, reaches μ_e = 0 at the isoelectric point (IEP), and afterwards increases to a

highly positive value. This behaviour of charge reversal of adsorbed polyelectrolytes onto oppositely charged surfaces was obtained in literature before (cf. literature review, Chapter 2.6.).

Table 6-1 summarizes the data obtained from the electrophoretic mobility measurements of the silica / PEI_{1393}^{qQ} –dispersions. The calculated logarithmic subunit ratios at the isoelectric point (IEP) and the adsorption saturation point (ASP), the calculated pH values at the IEP and the obtained values of the maximum electrophoretic mobility are listed. The values of $\log r_u^{IEP}$ and pH^{IEP} were calculated by linear regressions between the values determined of samples with the smallest positive and smallest negative electrophoretic mobility obtained in the presence of a particular polymer. The values of $\log r_u^{ASP}$ were determined at the intersects of two linear fitted functions, one with the slope of the electrophoretic mobility of samples, where adsorption occurred and one with the slope of μ_e of samples, after a full surface coverage was achieved.

Figure 6-8a) shows the logarithmic subunit ratio at the isoelectric point (IEP) and the adsorption saturation point (ASP) as a function of the degree of quaternization of the silica / PEI_{1393}^{qQ}–dispersions. The values of $\log r_u^{IEP}$ decrease with increasing the degree of quaternization and this decrease is approximately linear. A lower amount of polymer with a higher degree of quaternization is needed to neutralize the charge on the silica surface. The values of $\log r_u^{ASP}$ also decrease with an increasing degree of quaternization and also this decrease is approximately linear. This implies, that the maximum amount of polymer adsorbed on the silica surfaces decrease with an increasing degree of quaternization. Reasons for this can be the increasing diameter of the higher charged polymers or even more likely the stronger repulsive charges between the higher charged polymers, which prevent closer approach during adsorption.

Figure 6-8b) shows the dispersion pH at the calculated isoelectric point as a function of the degree of quaternization of the silica / PEI_{1393}^{qQ}–dispersions. The pH values at the isoelectric point decrease with increasing the degree of quaternization and this decrease is approximately linear.

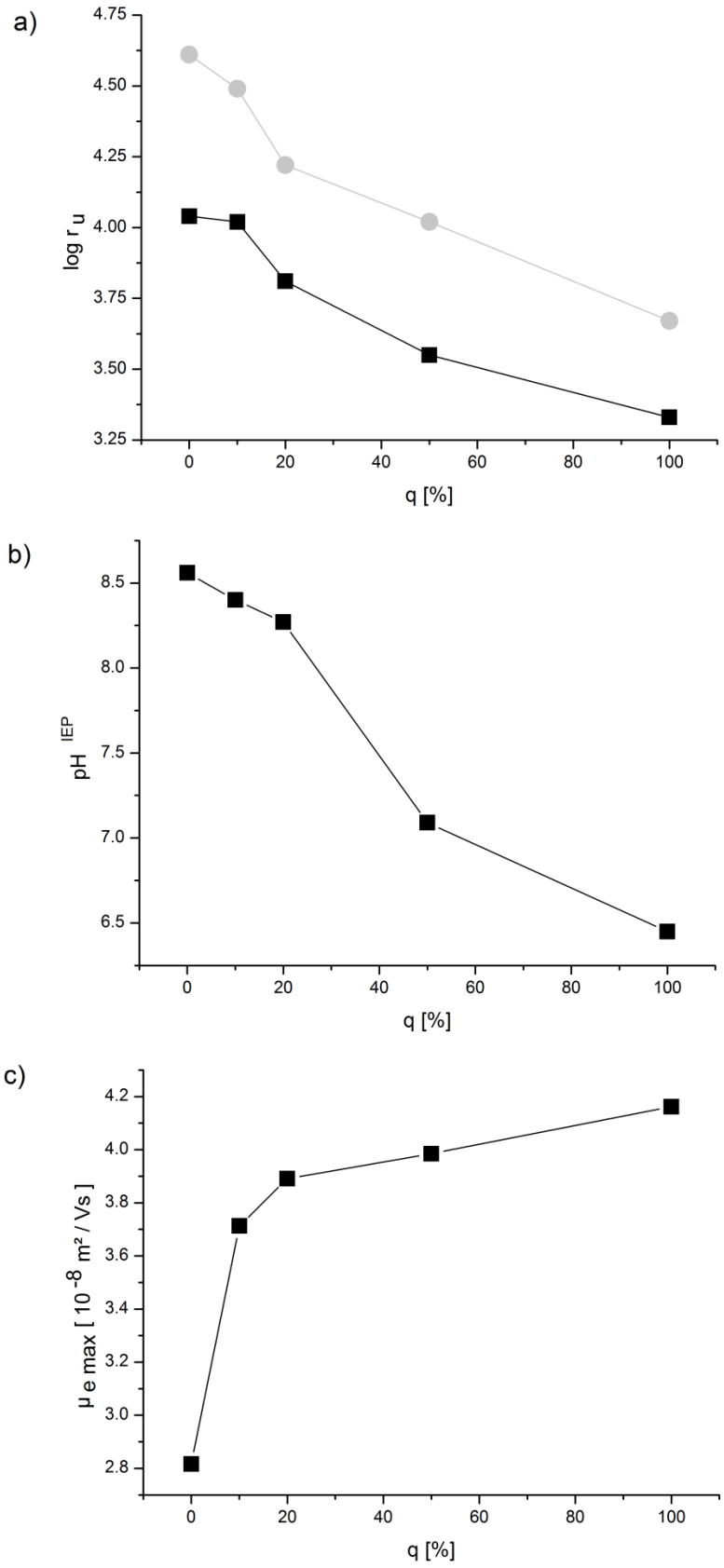

Figure 6-8a): Logarithmic subunit ratio of the isoelectric point (IEP; black squares) and the adsorption saturation point (ASP; grey circles), b) Dispersion pH at the isoelectric point and c) Maximum obtained electrophoretic mobility as a function of the degree of quaternization of silica / PEI_{1393}^{qQ} –dispersions

Figure 6-8c) shows the maximum obtained value of the electrophoretic mobility as a function of the degree of quaternization of the used silica / $\mathrm{PEI}_{1393}^{\mathrm{qQ}}$–dispersions. The value of $\mu_{e,max}$ increases with an increasing degree of quaternization. The increase in $\mu_{e,max}$ from the dispersions in the presence of PEI_{1393} (XIII) to $\mathrm{PEI}_{1393}^{10\mathrm{Q}}$ (XIV) equals nearly 25%, whereas the increase from the dispersions in the presence of $\mathrm{PEI}_{1393}^{10\mathrm{Q}}$ (XIV) to $\mathrm{PEI}_{1393}^{100\mathrm{Q}}$ (VII) is just around 10%.

Table 6-1: Data obtained by electrophoretic measurements of silica / PEI_{1393}^{qQ} –dispersions: Calculated logarithmic subunit ratios at the isoelectric point (IEP) and at the adsorption saturation point (ASP), calculated pH values at the IEP and obtained maximum electrophoretic mobility

No.	Polymer	$\log \mathrm{r_u^{IEP}}$	$\log \mathrm{r_u^{ASP}}$	$\mathrm{pH^{IEP}}$	$\mu_{e,max}$ [10^{-8} m²/Vs]
(XIII)	PEI_{1393}	4.04	4.61	8.56	2.816
(XIV)	$\mathrm{PEI}_{1393}^{10\mathrm{Q}}$	4.02	4.49	8.40	3.713
(XV)	$\mathrm{PEI}_{1393}^{20\mathrm{Q}}$	3.81	4.22	8.27	3.891
(XVI)	$\mathrm{PEI}_{1393}^{50\mathrm{Q}}$	3.55	4.02	7.10	3.985
(XVII)	$\mathrm{PEI}_{1393}^{100\mathrm{Q}}$	3.33	3.72	6.45	4.162

The μ_e (log r_u)-curves (see Figure 6-7) obtained from dispersions containing non-, or weakly charged amino-quat-primer derivatives (q = 0, 10, and 20%) exhibit a maximum electrophoretic mobility of the samples at log r_u between 4.60 and 4.86, with higher subunit ratios μ_e of the respective system decreases, where the slopes decrease with increasing the degree of quaternization. When PEI-dispersants of q ≥ 50% are used, the respective μ_e(log r_u)-curves increase to a maximum value and remain constant between log r_u = 4.44 and 5.46. With q = 50% samples at a logarithmic subunit ratio of 5.87, and 6.16 exhibit a decrease of the electrophoretic mobility of 44% from sample (XVI)-011 to (XVI)-013. This means that a decrease in μ_e for very high subunit ratios above the adsorption saturation point is also observed for highly quaternized derivatives, however these dispersions exhibit a much broader plateau of the maximum electrophoretic mobility.

6.3.2. Influence of the degree of polymerization on the particle surface charge

Figure 6-9 depicts the electrophoretic mobility μ_e of the silica / $\mathrm{PEI}_{\mathrm{X_n}}^{50\mathrm{Q}}$-dispersions as a function of the logarithmic subunit ratio log r_u (values listed in Table I-8, column 4, Appendix). The general trend of the plots of the electrophoretic mobility versus the subunit ratio is similar for all three investigated polymers with the same degree of quaternization. The graph starts at a highly negative value of the electrophoretic mobility and with an increasing subunit ratio, the magnitude of the negative electrophoretic mobility values decreases. After reaching the isoelectric point, μ_e increases to a highly positive value, stays constant, and finally decreases. The electrophoretic mobility has nearly identical values for all three degrees of polymerization at log r_u = 3.15 – 5.15. Above log r_u = 5.15, μ_e decreases for all degrees of polymerization. The electrophoretic mobility at log r_u = 5.86 is 2.694*10^{-8} m²/Vs for the intermediate degree of polymerization and 3.571*10^{-8} m²/Vs for the highest one. This indicates, that the decrease is more rapidly for a lower degree of polymerization.

Table 6-2: Data obtained by electrophoretic measurements of silica / $PEI_{X_n}^{50Q}$ –dispersions: Calculated logarithmic subunit ratios at the isoelectric point (IEP) and at the adsorption saturation point (ASP), calculated pH values at the IEP and obtained maximum electrophoretic mobility

No.	Polymer	$\log r_u^{IEP}$	$\log r_u^{ASP}$	pH^{IEP}	$\mu_{e,max}$ [10^{-8} m²/Vs]
(VI)	$\mathrm{PEI}_{28}^{50\mathrm{Q}}$	3.47	3.85	7.87	3.540
(XI)	$\mathrm{PEI}_{232}^{50\mathrm{Q}}$	3.59	3.91	7.15	3.916
(XV)	$\mathrm{PEI}_{1393}^{50\mathrm{Q}}$	3.55	4.02	7.10	3.985

Table 6-2 summarizes the data obtained from the electrophoretic mobility measurements of the silica / $\mathrm{PEI}_{\mathrm{X_n}}^{50\mathrm{Q}}$ -dispersions. The calculated logarithmic subunit ratios at the isoelectric point (IEP) and the adsorption saturation point (ASP), the calculated pH values at the IEP and the obtained maximum values of the electrophoretic mobility are listed. As explained earlier in Chapter 6.3.1., the values of $\log \mathrm{r_u^{IEP}}$ and pH^{IEP} were calculated by linear regressions using the values determined of samples with the smallest positive and smallest negative electrophoretic mobility obtained in the presence of a particular polymer. The values of $\log \mathrm{r_u^{ASP}}$ were determined at the intersections of two linear fitted functions, one with the

slope of the electrophoretic mobility of samples where adsorption occurred, and one with the slope of μ_e of samples, after a full surface coverage was achieved.

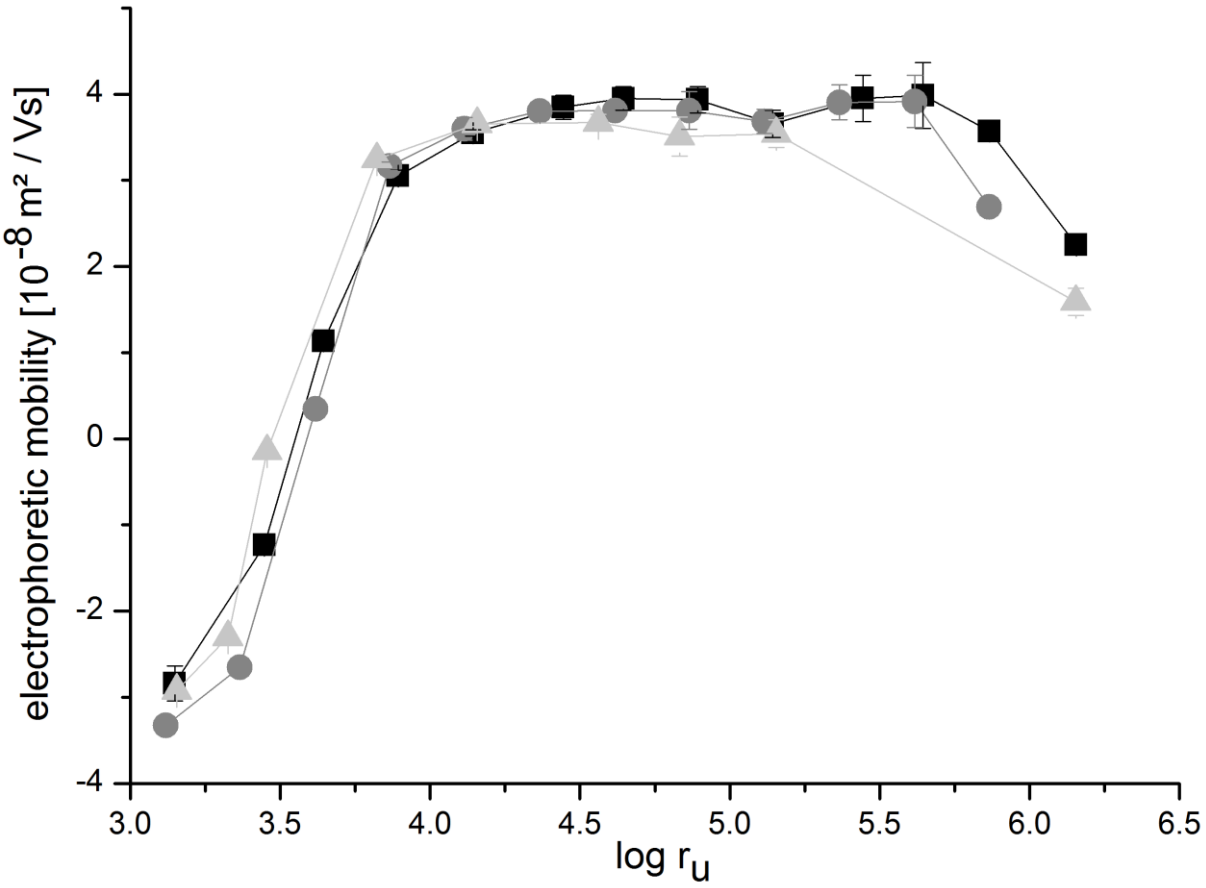

Figure 6-9: Electrophoretic mobility of silica / $PEI_{X_n}^{50Q}$ –dispersions as a function of the logarithmic subunit ratio; back squares: PEI_{28}^{50Q} (VI), dark grey circles: PEI_{232}^{50Q} (XI), light grey triangles: PEI_{1393}^{50Q} (XVI)

The calculated values of the subunit ratios at the isoelectric point vary between $\log r_u^{IEP}$ = 3.47 and 3.59 and are hence very similar for all three investigated polymers $PEI_{X_n}^{50Q}$. There is no recognizable trend for a higher or lower degree of polymerization. The calculated values of the subunit ratios at the adsorption saturation point increase with an increasing degree of polymerization (X_n = 28 : $\log r_u^{ASP}$ = 3.85; X_n = 1393 : $\log r_u^{ASP}$ = 4.02). The calculated pH values at the isoelectric point are nearly identical for the polymers with the both higher degrees of polymerization (X_n = 232 : pH^{IEP} = 7.15; X_n = 1393 : pH^{IEP} = 7.10) and the value for the smallest X_n is slightly higher (X_n = 28 : pH^{IEP} = 7.87). The maximum value of the electrophoretic mobility obtained for the intermediate and highest values of X_n are very similar with 3.916*10^{-8} m²/Vs and 3.985*10^{-8} m²/Vs, respectively. The obtained maximum value of μ_e for the lowest degree of polymerization, however, is smaller with 3.540*10^{-8} m²/Vs.

6.3.3. Relation between particle surface charge and dispersion stability

Figure 6-10 illustrates a superposition of the plots of the absorbance at 400nm and the electrophoretic mobility of silica-nanoparticle-dispersions prepared in the presence of a) PEI_{1393} (XIII) and b) $\mathrm{PEI}_{1393}^{100Q}$ (XVII) as functions of the logarithmic subunit ratio. The positions of the areas $\mathrm{D_I}$, $\mathrm{P_I}$, $\mathrm{D_{II}}$ and $\mathrm{P_{II}}$ are indicated, and areas of stability are shown by a grey colored background.

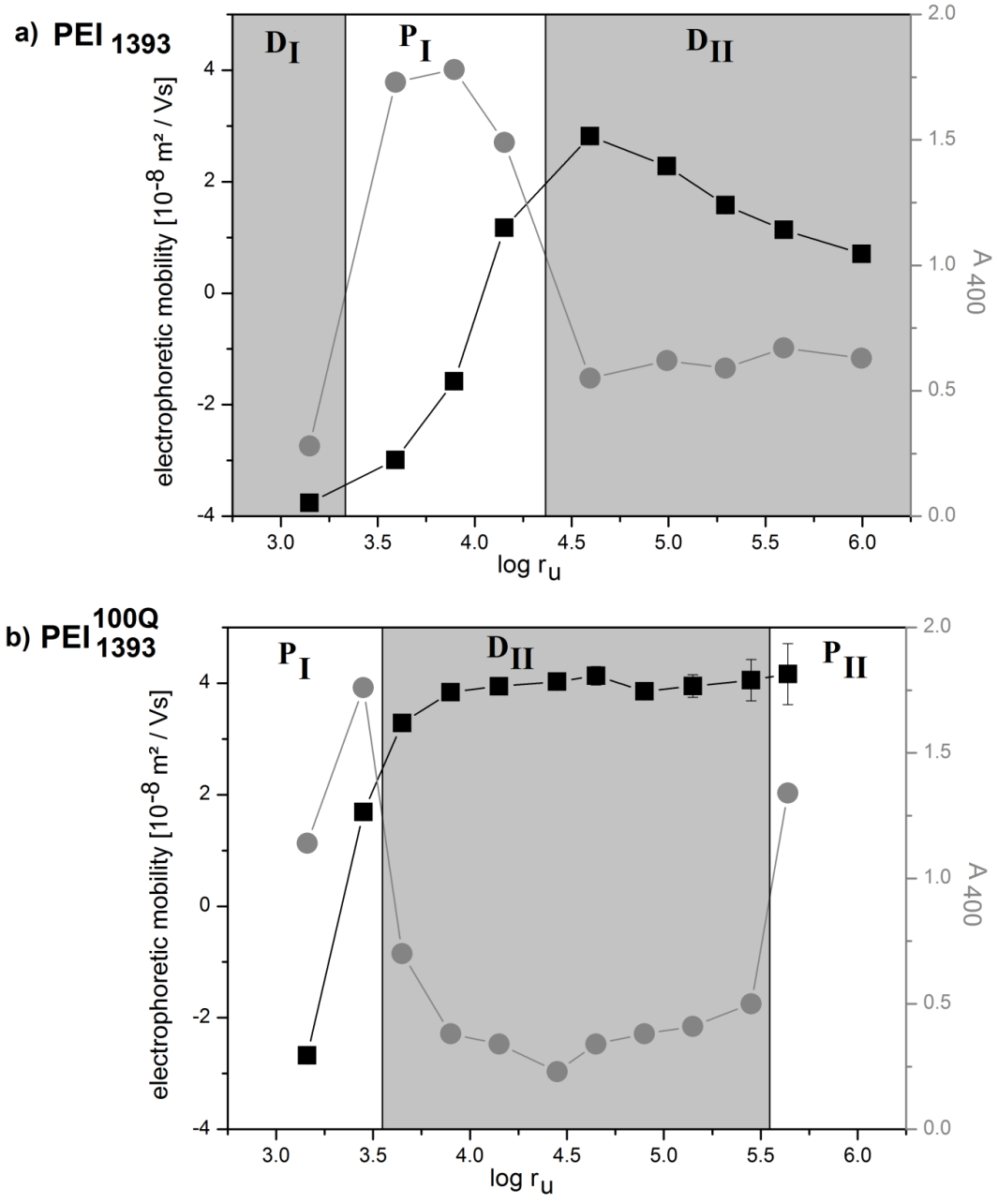

Figure 6-10: Superposition of the plots of the absorbance at 400nm and the electrophoretic mobility of silica-nanoparticle-dispersions prepared in the presence of a) PEI_{1393} (XIII) and b) PEI_{1393}^{100Q} (XVII) as functions of the logarithmic subunit ratio

In Figure 6-10a) in presence of PEI_{1393} (XIII) the low absorbance of the sample with the lowest subunit ratio (XIII)-001 in area D_I corresponds to the highly negative electrophoretic mobility of weakly PEI^Q-covered silica nanoparticles. The samples (XIII)-002 – (XIII)-004 in area P_I show a high absorbance, which corresponds to partially covered nanoparticles with a weakly negative or weakly positive electrophoretic mobility close to the isoelectric point. In area D_{II}, the sample (XIII)-005 exhibits a highly positive electrophoretic mobility, which corresponds to a charge-stabilized, polymer-covered nanoparticle. The electrophoretic mobility of the samples (XIII)-006 – (XIII)-009 decreases again, but the absorbance stays low, and the stability stays high. A similar relation is shown in Figure 6-10b) in the presence of PEI_{1393}^{100Q} (XVII). Samples (XVII)-001 and (XVII)-002 in area P_I have a high absorbance and a respectively weakly positive and weakly negative electrophoretic mobility close to the isoelectric point. The following samples (XVII)-003 – (XVII)-011 show a constantly high positive electrophoretic mobility. The absorbance of the samples (XVII)-003 – (XVII)-010 in area D_{II} is low, but the sample (XVII)-011 in area P_{II} shows a high absorbance.

The absorbance at 400nm and the electrophoretic mobility of the silica / $PEI_{X_n}^{qQ}$ –dispersions in the stability areas D_I, P_I and D_{II} are related to eachother. In area D_I particles are highly negatively charged and therefore stable, which is indicated by the highly negative μ_e values and the low values of A_{400}. In area P_I, the particles are slightly positively or negatively charged with a small positive or small negative electrophoretic mobility and therefore unstable indicated by the high absorbance. In area D_{II}, the particles are highly positively charged, therefore exhibit highly positive μ_e values and are stable with a low absorbance. In area P_{II}, the particles exhibit a highly to moderate positive electrophoretic mobility, however the absorbance increases strongly. The samples become highly turbid. The reason for the instability of in area P_{II} is not closely correlated to the surface charge of the nanoparticles.

6.3.4. Relation between particle surface charge and dispersion pH

Figure 6-11 depicts the superposition of the plots of the electrophoretic mobility and the pH of silica-nanoparticle-dispersions prepared in the presence of a) PEI_{1393} (XIII) and b) PEI_{1393}^{100Q} (XVII) as functions of the logarithmic subunit ratio.

In Figure 6-11a) for dispersions with PEI_{1393} (XIII), the pH increases with an increasing electrophoretic mobility for the dispersions (XIII)-001 – (XIII)-005. The change in the slope after the sample (XIII)-005 corresponds to the maximum in the electrophoretic mobility, which indicates a saturated adsorption. After the nanoparticle surface is fully covered the pH

increases with a constant slope. In Figure 6-11b) with $\mathrm{PEI}_{1393}^{100\mathrm{Q}}$ (XVII), the pH decreases with an increasing electrophoretic mobility for the dispersions (XVII)-001 – (XVII)-004. When the electrophoretic mobility reaches its saturation value for (XVII)-004, the pH starts to increase with a constant slope.

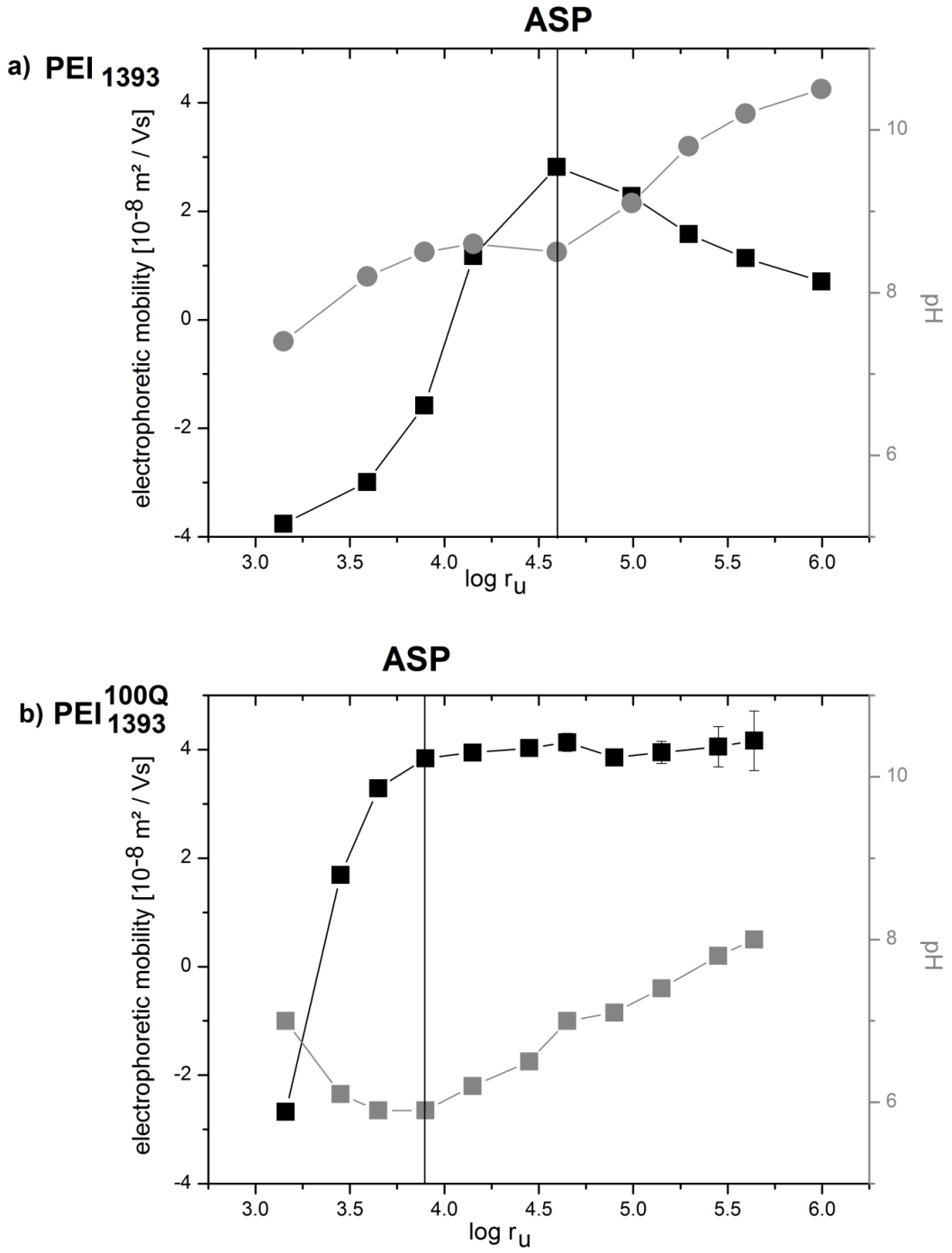

Figure 6-11: Superposition of the plots of the electrophoretic mobility and the pH of silica-nanoparticle-dispersions prepared in the presence of a) PEI_{1393} (XIII) and b) PEI_{1393}^{100Q} (XVII) as functions of the logarithmic subunit ratio

The subunit ratio of the change of the slope of the dispersion pH corresponds to the one of the adsorption saturation point (ASP) in the electrophoretic mobility measurement. Below the ASP, during the addition of amino-quat-primer polymer to the nanoparticle surface, chlorid counterions from the quaternized groups of the polymer and protons from the silica surface are released. The release of hydrochloric acid into the solution lowers the solution pH. Above the ASP the pH increases linearly upon the addition of partially quaternized poly(ethylenimine) to the dispersion.

6.4. Dispersion pH variation

The influence of a variation of the dispersion pH on the dispersion stability and the particle surface charge of silica-nanoparticle-dispersions in presence of amino-quat-primer polymers was investigated.

6.4.1. pH titration of polymer-covered silica-nanoparticle-dispersions

A bare silica-nanoparticle-dispersion, as well as dispersions containing PEI_{1393} (XIII) and $\mathrm{PEI}_{1393}^{50\mathrm{Q}}$ (XVI) at a logarithmic subunit ratio of log r_u = 4.44 were titrated with acidic and basic solutions (for employed samples and the titrant solutions see Table I-9, Appendix). Figure 6-12 illustrates the pH value as a function of added amount of protons and hydroxide ions.

While adding acid the pH of the bare particle dispersions decreases much stronger than of the dispersions with polymers. Furthermore the pH decrease is stronger with the partially quaternized polymer $\mathrm{PEI}_{1393}^{50\mathrm{Q}}$ (XVI) than with pure poly(ethylenimine) PEI_{1393} (XIII). The partially quaternized poly(ethylenimine) derivatives adsorbed on the silica surface act as a buffer, as it was shown with the pure polymer solutions in Chapter 4.7. The polymer can be protonated and because of this the pH of the dispersions containing polymer results in a higher pH under acid addition than the silica dispersion. The decrease is stronger with the partially quaternized polymer than with the pure polymer, because of the higher amount of primary and secondary amino groups of the pure polymer compared to the quaternized polymer, which are protonated more readily than tertiary amino groups.

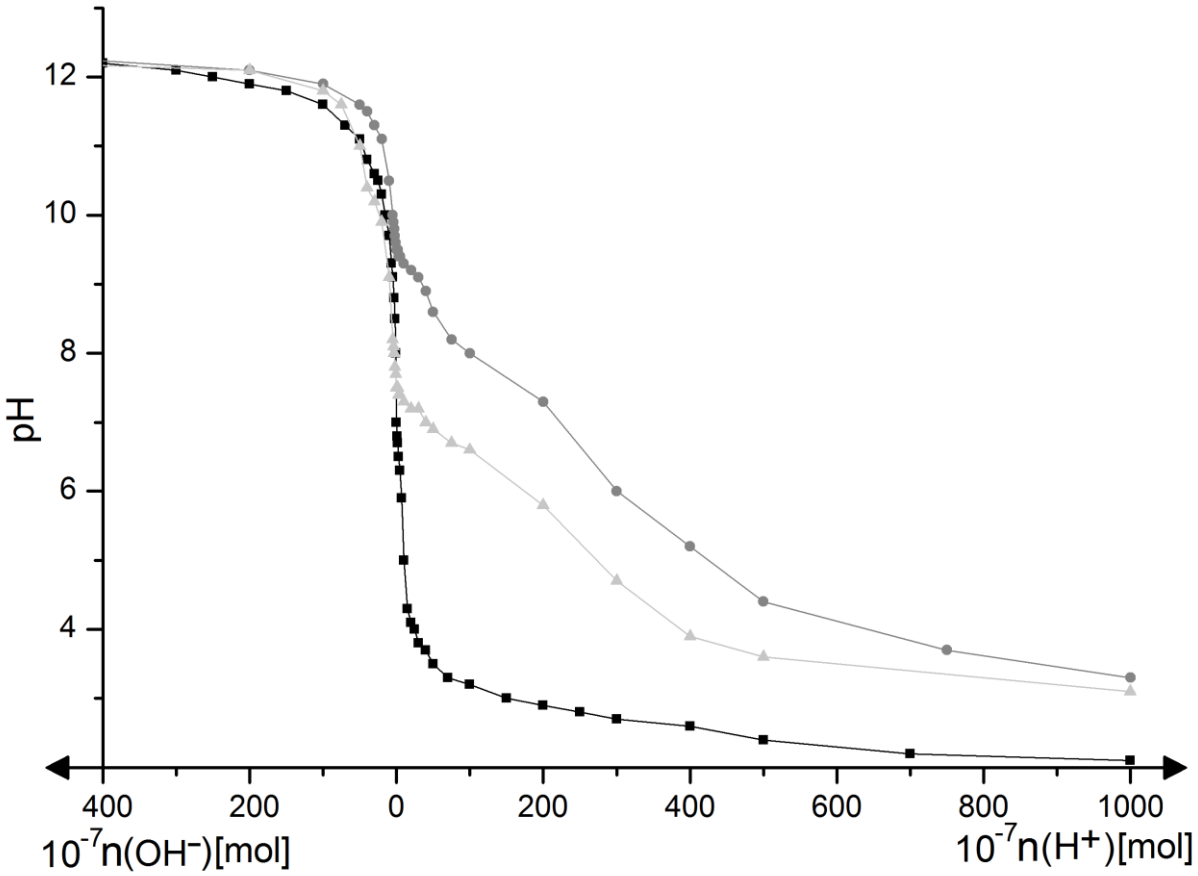

Figure 6-12: pH value as a function of added amount of protons and hydroxide ions of bare silica-nanoparticle-dispersions (black squares) and in the presence of PEI_{1393} (XIII) (dark grey circles) and PEI_{1393}^{50Q} (XVI) (light grey triangles) with a logarithmic subunit ratio of log r_u = 4.44

While adding base the pH of the bare particle dispersions increases slightly weaker than the one of the polymer containing dispersions, and the increase is stronger with the pure poly(ethylenimine) PEI_{1393} (XIII) than with the partially quaternized polymer $\mathrm{PEI}_{1393}^{50\mathrm{Q}}$ (XVI). Since the silica surfaces can be deprotonated by addition of base [1], the release of protons has a buffering effect on the pH increase.

6.4.2. Dispersion pH variation of polymer-covered silica-nanoparticle-dispersions

The influence of a pH variation after the preparation on the particle surface charge and the dispersion stability of stable dispersions of $\mathrm{PEI}^{\mathrm{Q}}$-covered silica nanoparticle was investigated. After the ultrasound treatment a specific amount of acid or base was added to modify the pH after the dispersion preparation (samples (XIII)-015 – (XIII)-020 and (XVI)-028 – (XVI)-033).

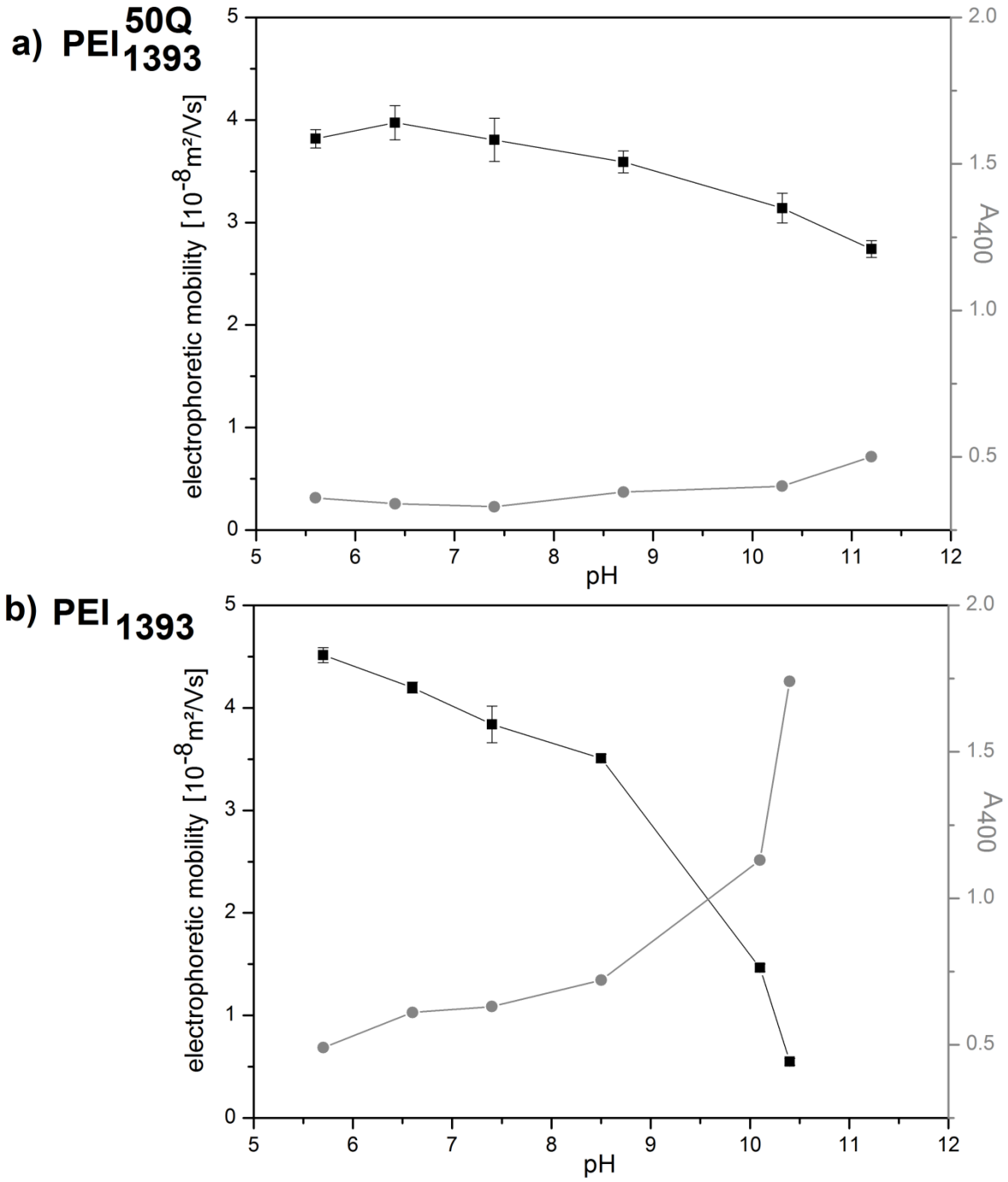

Figure 6-13: Superposition of the plots of the electrophoretic mobility and absorbance at 400nm as a function of the pH of silica-nanoparticle-dispersions prepared the presence of PEI_{1393} (XIII) and PEI_{1393}^{50Q} (XVI) at a logarithmic subunit ratio of log r_u = 4.44

Figure 6-13 depicts the superposition of the plots of the electrophoretic mobility and absorbance at 400nm as a function of the pH of the silica-nanoparticle-dispersions prepared the presence of (a) $\mathrm{PEI}_{1393}^{50Q}$ (XVI) and (b) PEI_{1393} (XIII) at log r_u = 4.44 (values listed in Table I-7, column 5 and Table I-8, column 3 in Appendix).

In the presence of the pure poly(ethylenimine) (Figure 6-13b), the dispersion exhibits a highly positive electrophoretic mobility of 4.515*10^{-8}m²/Vs for the smallest investigated pH of 5.7 with a low absorbance. With increasing pH the electrophoretic mobility decreases and reaches a value of 0.549*10^{-8}m²/Vs at a pH of 10.4. While the electrophoretic mobility decreases, the absorbance increases with an increasing pH. It has been observed that the dispersions become unstable for a pH of 10.1 and above.

In the presence of the partially quaternized poly(ethylenimine) derivative $\mathrm{PEI}_{1393}^{50\mathrm{Q}}$ (Figure 6-13a), the dispersions exhibit a highly positive electrophoretic mobility of all dispersions (μ_e = 2.741 – 3.974*10^{-8}m²/Vs), with a slightly decreasing magnitude with an increasing pH. The absorbance is low for all investigated samples, it only increases in the range from 0.33 to 0.50, which indicates that all dispersions in the presence of the partially quaternized poly(ethylenimine) derivative are stable at a pH between 5.6 and 11.2.

The dispersions containing pure poly(ethylenimine) are stronger affected by the pH change than the dispersions prepared in the presence of the partially quaternized derivative. The latter ones are also stable with a highly positive electrophoretic mobility for high pH values (pH 10 – 11).

6.5. Salt concentration variation

The influence of the salt concentration on the particle surface charge and dispersion stability of silica-nanoparticle-dispersions in presence of amino-quat-primer polymers was investigated.

6.5.1. Salt concentration variation of silica-polymer-dispersions

Figure 6-14 shows the superposition of the plots of the electrophoretic mobility and the absorbance at 400nm of silica-nanoparticle-dispersions prepared in the presence of $\mathrm{PEI}_{1393}^{50\mathrm{Q}}$ (XVI) with a logarithmic subunit ratio of log r_u = 4.44 as functions of the sodium chloride concentration (samples (XVI)-034 – (XVI)-041, values listed in Table I-6, column 5 and Table I-8, column 3, Appendix). The electrophoretic mobility of the silica / $\mathrm{PEI}_{1393}^{50\mathrm{Q}}$ – dispersions decreases from 3.849*10^{-8}m²/Vs without sodium chloride for about 40% to 2.218*10^{-8}m²/Vs at a sodium chloride concentration of 0.1mol/L. The corresponding absorbance increases from 0.30 without added sodium chloride to 0.77 for a sodium chloride concentration of 0.1mol/L.

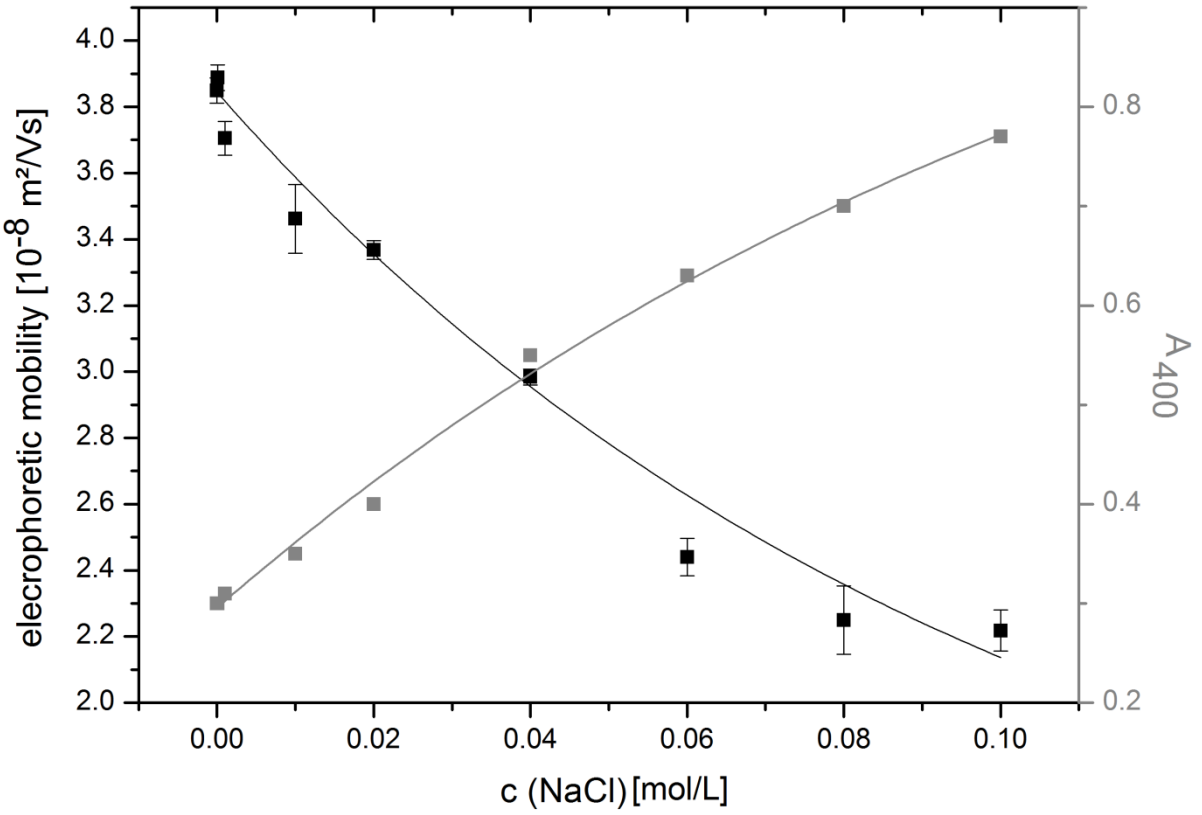

Figure 6-14: Superposition of the plots of the electrophoretic mobility and the absorbance at 400nm of silica-nanoparticle-dispersions prepared in the presence of PEI_{1393}^{50Q} (XVI) at a logarithmic subunit ratio of log r_u = 4.44 as functions of the sodium chloride concentration

The added salt screens the charges in the solution [2] and likely decreases the surface charge of the particles. The repulsive forces between two particles are decreased, causing stronger particle agglomeration, and an increase of the dispersion absorbance.

6.5.2. Salting-out effect by amino-quat-primer polymers

To investigate if the occurrence of stability area P_{II} (= the second area of instability) is caused by a salting out effect induced by free, i.e. not adsorbed polymer molecules in the solution, the influence of the effect of the free polymer is compared with the one of the monovalent salt sodium chloride. Two dispersions have been selected for this experiment: the dispersion (XVI)-006 is a stable dispersion of the silica nanoparticles in the presence of PEI_{1393}^{50Q} at a logarithmic subunit ratio of log r_u = 4.44, while the dispersion (XVI)-011 is an unstable dispersion of the silica nanoparticles containing PEI_{1393}^{50Q} at a logarithmic subunit ratio of log r_u = 5.64. The increase in the total number (Equation 6-1) and in the total concentration (Equation 6-2) of quaternized subunits of polymers free in solution from sample (XVI)-006 to

sample (XVI)-011 are calculated. Every quaternized subunit in a partially quaternized poly(ethylenimine) derivative carries a positively charged quaternary nitrogen atom and a negatively charged chloride counterion. The effect of the free polymer in sample (XVI)-011 on the particle surface charge and the dispersion stability (see Table 6-3) is compared with the one of sample (XVI)-039, which exhibits the same subunit ratio as dispersion (XVI)-006 ($\log r_u$ = 4.44) and additionally a salt concentration, which equals the increase in the concentration of quaternized subunits of polymers free in solution from sample (XVI)-006 to sample (XVI)-011 (c = 0.6 mol/L).

$$n_{u\ quat\ free} = (r_u^2 - r_u^1) \cdot \frac{q}{100} \cdot n_{np} = 3.62 \cdot 10^{20} \qquad \textit{Equation 6-1}$$

$$c_{u\ quat\ free} = \frac{n_{u\ quat\ free}}{N_A \cdot V} = 0.6\ \frac{mol}{L} \qquad \textit{Equation 6-2}$$

with $n_{u\ quat\ free}$: total number of quaternized subunits of polymers free in solution; r_u^1 : subunit ratio of the stable sample ($\log r_u^1$ = 5.64); r_u^2 : subunit ratio of the unstable sample ($\log r_u^2$ = 4.44); q: degree of quaternization (q = 50%); n_{np} : total number of silica nanoparticles (n_{np} = 1.77 * 10^{15}); $c_{u\ quat\ free}$: total concentration of quaternized subunits of polymers free in solution [mol/L] ; N_A : Avogadro constant; V : volume (V = 0.01L)

The electrophoretic mobility of sample (XVI)-039 with a sodium chloride concentration of 0.6mol/L equals only 60% of the one of sample (XVI)-011 with an increased concentration of quaternized subunits of polymers free in solution of 0.6mol/L. The absorbance of sample (XVI)-011 is nearly twice as high as the one of dispersion (XVI)-039. This means that the surface charge of the silica nanoparticle in solution is screened much more effectively by the monovalent salt than by the polymer. However, in presence of free polymer the PEI^Q-covered nanoparticles are much more unstable than the PEI^Q-covered nanoparticles in presence of sodium chloride. It is concluded that the main destabilization mechanism in area P_{II} caused by free quaternized poly(ethylenimine) in solution is not a salting-out effect.

Table 6-3: Electrophoretic mobility and absorbance at 400nm of dispersions (XVI)-011 and (XVI)-039

Dispersion	μ_e [10^{-8} m²/Vs]	A_{400}
(XVI)-011	3.985	1.25
(XVI)-039	2.440	0.63

6.5.3. Salt concentration variation of silica- and silica-polymer-dispersions

The influence of the variation of the salt concentration on the particle surface charge of dispersions containing bare silica nanoparticle and on dispersions containing additionally a partially quaternized poly(ethylenimine) derivative are compared.

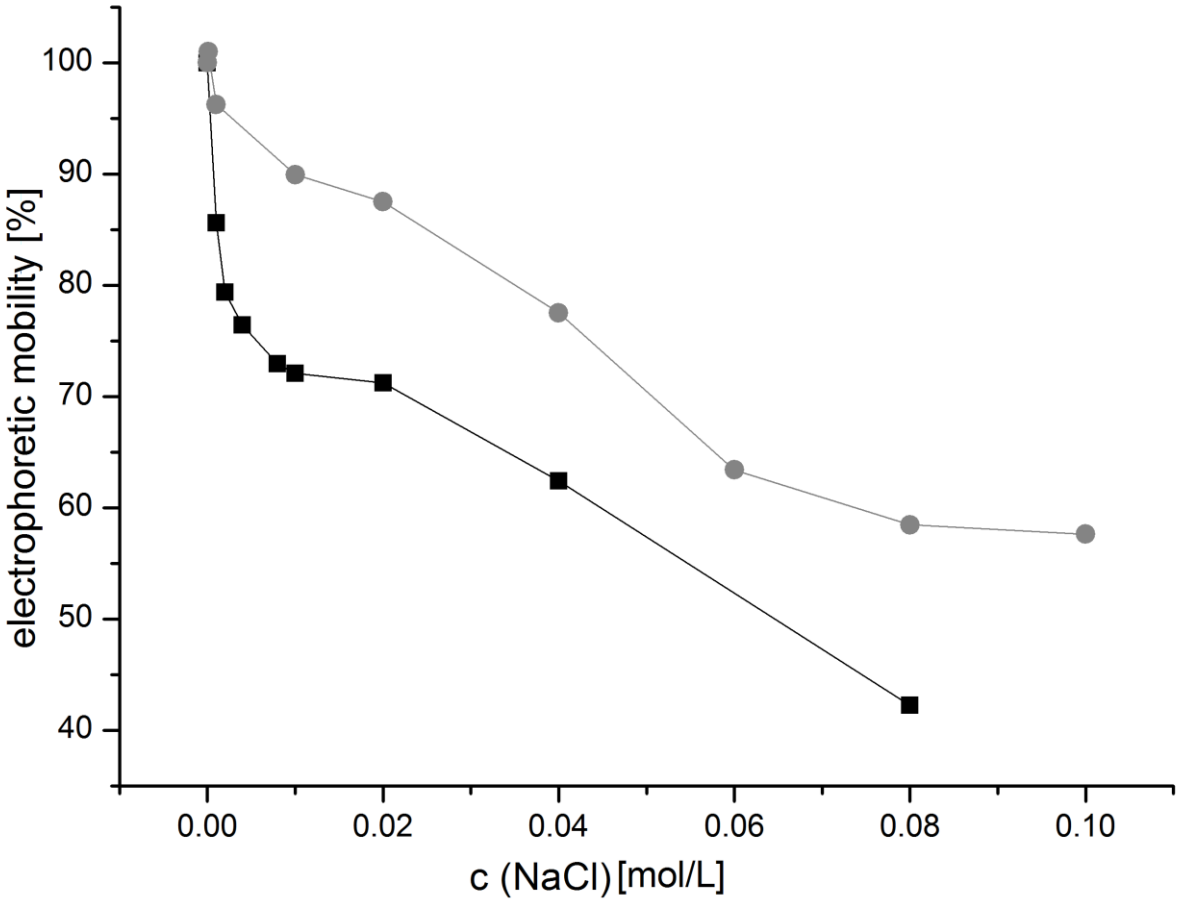

Figure 6-15: Comparison of the electrophoretic mobility of dispersions of bare silica nanoparticles (black squares) and in the presence of PEI_{1393}^{50Q} (XVI) at a logarithmic subunit ratio of log r_u = 4.44 (grey circles) as functions of the sodium chloride concentration

Figure 6-15 depicts the electrophoretic mobility of dispersions of bare silica nanoparticles and in the presence of PEI_{1393}^{50Q} (XVI) at log r_u = 4.44, as a function of the sodium chloride concentration. The values of the electrophoretic mobility of bare silica nanoparticles are negative and the ones of the polymer-covered particles positive. For comparison the electrophoretic mobility is shown as percentage of the value in absence of sodium chloride. The magnitude of the electrophoretic mobility decreases in the presence and in the absence of polymer with an increasing salt concentration. The increasing salt concentration screens the surface charge of the bare particles more effectively than of the PEI^Q-covered particles.

6.6. Results

The information gained in this chapter about the interaction of silica-nanoparticle-dispersions with amino-quat-primer polymers concerning the stability areas, the degree of quaternization, the degree of polymerization, the dispersion pH, the dispersion salt concentration and the surface deprotonation are summarized.

6.6.1. Stability areas

The investigation of the particle surface charge by means of electrophoretic mobility measurements and of the dispersion turbidity by means of absorption measurements at a fixed wavelength of 400nm revealed a charge reversal behavior and the occurrence of two areas of stability (D_I and D_{II}) and two areas of instability (P_I and P_{II}) in the stability maps. Figure 6-16 shows schematically the arrangement of polymers and particles in the four different stability regions, which occur alternatingly with increasing concentrations of partially quaternized poly(ethylenimine) derivatives in the silica-nanoparticle-dispersions.

In area D_I, the first area of stability, bare and weakly PEI^Q-covered silica nanoparticles exist, showing a highly negative electrophoretic mobility (see Figure 6-16a). Strong repulsive forces between the particles are present stabilizing the dispersions as it was confirmed by the low absorbance.

In area P_I, the first area of instability, the nanoparticles are partially PEI^Q-covered (see Figure 6-16b). Their electrophoretic mobility is weakly negative or weakly positive, close to the isoelectric point. Since the electrostatic repulsive forces between the nanoparticles are weak, the attractive van der Waals forces become dominant. The particles agglomerate, the dispersion exhibits a high absorbance, indicating its instability.

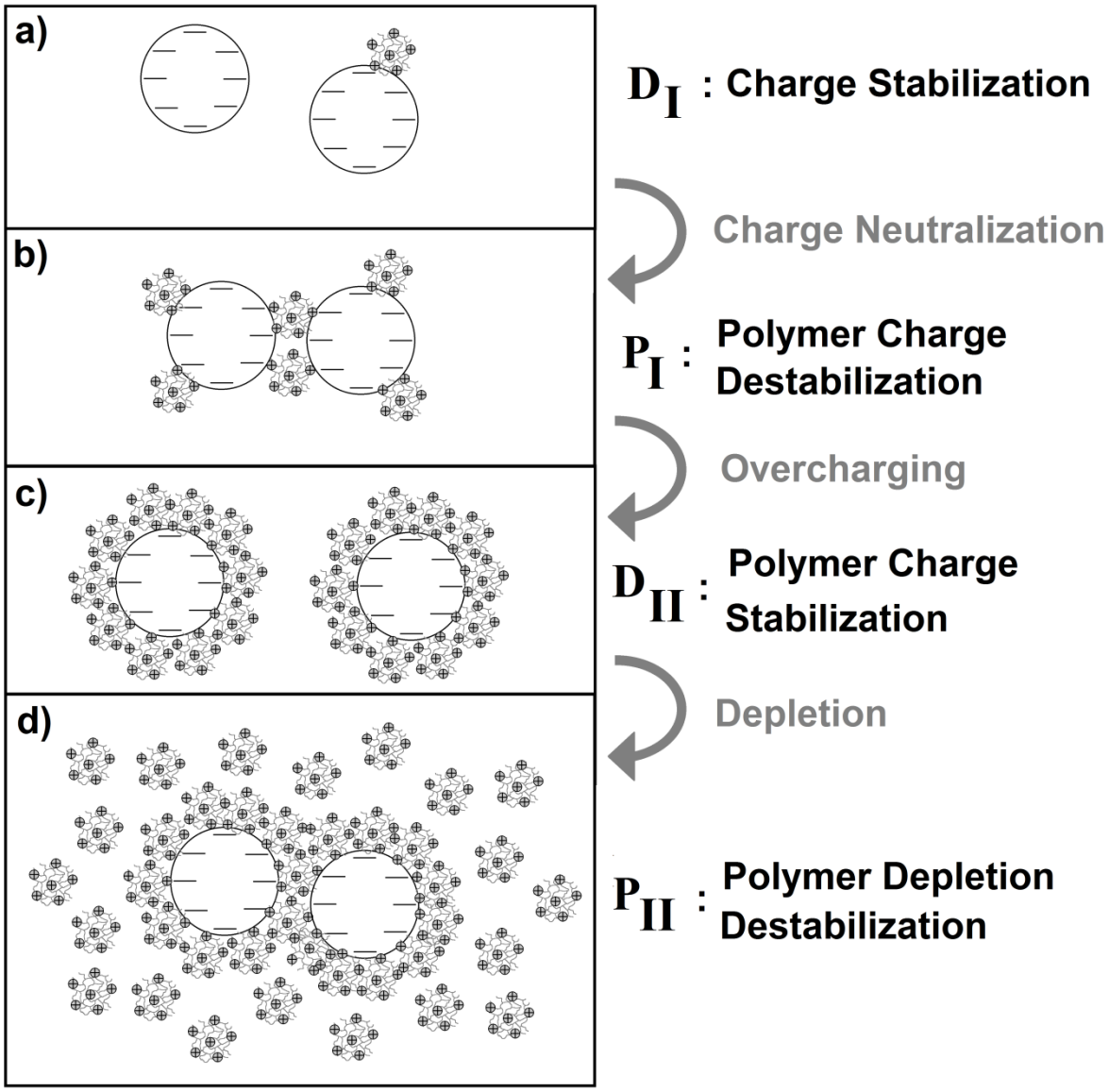

Figure 6-16: Four stability regions occur for the stability of silica nanoparticles against the addition of highmolecular, partially quaternized poly(ethylenimine) derivatives

In area D_{II}, the second area of stability, the particles are completely PEI^Q-covered (see Figure 6-16c). This causes a highly positive electrophoretic mobility and strong repulsive forces between the particles to occur, resulting in a high stability, which is shown by the low absorbances.

In area P_{II}, the particles are completely PEI^Q-covered and free, i.e. non-adsorbed PEI^Q molecules are present in the dispersion (see Figure 6-16d). Even though the particles exhibit a highly positive electrophoretic mobility, the turbidity of the dispersions is very high as proven by a high absorbance.

The appearance of the stability region D_I, P_I and D_{II} can be explained by means of the established DLVO theory based on the combination of attractive and repulsive forces (see Literature Review, Chapter 2.4.2.). The transition of areas D_I to area P_I occurs due to a neutralization of the surface charge of the silica nanoparticles by adsorption of the positively charged PEI^Q molecules. The particles exhibit only very weak repulsive forces close to the isoelectric point, so, that the attractive van der Waals forces dominate and the particles agglomerate. Because of the highly branched structure and the high charge density of the polymers, an adsorption as patches on the silica surface below the adsorption saturation point is assumed [3]. Hence, additional attractive non-DLVO, patch-charge-forces close to the IEP are expected (cf. literature review, Chapter 2.6.6.1.). However, non-DLVO bridging forces are excluded, because they are not observed for hyperbranched polymers [3].

The transition of P_I to D_{II} is attributed to the overcharging of the nanoparticle surface by further addition of positively charged PEI^Q molecules beyond the charge neutralization point. The increase in the particle surface charge was tracked by electrophoretic mobility measurements and the decrease in the turbidity, meaning an increase in the stability was observed by UV-absorption measurements.

The charge neutralization and overcharging are well known phenomena occurring for the adsorption of charged polyelectrolytes on oppositely charged surfaces (see Literature Review, Chapter 2.6.).

The appearance of the second area of instability, P_{II}, which is found for silica nanoparticles in the presence of partially quaternized poly(ethylenimine) derivatives at very high subunit ratios beyond full particle coverage cannot be explained by the DLVO theory and has not been yet observed in the case of the adsorption of charged polyelectrolytes on oppositely charged surfaces. The emergence of area P_{II} must be explained by non-DLVO forces. Different non-DLVO forces are known in literature, that are induced either by charged species, e.g. salting out effects [4] or by free, non-adsorbed polymer, e.g. depletion forces (see Literature Review, Chapter 2.6.6.4.). A salting-out effect by free charged polymer was excluded by proving that an equivalent amount of monovalent salt does not have such a strong destabilization effect (see Chapter 6.5.2.). The destabilization of particles by attractive depletion forces induced by free, neutral, non-adsorbing polymer is known in literature. Based on the current state of knowledge depletion destabilization by the free, non-adsorbed charged PEI^Q is assumed as the most plausible explanation of the origin of area P_{II}.

A special feature in the stability map for the smallest degree of quaternization, was the occurrence of a third area of stability D_{III} for very high polymer amounts for the unmodified poly(ethylenimine). Also a stabilizing effect of high amounts of free polymer in solution is known. The so called depletion stabilization effect [5] occurs at much higher amounts of free polymer then the depletion destabilization.

6.6.2. Degree of quaternization

With an increasing degree of quaternization, the position of the isoelectric point (IEP) and with it the position of the first area of instability P_I, as well as the position of the adsorption saturation point (ASP) are shifted to smaller amounts of polymer. The obtained maximum of electrophoretic mobility increases with an increasing degree of quaternization. The extent of the second area of stability D_{II} increases with an increasing degree of quaternization for the intermediate and the highest degree of polymerization (X_n = 232 and 1393), but decreases with an increasing degree of quaternization for the smallest degree of polymerization (X_n = 28).

6.6.3. Degree of polymerization

With the unmodified poly(ethylenimine) derivatives the position of the first area of instability P_I is independent of the polymers degree of polymerization, but starting from q ≥ 10% the position of P_I becomes shifted to higher polymer amounts with an increasing degree of polymerization. The extent of the second area of stability D_{II} increases with an increasing degree of polymerization for q ≥ 10%. The trend of the curves of the electrophoretic mobility vary in a similar mode independently of the degree of polymerization, however the final decrease of the electrophoretic mobility at very high polymer amounts is stronger with a smaller degree of polymerization. The position of the IEP is independent of the degree of polymerization. The position of the ASP is shifted to higher polymer amounts with a higher degree of polymerization. The obtained maximum value of electrophoretic mobility is similar for the intermediate and the highest degree of polymerization (X_n = 232 and 1393), but is smaller for the smallest degree of polymerization (X_n = 28).

6.6.4. Dispersion pH

The amino-quat-primer polymer act like a buffer against the addition of acid. In contrast to the pure poly(ethylenimine) containing dispersions, the dispersions with the quaternized derivatives are stable, exhibiting a highly positive electrophoretic mobility at high pH values.

6.6.5. Salt concentration

Added salt screens the surface charge of the PEI^{Q}-covered particles, which lowers the repulsive forces between two particles as predicted by the DLVO theory [2], more agglomeration occurs and the absorbance increases. The decrease of the particle surface charge is stronger of the bare nanoparticles than of the polymer-covered ones.

6.6.6. Deprotonation of the silica surface

It was found, that the pH of the silica-nanoparticle-dispersion decreases first upon addition of the partially quaternized poly(ethylenimine) (q ≥ 20%). Due to the adsorption of the PEI^{Q} molecules the silica surface is deprotonated, chlorid counterions become released from the quaternized groups of the polymer and protons leave the silica surfaces. The release of hydrochloric acid into the solution lowers the dispersion pH.

6.7. Conclusion

The stability of silica-nanoparticle-dispersions containing partially quaternized poly(ethylenimine) derivatives $PEI_{X_n}^{qQ}$ was investigated with respect to the subunit ratio r_u between the total number of polymer subunits and the total number of silica nanoparticles, the degree of polymerization X_n and the degree of quaternization q of the employed macromolecules, as well as the pH and the salt concentration of the dispersion.

Stability maps for each degree of quaternization and each degree of polymerization of the amino-quat primer as a function of the subunit ratio were constructed. Four different stability areas were found which occur alternatingly: Two areas of stability (area D_I and D_{II}) and two areas of instability (area P_I and P_{II}). In area D_I bare and few PEI^{Q}-covered charge-stabilized particles occur; in area P_I partially PEI^{Q}-covered, charge-destabilized particles are found; in area D_{II} fully PEI^{Q}-covered charge-stabilized particles are present; and in area P_{II} fully PEI^{Q}-covered particles and additional free PEI^{Q} lead to destabilization. The occurrence of the areas D_I, P_I and D_{II} can be explained based on the charge reversal of the bare, negatively charged silica nanoparticles to the PEI^{Q}-covered, positively charged particles ($D_I \rightarrow P_I$: charge neutralization, $P_I \rightarrow D_{II}$: overcharging). The occurrence of area P_{II} with the quaternized polymers cannot be explained based on the electrostatic interaction and is assumed to originate from depletion forces of non-adsorbed free polymer.

Stable, positively charged silica nanoparticles covered with partially quaternized poly(ethylenimine) were found for all degrees of quaternization (q = 0 – 100%) for the

intermediate and the highest degree of polymerization (X_n = 232 and 1393) and for a degree of quaternization of q ≥ 10% for the smallest degree of polymerization (X_n = 28).

The isoelectric point (IEP), the position of the first area of instability P_I, and the adsorption saturation point (ASP) are shifted to smaller amounts of polymer with an increasing degree of quaternization. Furthermore, the obtained maximum value of electrophoretic mobility increases with an increasing degree of quaternization.

With the quaternized derivatives (q ≥ 10%) the position of the first area of instability P_I becomes shifted to higher polymer amounts and the extent of the second area of stability D_{II} increases with an increasing degree of polymerization.

At high pH values (pH 10 – 11) in contrast to the pure poly(ethylenimine) containing dispersions, the dispersions with the quaternized derivatives are stable, exhibiting a highly positive electrophoretic mobility.

Added salt screens the surface charge of the PEI^Q-covered particles. The decrease of the particle surface charge is stronger of the bare nanoparticles than of the polymer-covered ones.

It was found that the adsorption of the amino-quat-primer polymers onto the silica nanoparticles happens under deprotonation of the silica surface and a hydrochloric acid release, which lowers the dispersion pH.

The surface of the silica nanoparticles was modified not by a chemical, but by a physical modification. The contact between the polymer and the surface is mediated by a cooperative ionic interaction, and therefore the stability of the interaction is very high. The density of functional groups on the surface is very high after the functionalization, due to the hyperbranched structure of the poly(ethylenimine). The new amino-functionalized surface can be used for further modifications.

[1] Sears, G.W.; Analytical Chemistry 1956, 28, 1981-1983

[2] Russel, W.B., Saville, D.A.; Schowalter, W. R. Colloidal Dispersions, Cambridge University Press, 1989

[3] Pfau, A.; Schrepp, W.; Horn, D.; Langmuir 1999, 15, 3219-3225

[4] Ikegami, A.; Imai, N.; Journal of Polymer Science 1962, 56, 133-152

[5] Feigin, R.I.; Napper, D.H.; Journal of Colloid and Interface Science 1980, 75, 525-541

Chapter 7:

Summary

7. Summary

The main goal of this thesis was to perform a systematic study on the factors influencing the interaction of colloidal silica nanoparticles with so-called “amino-quat-primer” polymers - hyperbranched poly(ethylenimine) polymers containing amino groups and quaternized groups. In order to investigate this interaction, firstly, these polymers were synthesized and characterized; secondly, silica-polymer-dispersions were prepared; and finally, the stability and the particle surface charge of these produced dispersions were studied.

Chapter 4 deals with the synthesis and characterization of amino-quat-primer polymers. Fourteen derivatives were synthesized, with degrees of polymerization of X_n = 28, 232, and 1393 and degrees of quaternization of q = (1, 5,) 10, 20, 50 and 100%. The structure of the products was determined using ^{1}H- and ^{13}C-NMR-spectroscopy and the degree of quaternization was confirmed employing ^{1}H-NMR-spectroscopy and elemental analysis. The charge density of poly(ethylenimine) was controlled by introducing covalently bonded positive charges into the polymer. The protonation behavior of the amino-quat-primer polymers in aqueous solution was investigated upon variation of polymer concentration, pH, and salt concentration. Solutions of the amino-quat-primer polymers in water exhibited an alkaline pH, which increased with increasing the polymer concentration and decreasing the degree of quaternization. Under acidic conditions the polymers became further positively charged. The quaternization of the polymers led to a weaker protonation and resulted in a more stable amount of positive charge against pH variation. DLS - and DOSY measurements led to the conclusion that single molecules associated in solution, which caused that average values of the size and the electrophoretic mobility of these associates, instead of values of single molecules were measured.

The preparation and optical investigation of silica-nanoparticle-dispersions containing amino-quat-primer polymers are discussed in Chapter 5. The size of the non-treated silica nanoparticles was determined to be 30 ± 5nm using dynamic light scattering and transmission electron microscopy. Titration and electrophoretic measurements confirmed that the particles carried slightly positive charge at low pH values and were highly negatively charged at high pH values. The preparation of silica-polymer-dispersions was conducted employing sonication. Prepared dispersions were optically judged as “dispersion” or as “precipitated” 24 hours after the ultrasound treatment. UV/Vis-absorption measurements were conducted and a correlation between the absorption value at 400nm and the turbidity of the sample was identified, which led to evaluation of the dispersion stability based on the absorbance at 400nm.

In Chapter 6, the stability of silica-nanoparticle-dispersions containing amino-quat-primer polymers was investigated with respect to five key factors: their polymer-particle-ratio, the degree of polymerization and the degree of quaternization of the employed macromolecules, as well as pH and salt concentration of the dispersion. One stability map was constructed for each degree of quaternization and for each degree of polymerization of the amino-quat-primer polymers as a function of the polymer-particle-ratio. Two areas of stability (area D_I and D_{II}) and two areas of instability (area P_I and P_{II}) were found, which occurred alternatingly. In area D_I bare and few PEI^Q-covered, charge-stabilized particles emerged; in area P_I partially PEI^Q-covered, charge-destabilized particles occurred; in area D_{II} fully PEI^Q-covered, charge-stabilized particles were found; and in area P_{II} fully PEI^Q-covered particles and additional free PEI^Q were present, which led to destabilization. The appearances of the areas D_I, P_I and D_{II} were interpreted based on the charge reversal of bare, negatively charged silica nanoparticles to PEI^Q-covered, positively charged particles [1]. The transition from D_I to P_I happened due to charge neutralization, while the one from P_I to D_{II} occurred due to overcharging. The occurrence of area P_{II} could not be explained based on electrostatic interactions and was assumed to arise from depletion forces of non-adsorbed free polymer [2]. Stable, positively charged silica nanoparticles covered with amino-quat-primer polymers occurred for all degrees of quaternization (q = 0 – 100%) for the intermediate and the highest degree of polymerization (X_n = 232 and 1393), as well as for a degree of quaternization of q ≥ 10% for the smallest degree of polymerization (X_n = 28). The adsorption of the amino-quat-primer polymers onto the silica surfaces took place under deprotonation of the surface and the release of hydrochloric acid, which lowered the dispersion pH. The isoelectric point (IEP), the position of the first area of instability P_I, and the adsorption saturation point (ASP) were shifted to smaller polymer-particle-ratios with increasing the degree of quaternization. The obtained maximum value of electrophoretic mobility increased with a growing degree of quaternization. With the quaternized derivatives (q ≥ 10%), the position of the first area of instability P_I was relocated at higher polymer-particle-ratios and the extent of the second area of stability D_{II} grew with increasing the degree of polymerization. In contrast to the pure poly(ethylenimine) containing dispersions, the dispersions containing the quaternized derivatives were stable and exhibited a highly positive electrophoretic mobility also at high pH values (pH 10 – 11). Upon addition of monovalent salt, the decrease of the particle surface charge was more strongly pronounced of the bare nanoparticles in comparison to the polymer-covered ones. By modifying the silica nanoparticle surfaces with “amino-quat-primer” polymers, the colloidal stability of the particles was enhanced by an electrosteric stabilization and a new amino-functionalized surface was generated.

In summary, in this thesis a systematic investigation on the factors influencing the interaction of aqueous silica-nanoparticle-dispersions with amino-quat-primer polymers was conducted. Optimized conditions regarding the following five key factors were established: the polymer-particle-ratio, the degree of polymerization and the degree of quaternization of the polymers, the dispersion pH and the salt concentration.

Outlook

It is suggested that the new amino-functionalized silica-nanoparticle-surface could be used for further modifications. For example, the surface could be equipped with polymer chains to result in a compatibility with a polymer matrix to fabricate highly functional polymer / inorganic hybrid materials. Moreover, the importance of the conducted investigations for an optimized stabilization by amino-quat-primer polymers was demonstrated in this work, which manifests the need for further examinations of additional systems.

[1] Hierrezuelo, J.; Sadeghpour, A.; Szilagyi, I.; Vaccaro, A.; Borkovec, M.; Langmuir Letter 2010, 26, 15109-15111

[2] Feigin, R.I.; Napper, D.H.; Journal of Colloid and Interface Science 1980, 74, 567-571

Chapter 8:

Zusammenfassung
(Summary in German language)

8. Zusammenfassung

Das Hauptziel dieser Arbeit war eine systematische Studie der Einflussfaktoren auf die Wechselwirkung von kolloidalen SiO_2-Nanopartikeln mit sogenannten „Amino-Quat-Primer" Polymeren – hochverzweigte Poly(ethylenimin) Polymere, die Aminogruppen und quaternisierte Gruppen enthalten. Erstens wurden diese Polymere synthetisiert und charakterisiert; zweitens wurden SiO_2-Polymer-Dispersionen hergestellt; und schließlich wurden die Stabilität und die Partikeloberflächenladung dieser erzeugten Dispersionen analysiert.

Kapitel 4 beschäftigt sich mit der Synthese und Charakterisierung von Amino-Quat-Primer Polymeren. Vierzehn Derivate wurden synthetisiert, mit Polymerisationsgraden von X_n = 28, 232, und 1393, sowie Quaternisierungsgraden von q = (1, 5,) 10, 20, 50 und 100%. Die Struktur der Produkte wurde mittels ^{1}H- und ^{13}C-NMR-Spectroskopie überprüft und der Quaternisierungsgrad wurde mittels ^{1}H-NMR-Spectroskopie und Elementaranalyse bestätigt. Die Ladungsdichte von Poly(ethylenimin) wurde durch Einbringen kovalent gebundener, positiver Ladungen ins Polymer gesteuert. Das Protonierungsverhalten der Amino-Quat-Primer Polymere in wässriger Lösung wurde unter Variation der Polymerkonzentration, des pH-Wertes und der Salzkonzentration untersucht. Wässrige Lösungen der Amino-Quat-Primer Polymere wiesen einen basischen pH-Wert auf, welcher bei ansteigender Polymerkonzentration und sinkendem Quaternisierungsgrad abnahm. Unter sauren Bedingungen wurden die Polymere zunehmend positiv geladen. Die Quaternisierung der Polymere führte zu einer schwächeren Protonierung und zu einer stabileren Ladungsmenge gegen eine pH-Wertänderung. DLS- und DOSY-Messungen ergaben, dass einzelne Moleküle in Lösung assoziierten, was zur Folge hatte, dass mittlere Werte der Größen und der elektrophoretischen Mobilität dieser Assoziate und nicht die einzelner Moleküle gemessen wurden.

Die Herstellung und optischen Untersuchungen der SiO_2-Nanopartikel-Dispersionen, die Amino-Quat-Primer Polymere enthalten, werden in Kapitel 5 diskutiert. Die Größe der SiO_2-Nanopartikel wurde mittels dynamischer Lichtstreuung und Transelektronenmikroskopie zu 30 ± 5nm bestimmt. Titrationsexperimente und elektrophoretische Messungen bestätigten, dass die Partikel eine schwache positive Ladung bei geringen pH-Werten und eine starke negative Ladung bei hohen pH-Werten trugen. Die Herstellung der SiO_2-Polymer-Dispersionen wurde mittels Ultraschallbehandlung durchgeführt. Hergestellte Dispersionen wurden optisch 24 Stunden nach der Ultraschallbehandlung als „dispergiert" oder „ausgefallen" beurteilt. UV/Vis-Absorptionsmessungen wurden ausgeführt und ein

Zusammenhang zwischen der Absorption bei 400nm und der Turbidität der Probe identifiziert, welcher eine Beurteilung der Dispersionsstabilität auf Basis der Absorption bei 400nm erlaubte.

In Kapitel 6 wurde die Stabilität der SiO_2-Nanopartikel-Dispersionen, die Amino-Quat-Primer Polymere enthalten, im Hinblick auf fünf Schlüsselfaktoren untersucht: Ihr Polymer-Partikel-Verhältnis, den Polymerisationsgrad und den Quaternisierungsgrad der benutzten Makromoleküle, sowie den pH-Wert und die Salzkonzentration der Dispersion. Eine Stabilitätskarte wurde für jeden Quaternisierungsgrad und für jeden Polymerisierungsgrad der Amino-Quat-Primer Polymere als eine Funktion des Polymer-Partikel-Verhältnisses erstellt. Zwei Stabilitätsbereiche (Bereich D_I und D_{II}) und zwei Instabilitätsbereiche (Bereich P_I und P_{II}), die alternierend auftraten, wurden gefunden. In Bereich D_I kamen wenig polymerbedeckte, ladungsstabilisierte Partikel vor; in Bereich P_I wurden teilweise polymerbedeckte, ladungsdestabilisierte Partikel gefunden; in Bereich D_{II} waren komplett polymerbedeckte, ladungsstabilisierte Partikel vorhanden; und in Bereich P_{II} traten komplett polymerbedeckte Partikel und zusätzliches, freies Polymer auf, was zu einer Destabilisierung führte. Das Auftreten der Bereiche D_I, P_I und D_{II} wurde basierend auf einer Ladungsumkehr von negativgeladenen SiO_2-Nanopartikeln zu polymerbedeckten, positivgeladenen Partikeln interpretiert [1]. Der Übergang von D_I zu P_I trat als Folge von Ladungsneutralisation auf, während der Übergang von P_I zu D_{II} durch Überladung erfolgte. Das Auftreten des Bereiches P_{II} konnte nicht durch elektrostatische Wechselwirkungen erklärt werden und deshalb wurde angenommen, dass es zu einer Destabilisierung kam durch „Depletion“-Kräfte von nicht-adsorbiertem, freiem Polymer [2]. Stabile, positivgeladene SiO_2-Nanopartikel, die mit Amino-Quat-Primer Polymere bedeckt waren, traten für alle Quaternisierungsgrade ($q = 0 – 100\%$) für den mittleren und höchsten Polymerisierungsgrad ($X_n = 232$ und 1393) auf, sowie für einen Quaternisierungsgrad von $q \geq 10\%$ für den kleinsten Polymerisierungsgrad ($X_n = 28$). Die Adsorption von Amino-Quat-Primer Polymeren auf SiO_2-Oberflächen wurde begleitet durch eine Deprotonierung der Oberfläche und eine Freisetzung von Chlorwasserstoff, welche den pH-Wert der Dispersion herabsetzte. Der isoelektrische Punkt (IEP), die Position des ersten Instabilitätsbereiches P_I und der Adsorptionssättigungspunkt (ASP) wurden mit einem wachsenden Quaternisierungsgrad zu kleineren Polymer-Partikel-Verhältnissen verschoben. Der gemessene Maximalwert der elektrophoretischen Mobilität wuchs mit einem zunehmenden Quaternisierungsgrad. Mit den quaternisierten Derivaten verschob sich die Position des ersten Instabilitätsbereiches P_I mit einem zunehmenden Polymerisationsgrad zu höheren Polymer-Partikel-Verhältnissen und die Ausdehnung des zweiten Stabilitäts-bereiches D_{II} wuchs. Im Gegensatz zu den Dispersionen, die das reine Poly(ethylenimin)

enthielten, waren die Dispersionen, die die quaternisierten Derivate enthielten, stabil, mit einer hohen elektrophoretischen Mobilität und das sogar bei hohen pH-Werten (pH 10 – 11). Unter Zugabe von einwertigem Salz war die Abnahme der Partikeloberflächenladung stärker ausgeprägt für die unbehandelten Nanopartikel als für die polymerbedeckten Partikel. Durch Modifizierung der SiO_2-Nanopartikeloberfläche mit Amino-Quat-Primer Polymeren wurde die kolloidale Stabilität der Partikel durch elektrosterische Stabilisierung verbessert und eine neue aminofunktionalisierte Oberfläche erzeugt.

Zusammenfassend wurde in dieser Arbeit eine systematische Untersuchung der Einflussfaktoren der Wechselwirkung von wässrigen SiO_2-Nanopartikel-Dispersionen mit Amino-Quat-Primer Polymeren durchgeführt. Optimierte Bedingungen bezüglich der folgenden fünf Schlüsselfaktoren wurden festgestellt: des Polymer-Partikel-Verhältnisses, des Polymerisationsgrades und des Quaternisierungsgrades der Polymere, sowie des pH-Wertes und der Salzkonzentration der Dispersion.

Ausblick

Es wird vorgeschlagen, dass die neue aminofunktionalisierte SiO_2-Nanopartikeloberfläche als Ausgangspunkt für weitere Funktionalisierung genutzt werden kann. Zum Beispiel könnte die Oberfläche mit Polymerketten ausgestattet werden um eine Kompatibilität mit einer Polymermatrix zu erzeugen um hochfunktionale makromolekular-anorganische Hybrid-materialien herzustellen. Des Weiteren wurde in dieser Arbeit die Bedeutung der durchgeführten Untersuchungen für die Optimierung der Stabilisierung durch Amino-Quat-Primer Polymere demonstriert, was die Notwendigkeit weiterführender Erforschung anderer Systeme aufzeigt.

[1] Hierrezuelo, J.; Sadeghpour, A.; Szilagyi, I.; Vaccaro, A.; Borkovec, M.; Langmuir Letter 2010, 26, 15109-15111

[2] Feigin, R.I.; Napper, D.H.; Journal of Colloid and Interface Science 1980, 74, 567-571

Appendix

Table I-1: pH values of polymer-water-solutions

Polymer	Sample	C_P [wt%]	pH
PEI_{1393}	P(XIII)-001	0.01	9.8
	P(XIII)-002	0.05	10.4
	P(XIII)-003	0.10	10.7
	P(XIII)-004	0.50	11.0
	P(XIII)-005	1.00	11.0
	P(XIII)-006	2.50	11.1
PEI_{1393}^{10Q}	P(XIV)-001	0.01	9.0
	P(XIV)-002	0.05	9.6
	P(XIV)-003	0.10	9.9
	P(XIV)-004	0.50	10.3
	P(XIV)-005	1.00	10.5
	P(XIV)-006	2.50	10.7
PEI_{1393}^{20Q}	P(XV)-001	0.01	8.3
	P(XV)-002	0.05	9.0
	P(XV)-003	0.10	9.6
	P(XV)-004	0.50	10.0
	P(XV)-005	1.00	10.2
	P(XV)-006	2.50	10.5
PEI_{1393}^{50Q}	P(XVI)-001	0.01	7.4
	P(XVI)-002	0.05	7.9
	P(XVI)-003	0.10	8.6
	P(XVI)-004	0.50	9.0
	P(XVI)-005	1.00	9.2
	P(XVI)-006	2.50	9.5
PEI_{1393}^{100Q}	P(XVII)-001	0.01	7.0
	P(XVI)-002	0.05	7.1
	P(XVI)-003	0.10	7.6
	P(XVI)-004	0.50	7.9
	P(XVI)-005	1.00	8.2
	P(XVI)-006	2.50	8.4

Table I-2: Polymer-water-solutions and their titration solutions

Polymer	Sample	Titration solution
PEI_{1393}	P(XIII)-007	0.01M HCl
	P(XIII)-008	0.001M HCl
	P(XIII)-009	0.001M NaOH
PEI_{1393}^{10Q}	P(XIV)-007	0.01M HCl
	P(XIV)-008	0.001M HCl
	P(XIV)-009	0.001M NaOH
PEI_{1393}^{20Q}	P(XV)-007	0.01M HCl
	P(XV)-008	0.001M HCl
	P(XV)-009	0.001M NaOH
PEI_{1393}^{50Q}	P(XVI)-007	0.01M HCl
	P(XVI)-008	0.001M HCl
	P(XVI)-009	0.001M NaOH
PEI_{1393}^{100Q}	P(XVI)-007	0.01M HCl
	P(XVI)-008	0.001M HCl
	P(XVI)-009	0.001M NaOH

Table I-3: Degree of protonation α of polymer-water-solutions as a function of pH (calculated from titration data)

pH	PEI_{1393}	PEI_{1393}^{10Q}	PEI_{1393}^{20Q}	PEI_{1393}^{50Q}	PEI_{1393}^{100Q}
5	0.56	0.49	0.52	0.41	0.28
5.5	0.52	0.43	0.46	0.38	0.26
6	0.47	0.36	0.40	0.31	0.18
6.5	0.42	0.30	0.34	0.22	0.13
7	0.35	0.25	0.27	0.14	0.06
7.5	0.28	0.19	0.21	0.06	0.01
8	0.21	0.12	0.15	0.01	0.00
8.5	0.13	0.06	0.05	0.00	0.00
9	0.07	0.02	0.00	0.00	0.00
9.5	0.02	0.00	0.00	0.00	0.00
10	0.01	0.00	0.00	0.00	0.00

Table I-4: Electrophoretic mobility of partially quaternized poly(ethylenimine) derivatives PEI_{1393} (XIII) – PEI_{1393}^{100Q} (XVII) for three different molar concentrations

Polymer	Sample	c_P [mM]	μ_e [10^{-8}m²/Vs]
PEI_{1393}	P(XIII)-010	3.33	2.034±0.413
	P(XIII)-011	6.66	1.791±0.200
	P(XIII)-012	13.33	1.390±0.369
$\mathrm{PEI}_{1393}^{10\mathrm{Q}}$	P(XIV)-010	3.33	2.905±0.283
	P(XIV)-011	6.66	2.922±0.188
	P(XIV)-012	13.33	2.942±0.273
$\mathrm{PEI}_{1393}^{20\mathrm{Q}}$	P(XV)-010	3.33	3.028±0.094
	P(XV)-011	6.66	3.099±0.147
	P(XV)-012	13.33	3.214±0.042
$\mathrm{PEI}_{1393}^{50\mathrm{Q}}$	P(XVI)-010	3.33	3.157±0.124
	P(XVI)-011	6.66	3.410±0.110
	P(XVI)-012	13.33	3.087±0.049
$\mathrm{PEI}_{1393}^{100\mathrm{Q}}$	P(XVII)-010	3.33	1.927±0.154
	P(XVII)-011	6.66	1.627±0.183
	P(XVII)-012	13.33	1.997±0.278

Table I-5: Silica-nanoparticle-dispersions and their titration solutions

Sample	Titration solution
009	0.1M HCl
010	0.01M HCl
011	0.001M HCl
012	0.1M NaOH
013	0.01M NaOH
014	0.001M NaOH

Table I-6: pH and electrophoretic mobility of silica-nanoparticle-dispersions

Sample	pH	μ_e [10^{-8} m²/Vs]
015	2.4	7.633±0.253
016	3.5	-1.781±0.033
017	4.8	-2.151±0.087

Sample	pH	μ_e [10^{-8} m²/Vs]
018	6.1	-2.390±0.062
019	6.6	-2.540±0.166
020	7.1	-2.757±0.119
021	8.2	-3.004±0.109
022	9.2	-3.145±0.132
023	10.1	-3.218±0.096
024	10.7	-3.161±0.145
025	11.4	-3.116±0.374

Table I-7: Logarithmic mass and number ratio, the absorbance at 400nm and optical judgment for the pure silica-water-dispersion and all silica dispersions in presence of partially quaternized poly(ethylenimine) derivatives

Polymer	Dispersion	log r_m	log r_u	A_{400nm}	Optical judgment
	001	---	---	0.06	D
PEI_{28}	(I)-001	-4.00	1.60	0.22	D
	(I)-002	-3.14	2.44	0.10	D
	(I)-003	-3.00	2.60	0.08	D
	(I)-004	-2.85	2.74	0.10	D
	(I)-005	-2.67	2.92	0.09	D
	(I)-006	-2.45	3.15	0.11	D
	(I)-007	-2.27	3.33	0.17	D
	(I)-008	-2.14	3.45	0.25	D
	(I)-009	-2.01	3.59	1.55	P
	(I)-010	-1.66	3.94	1.93	P
	(I)-011	-1.33	4.27	1.55	P
	(I)-012	-0.99	4.61	1.70	P
	(I)-013	-0.61	4.99	1.69	P
	(I)-014	-0.30	5.30	1.70	P
	(I)-015	0.00	5.60	1.70	P
	(I)-016	0.40	5.99	1.41	P
	(I)-017	1.00	6.60	0.26	D
	(I)-018	1.17	6.77	0.10	D
	(I)-019	1.30	6.90	0.10	D

Polymer	Dispersion	log r_m	log r_u	A_{400nm}	Optical judgment
PEI_{28}^{1Q}	(II)-001	-4.00	1.58	0.05	D
	(II)-002	-3.00	2.58	0.06	D
	(II)-003	-2.65	2.92	0.04	D
	(II)-004	-2.32	3.26	0.17	D
	(II)-005	-2.00	3.58	0.39	P
	(II)-006	-1.65	3.93	1.80	P
	(II)-007	-1.33	4.25	1.47	P
	(II)-008	-1.00	4.58	1.75	P
	(II)-009	0.00	5.58	1.68	P
	(II)-010	1.00	6.58	1.60	P
PEI_{28}^{5Q}	(III)-001	-4.00	1.52	0.11	D
	(III)-002	-3.00	2.53	0.06	D
	(III)-003	-2.65	2.87	0.09	D
	(III)-004	-2.32	3.21	0.18	D
	(III)-005	-2.00	3.53	0.35	P
	(III)-006	-1.66	3.86	1.79	P
	(III)-007	-1.33	4.19	1.26	P
	(III)-008	-1.00	4.52	1.77	P
	(III)-009	0.00	5.53	1.94	P
	(III)-010	1.00	6.53	1.93	P
PEI_{28}^{10Q}	(IV)-001	-4.00	1.47	0.09	D
	(IV)-002	-3.01	2.47	0.06	D
	(IV)-003	-2.71	2.74	0.09	D
	(IV)-004	-2.54	2.93	0.10	D
	(IV)-005	-2.32	3.15	0.14	D
	(IV)-006	-2.14	3.33	0.19	D
	(IV)-007	-2.01	3.45	0.32	D
	(IV)-008	-1.66	3.81	1.48	P
	(IV)-009	-1.32	4.14	0.38	D
	(IV)-010	-1.00	4.46	0.52	D
	(IV)-011	-0.61	4.86	0.34	D
	(IV)-012	-0.30	5.16	0.38	P
	(IV)-013	0.00	5.46	0.38	P

Polymer	Dispersion	log r_m	log r_u	A_{400nm}	Optical judgment
	(IV)-014	0.39	5.85	1.68	P
	(IV)-015	1.00	6.47	0.92	P
PEI_{28}^{20Q}	(V)-001	-4.00	1.36	0.16	D
	(V)-002	-2.99	2.37	0.07	D
	(V)-003	-2.66	2.71	0.11	D
	(V)-004	-2.33	3.04	0.14	D
	(V)-005	-2.00	3.36	0.41	P
	(V)-006	-1.65	3.72	1.77	P
	(V)-007	-1.33	4.04	0.20	D
	(V)-008	-0.99	4.37	0.24	D
	(V)-009	-0.66	4.71	0.48	P
	(V)-010	-0.33	5.03	0.70	P
	(V)-011	0.00	5.36	0.90	P
	(V)-012	1.00	6.37	1.66	P
PEI_{28}^{50Q}	(VI)-001	-4.00	1.15	0.18	D
	(VI)-002	-3.00	2.16	0.07	D
	(VI)-003	-2.70	2.46	0.08	D
	(VI)-004	-2.40	2.76	0.11	D
	(VI)-005	-2.22	2.93	0.17	D
	(VI)-006	-2.00	3.16	0.64	P
	(VI)-007	-1.83	3.33	1.41	P
	(VI)-008	-1.70	3.46	1.38	P
	(VI)-009	-1.33	3.82	0.24	D
	(VI)-010	-1.00	4.16	0.39	D
	(VI)-011	-0.59	4.56	0.69	P
	(VI)-012	-0.32	4.83	0.85	P
	(VI)-013	0.00	5.16	0.78	P
	(VI)-014	1.00	6.15	1.34	P
PEI_{28}^{100Q}	(VII)-001	-4.00	0.94	0.15	D
	(VII)-002	-2.99	1.94	0.09	D
	(VII)-003	-2.49	2.45	0.10	D
	(VII)-004	-2.19	2.75	0.17	D
	(VII)-005	-1.99	2.94	0.59	P

Polymer	Dispersion	log r_m	log r_u	A_{400nm}	Optical judgment
	(VII)-006	-1.78	3.16	1.41	P
	(VII)-007	-1.62	3.32	0.32	D
	(VII)-008	-1.49	3.45	0.24	D
	(VII)-009	-1.33	3.61	0.27	D
	(VII)-010	-1.00	3.94	0.91	P
	(VII)-011	-0.66	4.28	0.53	P
	(VII)-012	-0.33	4.62	0.59	P
	(VII)-013	0.00	4.94	1.00	P
	(VII)-014	1.00	5.94	0.97	P
	(VIII)-001	-3.23	2.37	0.10	D
	(VIII)-002	-2.48	3.12	0.19	D
	(VIII)-003	-2.00	3.60	1.39	P
	(VIII)-004	-1.48	4.12	1.80	P
PEI_{232}	(VIII)-005	-1.00	4.60	0.53	D
	(VIII)-006	-0.60	5.00	0.77	D
	(VIII)-007	-0.30	5.30	0.81	D
	(VIII)-008	0.00	5.60	0.71	D
	(VIII)-009	0.40	6.00	0.62	D
	(VIII)-010	0.77	6.37	0.31	D
	(IX)-001	-4.00	1.48	0.05	D
	(IX)-002	-3.00	2.47	0.06	D
	(IX)-003	-2.60	2.87	0.43	D
	(IX)-004	-2.29	3.17	0.23	D
	(IX)-005	-2.12	3.35	0.35	D
	(IX)-006	-2.00	3.47	0.63	D
PEI_{232}^{10Q}	(IX)-007	-1.53	3.94	1.69	P
	(IX)-008	-1.30	4.16	1.50	P
	(IX)-009	-1.12	4.34	0.65	D
	(IX)-010	-1.00	4.46	0.25	D
	(IX)-011	-0.82	4.64	0.27	D
	(IX)-012	-0.70	4.77	0.28	D
	(IX)-013	-0.60	4.86	0.24	D
	(IX)-014	-0.52	4.94	0.34	D

Polymer	Dispersion	log r_m	log r_u	A_{400nm}	Optical judgment
	(IX)-015	-0.40	5.07	0.33	D
	(IX)-016	-0.30	5.16	0.24	D
	(IX)-017	-0.12	5.34	0.34	D
	(IX)-018	0.00	5.47	0.30	D
	(IX)-019	0.40	5.87	1.10	P
	(IX)-020	0.70	6.17	1.31	P
	(IX)-021	0.88	6.34	1.15	P
	(IX)-022	1.00	6.47	1.12	P
PEI_{232}^{20Q}	(X)-001	-3.00	2.37	0.20	D
	(X)-002	-2.75	2.62	0.11	D
	(X)-003	-2.50	2.87	0.14	D
	(X)-004	-2.25	3.11	0.22	D
	(X)-005	-2.00	3.37	0.49	D
	(X)-006	-1.75	3.62	1.76	P
	(X)-007	-1.50	3.87	1.47	P
	(X)-008	-1.25	4.12	0.92	D
	(X)-009	-1.00	4.36	0.47	D
	(X)-010	-0.75	4.62	0.26	D
	(X)-011	-0.50	4.87	0.27	D
	(X)-012	-0.25	5.12	0.70	D
	(X)-013	0.00	5.36	0.99	P
	(X)-014	0.25	5.62	1.19	P
	(X)-015	0.50	5.86	1.34	P
PEI_{232}^{50Q}	(XI)-001	-2.79	2.37	0.12	D
	(XI)-002	-2.54	2.62	0.14	D
	(XI)-003	-2.29	2.87	0.18	D
	(XI)-004	-2.04	3.12	0.41	D
	(XI)-005	-1.79	3.36	1.76	P
	(XI)-006	-1.54	3.62	1.46	P
	(XI)-007	-1.29	3.87	0.75	D
	(XI)-008	-1.04	4.12	0.36	D
	(XI)-009	-0.79	4.37	0.27	D
	(XI)-010	-0.54	4.62	0.29	D

Polymer	Dispersion	log r_m	log r_u	A_{400nm}	Optical judgment
	(XI)-011	-0.29	4.86	0.27	D
	(XI)-012	-0.04	5.12	0.75	D
	(XI)-013	0.21	5.37	0.92	P
	(XI)-014	0.46	5.62	1.07	P
	(XI)-015	0.71	5.86	1.18	P
PEI_{232}^{100Q}	(XII)-001	-2.58	2.37	0.12	D
	(XII)-002	-2.33	2.62	0.15	D
	(XII)-003	-2.08	2.86	0.20	D
	(XII)-004	-1.83	3.11	1.38	P
	(XII)-005	-1.58	3.36	1.77	P
	(XII)-006	-1.33	3.61	0.69	D
	(XII)-007	-1.08	3.86	0.32	D
	(XII)-008	-0.83	4.11	0.25	D
	(XII)-009	-0.58	4.36	0.26	D
	(XII)-010	-0.33	4.62	0.27	D
	(XII)-011	-0.08	4.87	0.28	D
	(XII)-012	0.17	5.11	0.79	D
	(XII)-013	0.42	5.37	0.91	P
	(XII)-014	0.67	5.61	1.03	P
	(XII)-015	0.92	5.86	1.15	P
PEI_{1393}	(XIII)-001	-2.45	3.15	0.28	D
	(XIII)-002	-2.01	3.59	1.73	P
	(XIII)-003	-1.70	3.89	1.78	P
	(XIII)-004	-1.44	4.15	1.49	P
	(XIII)-005	-1.00	4.59	0.55	D
	(XIII)-006	-0.61	4.99	0.62	D
	(XIII)-007	-0.30	5.29	0.59	D
	(XIII)-008	0.00	5.59	0.67	D
	(XIII)-009	0.40	6.00	0.63	D
	(XIII)-015	-1.15	4.44	1.74	P
	(XIII)-016	-1.15	4.44	1.13	P
	(XIII)-017	-1.15	4.44	0.72	D
	(XIII)-018	-1.15	4.44	0.63	D

Polymer	Dispersion	log r_m	log r_u	A_{400nm}	Optical judgment
	(XIII)-019	-1.15	4.44	0.61	D
	(XIII)-020	-1.15	4.44	0.49	D
PEI_{1393}^{10Q}	(XIV)-001	-2.32	3.15	0.23	D
	(XIV)-002	-2.02	3.44	0.47	D
	(XIV)-003	-1.81	3.65	0.95	D
	(XIV)-004	-1.57	3.89	2.19	P
	(XIV)-005	-1.22	4.24	0.89	D
	(XIV)-006	-1.00	4.46	0.57	D
	(XIV)-007	-0.60	4.86	0.40	D
	(XIV)-008	-0.31	5.16	0.45	D
	(XIV)-009	0.00	5.46	0.43	D
	(XIV)-010	0.18	5.65	0.91	D
	(XIV)-011	0.40	5.87	1.42	P
	(XIV)-012	0.68	6.14	0.95	P
PEI_{1393}^{20Q}	(XV)-001	-2.22	3.14	0.37	D
	(XV)-002	-1.91	3.45	0.68	D
	(XV)-003	-1.72	3.65	1.78	P
	(XV)-004	-1.47	3.89	1.49	P
	(XV)-005	-1.22	4.14	0.79	D
	(XV)-006	-0.92	4.44	0.48	D
	(XV)-007	-0.72	4.64	0.37	D
	(XV)-008	-0.47	4.89	0.31	D
	(XV)-009	-0.22	5.14	0.30	D
	(XV)-010	0.08	5.44	0.53	D
	(XV)-011	0.28	5.65	1.02	P
PEI_{1393}^{50Q}	(XVI)-001	-2.01	3.15	0.48	D
	(XVI)-002	-1.71	3.45	1.47	P
	(XVI)-003	-1.51	3.65	1.64	P
	(XVI)-004	-1.26	3.89	0.80	D
	(XVI)-005	-1.01	4.14	0.46	D
	(XVI)-006	-0.71	4.44	0.30	D
	(XVI)-007	-0.51	4.64	0.30	D

Polymer	Dispersion	log r_m	log r_u	A_{400nm}	Optical judgment
	(XVI)-008	-0.26	4.89	0.31	D
	(XVI)-009	-0.01	5.14	0.30	D
	(XVI)-010	0.29	5.44	0.49	D
	(XVI)-011	0.49	5.64	1.25	P
	(XVI)-012	0.71	5.87	1.29	P
	(XVI)-013	1.00	6.16	1.33	P
	(XVI)-014	-2.01	3.14	1.20	P
	(XVI)-015	-1.51	3.65	2.02	P
	(XVI)-016	-1.01	4.15	1.92	P
	(XVI)-017	-0.51	4.64	1.67	P
	(XVI)-018	-0.01	5.14	0.64	P
	(XVI)-019	-1.51	3.65	1.71	P
	(XVI)-020	-1.51	3.65	1.73	P
	(XVI)-021	-1.01	4.15	0.49	D
	(XVI)-022	-1.01	4.15	0.47	D
	(XVI)-028	-0.71	4.44	0.50	D
	(XVI)-029	-0.71	4.44	0.40	D
	(XVI)-030	-0.71	4.44	0.38	D
	(XVI)-031	-0.71	4.44	0.33	D
	(XVI)-032	-0.71	4.44	0.34	D
	(XVI)-033	-0.71	4.44	0.36	D
	(XVI)-034	-0.71	4.44	0.30	D
	(XVI)-035	-0.71	4.44	0.31	D
	(XVI)-036	-0.71	4.44	0.35	D
	(XVI)-037	-0.71	4.44	0.40	D
	(XVI)-038	-0.71	4.44	0.55	D
	(XVI)-039	-0.71	4.44	0.63	D
	(XVI)-040	-0.71	4.44	0.70	D
	(XVI)-041	-0.71	4.44	0.77	D
PEI_{1393}^{100Q}	(XVII)-001	-1.79	3.16	1.14	P
	(XVII)-002	-1.49	3.45	1.76	P
	(XVII)-003	-1.29	3.65	0.70	D
	(XVII)-004	-1.04	3.90	0.38	D

Polymer	Dispersion	log r_m	log r_u	A_{400nm}	Optical judgment
	(XVII)-005	-0.79	4.15	0.34	D
	(XVII)-006	-0.50	4.45	0.23	D
	(XVII)-007	-0.29	4.65	0.34	D
	(XVII)-008	-0.04	4.90	0.38	D
	(XVII)-009	0.21	5.15	0.41	D
	(XVII)-010	0.50	5.45	0.50	D
	(XVII)-011	0.70	5.64	1.34	P

(D: dispersion; P: precipitation)

Table I-8: pH-values and electrophoretic mobility of the silica dispersions in presence of partially quaternized poly(ethylenimine)

Polymer	Dispersion	pH	μ_e [10^{-8} m²/Vs]
	001	7.0	-4.094±0.085
PEI_{28}^{50Q}	(VI)-006	8.1	-2.923±0.036
	(VI)-007	8.1	-2.302±0.018
	(VI)-008	7.9	-0.145±0.047
	(VI)-009	7.1	3.245±0.012
	(VI)-010	7.5	3.653±0.028
	(VI)-011	8.1	3.670±0.098
	(VI)-012	8.5	3.508±0.226
	(VI)-013	8.8	3.540±0.161
	(VI)-014	9.5	1.591±0.160
PEI_{232}^{50Q}	(XI)-004	7.8	-3.327±0.039
	(XI)-005	7.4	-2.651±0.040
	(XI)-006	7.1	0.345±0.021
	(XI)-007	6.8	3.163±0.052
	(XI)-008	6.8	3.599±0.131
	(XI)-009	7.2	3.802±0.081
	(XI)-010	7.4	3.809±0.094
	(XI)-011	7.8	3.809±0.219
	(XI)-012	8.2	3.683±0.139
	(XI)-013	8.5	3.905±0.203
	(XI)-014	8.8	3.916±0.304
	(XI)-015	8.9	2.694±0.020

Polymer	Dispersion	pH	μ_e [10^{-8} m²/Vs]
PEI_{1393}	(XIII)-001	7.4	-3.761±0.117
	(XIII)-002	8.2	-2.990±0.119
	(XIII)-003	8.5	-1.581±0.145
	(XIII)-004	8.6	1.176±0.069
	(XIII)-005	8.5	2.816±0.048
	(XIII)-006	9.1	2.278±0.038
	(XIII)-007	9.8	1.579±0.018
	(XIII)-008	10.2	1.137±0.036
	(XIII)-009	10.5	0.709±0.015
	(XIII)-015	10.4	0.549±0.033
	(XIII)-016	10.1	1.465±0.037
	(XIII)-017	8.5	3.508±0.042
	(XIII)-018	7.4	3.839±0.178
	(XIII)-019	6.6	4.198±0.053
	(XIII)-020	5.7	4.515±0.073
PEI_{1393}^{10Q}	(XIV)-001	8.4	-3.656±0.324
	(XIV)-002	8.4	-3.758±0.151
	(XIV)-003	8.4	-3.484±0.216
	(XIV)-004	8.4	-1.542±0.262
	(XIV)-005	8.4	2.826±0.142
	(XIV)-006	8.4	3.542±0.059
	(XIV)-007	8.9	3.713±0.104
	(XIV)-008	9.5	3.203±0.120
	(XIV)-009	9.7	2.740±0.070
	(XIV)-010	10.1	2.698±0.060
	(XIV)-011	10.2	2.632±0.119
	(XIV)-012	10.5	2.178±0.118
PEI_{1393}^{20Q}	(XV)-001	8.4	-3.307±0.245
	(XV)-002	8.5	-3.469±0.057
	(XV)-003	8.4	-1.939±0.054
	(XV)-004	8.2	1.031±0.069
	(XV)-005	7.9	3.211±0.026
	(XV)-006	8.3	3.516±0.055
	(XV)-007	8.4	3.891±0.111

Polymer	Dispersion	pH	μ_e [10^{-8} m²/Vs]
	(XV)-008	8.8	3.696±0.094
	(XV)-009	9.2	3.491±0.068
	(XV)-010	9.5	3.429±0.173
	(XV)-011	9.7	3.336±0.206
PEI_{1393}^{50Q}	(XVI)-001	7.3	-2.839±0.202
	(XVI)-002	7.3	-1.234±0.032
	(XVI)-003	6.9	1.136±0.051
	(XVI)-004	6.8	3.050±0.070
	(XVI)-005	7.0	3.549±0.038
	(XVI)-006	7.3	3.849±0.139
	(XVI)-007	7.8	3.949±0.137
	(XVI)-008	8.1	3.935±0.154
	(XVI)-009	8.4	3.655±0.157
	(XVI)-010	8.7	3.951±0.269
	(XVI)-011	8.9	3.985±0.380
	(XVI)-012	9.1	3.571±0.089
	(XVI)-013	9.4	2.250±0.030
	(XVI)-028	11.2	2.741±0.082
	(XVI)-029	10.3	3.141±0.144
	(XVI)-030	8.7	3.591±0.107
	(XVI)-031	7.4	3.806±0.210
	(XVI)-032	6.4	3.974±0.167
	(XVI)-033	5.6	3.817±0.089
	(XVI)-034	7.2	3.888±0.039
	(XVI)-035	7.4	3.705±0.051
	(XVI)-036	7.7	3.462±0.104
	(XVI)-037	7.8	3.368±0.028
	(XVI)-038	7.9	2.984±0.024
	(XVI)-039	7.9	2.440±0.057
	(XVI)-040	8.0	2.250±0.103
	(XVI)-041	8.0	2.218±0.062
PEI_{1393}^{100Q}	(XVII)-001	7.0	-2.675±0.083
	(XVII)-002	6.1	1.689±0.090
	(XVII)-003	5.9	3.284±0.082

Polymer	Dispersion	pH	μ_e [10^{-8} m²/Vs]
	(XVII)-004	5.9	3.840±0.124
	(XVII)-005	6.2	3.944±0.155
	(XVII)-006	6.5	4.026±0.120
	(XVII)-007	7.0	4.132±0.167
	(XVII)-008	7.1	3.853±0.140
	(XVII)-009	7.4	3.948±0.204
	(XVII)-010	7.8	4.053±0.372
	(XVII)-011	8.0	4.162±0.547

Table I-9: Samples and the titrant solutions used for the titration of silica-nanoparticle-dispersions in the presence of PEI_{1393} (XIII) and PEI_{1393}^{50Q} (XVI) with a logarithmic subunit ratio of log r_u = 4.44

	0.001M HCl	0.01M HCl	0.1M HCl	0.001M NaOH	0.01M NaOH
PEI_{1393}	(XIII)-010	(XIII)-011	(XIII)-012	(XIII)-013	(XIII)-014
$\mathrm{PEI}_{1393}^{50\mathrm{Q}}$	(XVI)-023	(XVI)-024	(XVI)-025	(XVI)-026	(XVI)-027

Abbreviations

Methods

AFM	Atomic force microscopy
ATR	Attenuated total reflection
DLS	Dynamic light scattering
DOSY	Diffusion-ordered spectroscopy
DSC	Differential scanning calorimetry
EA	Elemental analysis
FTIR	Fourier transform infrared
GPC	Gel permeation chromatography
LS	Light scattering
NMR	Nuclear magnetic resonance
SFG	Sum frequency generation
TEM	Transmission electron microscopy
UV/Vis	Ultraviolet/visible

Formula Symbols

B	Baseline
c	Concentration
ccc	Critical coagulation concentration
D	Diffusion coefficient
E	Electric field strength
f_D	Doppler frequency shift
F_{el}	Electrical field force
F_f	Hydrodynamic friction force
G	Distribution of decay rates
g_1	Electric field correlation
g_2	Intensity correlation function
I (scattering)	Intensity
I (stability)	Ionic strength
k^{-1}	Debye length
k_b	Boltzmann constant
M	Molar mass

m (graphical analysis)	Slope
m (synthesis)	Mass
M_W	Mass average molar mass
M_N	Number average molar mass
N	Number
n (diffusion)	Refractive index
n (screening)	Counterions valency
n (synthesis)	Amount of substance
N_A	Avogadro number
q (diffusion)	Wave vector
q (polymer composition)	Degree of quaternization
r	Radius, distance
T	Temperature
t	Time
T_G	Glass temperature
V (electrokinetics)	Potential
V (geometry)	Volume
v (diffusion)	Wave number
v (electrokinetics)	Particle drift velocity
wt	Weight
X_n	Degree of polymerization
z	Charge number
α	Degree of protonation
β (light scattering)	Instrumental constant
β (electrokinetics)	Angle between the measured component and the flow
Γ	Decay constant
Δ	Difference
ε_0	Dielectric constant
ε_r	Permittivity of free space
Z	Zeta potential
H	Dynamic viscosity
Θ	Angle between two beams
Λ	Fringe spacing
λ	Wavelength
μ_e	Electrophoretic mobility
ρ	Density

σ_S	Surface charge
τ	Delay time
Φ	Volume fraction

Units

°	Degree
%	Percent
C	Celsius
g	Gram
h	Hour
Hz	Hertz
K	Kelvin
L	Liter
M	Molar
m	Meter
m^{-1}	Number of waves per meter
min	Minute
ppm	Parts per million
s	Second
V	Volt

Prefix

c	Centi
k	Kilo
M	Mega
m	Milli
n	Nano
µ	Micro

Chemicals

Ac	Acetone
BPEI	Branched poly(ethylenimine)
DMF	Dimethylformamide

DPEI	Dendritic poly(ethylenimine)
EA	Ethyl acetate
EI	Ethylenimine
EtOH	Ethanol
LPEI	Linear poly(ethylenimine)
MeOH	Methanol
PAMAM	Poly(amidoamine)
PDADMAC	Poly(diallyldimethylammonium chloride)
PEI	Poly(ethylenimine)
$\mathrm{PEI}_{\mathrm{X_n}}^{\mathrm{qQ}}$	Poly(ethylenimine) derivative with a degree of quaternization of "q" percent and a degree of polymerization of "X_n"
PE	Petroleum ether
PMMA	Poly(methyl methacrylate)
$\mathrm{quat}_{\mathrm{R}}$	Glycidyltrimethylammonium chloride
TEOS	Tetraethyl orthosilicate
THF	Tetrahydrofuran
Tol	Toluene

Substances

(I)	PEI_{28}
(II)	$\mathrm{PEI}_{28}^{1\mathrm{Q}}$
(III)	$\mathrm{PEI}_{28}^{5\mathrm{Q}}$
(IV)	$\mathrm{PEI}_{28}^{10\mathrm{Q}}$
(V)	$\mathrm{PEI}_{28}^{20\mathrm{Q}}$
(VI)	$\mathrm{PEI}_{28}^{50\mathrm{Q}}$
(VII)	$\mathrm{PEI}_{28}^{100\mathrm{Q}}$
(VIII)	PEI_{232}
(IX)	$\mathrm{PEI}_{232}^{10\mathrm{Q}}$
(X)	$\mathrm{PEI}_{232}^{20\mathrm{Q}}$

(XI)	PEI_{232}^{50Q}
(XII)	PEI_{232}^{100Q}
(XIII)	PEI_{1393}
(XIV)	PEI_{1393}^{10Q}
(XV)	PEI_{1393}^{20Q}
(XVI)	PEI_{1393}^{50Q}
(XVII)	PEI_{1393}^{100Q}

Samples

(Consecutively number)	Silica-dispersion
P(Roman numberal)-(Consecutively number)	Polymer-solution
(Roman numeral)-(Consecutively number)	Silica-polymer-dispersion

Reaction

ACE	Active chain end
R	Rest
1°	Primary
2°	Secondary
3°	Tertiary

Structure

A, B, G, N (NMR)	Backbone methylene carbon atoms
C, H, O (NMR)	α-backbone ammonium bonded-methylene carbon atoms
D, M, P (NMR)	Hydroxyl-bonded methine carbon atoms
E, J, Q (NMR)	α-ammonium bonded-methylene carbon atoms

F, K, R (NMR)	Methyl carbon atoms of the ammonium groups
I (NMR)	α-oxygen bonded-methylene carbon atoms
J (NMR)	α-oxygen bonded-methine carbon atoms
td (NMR)	Terminal and dendritic unit
tl (NMR)	Terminal and linear unit
dd (NMR)	Two dendritic units
ld (NMR)	Linear and a dendritic unit
ll (NMR)	Two linear units
b_1 (NMR)	Carbon atom next to terminal group (for terminal and dendritic unit)
b_2 (NMR)	Carbon atom next to terminal group (for terminal and linear unit)
b_3 (NMR)	Carbon atom next to linear group (for linear and dendritic unit)
b_4 (NMR)	Carbon atom next to linear group (for two linear units)
b_5 (NMR)	Carbon atom next to linear group (for terminal and linear unit)
b_6 (NMR)	Carbon atom next to dendritic group (for two dendritic units)
b_7 (NMR)	Carbon atom next to dendritic group (for linear and dendritic unit)
b_8 (NMR)	Carbon atom next to dendritic group (for terminal and dendritic unit)
b_x (NMR)	Carbon atom in the backbone bonded to a nitrogen atom that reacted with $quat_R$
A_1, A_2, A_3 (NMR)	Integration regions
A_N, A_C (EA)	Atomic weight of nitrogen / carbon
N_+	Quaternized ethylenimine units
p_N, p_C (EA)	Percentage of nitrogen / carbon
n, x, y, z (NMR)	Subunits

Stability

A_{400}	Absorbance at a wavelength of 400nm
D	Dispersion (optical judgement)
D_I	First area of stability
D_{II}	Second area of stability
D_{III}	Third area of stability
P	Precipitation
P_I	First area of instability
P_{II}	Second area of instability
r_m	Mass ratio
r_u	Subunit ratio

Surface charge

ASP	Adsorption saturation point
CR	Charge ratio
c+	Fixed positive charges
IEP	Isoelectric point
n+	Nominal charge
neff	Effective charge
quat free	Quaternized subunits of polymers free in solution

Shortcuts

calc.	Calculated
cf.	Compare
DLVO	Derjaguin, Landau, Verwey, Overbeek
e.g.	For example
G	Generation
g	Grafted
k	Proportionality constant
log	Logarithm to the base of 10
max	Maximum
NP	Nanoparticle
P	Polymer

PEL	Polyelectrolyte
PS	Polymer solution
Q	Quaternization
REP	Repulsive
SU	Subunit
THEO	Theoretical
TOT	Total
VDW	Van der Waals
X	Soluble
---	Insoluble

Danksagung

Ich bedanke mich bei Herrn Professor Beginn für die Möglichkeit diese Arbeit anzufertigen, für die Bereitstellung der Mittel, sowie die wissenschaftliche Betreuung, die Diskussionen und die Unterstützung während meiner Studien- und Promotionszeit.

Ich danke Herrn Professor Lorenz Walder für die Übernahme des Zweitgutachtens.

Ich bedanke mich bei Herrn Professor Markus Haase und Herrn Doktor Karsten Kömpe für ihre Teilnahme an der Prüfungskommission.

Großer Dank gilt den Mitarbeitern des Institutes für die Durchführung von Messungen und für jegliche weitere Hilfe im Laboralltag: Petra Bösel, Marianne Gather, Elisabeth Michalek, Iris Helms, Eva Becker, Anja Schuster und Henning Eickmeier.

Ich bedanke mich bei Gertraud Strunk und Monika Dubiel für die Hilfe bei der Bewerkstelligung von Formalien.

Ich danke all meinen Kollegen der Arbeitsgruppe OMC für die kollegiale Atmosphäre: Dr. Ralf Beckmann, Dr. Enfeng Song, Dr. Sandra Schwitke, Dr. Marina Zorn, Dr. Marius Ciobanu, Ana-Maria Lepadatu, Eduard Belke, Xihomara Casallas Cruz, Nadine Diek, Martin Frosinn, Eugen Leinweber und Irina Weimer.

Ich bedanke mich bei meinen Eltern, die mich immer in meinen Entscheidungen unterstützt haben und denen der größte Dank dafür gilt, dass ich diesen Weg gegangen bin und mich für diese Promotion qualifizieren konnte.

Ich danke meinem Freund Mohsen für die konstante Unterstützung in diesen Jahren, die mir die größte Motivation zur Fertigstellung dieser Arbeit war.

Ich erkläre hiermit, dass ich die vorliegende Arbeit ohne unzulässige Hilfe Dritter und ohne Benutzung anderer als der angegebenen Hilfsmittel angefertigt habe. Die aus anderen Quellen direkt oder indirekt übernommenen Daten und Konzepte sind unter Angabe der Quelle gekennzeichnet. Niemand hat von mir unmittelbar oder mittelbar geldwerte Leistungen für Arbeiten erhalten, die im Zusammenhang mit dem Inhalt der vorgelegten Dissertation stehen.

Die Arbeit wurde bisher weder im In- noch im Ausland in gleicher oder ähnlicher Form einer anderen Prüfungsbehörde vorgelegt.

Osnabrück, den 15. September 2015

Miriam Brandt